Exploring the Cellular and Molecular Mechanisms Driving Connexin-36 Electrical Plasticity and the Functional Consequences of its Loss on the Sensorimotor Behaviors of Zebrafish (*Danio Rerio*)

CHERIE BROWN

A DISSERTATION SUBMITTED TO
THE FACULTY OF GRADUATE STUDIES
IN PARTIAL FULFILLMENT OF THE REQUIREMENTS
FOR THE DEGREE OF
DOCTOR OF PHILOSOPHY

GRADUATE PROGRAM IN BIOLOGY
YORK UNIVERSITY
TORONTO, ONTARIO

August 2022

ABSTRACT

In mammals, connexin-36 (Cx36) is the major component of electrical synapses, also found alongside chemical synapses throughout the brain. An equivalent form of long-term potentiation (LTP) exclusively at Cx36 electrical synapses, termed the run-up, has been previously identified; however, the mechanism and molecular machinery involved remains elusive. We hypothesized an LTP-like mechanism was involved at Cx36 electrical synapses, potentiating the run-up. To address this, we investigated the tubulin-dependent delivery of Cx36 connexons to the plasma membrane in Neuro2a cells. A putative Cx36-tubulin binding motif was elucidated via sequence alignment, and the direct binding of tubulin with the C-terminal tail of Cx36 was confirmed via BioID. TIRF and FRAP microscopy techniques established that Cx36 is transported from the trans-Golgi network to the plasma membrane via interactions with the tubulin-cytoskeleton. Manipulating the Cx36-tubulin interaction via mutations and pharmacological inhibition reduced Cx36 trafficking to the gap junction plaque and inhibited run-up. While we identified tubulin as a driving force in achieving Cx36 run-up, we found that its transport occurred independently of CaM-CaMKII activity. Despite the similarities in machinery used between chemical and electrical synapses, the functional consequence of Cx36 asymmetry at homotypic aggregates had yet to be addressed. Next, we investigated the role of Cx36 in sensorimotor circuitry in zebrafish (*Danio rerio*), where the teleost orthologs are expressed distinctly. Here, we targeted the *gjd2b* gene since its corresponding ortholog, Cx35b, is expressed presynaptically. Based on current literature, we hypothesized that complex alterations to neuronal circuitry via Cx35b knock-out (KO) would affect vision, sensorimotor gating, and plasticity-dependent cognitive processing. We found that Cx35b expression coincides with photoreceptor cell specificity and expression in the inner plexiform layer. Cx35b KO resulted in developmental deviances, cranial defects, visual ambiguities (discrimination of light stimulus brightness, arrangement, and temporal properties), and increased levels of anxiety; however, KO did not impair non-associative learning and memory. Genetically, loss of the *gjd2b* gene resulted in changes primarily in connexin, dopaminergic, and immediate early gene regulation. Taken together, we concluded that Cx36 shares molecular machinery with chemical synapses to rectify neuronal communication, and this molecular asymmetry is critical in driving behavioral outcomes.

DEDICATION

In loving memory of my father

Charles Denton Brown
February 12, 1954 – February 19, 2022

Oh I miss those days, yes
I miss those days, yeah
Remember the songs use to make you rockaway,
Those were the days.

ACKNOWLEDGEMENTS

First and foremost, to God be the glory forever and ever. Amen.
Joel 2:25

I want to give my wholehearted thanks to:

Georg Zoidl.
I will never be able to completely articulate the level of deep respect and gratitude I have towards you. I want to thank you for choosing me as your student and treating me as your friend. You have been more than a supervisor, but also my mentor, advocator, cheer captain, and, greatest of all, my family. Your trust in me has never wavered, and it has not gone unnoticed or taken for granted. So here, I want to thank you immensely for your support and guidance through both my highs and lows. You have been instrumental in my growth from a young girl with a dream to a woman achieving her goals. I hope the person and scientist I am today is somebody you can be very proud of. One thing for sure is that we will meet again, perhaps in an interesting city over some good food, drinks, laughs, and music! Again, from the bottom of my heart, thank you.

Christiane Zoidl.
You have been such a great resource to me in both your technical knowledge and the operation of the lab. I would not have grown as much as a scientist as I have if it weren't for you. I have learned so much and look up to you and the example/standard you have set. This is what I can only hope to achieve in my future career. More than that, you are such a sweet, thoughtful, and kind soul. Thank you for always checking in with me and finding ways to make me feel loved. I appreciate our friendship and look forward to meeting you for another lunch date somewhere in the world. It should go without saying that you, like Georg, have become my family.

Janet Flores.
I must credit my knowledge of zebrafish husbandry to you. You have gone above and beyond to teach me about caring for the fish, identifying behavioral patterns and techniques necessary for my dissertation to come together. I could not have achieved this without you. I also want to thank you for your friendship and fellowship; for being my sister in Christ. With the adversity we shared, it was such an encouragement to have your ongoing prayers and continuous support. You are family now, and I look forward to seeing you again.

Club Zoidl.
Paige, Ryan, Nickie, Anna, Ksenia, Daria, Baby Georg and past members. You all have forever impacted my life through our conversations and friendships both inside and outside of the lab. I wish you all the greatest success and look forward to seeing you thrive in life, past your degrees. A special thank you to Paige Whyte-Fagundes for being more than a lab mate to me. Our friendship is one of the best things I can take away from my experience. You are an inspiration and the best Irish dancer I will ever know. We started together and are now stuck forever.

LSB & Research Colleagues.
Never did I imagine that I would have such supportive professors during my journey at York University. I want to thank my research colleagues and collaborators for working with me, teaching me, and serving as members of my committee (both past and present). All your input has been instrumental in my development as an academic, and I often admire your knowledge base. Thank you for challenging me because, without this, I would not have been able to develop my critical thinking skills. I hope to be just as brilliant as I believe you all to be one day. I would also like to thank Roger Thompson for welcoming me into his lab as a post-doctoral fellow. You have already been a great support for me and I look forward to accomplishing great work under your guidance.

Friends & Family.
A special thank you to my friends and family who have really been my tribe. When they say it takes a village to raise a child, you are the village they speak of. To my aunt Carlene, I am so grateful to have you in my life. Thank you for your endless support, prayers, advice, and encouragement. I know you will always have my back, and I appreciate you so much. To my brothers Chris and Michael, whom I've always looked up to. Thank you for being such supportive brothers and for being my protectors. I know you both have never doubted my abilities, and I hope this achievement has made you proud. To my cousins and close friends, thank you for always pouring so much love into me; your big hearts never cease to amaze me.

Tremayne & Children.
When I think of my reasons, I think of you, my family. Not only are you a source of motivation for me, but you are the ones that lift me up.
Tremayne, you have seen me when I am standing and when I have fallen; I thank you for always choosing to see the best in me regardless. I also thank you for allowing me to pursue my dreams wherever they may take me; I recognize not everybody is fortunate in this manner. I also want to thank you for being such a great provider for the family, and I look forward to smashing more goals and attaining the life we are working towards.
My children, you have been, and will always be, my greatest achievement in life. God has blessed me with your lives, and I am thankful to be your mother. I pray for you daily and know you are blessed and highly favored. I will always be your mommy first and scientist second. I hope mommy has, and will continue to, make you proud.

Mom.
I must thank you for reinforcing my faith by leading such a great example. You have always encouraged me to continue pressing forward, especially in my academic career. Thank you for your love and support, for your cheers, and for your prayers. I am eternally grateful to have you here with me to witness my dreams come to fruition. I know how proud of me you already are, and I hope that continues as I advance further in my career. Just like dad, know that I will always be there for you in whatever capacity I can and for whatever you may need.

Dad.
You first said it, I am going to be a doctor. What prophetic words these were. Dad, I miss you so much, and I wish you could've been here with me for this day. I know how excited you were to see me continue my education and excel at it. While I hope I've made you proud, I already know you were proud of me long before this. I consider it an honor to have been by your side through your trials. I know God works everything out for the good of those who love him, so I am confident your life will be a testament. Thank you for providing me with all the tools, resources, love, and support necessary for this pursuit. Until we meet again, xoxo from your baby girl.

I am fortunate to have such a loving system supporting me. It has been nothing short of a blessing to have you all in my life and I am continually reminded everyday of this. I consider this to be nothing less but the grace and favor of God over my life. To everyone I mentioned, or anyone I missed, I love you, I'm praying for you, and I thank you.

Isaiah 61

TABLE OF CONTENTS

LIST OF TABLES

LIST OF FIGURES

Supplementary Figures

LIST OF ABBREVIATIONS

Symbol	Definition
(RTq)PCR	(Real-Time Quantitative) Polymerase Chain Reaction
[X]i	intracellular concentration
µL	microliter
µM	micromolar
µm	micrometer
A	Angstrom
A.U.	Airy Units
AC	Adenylyl Cyclase
AMPA(R)	α-amino-3-hydroxy-5-methyl-4-isoxazolepropionic acid (receptor)
ATP	adenosine triphosphate
BAPTA-AM	1,2-Bis(2-aminophenoxy)ethane-N,N,N′,N′-tetraacetic acid tetrakis(acetoxymethyl ester)
BioID	Biotin Identification
BLITZ	Biotin Labelling In Tagged Zebrafish
bp	base pair
Ca2+	Calcium ion
CaM	Calmodulin
CaMK	Calmodulin Kinase
cAMP	3',5'-cyclic adenosine monophosphate
CL	Cytoplasmic loop
CNS	Central Nervous System
cpd	cycles per degree
CPG	Central Pattern Generators
CREB	cAMP response element-binding protein
CRISPR	clustered regularly interspaced short palindromic repeats
C-terminal	Carboxyl terminal
Cx	Connexin
DIC	Differential interference contrast microscopy
DMEM	Dulbecco's Modified Eagle Medium
DMSO	Dimethyl sulfoxide
dpf	days post fertilization
dr	*Danio Rerio*
DsRed	Discosoma Red
EGFP	Enhanced green fluorescent protein
EPSP	Excitatory postsynaptic potential
ER	Endoplasmic Reticulum
EtBr	Ethidium Bromide
FRAP	Fluorescence recovery after photobleaching
FSTR	Flash Stimuli Threshold Response

fwd	Forward
GABA	Gamma aminobutyric acid
GC	Ganglion cell
GJP	gap junction plaque
hr	Hour
IEG	Immediate Early Genes
i-IN	inhibitory interneuron
IM	ionomycin
Inx	Innexin
IPL	inner plexiform layer
IPSP	Inhibitory postsynaptic potential
K^+	postassium ion
kDa	kilodalton
KDEL	Lysine-Aspartic acid-Glutamic acid-Leucine.
KN93	N-[2-[N-(4-Chlorocinnamyl)-N-methylaminomethyl]phenyl]-N-(2-hydroxyethyl)-4-methoxybenzenesulfonamide
KO	Knock-out
LTD	long-term depression
LTP	long-term potentiation
M	Molar
MAP	microtubule associating protein
M-cell	mauthner neuron
MD	midbrain diameter
Mg^{2+}	magnesium ion
mi	missense
min	Minute
mL	Milliliter
mM	Millimolar
MN	motor neuron
MT	microtubule
N2a	Neuro-2a
NGS	Normal Goat Serum
nl	Nanolitre
nm	nanometre
NMDA(R)	N-methyl-D-aspartate (receptor)
nMLF	Nucleus of the Medial Longitudinal Fasciculus
NMR	Nuclear Magnetic Resonance
BLITZ	Biotin Labelling In Tagged Zebrafish
BioID	Biotin Identification
N-terminal	amino-terminal
OKR	optokinetic response
Panx	pannexin
PBS	Phosphate Buffered Saline
pg	picogram
PKA	protein kinase A

PRC	photoreceptor cell
PSD	postsynaptic density
px	Pixel
ROI	region of interest
rv	Reverse
s/sec	Second
SCN	suprachiasmatic nucleus
SD	standard deviation
SEM	standard error of the mean
Ser	serine
TALEN	Transcription activator-like effector nucleases
TH	Tyrosine Hydroxylase
Thr	threonine
TIRF	Total internal reflection fluorescence
TL	Tupfel long-fin
VMR	visual-motor response
WT	wild-type

1

INTRODUCTION

Connexin 36 (Cx36) is a major constituent of neural gap junctions in the mammalian retina and the brain, most notably in the cerebral cortex and hippocampal regions (Güldenagel *et al.*, 2001; Deans *et al.*, 2002; Feigenspan *et al.*, 2004). In Cx36-deficient ($Cx36^{-/-}$) mice, dendro-dendritic coupling in the hippocampus was nearly abolished. Moreover, the synchronization of interneurons in the cortex and hippocampus was significantly disrupted without any indication of a compensatory mechanism. At the behavioral level, this translates to learning and memory deficits, particularly with long-term memory and short-term spatial memory (Deans *et al.*, 2001; Hormuzdi *et al.*, 2001, 2004; Frisch *et al.*, 2005; Allen *et al.*, 2011), indicating the significant, yet relatively unexplored, contributions of Cx36 to plasticity-dependent cognition. In this dissertation, I explore how the plasticity of Cx36 electrical synapses is modulated, drawing inspiration from the chemical synapse model of transmission. The overarching goal is to provide a greater understanding of the interplay between chemical and electrical synapses, starting at the cellular and molecular level. To further this, I then applied a 'bird's eye view' approach and investigated how gap junctional (a)symmetry may affect the functionality of the retina and brain by analyzing outcomes in vision and cognition in Cx35b knock-out zebrafish (*Danio rerio*). The zebrafish animal model was chosen over the favorable murine animal model for its similarity in color vision to humans. Investigations carried out in this dissertation provide insight into the functions of Cx36, from cells to systems to behavior.

1.1 Neuronal Communication in the Vertebrate Central Nervous System

1.1.1 Modalities of Neuronal Communication

Communication between neurons and glia is vital for the optimization and regulation of brain function in higher organisms. Synapses, the dynamic regions that allow for this cross-talk between neurons, are recognized as protein-dense areas that operate under two primary modalities of synaptic transmission referred to as chemical and electrical synapses. At the chemical synapse, the release of neurotransmitters from the presynaptic neuron is detected by receptors of the postsynaptic membrane, allowing for the unidirectional transfer of information and appropriate cellular response. Alternatively, under the electrical transmission model, signaling molecules may be transmitted bi-directionally between adjacent neurons through channels known as gap junctions. Although both models of synaptic transmission are often studied individually, chemical and electrical synapses are now known to co-exist (Pereda, 2014). Evidence to

support the properties and distribution of these two modalities at mixed synapses is still emerging yet allows for the opportunity to identify commonalities in machinery and operation between the two.

1.1.1.1 Chemical Transmission

The discovery of chemical transmission is jointly awarded to Otto Loewi and Henry Dale following the infamous 1921 Loewi experiment. After a series of dreams, Loewi stimulated the vagus nerve from a beating frog heart submerged in a saline bath, causing the heart to slow. The saline bath also flowed into a second chamber housing a frog heart with the vagus nerve removed. Here, he found that stimulation of the vagus nerve was sufficient to impact the second heart; this result was attributed to chemical neurotransmission. Follow-up studies by Henry Dale revealed that this chemical neurotransmission was due to the actions of acetylcholine (Loewi, 1924; Todman, 2008). To date, chemical transmission is the most studied modality of neuronal communication, involving an intricate and well-defined network of neurotransmitters and receptors. Morphologically, chemical synapses are asymmetric with a distinct pre- and postsynapse, creating uni-directionality between cells. Due to the enlarged extracellular space (200-300A/ 20-5nm) between the pre- and postsynapse, known as the synaptic cleft, chemical neurotransmission is slower than the electrical counterpart by an approximate delay of 0.4-5 milliseconds (Kats and Miledi, 1965).

In the chemical synapse model, the release of neurotransmitters from the presynaptic terminal into the synaptic cleft occurs upon neuronal depolarization. A combination of metabotropic and ionotropic receptors embedded in the postsynaptic membrane subsequently bind to their respective neurotransmitter, thus evoking a response intracellularly through a defined series of signaling cascades (Sheng, Sabatini and Sudhof, 2012). Two ionotropic receptors of importance in long-term potentiation (LTP), the underlying basis of the learning, memory, and behavioral cascades, are the N-methyl-D-aspartate receptor (NMDAR) and α-Amino-3-hydroxy-5-methyl-4-isoxazolepropionic acid receptor (AMPAR). Previous studies have shown that upon the release of glutamate presynaptically, the postsynaptic membrane responds by depolarizing. The combination of glutamate binding to NMDAR and neuronal depolarization, in turn, activates NMDARs, relieving the Mg^{2+} blockade. Active NMDARs allow for the influx of calcium (Ca^{2+}), triggering several signaling cascades critical for LTP (Collingridge, Isaac and Wang, 2004; Traynelis *et al.*, 2010). Most notably, the rapid rise in intracellular calcium levels activates Ca^{2+}/calmodulin-dependent kinase II (CaMKII), a protein kinase responsible for phosphorylating numerous targets, upon the initial binding of calmodulin (Ca^{2+}-CaM) (Fukunaga *et al.*, 1993). AMPA receptors, a target of CaMKII, increase in activity levels, trafficking, and insertion into the postsynaptic membrane in response to phosphorylation. This is of significance since an abundance of receptors is a crucial regulator in synaptic strength (Sheng and Hoogenraad, 2007). Phosphorylation of NMDAR by CaMKII increases calcium conductance, thus

providing an additional means for controlling synaptic strength (Derkach *et al.*, 2007; Zhou *et al.*, 2007; Sanhueza *et al.*, 2011). These two events are critical for the LTP of chemical synapses and have been widely accepted as a cellular mechanism contributing to learning and memory formation (**Figure 1.1**).

1.1.1.2 Electrical Transmission

Neuronal gap junctions, the electrical synapses of the central nervous system (CNS), are specialized channels that mediate bi-directional communication between adjacent neurons. Permeability of gap junctions has been attributed to the channel size, as the large hydrophobic pore has an estimated diameter of 1.2 nm (Bennett and Zukin, 2004). As such, these structures provide an efficient means for the exchange of small molecules and metabolites (up to 1 kDa), including but not limited to second messengers, glucose, ATP, cations, and anions (Söhl, Maxeiner and Willecke, 2005; Jabeen and Thirumalai, 2013) (**Figure 1.1**). Functionally, gap junctions have demonstrated involvement in signal transduction pathways, maintenance of cellular homeostasis, and the regulation of synchronous activity of electrically excitable neuronal networks; consequently, the term "electrical synapse" was derived accordingly (Weidmann, 1952; Revel and Karnovsky, 1967; Paul, 1995; Bennett and Zukin, 2004). Gap junctions differ from most membrane channels in that they exist between two opposing cells rather than function as single membrane units. Evaluation under electron microscopy determined that a narrow gap (2-4nm) exists between the adjoining cells, which in turn led to its designated title as a "gap junction" (Revel and Karnovsky, 1967). Typically, gap junctions are localized to the plasma membrane at confined aggregates, referred to as gap junction plaques (GJPs), consisting of up to thousands of intercellular channels (Simon and Goodenough, 1998). Although the opening of gap junction channels typically requires a sizeable amount of aggregates (in the order of hundreds) as a prerequisite, in established gap junction plaques meeting this requirement, approximately 1 in 10 remain open at a time (Bukauskas *et al.*, 2000).

From their initial discovery in the crayfish giant motor synapse, gap junctions were later demonstrated to exist in most vertebrate and invertebrate tissues except spermatozoa, erythrocytes, thrombocytes, and adult skeletal muscle cells (Dermietzel and Spray, 1993; Söhl *et al.*, 2004). However, the evolutionary divergence of gap junctions led to the identification of protein families with similar morphological and physiological properties; in chordates, gap junctions are formed by the family of proteins termed connexins (Cx), whereas the innexin (Inx) protein family is found exclusively in invertebrates. A third family of proteins termed pannexins (Panx), are found in both invertebrates and chordates; however classification of pannexins as belonging to the gap junction family of proteins is currently debated since their glycosylation state does not allow for adjacent channels to dock together (Bruzzone, White and Paul, 1996; Kumar and Gilula, 1996; Phelan *et al.*, 1998; Baranova *et al.*, 2004). Although innexins and

pannexins will not be described here, it is important to acknowledge that all serve to allow for membrane permeability through their oligomerization into channels (Scemes, Spray and Meda, 2009).

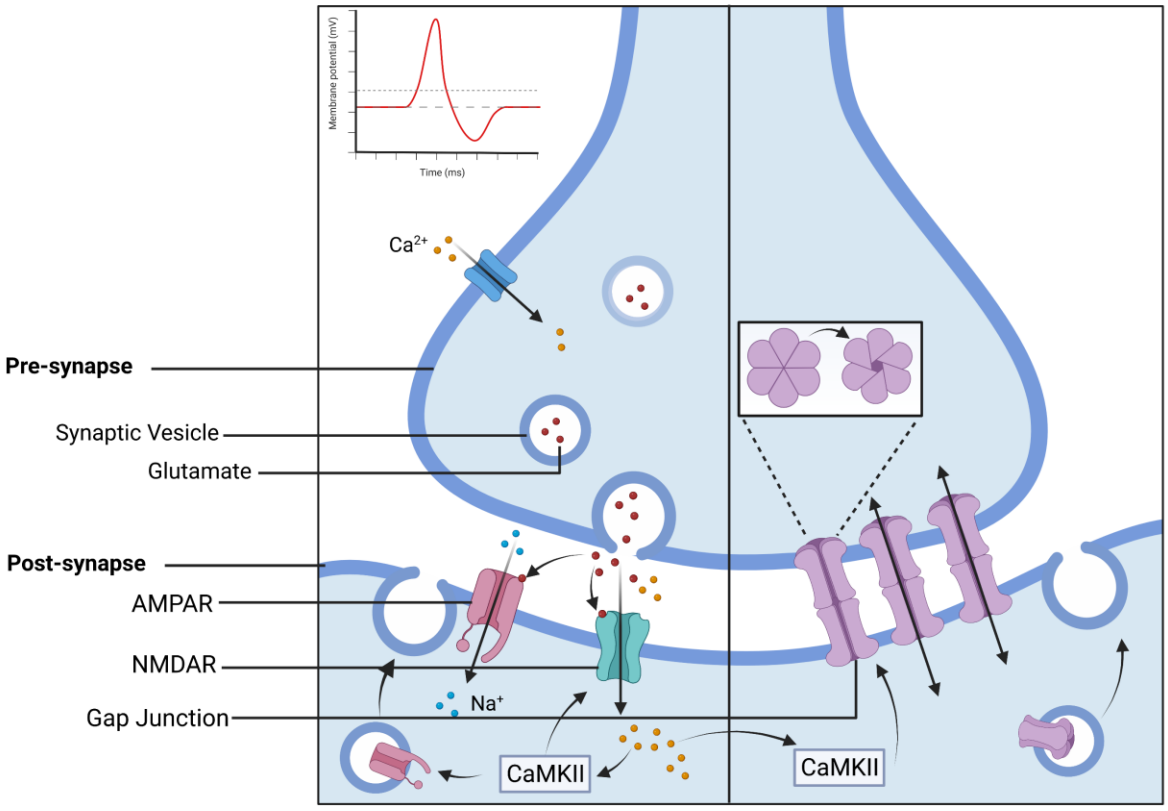

Figure 1.1. Overview of the Mixed Chemical and Electrical Synapses.

Chemical synapses (left panel) are asymmetric and drive neuronal communication from the presynapse to the postsynapse. During LTP, chemical synapses respond to depolarization by releasing presynaptic vesicles containing glutamate into the synaptic cleft. NMDARs dislodge the Mg^{2+} blockage upon the binding glutamate and allow for an influx of Ca^{2+}. Elevating intracellular calcium concentrations subsequently activates CaMKII activity which targets AMPARs, increasing receptor abundance through trafficking mechanisms. In contrast, electrical synapses (right panel) are formed by two docking connexons from adjacent cells and allow for the bi-directional communication of ions and metabolites. Current literature has identified that both modalities use CaMKII to modulate plasticity. Figure was created with BioRender.com by Brown (2022).

1.1.1.3 The Electro-Chemical Relationship and Mixed Synapses

While studies focusing on the interplay between chemical and electrical synapses during synaptogenesis are still emerging, it is well established that an increase in gap junctional coupling precedes chemical synaptogenesis (Fischbach, 1972; Lopresti, Macagno and Levinthal, 1974; Connors, Benardo and Prince, 1983; Jabeen and Thirumalai, 2013). Belluardo et al. (2000) determined that the expression and

coupling of Cx36 gap junctions increase from postnatal days 0-14 (P0-P14) in the developing neocortex of rats; this increase is transient as expression levels decrease during the late stages of postnatal development (Söhl *et al.*, 1998; Belluardo *et al.*, 2000). Moreover, excitatory synapses in the olfactory bulb failed to form in a Cx36 knock-out mice model, providing further evidence of the involvement of gap junction activity in chemical synaptogenesis (Maher, McGinley and Westbrook, 2009). In the same regard, chemical neurotransmission is also capable of regulating gap junctional communication. Park et al. (2011) demonstrated that upregulation in Cx36 gap junctions was mediated by the binding of glutamate to group II metabotropic receptors during the early development (P0-P15) of the rodent hippocampus and cortex. In contrast, the actions of gamma-aminobutyric acid (GABA) on the $GABA_A$ receptor inhibited the upregulation of Cx36 expression (Park *et al.*, 2011). These studies have established an interrelationship between electrical and chemical transmission, suggesting that these two modalities do not act in isolation but rather in unison throughout the nervous system. This provides a greater basis for investigating the commonalities in molecular machinery and signaling pathways, particularly at mixed (chemical and electrical) synapses.

Mixed synapses were initially discovered throughout neurons of the mammalian spinal cord when it was previously accepted that synaptic activity here was exclusively due to chemical neurotransmission (Rash *et al.*, 1996). Since then, the presence and functionality of mixed synapses have been well documented at the giant club-endings of teleost Mauthner neurons (Pereda *et al.*, 2003, 2004). Here, it was found that electrical synapses were intermixed with NMDA glutamate receptors and possessed a distinct electrophysiological signature whereby a large electrical pre-potential is followed by an excitatory postsynaptic potential (Pereda *et al.*, 2003, 2004). To date, mixed synapses have also been described in the adult rat hippocampus. For example, Hamzei-Sichani et al. (2012) determined that mixed synapses on both principal cells and interneurons were primarily composed of glutamatergic chemical synapses and Cx36 electrical synapses (Hamzei-Sichani *et al.*, 2012). Considering the vast amount of evidence supporting the reciprocal modulation between Cx36 gap junctions and chemical synapses, in conjunction with its confirmed precedence at mixed synapses, Cx36 serves as an ideal candidate to study the interrelationship between electrical and chemical synapses.

1.1.2 Connexins and the Connexin-36 Electrical Synapse

The first gap junction proteins were discovered in mouse hepatocytes in 1974 and were classified into the connexin family of proteins. Initially, the names connexin A and B were proposed to coincide with the two identified components of differing molecular weight; protein isolates were generated by bulk preparation (Goodenough, 1974). Since then, numerous connexin isoforms have been identified. To date, there are 20 known connexin genes in murines, 21 in the human genome, and 37 genes in zebrafish. Of the

37 genes expressed in zebrafish, 23 are related to 16 mammalian connexins, and 14 connexins are unique (Eastman, Chen, Falk, Mendelson, & Iovine, 2006; Cruciani and Mikalsen, 2007). Likewise, between the mouse and human genome, 19 genes are orthologs (Söhl and Willecke, 2003). The connexin family of proteins is further classified into the alpha (α-), beta (β-), gamma (γ-), delta (δ), or epsilon (ε-) subclasses depending on gene sequence similarity (Söhl and Willecke, 2003). It is now understood that connexins form gap junctions exclusively in chordates, a phylum consisting of organisms characterized by the presence of a notochord, dorsal neural tube, pharyngeal slits, post-anal tail and an endostyle at some stage throughout development (Holland, 2005).

Among the connexin genes identified in mammalian cells, more than half are expressed in the nervous system. As such, several connexins have been identified as significant contributors to neuronal activity; among these are Cx29 (*GJE1*), Cx30 (*GJB6*), Cx30.2 (*GJC3*), Cx31.1 (*GJB5*), Cx32 (*GJB1*), Cx36 (*GJD2*), Cx43 (*GJA1*), Cx45 (*GJC1*), Cx47 (*GJC2*), and Cx50 (*GJA8*) (Söhl, Maxeiner and Willecke, 2005; Pereda *et al.*, 2013; Shimizu and Stopfer, 2013). Of the known neuronal gap junction proteins, Cx36 was the first isoform to be described in mammalian neurons (Condorelli *et al.*, 1998).

1.1.2.1 Connexin Topology and Formation into Gap Junction Channels

In vertebrates, each gap junction channel is composed of two docking connexons (i.e., hemichannels), each formed by the oligomerization of six connexin proteins (Bennett, 1977; Kumar and Gilula, 1996). Topologically, connexins are recognized as tetraspan membrane proteins with two extracellular loops that possess three conserved cysteine residues crucial for docking; both the N-terminal and C-terminal domains are located intracellularly. As connexins are named according to their molecular weight (in kDa), variation between connexin isoforms is mainly due to residual differences in the cytoplasmic loop and carboxyl-terminal (Söhl, Maxeiner and Willecke, 2005). Once oligomerization is complete, connexons can arrange either homomerically, where each connexin subunit is identical, or heteromerically. Similarly, connexons localized in the plasma membrane may dock to form gap junction channels in a homotypic (i.e., same composition) or heterotypic manner. The composition of the gap junction channel affects both its localization and conductance properties (voltage dependence, open probability, permeability, and gating kinetics), allowing for greater regulatory variety (Cao *et al.*, 1998; Bennett and Zukin, 2004; Weber *et al.*, 2004). Although less studied, functional hemichannels have also been described both *in vivo* and *in vitro*, allowing for the passage of molecules between the intracellular and extracellular space (Paul *et al.*, 1991; Kamermans *et al.*, 2001).

Properly folded connexin proteins are transferred from the endoplasmic reticulum to the Golgi apparatus before transport to the plasma membrane; in the case of Cx26, trafficking to the plasma membrane occurs in a Golgi-independent manner. Connexon assembly may occur in an isoform-specific manner

(Sarma, Wang and Koval, 2002) with evidence supporting assembly at the ER (Falk *et al.*, 1997; Ahmad *et al.*, 1999), *trans*-Golgi network (Musil and Goodenough, 1993) or ER-Golgi intermediate (Diez, Ahmad and Evans, 1999). Upon exiting the *trans*-Golgi network, connexons are packaged into vesicles for delivery to the cell surface. Once transport vesicles fuse with the phospholipid bilayer, connexons diffuse laterally and dock with the connexons of the adjacent cell with the aid of N- and E-cadherins, thus forming gap junctions (Jongen *et al.*, 1991; Meyer *et al.*, 1992; Lauf *et al.*, 2002; Thomas *et al.*, 2005; Wei *et al.*, 2005). Although functional activity is typically delayed until the coalescence into gap junction plaques, recent studies have confirmed that gap junction channels could acquire an active state in the absence of microscopically identifiable plaques (Essenfelder *et al.*, 2004). Clustering of gap junctions is a continual dynamic event as the turnover rate of connexin-forming gap junctions is typically 1-5 hours, although longer turnover rates have been recorded (J. C. Hervé *et al.*, 2007) (**Figure 1.2**).

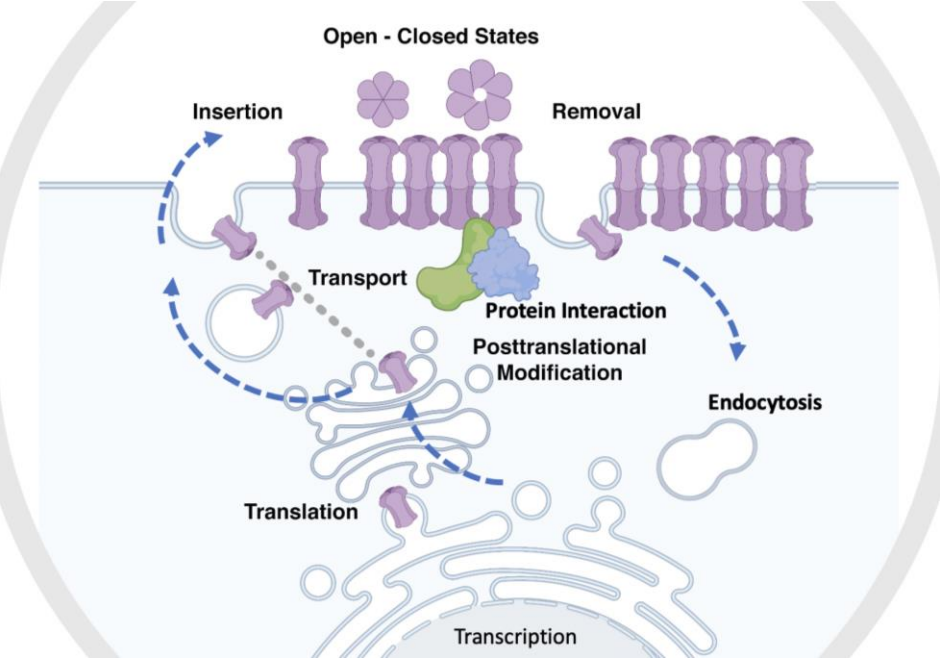

Figure 1.2. Trafficking and Turnover of Electrical Synapses.

Following translation, properly folded connexin proteins oligomerize into connexons at the ER-Golgi complex and are transported to the plasma membrane via vesicles. Connexons shuffle laterally and incorporate into the gap junction plaque by docking with adjacent connexons. Here, connexons interact with various proteins to modulate their stability and open/close probabilities. Removal of connexons takes place centrally via endocytosis. Figure was created with BioRender.com by Zoidl (2022).

1.1.2.2 Connexin 36 Gene and Protein

Connexin 36 (Cx36), encoded by the *GJD2* gene, is a 321 amino acid protein identified as a major component of neural gap junctions in the CNS. The connexin gene is highly conserved, displaying 98%

sequence identity between the rat, mouse, and human genomes and 80% identity to its fish ortholog connexin-35b (Cx35b) (Belousov and Fontes, 2013). Based on the gene structure, Cx36 is classified as belonging to the gamma (γ) sub-family, determined by the presence of an intron located within its coding region (O'Brien, Al-Ubaidi and Ripps, 1996; Condorelli *et al.*, 1998; Söhl *et al.*, 1998; Abascal and Zardoya, 2012). Typically, Cx36 proteins are found between dendro-dendritic and dendro-somatic contacts but have also been described at axon terminals (Hamzei-sichani *et al.*, 2007). Interestingly, experimental evidence to date has suggested that Cx36 primarily forms homomeric/homotypic intercellular channels (Teubner *et al.*, 2000; Li *et al.*, 2008); this is in contrast to the configurations observed with other connexins (Orthmann-Murphy *et al.*, 2007; Yum *et al.*, 2007).

1.1.2.3 Channel properties of Cx36

Relative to other connexin isoforms, Cx36 is described as having one of the lowest voltage sensitivities (half-inactivation voltage ±75 mV) and single-channel conductance (10-15 pS). With a low unitary conductance, it is inferred that Cx36 allows for in-depth precision of electrical coupling through the regulation of the number of channels present in the gap junction plaque. Further, during neuronal activity and development, low voltage sensitivity prevents uncoupling in cells that have acquired a high resting potential (Srinivas *et al.*, 1999). Regulation of Cx36 channel gating open probability has been attributed to intracellular [Mg^{2+}] in an ATP-dependent manner (Palacios-Prado *et al.*, 2012) and pH (González-Nieto *et al.*, 2008). Experimental efforts aimed at defining the molecular mechanism of connexin gating have proposed a dual mechanism of "slow V_j-gating," inferring the involvement of the N-terminal domain and "fast V_j-gating" involving the cytoplasmic domain in a connexin-specific manner (Verselis, Ginter and Bargiello, 1994; Anumonwo *et al.*, 2001; Moreno *et al.*, 2002; González, Gómez-Hernández and Barrio, 2007; Beyer *et al.*, 2012). Studies on Cx36 channel gating properties have supported this two-tier mechanism for opening and closing probabilities in a pH-dependent manner (González-Nieto *et al.*, 2008). Additionally, coupling of Cx36 gap junction channels has been shown to be mediated by calcium, where high intracellular [Ca^{2+}] results in the uncoupling of junctions (Baux *et al.*, 1978; Rao, Barnes and McNaughton, 1987).

1.1.2.4 Cx36 Expression in the Central Nervous System

In the mammalian brain, Cx36 is expressed in a variety of regions, including the cerebral cortex and hippocampus (Condorelli *et al.*, 1998). Both the hippocampus and neocortical regions are dictated by the highly regulated synchronous oscillations of neuronal networks and, in turn, correlate to cognitive and sensory function, attention, and memory formation (Buzsaki *et al.*, 1992; Csicsvari *et al.*, 1999; Cape *et al.*, 2000). The hippocampus, a member of the limbic system, is most notably known for its role in the integration of short-term and long-term memory in addition to spatial navigation. In Cx36 deficient ($Cx36^{-}$

$^{/-}$) mice, dendro-dendritic coupling in the hippocampus was nearly abolished. At the behavioral level, Cx36$^{-/-}$ mice showed impairments in object recognition, displaying an inability to distinguish between new and old objects after short delays of 15 and 45 minutes. Additionally, the lack of Cx36 expression in mice also resulted in an impairment in short-term spatial memory as determined by their poor performance on a rewarded alternation T-maze task in comparison to wild-type mice (Frisch *et al.*, 2005; Allen *et al.*, 2011). Again, the significance of Cx36 in the hippocampus must be elaborated since this demonstrates that Cx36$^{-/-}$ mice display impairments in learning and memory formation. Furthermore, the knock-out of Cx36 significantly disrupted the synchrony of interneurons in both the cortex and hippocampus without any signs of a compensatory mechanism (Deans *et al.*, 2001; Hormuzdi *et al.*, 2001, 2004).

The retina, a light-sensitive tissue, is organized into distinct layers of neuronal cells interconnected by synapses. Functionally, the retina is responsible for receiving and transmitting visual input through the optic nerve to the brain for visual processing. In the mouse retina, Cx36 is expressed between AII amacrine cells, OFF cone bipolar cells, as well as the light-sensitive photoreceptors located at the base of the retina. Photoreceptors are divided into two classes known as cones and rods and mediate photopic and scotopic vision, respectively. Although Cx36$^{-/-}$ mice show the normal cellular organization of the retina, coupling between AII amacrine cells and bipolar cells was disrupted. Furthermore, rod-mediated transmission to ganglion cells was impaired in Cx36 knock-out mice, indicating that Cx36 is critical for rod signal propagation and essential for night vision (Güldenagel *et al.*, 2001; Deans *et al.*, 2002; Feigenspan *et al.*, 2004).

Knock-out of Cx36 typically displays a broad range of consequences, including deficits in circadian activity, regulated by the suprachiasmatic nucleus (SCN). Moreover, behavioral phenotypes are also impacted as Cx36$^{-/-}$ mice showed an increase in locomotion and running speed, a reduction in object exploration, and displayed more anxiety-like behavior (Long *et al.*, 2005; Zlomuzica *et al.*, 2012). It is also interesting to acknowledge that in the rat hippocampus and cortex, Cx36 knock-out resulted in the impairment of long-term potentiation of chemical synapses reiterating a synonymous relationship between electrical and chemical synapses (Postma *et al.*, 2011; Wang and Belousov, 2011).

1.1.2.5 The Run-Up Model of Cx36 Electrical Plasticity

Synaptic plasticity, the ability of neuronal synapses to strengthen or weaken over time, serves as the fundamental basis underlying learning, memory, and behavior. As such, delineating the mechanism(s) governing synaptic plasticity will drive our fundamental understanding of the regulatory means by which these processes operate. Although research aimed at defining the cellular signaling cascade(s) involved in learning, memory, and behavior has largely focused on chemical synapses, emerging evidence supports a significant role of electrical synapses in the contribution of neuronal plasticity.

The dynamic trafficking and turnover of ion channels and membrane proteins is a highly regulated process, constitutive of cellular homeostasis and particularly synaptic plasticity. The flexibility of chemical and mixed neuronal synapses, achieved through long-term potentiation or depression (LTP/LTD), is well-described in various regions of the brain and serves as the hallmark of the CNS. During LTP or LTD, presynaptic axon terminals and postsynaptic dendrites are regulated in tandem, demonstrating unique cellular and molecular responses which in turn correlate to higher brain functions (Hughes, 1958). As previously outlined, the molecular machinery involved in LTP and the respective signaling network has been extensively described at chemical synapses, and its influence on learning and memory has been well established. However, less is known about the electrical modality.

In a recent study, the LTP-like phenomenon, coined the "run-up," demonstrated a 10-fold increase in gap junctional conductance exclusively at Cx36 GJPs; an observation later shown to occur in a Ca^{2+}/calmodulin-dependent kinase II (CaMKII)-dependent manner (Zoidl *et al.*, 2002; Alev *et al.*, 2008; Del Corsso *et al.*, 2012). The run-up phenomenon closely resembles CaMKII-mediated phosphorylation of NMDA receptors, promoting the transient influx of Ca^{2+}, a critical mediating step in LTP-based plasticity. At the chemical synapse, the increase in calcium conductance via NMDA receptors potentiates the increase in activity, trafficking, and insertion of AMPA receptors, thus regulating synaptic strength through receptor abundance (Fukunaga *et al.*, 1993; Collingridge, Isaac and Wang, 2004; Derkach *et al.*, 2007; Sheng and Hoogenraad, 2007; Zhou *et al.*, 2007; Traynelis *et al.*, 2010; Sanhueza *et al.*, 2011). Likewise, the run-up phenomenon would be indicative of an increase in channel opening probability, elevated channel recruitment, or a combination of these two events (**Figure 1.1**). However, the mechanism and molecular machinery involved in the run-up currently remain elusive.

1.1.3 The Dynamic Cytoskeleton

In eukaryotes, the neuronal cytoskeleton is a dynamic network comprised of microtubules, actin microfilaments, and neurofilaments/intermediate filaments. Collectively, the cytoskeleton is responsible for nerve signal propagation, cell structure, axonal growth, and intracellular trafficking of organelles or cargo-carrying vesicles in eukaryotes (Gendron and Petrucelli, 2009; LaPointe *et al.*, 2009). All three filaments of the cytoskeleton differ in a variety of ways, including assembly dynamics, polarity, and associating motor proteins (Fletcher and Mullins, 2010). However, most notably is the organization within neuronal cells. Actin, for example, can be found within the dendritic and axon terminal ends, highly concentrated at protein-rich areas known as postsynaptic densities (PSD) beneath the synapse (Sheng and Hoogenraad, 2007; Hotulainen and Hoogenraad, 2010). In contrast, microtubules are excluded from end terminals and are restricted to the dendritic spine (Gu, Firestein and Zheng, 2008). As such, the transport of proteins destined for the synapse often requires a combination of tubulin- and actin-dependent transport. In more

recent years, the microtubule network has been of particular interest due to its ability to achieve fast transport of cargo to the dendritic spines, a key component in modulating synaptic events. (Gu, Firestein and Zheng, 2008; Hu *et al.*, 2008; Jaworski *et al.*, 2009; Kapitein *et al.*, 2011; Merriam *et al.*, 2011, 2013). As such, we hypothesized that in parallel to LTP, the run-up phenomenon of electrical plasticity would be mediated by the microtubule-dependent transport of Cx36, allowing for greater channel recruitment to the GJP. Although trafficking mechanisms were previously described for several connexin isoforms, and most notably for Cx43 (Giepmans *et al.*, 2001; Giepmans, Verlaan and Moolenaar, 2001; Lauf *et al.*, 2002), no such characterization with the cytoskeleton currently exists for Cx36 or its respective orthologs. Since the investigations pertaining to this dissertation primarily describe the interaction between Cx36 and tubulin with a lesser focus on actin, neurofilaments will not be described.

1.1.3.1 Actin

Actin in its free monomeric form is a 42 kDa globular protein (G-actin) that polymerizes to form microfilaments (F-actin), a major contributor to the cytoskeleton, particularly at synapses. Of the three classes of actin that have been described: α, β and γ, the latter two are involved in F-actin polymerization. Both G-actin and F-actin are essential for maintaining cell morphology, motility, and cell signaling, as well as the trafficking of organelles and vesicles in a highly dynamic manner. Typically, actin localizes beneath the plasma membrane where, in addition to structural support, it interacts with membrane proteins to facilitate receptor mobility and anchoring with the aid of scaffolding proteins (Dillon and Goda, 2005). Interestingly, it was recently determined that the actin cytoskeleton and associating proteins, being functionally linked to synaptic receptors, are also necessary entities in memory formation (Fischer *et al.*, 2004; Hou *et al.*, 2009; Bi *et al.*, 2010; Nelson *et al.*, 2012; Young *et al.*, 2014).

Interactions between gap junctions and actin have only recently been described in the past few years. Although Cx30 has been shown to interact directly with actin, more often, gap junctions require adaptor proteins to facilitate indirect contact, such in the case of Cx43 (Butkevich *et al.*, 2004; Qu, Gardner and Schrijver, 2009; Bhalla-Gehi *et al.*, 2010). Early reports have indicated that actin is involved in turnover and endocytosis of gap junctions. This typically occurs in cells expressing connexins known to interact indirectly with actin through an invagination event into the cytoplasm prior to degradation (Watanabe, Washioka and Tonosaki, 1988). However, a more recent study on connexin 30 (Cx30) proposed that actin is likely involved in the anchoring of connexons and short-distance transport rather than in the facilitation of internalization (Qu, Gardner and Schrijver, 2009).

1.1.3.2 Tubulin

Microtubules (MTs) are hollow tubes approximately 25 nm in diameter formed by protofilaments of α-, β-tubulin heterodimers running lengthwise. The α- and β-tubulin monomers responsible for the

configuration of microtubules are approximately 55kDa in size with 450 amino acid residues. Throughout evolution, the tubulin monomers have remained highly conserved, showing approximately 60% sequence identity across species; between the tubulin monomers themselves, there is approximately 40% conservation (Wade, 2009). Multiple copies of the tubulin gene exist in both human and murine genomes, leading to the identification of 19 isoforms in humans (10 of which belong to the alpha isotype and 9 to the beta) and 16 in murines (8 alpha and beta) (Saillour *et al.*, 2014). During assembly, tubulin heterodimers are typically added to the plus (+) end, giving MTs a characteristic structural polarity, while the minus (-) end grows at a slower rate. Microtubule assembly is a GTP-dependent process with GTP being hydrolyzed to GDP, forming a stable GDP-tubulin cap at the plus end. Several proteins have been shown to interact with MTs, including microtubule-associated proteins (MAPs), responsible for stabilizing MTs, and motor proteins dynein and kinesin, essential for microtubule-dependent trafficking (Wade, 2009).

As previously mentioned, evidence suggests that upon leaving the Golgi apparatus, connexons are assembled and transported in vesicles to the plasma membrane. In support of this, it was found that Cx43 binds to both α- and β-tubulin with equal affinity and trafficking to the membrane was indeed dependent on microtubules (Giepmans *et al.*, 2001; Giepmans, Verlaan and Moolenaar, 2001; Lauf *et al.*, 2002). Although microtubules facilitate the transport of connexons to the plasma membrane, thus improving efficiency, it is thought that under some circumstances, MTs may not be essential (Laird, 2010). Nevertheless, recent reports have indicated that upon binding of tubulin, the Cx43-tubulin binding site and surrounding region (encompassing amino acids K243-D259) adopt a helical structure to facilitate the protein-protein interaction. Mediation of interaction between tubulin and Cx43 is achieved by phosphorylation, where phosphorylation of Tyr247 by v-Src prevents association with tubulin. The microtubule-binding region, located within the C-terminal (CT) domain of Cx43, is enriched in the basic amino acids lysine (K), glycine (G), proline (P), valine (V), and arginine (R).

1.1.4 Calcium Signaling

It is important to acknowledge that the dynamic nature of the tubulin-cytoskeleton can be attributed to protein-protein interactions as well as intracellular ion concentration (Wolff *et al.*, 1996). In theory, alterations of intracellular ion concentrations would allow for intrinsic manipulation to either promote neuronal plasticity or avoid excitotoxicity. While elevated intracellular Ca^{2+} and subsequent activation of signaling partners is a critical mediating step in both LTP and the run-up, the manipulation of microtubule dynamics under calcium activation, as it pertains to synaptic plasticity, has been loosely established. Interestingly, CaMKII is known to co-localize robustly with microtubules throughout the somatodendritic regions after calcium-mediated global activation; however, the functional role remains unresolved (Mcvicker, Millette and Dent, 2015). Instead, the link between Cx36 and the various components of calcium

signaling is slowly being elucidated, providing insight into how calcium mediates the run-up model of plasticity. Calcium signaling has previously been identified as a critical component of activity-dependent plasticity of electrical synapses via the regulation of protein kinase and phosphatase activity in numerous reports (Pereda *et al.*, 2013; Haas, Greenwald and Pereda, 2016; Coulon and Landisman, 2017; Sevetson *et al.*, 2017; O'Brien, 2019). As such, this dissertation also aimed to provide additional evidence for calcium-mediated modulation of Cx36 by addressing how calcium manipulation affects the transport and incorporation of Cx36 into gap junction plaques; the role of calcium modulation and channel open probability was previously addressed (Siu *et al.*, 2016).

1.1.4.1 Calcium

The calcium ion (Ca^{2+}) serves as an essential second messenger supporting numerous signal transduction pathways influencing the maintenance, plasticity, and apoptosis of neurons. Modulation of calcium concentrations is tightly regulated; in the cytoplasm, the concentration of calcium ions is typically low (10^{-7} M) and higher extracellularly (10^{-3} M), creating an electrochemical potential gradient across the membrane. Additional Ca^{2+} is also stored intracellularly in membrane-bound organelles such as the mitochondria. Upon stimulation, neuronal cells are triggered to either (1) release calcium from internal organelle stores and/or (2) open calcium-permeable channels to allow for an influx of Ca^{2+} (Endo, 2006). Although calcium has many targets, the primary ligand it interacts with is the calcium modulated protein, otherwise known as calmodulin.

1.1.4.2 Calmodulin

The binding of calcium to calmodulin (abbreviated at Ca^{2+}-CaM) triggers critical downstream processes at both the pre- and postsynapse. The direct binding of Ca^{2+}-CaM to Cx36 was independently illustrated by Siu et al. (2016) and Burr et al. (2005) (Burr *et al.*, 2005a; Siu *et al.*, 2016). Further analysis revealed that the calmodulin-binding domain is localized to the carboxyl-terminal tail of Cx36, where it coincides with the CaMKII binding site also (Burr *et al.*, 2005b; Siu *et al.*, 2016). While Siu et al. (2016) demonstrated that Ca^{2+}-CaM interactions with Cx36 occur primarily outside of the GJP, the actions of CaM binding at the GJP remain debatable since numerous studies have reported conflicting evidence on how CaM binding influences junctional coupling (Török, Staugger and Evans, 1997; Stauch, Kieken and Sorgen, 2012; Siu *et al.*, 2016; Aseervatham *et al.*, 2020). Nevertheless, the rapid binding and dissociation kinetics suggest that the binding of CaM to Cx36 is transient and dynamically regulated depending on the levels of cellular activity.

1.1.4.3 CaMKII

Ca^{2+}/calmodulin-dependent protein kinase II, otherwise known as CaMKII, is a serine/threonine-specific protein kinase that is critical in numerous signaling cascades. The CaMKII family of proteins contains approximately 25 isoforms of the dodecameric holoenzyme and is further classified into the α-, β-, γ-, and δ- subclasses; though the α- and β-isoforms are the most prominent in the mammalian brain (Brocke *et al.*, 1999; Hudmon and Schulman, 2002). Each CaMKII protein has a distinct structural profile comprised of a catalytic domain where phosphorylation activity occurs and an autoinhibitory domain that controls that activity state of the kinase. More specifically, phosphorylation of threonine-286 within the autoinhibitory domain relieves the autoinhibition mechanism, allowing CaMKII to remain active following the dissociation of Ca^{2+}-CaM. The variable segment and self-association domains also found in each CaMKII protein contribute to the diversity and classification of CaMKII isoforms (Rosenberg *et al.*, 2005; Thaler *et al.*, 2009; Chao *et al.*, 2010).

The Ca^{2+}-CaM interaction is the prerequisite for the binding and activation of calcium/calmodulin-dependent kinase II (CaMKII). As previously mentioned, CaMKII activation is a critical mediating event in both chemical and electrical models of plasticity, and its binding site is localized to the carboxyl-terminal tail of Cx36. It is hypothesized that the binding of CaMKII to Cx36 resembles that of the NR2B subunit of NMDARs, requiring dual binding motifs that act sequentially. Nevertheless, activated CaMKII phosphorylates Cx36 at Ser110/Thr111, regulating junctional conductance.

1.1.5 Main Research Aim and Hypotheses

The research investigations outlined thus far have demonstrated that Cx36 electrical synapses and chemical synapses are interrelated and share commonalities in their molecular machinery during synaptic plasticity. As such, I aimed to delineate the molecular machinery involved in supporting the Cx36 run-up model of plasticity (see section 2). **Firstly, I hypothesized that the tubulin cytoskeleton directly interacted with Cx36 and subsequently mediated its transport to the GJP**. The contribution of the tubulin cytoskeleton to Cx36 transport as a mediator of the run-up phenomenon was explored in section 2.2. Since CaMKII activation has been established in both the electrical and chemical models of synaptic plasticity, calcium manipulation was also of particular interest. Once the transport mechanisms of Cx36 were resolved, **I then hypothesized that manipulating intracellular calcium concentrations, and thus CaM and CaMKII activity levels, would modulate Cx36 transport**; this was addressed in section 2.3.

1.2 Zebrafish Visual-Locomotor Circuitry

While chemical synapses are known to be functionally asymmetrical, the molecular architecture of electrical synapses is brought into question when considering that electrical and chemical synapses share similar molecular machinery during synaptic plasticity. In fact, the notion that electrical synapses exist in perfect symmetry seems counterintuitive to the well-established discovery of mixed chemical and electrical synapses capable of driving neuronal communication from the pre- to the postsynapse. As such, it is reasonable to inquire how gap junctions are modulated distinctly pre- and postsynaptically, particularly at homotypic aggregates. New evidence is emerging supporting the functional asymmetry of gap junctions achieved through (1) connexin post-translational modifications, (2) variations of signaling complexes interacting with either side of the gap junction plaque, and (3) the overall asymmetric properties of the pre- and postsynaptic membrane (Li *et al.*, 2004; Li, Lynn and Nagy, 2012; A. C. Miller *et al.*, 2017; Bazzigaluppi *et al.*, 2017; Nagy and Lynn, 2018; O'Brien, 2019). Of these three means to achieve asymmetry at the electrical synapse, the first two are, in part, directly related to the connexin protein sequence itself. As such, the most feasible means to understand electrical asymmetry was to utilize a model where the unique differences in the protein sequence cause differential localization pre- and postsynaptically. Here, the zebrafish animal model was chosen since the teleost orthologs of Cx36 are known to be expressed in such a manner; Cx35 proteins are known to be expressed at the presynapse, and the Cx34.7 ortholog is expressed postsynaptically (Rash *et al.*, 2013).

1.2.1 Examining *GJD2* Expression in the Central Nervous System of Larval Zebrafish

1.2.1.1 The Zebrafish Animal Model in Modern Research

Recently, zebrafish (*Danio rerio*) have been brought to the forefront of alternative animal models since breeding and animal housing is compatible with high-throughput assessments and large stock maintenance, respectively; a challenge otherwise faced with murine animal models. Since the larvae are transparent and develop *ex utero* rapidly, the progression of organogenesis and tissue formation under wild-type, knock-out or other manipulative conditions are easily monitored post-fertilization (Zhdanova *et al.*, 2001; Guo, 2004; Orger *et al.*, 2008). The physiological nature of zebrafish also permits rapid drug delivery without any physical manipulation, reducing animal stress and subsequent behavioral consequences. This non-invasive approach, in turn, reduces confounding factors in behavioral screens which may, if severe, alter neuronal plasticity. Experimentally, a plethora of methodologies is available and suitable for the zebrafish animal model. Overexpression (Kawakami *et al.*, 2004; Soroldoni, Hogan and Oates, 2009) and the selective knockdown of targeted genes (Nasevicius and Ekker, 2000) have been described allowing for the *in vivo* analysis of gene functionality. Furthermore, the use of fluorescent reporters provides a direct means to visualize the morphology and physiology of individual cells (Peters *et al.*, 1995; McLean and

Fetcho, 2008; Peri and Nüsslein-Volhard, 2008; Wen *et al.*, 2008). Zebrafish also exhibit a rich repertoire of behavioral phenotypes, such as sleep, learning, and memory, quantifiable through several neurobehavioral tasks (Zhdanova *et al.*, 2001; Cahill, 2002; Guo, 2004; Orger *et al.*, 2004; Ninkovic and Bally-Cuif, 2006).

Since microglia, astrocytic-like cells, oligodendrocytes, myelin, and a blood-brain barrier (BBB) are present (Tomizawa, Inoue and Nakayasu, 2000; Yoshida and Macklin, 2005; Bernardos and Raymond, 2006; Kirby *et al.*, 2006; Schweitzer *et al.*, 2006; Avila *et al.*, 2007; Peri and Nüsslein-Volhard, 2008), zebrafish recapitulate conditions representative of that found in human tissue. Genome organization and genetic pathways that modulate signal transduction cascades are conversed between humans and zebrafish (Postlethwait *et al.*, 2000), thus confirming its use as a suitable and representative model to study complex human neurobiological or neurobehavioral processes. An important difference between zebrafish and mammals, however, is the presence of more neuronal connexins; this is attributed to genome duplications causing the expression of multiple homolog genes for most mammalian connexins (Volff, 2005; Eastman *et al.*, 2006). As such, the increase in possible connexon coupling configurations adds an additional layer of complexity that can be exploited to understand how changes in functional demands create electrical asymmetry.

1.2.1.2 Cx36 Teleost Orthologs

The *GJD2* gene is highly conserved, displaying 98% sequence identity between the rat, mouse, and human genomes and 80% identity to its fish orthologs (Belousov and Fontes, 2013). Unlike their human or murine counterpart, zebrafish are unique in that they express four *GJD2* homologs, corresponding to Cx35a/Cx35.5 (*gjd2a*), Cx35/Cx35b/Cx35.1 (*gjd2b*), and Cx34.7 (*gjd1b*) protein expression; this is due to multiple duplication events in the teleost genome that were sustained throughout evolution. In much controversy, the potential fourth isoform was described at the genetic level in an earlier report, however, evidence to support that this isoform is expressed was limited (Jabeen and Thirumalai, 2013). Miller et al. (2017) provides one of the few reports demonstrating that Cx34.1 (*gjd1a*) is expressed in Mauthner neurons (A. C. Miller *et al.*, 2017). Nevertheless, the *gjd2b* ortholog showed the highest sequence similarity (approximately 90%) to mammalian *GJD2* and was the focus of our investigations. It is important to acknowledge that the *gjd2b* gene adopts various nomenclature in the literature when referring to the protein itself. For clarification purposes, protein expression of the *gjd2b* gene will be denoted as Cx35b throughout the remainder of this dissertation.

1.2.1.3 Cx35b Expression throughout the Brain

Cx35b is most notably known for its localization to the mixed synapses formed by the auditory nerve afferents on the Mauthner neuron, a reticulospinal neuron critical for the fast motor movements

during teleost escape responses. Pereda et al. (2003) demonstrated that Cx35b is expressed at the large myelinated club endings located on the lateral dendrite in both the zebrafish and goldfish animal models (Pereda *et al.*, 2003). This was later followed up by Rash et al. (2004), confirming that these synapses were indeed mixed (chemical and electrical) and detailed that Cx35b expression coincided with the presence of NMDA receptors (Rash *et al.*, 2004). Interestingly, matched double-replica freeze-fracture immunogold labeling revealed that Cx35b was restricted to the presynapse and Cx34.7 to the postsynapse. Moreover, GJ resistance exhibited a difference in conductance nearly 4-fold, allowing for electrical rectification (Rash *et al.*, 2013).

The distribution of Cx35b throughout the CNS of the developing zebrafish larvae was previously described using immunoradioactivity (Jabeen and Thirumalai, 2013). Here, the authors claimed to have used an antibody where the antigen was raised against the intracellular loop of perch Cx35. Since the other orthologs have minimal similarity in this region, no cross-reactivity with the other orthologs was previously reported (Pereda *et al.*, 2003). Staining in the rhombencephalon, tectal neuropil, and motor-controlling Mauthner neurons was present as early as 2-days post-fertilization (dpf). Retinal ganglion cell axons begin innervating the tectum at 3dpf with prominent staining of Cx35b in the tectal neuropil at this stage of development. By 4dpf, Cx35b is also present in the habenulae, cerebellum, and radial glia. The staining of these brain regions remained consistent with age, up to the tested 15dpf. To date, Jabeen and Thirumalai (2013) provide the only report describing Cx35b expression in the developing brain of larval zebrafish.

1.2.1.4 Cx35b Expression in the Retina

Similar to the brain and other organs, the structure and development of the eye during embryogenesis are conserved between zebrafish and mammals (Bibliowicz, Tittle and Gross, 2011; Stenkamp, 2015). However, the retina is of particular interest in most research investigations due to its role in the detection and processing of visual input prior to relaying the information to the appropriate visual centers of the brain. The retina is a highly organized structure that is arranged into multiple yet distinct layers capable of distinguishing between different types of visual input (Gollisch and Meister, 2010) (**Figure 1.3**). The processing of a visual stimulus is initiated by the detection of light via the rod and cone photoreceptors lying at the base of the retina. Whereas rod photoreceptor activity is primarily increased under dim/scotopic light, cone photoreceptors function under bright/photopic light, reminiscent of lighting conditions between dawn and dusk. Although the murine model is commonly used in retinal research, the zebrafish animal model provides a more accurate and translatable comparison to the human retina. This is due to zebrafish having a cone-dominated retina (approximately 60% cones) rather than the rod-dominated retina found in murines (approximately 97% rods) (Carter-Dawson and Lavail, 1979; Fadool, 2003). Zebrafish possess four different cone photoreceptor subtypes: (1) UV-cones expressing the opsin gene *sws1*

capable of detecting visual input in the ultraviolet range (354 nm) are not expressed in mammals, (2) S-cones expressing *sws2* detect short wavelengths (416 nm), (3) M-cones express the Rh2 class of opsins (Rh2-1 to Rh2-4) and detect medium wavelengths (467 nm, 476 nm, 488 nm, and 505 nm), and (4) L-cones expressing lws class opsins detect long wavelengths (548nm and 558 nm). Interestingly, M- and L-cones are arranged as a double cone morphologically (Vihtelic, Doro and Hyde, 1999; Chinen *et al.*, 2003).

The phototransduction cascade is initiated when light triggers the activation of rhodopsins and/or opsins of the rod and cone photoreceptors. Rhodopsin and opsin proteins are both classified into the G-protein-coupled receptor superfamily and respond by dissociating the alpha-subunit G_{α}-GTP, which interacts with downstream targets to affect intracellular signaling. The subsequent change in membrane potential triggers an action potential and transmits this information via neurochemicals to horizontal and bipolar cells. Horizontal cells are inhibitory interneurons that act to fine-tune synaptic output, whereas bipolar cells are glutamatergic neurons that transmit light signals to the glutamatergic ganglion cells. Similar to horizontal cells, amacrine interneurons modulate the activity pre- and postsynaptically at this later stage. The axons of retinal ganglion cells converge to form the optic nerve and relay the visual input collected by the photoreceptors to the visual centers in the brain. While the phototransduction cascade is well-defined, it is now recognized that electrical coupling serves as an important modulator in the process. Here, gap junctions serve as a means of rapidly transmitting information through the multiple layers of the retina, improving signal: noise ratio and 'bridging the gap' between rod-cone signaling.

Although Cx35b expression in the retina resembles Cx36, which was previously addressed (see section 1.1.2.4), it is worth reiterating that Cx35b/Cx36 protein expression is well established and known to be enriched in the retina of teleosts and mammals. Previous reports demonstrated that Cx35b gap junction aggregates were found between cone-cone and rod-cone contacts, and coupling was regulated by lighting conditions. More specifically, Cx35b junctional coupling between cone contacts increased at night; however, it was downregulated in the daytime. Further analysis revealed that this result was due to the phosphorylation state of Cx35b at Ser110 and Ser276, where PKA-dependent phosphorylation had increased at night. As such, it was predicted that increasing cone-cone coupling at night served as a compensatory means to code for increases in light when the rod-rod bipolar pathway is saturated (Kothmann *et al.*, 2007; Li, Chuang and O'Brien, 2009; Li *et al.*, 2013).

Follow-up studies to date have now explored the relationship between the dopaminergic pathway and the coupling of Cx36/Cx35b gap junctions in the retina. In the retina, dopaminergic signaling originates from the amacrine cells and is released with an increase in lighting conditions (Witkovsky, 2004). Kothman et al. (2009) demonstrated that Cx36 uncoupling of AII amacrine cells was driven by dopamine (D1) receptor activation, which subsequently increased PKA and the protein phosphatase PP2A activity

(Kothmann, Massey and O'Brien, 2009). A strong correlation between Cx35b-mediated photoreceptor coupling and dopaminergic signaling was also established by Li et al. (2013). Here, it was reported that dopamine (D4/D2-like) receptor activation inhibits adenylyl cyclase, reducing cAMP and PKA activity. As a result, Cx35b photoreceptor contacts are uncoupled, confirming the influence of the dopaminergic pathway on the modulation of Cx35b gap junctional coupling (Li, Chuang and O'Brien, 2009; Li *et al.*, 2013). Adenosine, a neuromodulator that is abundant under scotopic light conditions, is now understood to be a co-regulator of adenylyl cyclase and thus affects Cx35b phosphorylation and coupling also (Li, Chuang and O'Brien, 2014).

1.2.2 Overview of Zebrafish Larval Locomotor Behaviors

Larval locomotor activity is essential to zebrafish hunting, predator defense, and social interaction. Subsequently, this behavior is also a direct reflection of neural activity of the CNS and is modulated by external stimuli targeting various sensory systems. In vertebrates, the basal ganglion is highly conserved, both anatomically and functionally, and considered to be a critical component in the initiation and control of locomotion (Grillner, Robertson and Stephenson-Jones, 2013). Neuronal circuits originating from the basal ganglia and descending through the mesencephalon and caudal brainstem regions are linked to the spinal cord, where locomotor central pattern generators (CPGs) reside to influence locomotor output (Chong and Drapeau, 2007; Wyart *et al.*, 2009; Kyriakatos *et al.*, 2011; Grillner, Robertson and Stephenson-Jones, 2013; Severi *et al.*, 2014). More specifically, the mesencephalic locomotor region was shown to initiate locomotion and modulate its speed upon electrical excitation (Shik, Orlovskiĭ and Severin, 1966; Shik, Severin and Orlovskiĭ, 1966). These signals are transmitted in sequence, first to the reticulospinal neurons located in the mid- and hindbrain, where sensory input is thought to be received, and next to the synaptic terminals converging on the CPGs during dominant swim (Buchanan and Grillner, 1987; Jordan, 1998; Deliagina, Zelenin and Orlovsky, 2002; Sato *et al.*, 2007; Kohashi and Oda, 2008; Haehnel, Taguchi and Liao, 2012). Slow motor neurons then receive excitatory input from the CPGs to induce dominant swimming behavior (T. H. Miller *et al.*, 2017) (**Figure 1.3**).

1.2.2.1 The Zebrafish Larval Startle Response

Startle responses are species-specific adaptive evolutionary behaviors exhibiting short-latency combined with high acceleration (Hale *et al.*, 2016). In zebrafish larvae, startle responses are a reflection of escape behaviors that are characterized by an increase in high-speed movements, known as burst swimming, and specific body curvature (Budick and O'Malley, 2000; Buss and Drapeau, 2001). Typically, startle responses occur in tandem with anxiety-like behavior, and larvae demonstrate larger durations of freezing in such circumstances (Blaser, Chadwick and McGinnis, 2010; Kalueff *et al.*, 2013). Burst activity

is also seen in zebrafish burst-and-coast behavior, a sequence of swimming movements since larvae are unable to perform continuous swimming bouts (Müller and van Leeuwen, 2004).

As previously mentioned, motor commands from the basal ganglia and subcortical regions are conveyed to the reticulospinal neurons prior to converging on the CPGs (Chong and Drapeau, 2007; Wyart *et al.*, 2009; Kyriakatos *et al.*, 2011; Grillner, Robertson and Stephenson-Jones, 2013; Severi *et al.*, 2014). However, larval escape behavior is largely dictated by the motor-controlling Mauthner neuron, which fires action potentials to excite the fast motor neurons and trigger the escape response (also referred to as subordinate locomotion; **Figure 1.3**) (Zottoli, 1977; Kimmel, Eaton and Powell, 1980; Eaton, Lavender and Wieland, 1981; Faber, Fetcho and Korn, 1989; T. H. Miller *et al.*, 2017). The segmental homologs MiD2 and MiD3, which are similar anatomically to Mauthner neurons, are also involved in escape responses (Zottoli, Hordes and Faber, 1987; Faber, Fetcho and Korn, 1989; Eaton, DiDomenico and Nissanov, 1991; O'Malley, Kao and Fetcho, 1996; Svoboda and Fetcho, 1996; Liu and Fetcho, 1999; Eaton, Lee and Foreman, 2001). Although Cx35b expression in the MiD2 and MiD3 neurons has not been explicitly described, Cx35b expression has been well established as a presynaptic component of mixed chemical/electrical synapses in Mauthner neurons as previously outlined (Rash *et al.*, 2013). Altogether, it was reasonable to suspect that presynaptic Cx35b expression and functionality would be critical in modulating the visuomotor aspects of larval zebrafish behavior.

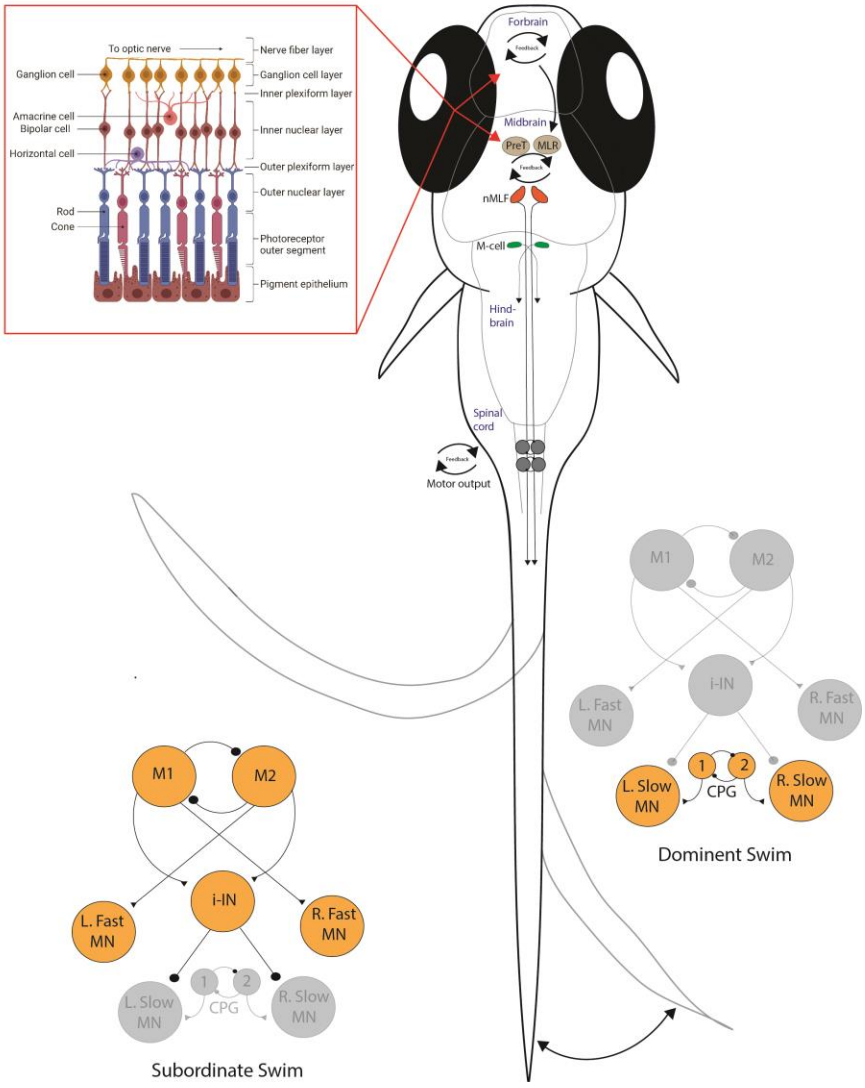

Figure 1.3. General Overview of the Zebrafish Retina and Locomotion Circuitry.

Visual input is received by rod- and cone photoreceptor cells and is first relayed to the bipolar cells (BC), then subsequently to the retinal ganglion cells (GC). Horizontal and amacrine cells serve as interneurons modulating the PRCs-BC cell and BC-GC synaptic connections. The organization of the retina is outlined in red at the upper left of the diagram. Signaling is then communicated to the visual processing centers of the brain via the optic nerve. Visuomotor behavior originates from the basal ganglia, located in the forebrain, and descends through the midbrain where the mesencephalic motor region (MLR) resides. Visual information is also received by the pretectum (pre-T). These synaptic inputs converge on the nucleus of the medial longitudinal fasciculus and descend through caudal brainstem regions into the spinal cord. During the dominant swim, central pattern generators in the spinal cord synapse on slow motor neurons (MN) to provoke swimming behavior. In contrast, Mauthner neurons (M-cell; M1 and M2) are activated and synapse on fast motor neurons to influence subordinate swimming behavior seen during the startle response. Overview of the retina was adapted from the "Structure of the Retina" template by BioRender.com (2022); retrieved from https://app.biorender.com/biorender-templates. All else was illustrated in Adobe CC 2015 by Brown (2022).

1.2.2.2 Visuomotor Behavioral Assays

Alterations in neuronal circuitry can be established by measuring visual-motor behavioral outcomes; the advantages of utilizing the zebrafish animal model over the murine model have been previously outlined. With the rise in interest in zebrafish research, numerous behavioral screens have been well-documented. Currently, only one report has explored behavioral outcomes in a *gjd2b* knock-out line of zebrafish. Quint et al. (2021) demonstrated that the loss of either *gjd2a* or *gjd2b* led to refractive errors but had a limited effect on the spatial acuity measured by the optokinetic reflex/response (OKR), an experiment designed to measure the eye movements in response to moving objects while the head is stationary. Here, the authors demonstrated that Cx35b$^{-/-}$ mutant zebrafish displayed reduced positive responses at spatial frequencies above 0.25cpd and reduced eye tracking movements (Quint *et al.*, 2021). Moreover, this report demonstrated that Cx35a is expressed in the retina, where previously, the commonly held notion was that the retinal tissues primarily expressed Cx35b (Quint *et al.*, 2021). Given the lack of literature exploring the behavioral outcomes in the *gjd2b* knock-out model, our overarching goal was to establish how the loss of Cx35b impacted visuomotor behaviors. Here, a brief catalog of behavioral screens achieved via high-throughput automated video-tracking systems utilized in this dissertation is provided.

1.2.2.2.1 Visual-Motor Response (VMR) Assay

Previously, a mutant zebrafish (known as *nrc* mutants) was reported to be completely blind based on its failure to respond to the OKR assay. However, this was challenged when it was demonstrated that *nrc* mutant fish could detect simple increments and decrements in lighting conditions; thus, *nrc* mutant fish were not completely blind. As such, Emran et al. (2008) published the visual-motor behavioral assay (VMR) that is now commonly adopted as a means to measure the responsiveness of zebrafish to changes in light intensities (Emran, Rihel and Dowling, 2008). Here, locomotion is measured using a video-tracking system during alternating periods of light ON and light OFF, each lasting 30 minutes. Due to the sudden change in light intensity, zebrafish larvae exhibit a sharp increase in their locomotion during each transition attributed to the startle response; blind fish, however, fail to do so. This sharp increase in locomotion is then analyzed to determine the efficacy of the visual system.

1.2.2.2.2 Light-Dark Locomotion Assay

The light-dark locomotion test has been proposed as an appropriate *in vivo* screening assay for psychoactive substances. Similar to the VMR assay, zebrafish larvae are exposed to alternating light and dark conditions, though typically for shorter time durations. Here, the locomotion activity following each transition is measured. The expected outcomes of the light-to-dark transition are an elevation in larval locomotion. In contrast, dark-to-light transitions reduce locomotor activity (Ellis, Seibert and Soanes, 2012; Schnörr *et al.*, 2012; Peng *et al.*, 2016; Luchtenburg, Schaaf and Richardson, 2019; Faught and Vijayan,

2022). A variety of locomotor parameters can be measured here, including speed, acceleration, distance traveled, and/or turning radius. Consequently, the light-dark locomotion assay is also used as an anxiety index.

1.2.2.2.3 Innate Color Preference

Color vision plays a critical role in visual perception and can be assessed based on the previous work of Park et al. (2016). A color-coordinated T-maze was used, and zebrafish larvae were left to swim freely. Color preference was measured by the cumulative time spent in each arm of the T-maze, associated with a distinct color. Here, 5dpf zebrafish strongly preferred blue over the remaining colors tested. Nevertheless, innate color preference was established as Blue > Red > Green > Yellow. In *tyr* mutant zebrafish, lacking the tyrosinase protein, color preference could not be established, suggesting that this assay was sufficient to assess color blindness visual phenotypes. Park et al. (2016) also reported that light intensity, the number of larvae within each test group, or pre-exposure to the colors did not affect the innate color preference (Park *et al.*, 2016).

1.2.2.2.4 Thigmotaxis

Thigmotaxis, otherwise known as wall-hugging, is the most well-established anxiety index in animals and humans. During a thigmotaxic response, animals avoid the center of their testing chamber and remain in close contact with the boundaries. Thigmotaxic behavior in zebrafish larvae was validated by Schnörr et al. (2012) by measuring this behavior while zebrafish were triggered by sudden light-dark transitions. Diazepam, a known anxiolytic, attenuated thigmotaxic behavior, and caffeine, an anxiogenic, enhanced wall-hugging. Thigmotaxic behavior was established as early as 5dpf (Schnörr *et al.*, 2012).

1.2.2.2.5 Non-associative Learning and Memory Model

Zebrafish larvae exhibit different types of learning and memory abilities, allowing for a variety of paradigms to be tested. Of particular interest is the non-associative (non-declarative) form of learning achieved through habituation assays. During habituation studies, a repetitive stimulus is delivered of fixed intensity. As a result, animals decrease their response (Thompson and Spencer, 1966; Rankin *et al.*, 2009). Habituation in zebrafish is best measured by exploiting the innate startle response behavior when exposed to an abrupt sensory stimulus such as auditory, visual, or tactile cues (Eaton *et al.*, 1977; Eaton, Nissanov and Wieland, 1984; Weiss *et al.*, 2006). Currently, the neurobiology underlying habituation is poorly understood.

1.2.3 Linking Visual Changes to Cognitive Indexes

One of the fundamental questions in neuroscience research is how specific genes, signaling pathways, and the overall architecture of neuronal connectivity influence higher-order behaviors. While the

relationship between anxiety and memory is established, the neurobiology of their interplay remains poorly understood; only a few studies have addressed the link between anxiety and memory in the zebrafish animal model. However, the collection of results thus far suggests that acute and chronic stress impair memory formation, similar to rodent and clinical data (de Castro *et al.*, 2009; Gaikwad *et al.*, 2011; Piato *et al.*, 2011). As an added layer of complexity, how changes in individual sensory systems contribute to this interplay is even lesser understood. As such, in Chapter 3 of this dissertation, I explore the role of Cx35b in visual behaviors and describe how its loss influences anxiety and memory capacity.

1.2.4 Main Hypothesis and Research Aims

In mammals, connexin-36 (Cx36) is the major component of electrical synapses, also found alongside chemical synapses in mixed synapses throughout the vertebrate brain. This research aims to elucidate the role of Cx36 in sensorimotor circuitry in an animal model suitable for fundamental and statistically strong *in-vivo* studies. The zebrafish (*Danio rerio*) is ideal for this purpose as a well-characterized model for genetic, developmental, and behavioral studies. Here, targeting the *gjd2b* gene was the primary focus since its corresponding ortholog, Cx35b, demonstrates the highest sequence similarity to Cx36. Although previous studies have demonstrated that Cx35b is highly expressed in the visual system, the motor-controlling Mauthner neurons, and throughout the brain, current literature has yet to explicitly explore its contributions to circuitry or behavioral phenotypes. As such, **I hypothesized that complex alterations to neuronal circuitry via a Cx35b knock-out (KO) would affect vision, sensorimotor gating, and plasticity-dependent cognitive processing**. It is reasonable to suspect that the evolutionary divergence of the *GJD2* gene has led to the unique morphological and physiological properties of each Cx36 ortholog. As such, zebrafish served as an ideal model organism to investigate the functionality of Cx35b *in vivo* and to better elucidate the multiple cellular roles of mammalian Cx36. For high-throughput analyses, sensorimotor phenotypes were determined in seven-day-old (7dpf) larvae when all major brain areas, including sensory organs, were developed, which allowed for testing of locomotor behavior under different light conditions.

2

DELINEATING THE MOLECULAR MACHINERY INVOLVED IN CX36 TRANSPORT & INSERTION INTO THE GAP JUNCTION PLAQUE

2.1 Materials & Methods

2.1.1 Plasmid Constructs

Rattus norvegicus Cx36 (Accession number: NP_062154.1) was used in this study. Wild-type Cx36-EGFP and the carboxyl-terminal mutant Cx36Δ279-292-EGFP (denoting the deletion of amino acids 279-292) expression plasmids were generated previously (Zoidl *et al.*, 2002; Del Corsso *et al.*, 2012). Cx36Δ279-292 was isolated and subcloned into the EGFP expression vector pEGFP-N1 (Clontech, Mountain View, CA, USA). EGFP expression plasmids for wild-type Cx36 and Cx36 (Δ279-292 were used for the subcloning of Cx36 sequences into pcDNA 3.1-MCS-BirA (R118G)-HA. The expression vector pcDNA 3.1-MCS-BirA (R118G)-HA (pcDNA3.1 BirA*) was purchased from Addgene (Cambridge, MA, USA). Oligonucleotides for single amino acid substitutions in the tubulin-binding region were designed using the NEBaseChanger tool (New England Biolabs Inc., Boston, MA, USA) and synthesized by IDT. Alanine scanning was performed using the Q5 Site-Directed Mutagenesis Kit as per the manufacturer's protocol (New England Biolabs Inc., Boston, MA, USA). All plasmid constructs were screened to confirm the correct directionality by restriction endonuclease digest and sequence-verified by Eurofins MWG Operon LLC (Huntsville, AL, USA). The pmCherry-alpha-tubulin (Addgene, 49149), pDsRed2-ER (Clontech, 6982-1), pDsRed-Monomer-Golgi Vector (Clontech, 632480) and the pDsRed-Monomer-Caveolin 1 (Clontech) vectors were purchased as described.

2.1.2 Cell line, Cell Culture, and Transient Transfection

Mouse neuroblastoma 2a (Neuro-2a) cells (ATCC®, CCL-131, Manassas, VA, USA) were cultured in high glucose Dulbecco's Modified Eagle Medium (DMEM) supplemented with 10% fetal bovine serum (FBS), 1% non-essential amino acids (NEAA), and 1% penicillin/streptomycin as described (Zoidl *et al.*, 2002). The cell line was previously authenticated in-house using a combination of morphological confirmation, differentiation capacity, and identifying neuronal markers via PCR. There was no evidence of mycoplasma contamination. All cell culture reagents were purchased from Thermo Fisher Scientific (Burlington, ON, Canada) or Sigma-Aldrich (Oakville, ON, Canada). For transient transfections Neuro-2a

cells were grown to 60% confluency (approximately 0.3-1.92 x 10^6) overnight in 19mm (24 well), 100mm or 35mm MatTek culture dishes. Cells were transfected using the Effectene Transfection Reagent Kit (Qiagen, Valencia, CA, USA) with 200 ng DNA, as per the manufacturer's protocol, and all analyses were performed 48 hrs post-transfection.

2.1.3 Protein Isolation and Immunoblot Analysis

Transiently transfected Neuro-2a cells were washed once with divalent free (DF) phosphate-buffered saline (PBS) prior to lysis. Whole-cell protein lysates were prepared directly in 1X Laemmli sample buffer (50 mM Tris-HCl, pH 6.8, 2% SDS, 3% β-mercaptoethanol) and heated for 3 min before gel separation. Twenty micrograms of proteins were fractionated by sodium dodecyl sulfate-gel electrophoresis (SDS-PAGE) on a 5% stacking and 10% running gels and transferred onto a 0.2 µm nitrocellulose membrane using the Trans-Blot® Turbo™ Transfer System (both Bio-Rad, Mississauga, ON, CA). Membranes were blocked with 1X iBind™ Solution (HRP or AP detection), and immunoblotting was carried out using the iBind Western System (Thermo Fisher Scientific, Burlington, ON, Canada) as per the manufacturer's protocols. Primary antibodies and enzyme conjugates were diluted at 1:10,000 (anti-β-actin: clone AC-15, A5441, and anti-HA: clone HA-7, H9658, Sigma-Aldrich, Oakville, Canada), 1:1000 (anti-GFP: clone F56-6A1, sc-53882, Santa Cruz Biotechnology, Dallas, TX, USA; anti- β-tubulin: clone TUB 2.1, ascites fluid, T4026, Sigma-Aldrich, Oakville, Canada), and 1:2500 (Streptavidin-HRP: 926-68079, Invitrogen, Burlington, ON, Canada). Secondary antibodies were diluted at 1:10,000 (IRDye®800CW Goat Anti-Mouse: 926-32210, Li-Cor Biosciences, Lincoln, NE, USA) and 1:15,000 (IRDye®680LT Donkey Anti-Rabbit, Li-Cor Biosciences Lincoln, NE, USA). Fluorescent signals were detected using the Odyssey® CLx Infrared Imaging System (Li-Cor Biosciences, Lincoln, NE, USA) as per the manufacturer's protocol using default settings.

2.1.4 *In vivo* affinity capture of biotinylated tubulin using BioID

On a 100mm dish (approximately 5.28 x 10^6), transfected Neuro-2a cells expressing Cx36 wild-type or Cx36Δ279-292-BirA* fusion proteins were incubated with 50 µM biotin for 24 hours as previously described (Roux *et al.*, 2012). Cells were washed three times with PBS (-/-) and lysed at 4°C with NP-40 cell lysis buffer (Invitrogen, Camarillo, CA, USA) supplemented with 1X protease inhibitor cocktail (Thermo Scientific, Burlington, ON, Canada) and 5 units/ml benzonase (EMD Millipore, Etobicoke, ON, Canada). Approximately 400 µl of extracts were subjected to centrifugation at 13,000 rpm and incubated at 4°C overnight with 180 µl of Dynabeads (MyOne Streptavidin C1, Invitrogen, Burlington, ON, Canada). Collection of the beads with protein candidates attached, washes, elution, and preparation for western blot or mass spectrometry analysis were performed as described (Roux *et al.*, 2012).

2.1.5 Pharmacology

Tubulin-dependent trafficking of Cx36 to the gap junction plaque was analyzed using Neuro-2a cells expressing EGFP-tagged wild-type Cx36 protein treated with either colchicine (100 µM, Sigma-Aldrich) or paclitaxel (20 µM, Sigma-Aldrich) to disrupt or stabilize microtubules respectively. Trafficking of Cx36 was also analyzed under calcium-stimulation/inhibition conditions by treating single or double-transfected Neuro-2a cells (see section 2.1.7) with 2µM ionomycin (Sigma-Aldrich) or 24M BAPTA-AM (Thermo Fisher Scientific, Burlington, ON, Canada). The CaM and CaMKII antagonists W7 (10µm) and KN-93 (50µm) were purchased from Thermo Fisher Scientific (Burlington, ON, Canada). Neuro-2a cells were incubated with a drug at 37°C, 5% CO_2, for 10 minutes prior to use in FRAP or TIRF studies; see section 2.1.7 for more detail.

2.1.6 Electrophysiology

Neuro-2a cell pairs expressing EGFP-tagged wild-type Cx36 or Cx36Δ279-292 were used for dual whole-cell patch-clamp recording. In brief, Neuro-2a cells were perfused in a bathing solution supplemented with 100 µM colchicine for 1, 3 or 24 hours, and the run-up was induced as previously described (Del Corsso *et al.*, 2012). Perforated patch-clamp recordings were performed as previously described (del Corsso *et al.*, 2006; Del Corsso *et al.*, 2012) over a time course of up to 70 min at room temperature.

2.1.7 Fluorescence Microscopy and Image Processing

2.1.7.1 Fluorescent Imaging and Gap Junction Plaque Measurements.

Transfected Neuro-2a cells were fixed with 4% formalin for 15 min at room temperature. Cells were subsequently rinsed with PBS (+/+) and distilled water prior to mounting with Fluoroshield™ with DAPI (Sigma, Oakville, ON, Canada) mounting medium. Mounted slides were visualized using a Zeiss LSM 700 confocal microscope controlled by the ZEN 2010 software program at room temperature. Cells were imaged using the Plan-Apochromat 63x/1.40 Oil DIC M27 or the EC Plan-Neofluar 40x/1.3 Oil M27 oil immersion lenses. Images were generated at a high resolution of up to 2048x2048 pixels and an average of 4 scanning repetitions in the single plane or each plane of a Z-stack. The single or multi-track mode was selected accordingly for the compilation of localization studies. The gap junction plaque area (µm²) was measured using the ImageJ (NIH, Bethesda, MD, USA) free-hand tool. The percentage of Cx36 gap junction-paired cells versus the total paired Cx36 expressing cells was measured as previously described (Qu, Gardner and Schrijver, 2009). Mander's overlap coefficient was used to quantify the overlap between corresponding fluorescent signals deriving from Cx36 and cell organelles in co-transfected cells. Mander's overlap coefficient was calculated using the ZEN2010 program. Co-localization was accepted at a Mander's

coefficient at and above 0.5; this threshold indicated that the occurrence of true co-localization surpassed the probability of chance.

2.1.7.2 Fluorescence recovery after photobleaching (FRAP).

For the quantitative analysis of connexon trafficking and gap junction regeneration, FRAP was performed 48h post-transfection using the Zeiss LSM 700 confocal microscopy in combination with Zeiss 63X (Plan-Apochromat, DIC M27 1.4) oil immersion lens and the Zen 2010 software. The microscope was equipped with an incubation chamber to maintain cells at 37°C in DMEM without phenol red. Since previous reports (Giepmans *et al.*, 2001; Lauf *et al.*, 2002) have described connexon replenishment occurring at the lateral ends of the gap *junction* plaque, this was selected as the region of interest (ROI). ROIs were manually drawn at the nonjunctional plasma membrane and lateral ends of the gap junction plaque using the rectangle tool. ROIs were bleached using the 405 nm laser line at 70% emission strength with a single event of 20 iterations. Prior to recording, confocal images were optimized along the focal plane yielding the largest GJP surface area. The mobile fraction (%) and intensity of fluorescence (RFU) were recorded *in vivo* for up to 200 seconds per ROI, and fluorescence values were collected at 1-second intervals. Observations were recorded with a pinhole of 1.0 airy units (AU) with a scan area of 31.1µm x 31.1µm, zoom level between 1-3, and resolution of 512x512 pixels. Consistent parameters were used across all experiments. Experiments with considerable fluctuations in fluorescence intensity or ROI frame shifts were not included in the analyses. Background subtraction was carried out with an ROI of the extracellular space to improve the signal-to-noise ratio. Loss of fluorescence was corrected next by expressing the previous values as a fraction of an unbleached control ROI. FRAP recordings were then normalized by expressing the corrected fluoresces as a fraction of the averaged pre-bleached values. The mobile fraction ($M_f = (F_{max} - F_0)(1 - e^{-kt})$) and half-time of recovery ($T_{1/2} = \ln 2/k$) were calculated by the monoexponential association equation in GraphPad: $F_t=F_0 + (F_{max} - F_0)(1 - e^{-kt})$ where F_t is the fluorescence after background subtraction at time t, F_0 and F_{max} are the fluorescence values immediately after, and at the end of recovery, following the bleaching event respectively, and k is the first-order rate constant for recovery. Repopulation figures and X-Y scatterplots were done using the R software. Sample sizes ranged based on the efficiency of gap junction plaque formation.

2.1.7.3 Total internal reflection fluorescence (TIRF).

For all experiments, Neuro-2a cells were plated onto 35mm MatTek dishes and co-transfected with pShuttle-mCherry-Tubulin and the pEGFP-Cx36 wild-type or mutants as previously outlined. Time-lapse TIRF microscopy was performed using the Zeiss Observer.Z1 spinning-disk microscope in combination with the Zeiss 100X (Plan-Apochromat, DIC M27, 1.46) oil immersion lens, Photometrics Evolve™512 camera, and the Zen 2 (2014) software. The microscope was equipped with an incubation chamber to

maintain the temperature at 37°C and CO_2 levels at 5%. Cells were imagined in DMEM without phenol red. Images were acquired at a resolution of 512 x 512 pixels in 20-second intervals for a total duration of 400 seconds. Images were processed in Imaris (Zurich, Switzerland) by tracking single particles expressing EGFP within the TIRF field.

2.1.8 Molecular modeling

A helical region spanning amino acids 47-62 of the RB3 protein stathmin-like-domain(Gigant *et al.*, 2005) (PDB: 1Z2B;) was substituted with a sequence from the Cx36 carboxy tail region (277-292) using PyMOL 1.8.6 (Schrödinger) and further refined with the FlexPepDock module of Rosetta 3.9 (Raveh, London and Schueler-Furman, 2010)

2.1.9 Statistics

Generation of beeswarm boxplots was completed in GraphPad Prism 6 (GraphPad Software, La Jolla, CA, USA). Plaque repopulation graphs and mobile fraction vs. half-time of recovery XY scatterplots were created in R-statistical program (The R Foundation, Aukland, New Zealand). All data is represented as the mean ± SEM. Statistical analysis was carried out using SPSS (IBM Corporation; Armonk, NY, USA) or GraphPad Prism 6. Significance was determined by the Kruskal-Wallis. For the FRAP data, statistical significance was determined by the Kruskal-Wallis test followed by a Dunn's multiple comparison test. $P < 0.05$ was considered significant. XY plots of the mobile fraction and half-time of recovery represented the mean±CI. All comparisons were made to the WT control unless otherwise stated. Sample sizes and p-values are provided throughout the manuscript and/or figure captions.

2.2

Tubulin-Dependent Transport of Connexin-36 Potentiates the Size and Strength of Electrical Synapses

Cherie A. Brown[1], Cristiane del Corsso[2], Christiane Zoidl[1], Logan Donaldson[1], David C. Spray[3,4], Georg Zoidl[1,5]

[1] Department of Biology, York University, Toronto, ON M3J 1P3, Canada, [2] Department of Biophysics and Physiology, Federal University of Rio de Janeiro-RJ, 21941-901 Rio de Janeiro, Brazil, [3] Department of Neuroscience, Albert Einstein College, Bronx, NY 10461, USA, [4] Department of Medicine, Albert Einstein College, Bronx, NY 10461, USA, [5] Department of Psychology, York University, Toronto, ON M3J 1P3, Canada

Author Contributions: Conceptualization, D.C.S., and G.Z.; investigation, C.A.B. (BioID, Immunoblot, Imaging, GJP size, GJP frequency, Mander's overlap coefficient, TIRF, FRAP, and site-directed mutagenesis), C.d.C. (electrophysiology), C.Z. (cell and molecular biology resources), and L.W.D. (structural modeling); writing—original draft preparation, C.A.B., L.W.D., D.C.S., and G.Z.; writing—review and editing, C.A.B., C.d.C., C.Z., D.C.S., L.W.D. and G.Z.; supervision, D.C.S., and G.Z.; funding acquisition, D.C.S., and G.Z

2.2.1 Abstract

Connexin-36 (Cx36) electrical synapses strengthen transmission in a calcium/calmodulin (CaM)/CaMKII-dependent manner, like a mechanism whereby the NMDA receptor subunit NR2B facilitates chemical transmission. Since NR2B-microtubule interactions recruit channels to the cell membrane during plasticity, we hypothesized an analogous modality for Cx36. We determined that Cx36 binds to tubulin at the carboxy-terminal domain were distinct from Cx43 and NR2B by binding a motif overlapping with the CaM and CaMKII binding motifs. Dual patch-clamp recordings demonstrated that pharmacological interference of the cytoskeleton and deleting the binding motif at the Cx36 CT reversibly abolished Cx36 plasticity. Mechanistic details of trafficking to the gap junction plaque (GJP) were probed pharmacologically and through mutational analysis, all of which affected GJP size and formation between cell pairs. Lys279, Ile280, and Lys281 positions were particularly critical. This study demonstrates that tubulin-dependent transport of Cx36 potentiates synaptic strength by delivering channels to GJPs,

reinforcing the role of protein transport at chemical and electrical synapses to fine-tune communication between neurons.

2.2.2 Cx36 Interaction with the Tubulin-Cytoskeleton is Required for Electrical Plasticity

The interaction between tubulin at the carboxy-terminal (CT) of Cx36 was initially identified by mass spectrometry using both affinity-purified samples and immunoprecipitated protein complexes from murine brain lysates (Alev, Zoidl and Dermietzel, 2013). This result was independently confirmed by a BioID screen using a full-length rat Cx36 protein as bait in the Neuro-2a mouse neuroblastoma cell line (**Figure 2.1A**). Within the Cx36-CT, a potential tubulin site was identified by sequence comparison with the analogous tubulin-binding sequence in connexin-43 (Cx43) (Giepmans *et al.*, 2001; Giepmans, Verlaan and Moolenaar, 2001). This sequence overlapped with the previously reported binding sites for calmodulin (CaM) (Burr *et al.*, 2005b; Siu *et al.*, 2016), and the calcium/calmodulin-dependent protein kinase II (CaMKII) (Alev *et al.*, 2008), all of which demonstrated high conservation across Cx36 orthologs belonging to the major vertebrate Chordata subphylum (**Figure 2.1B**). Since the predicted tubulin binding site and the established CaMKII / CaM binding sites are situated within a fourteen amino acid segment, any mechanistic model must consider competition among these proteins. This signature motif was absent in other connexin isoforms (**Figure S2.1**).

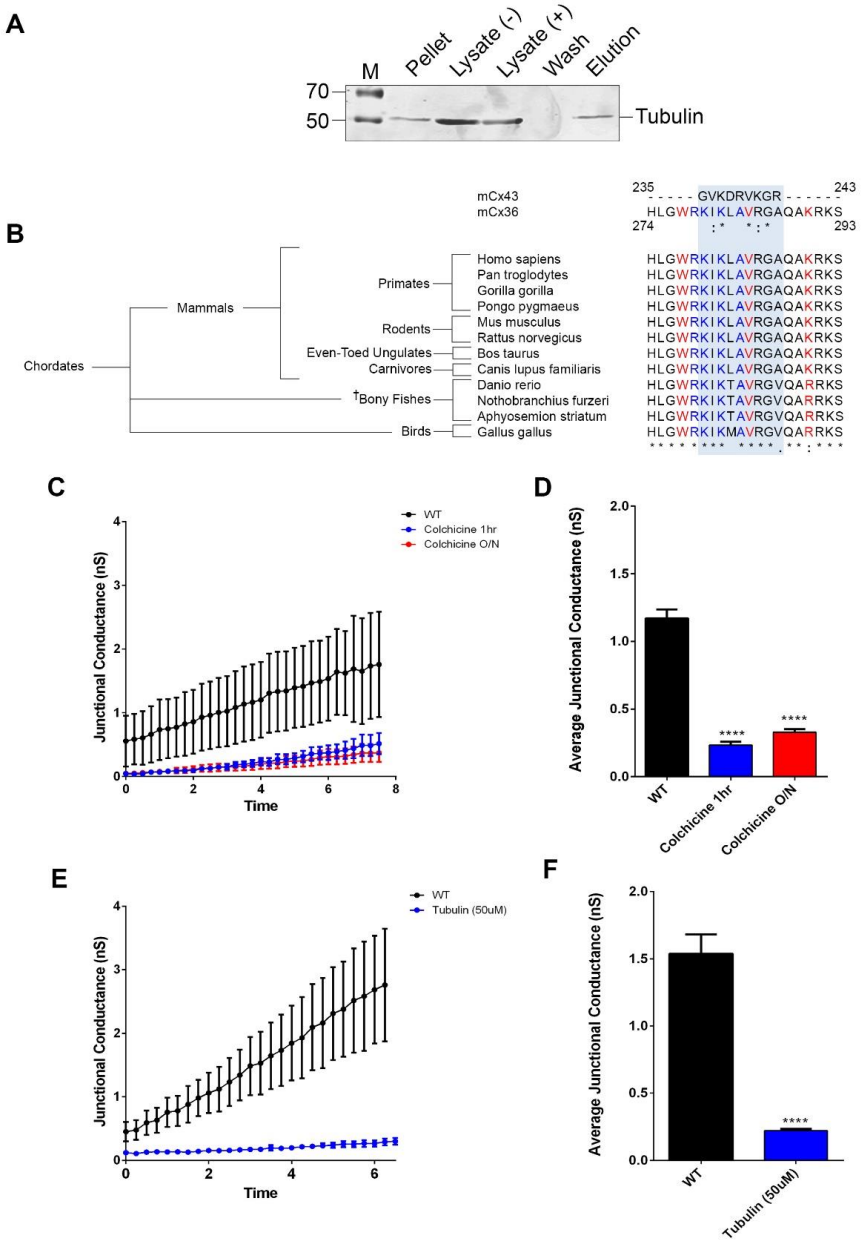

Figure 2.1. Tubulin interaction at the Cx36 Carboxyl Terminus Potentiates Electrical Plasticity.

*(**A**) Full-length Cx36 protein was expressed as a fusion protein with the BirA* ligase to perform a BioID assay using Neuro-2a cell lysate. Lysates were subjected to western blot analysis before (-) and after (+) the addition of streptavidin-conjugated beads. Immunodetection identified tubulin as an interaction candidate of Cx36. (**B**) Sequence alignment of the tubulin-binding motif confirmed in Cx43 elucidated the potential Cx36 interface localized to the Cx36 carboxyl terminus (CT). The putative binding motif of Cx36, shaded in blue, demonstrated robust conservation across orthologs belonging to the major vertebrate Chordata subphylum. The † symbol indicates the selective use of the Cx35b protein corresponding to the gjd2b gene. Conserved residues within the Cx36 CT are indicated by the asterisks. Both CaM and CaMKII binding sites appeared to share some overlap with the tubulin-binding motif, potentially indicating*

*competitive or cohesive binding mechanisms. The CaMKII binding motif is outlined in blue, and the CaM motif is in red. (**C-D**) Neuro-2a cells cultured in bathing solution supplemented with 100 µM Colchicine for 1 hour (n=5) or 24 h (n=6) demonstrated a significant reduction in GJ conductance relative to the untreated wild-type (n=6). Data are the mean±SEM, ****, p < 0.0001, Kruskal-Wallis test, each sample was compared to the untreated WT. Time is measured in minutes. (**E-F**) Intracellular perfusion with monomeric tubulin (50µM) (n=5) through the recording electrode was equally sufficient to block an increase in junctional currents in comparison to the untreated WT (n=4). Data are the mean±SEM, ****, p < 0.0001, Mann-Whitney test. Time is measured in minutes.*

In previous studies (Zoidl *et al.*, 2002; Alev *et al.*, 2008; Del Corsso *et al.*, 2012), we have proposed that microtubule-dependent trafficking of Cx36 serves as a potential modality in achieving run-up plasticity by facilitating activity-dependent transport of Cx36 to gap junction plaques. Here, the predicted role of Cx36 in run-up plasticity was demonstrated by dual whole-cell patch-clamp experiments measuring electrical coupling dynamics in pairs of Neuro-2a cells expressing EGFP-tagged Cx36 constructs. Targeted ablation of the putative tubulin-binding motif (Zoidl *et al.*, 2002; Del Corsso *et al.*, 2012) was used to investigate the involvement of this motif in run-up plasticity. In Neuro-2a cell pairs with a gap junction plaque (GJP) present at the juxtamembrane, gap junctional (GJ) conductance increased by a factor of about 10 during a ten-minute recording; by contrast, in cells expressing the Cx36Δ279-292 mutant, this run-up was severely blunted (**Figure S2.2**). This result showed that GJPs formed by Cx36 without the shared binding region for tubulin and CaM/CaMKII had reduced potential for plasticity.

To determine whether a tubulin-specific component was involved in run-up plasticity, the microtubule network was manipulated by bath application with Colchicine, a selective agent which inhibits tubulin polymerization. The application of 100 µM Colchicine for either 1 hr or over-night suppressed the junctional currents approximately 70% (1hr) or 80% (24hrs) compared to untreated controls (*in nS*, WT: 1.17±0.07, n=6; 1hr Colc: 0.23±0.03, n=5, $p < 0.01x10^{-2}$; O/N Colc: 0.33±0.02, n=6, $p < 0.01x10^{-2}$) (**Figure 2.1C-D**). An increase in GJ conductance was reversibly blocked when 100 µM Colchicine was applied for 20 min and washed out afterward (**Figure S2.3**). In a related experiment, monomeric tubulin (50µM) was utilized as a competitive inhibitor to polymerized microtubules, which are known to be responsible for transport mechanisms. Here, intracellular perfusion with monomeric tubulin through the recording electrode was equally sufficient to block the time-dependent increase in junctional currents (in nS, WT: 1.54±0.14, n=4; tubulin: 0.22±0.19, n= 5, $p < 0.01x10^{-2}$) (**Figure 2.1E-F**). These results showed that the inhibition of tubulin polymerization was sufficient to abolish run-up plasticity.

2.2.3 Inhibition of the Cx36-Tubulin Interaction Promotes Intracellular Localization

The involvement of the microtubule network in Cx36 delivery to the plasma membrane was studied by comparing the Cx36Δ279-292 mutant and wild-type control. Forty-eight hours post-transfection, no apparent expression differences were detected by immunoblot analysis (**Figure 2.2A**). Localization studies

confirmed Cx36 protein forming gap junction plaques (GJPs) at the juxtamembrane (**Figure 2.2B**); however, Cx36Δ279-292-expressing cells showed frequent annular junctions (**Figure 2.2C**). Quantitatively, the mean area of Cx36Δ279-292 GJPs was significantly smaller than the WT control (WT: 2.2±0.2 μm^2, n=28; Δ279-292: 1.6±0.1 μm^2, n=26, $p=0.17x10^{-1}$) **(Figure 2.2D)** and less GJPs were formed between cell-pairs expressing Cx36Δ279-292 (WT: 31.11±3.78%, n=30; Δ279-292: 8.72±1.57%, n=30, $p<0.01x10^{-1}$) (**Figure 2.2E**). We conclude that the Cx36Δ279-292 mutation interfered with transport to the cell membrane accounting for the smaller and less frequent GJPs.

To determine the subcellular localization of the tubulin-binding deficient mutant, Cx36Δ279-292-EGFP or the Cx36 wild-type control were co-expressed with mCherry-tagged tubulin or the DsRed-monomeric protein tagged with *(i)* the ER retention signal KDEL, *(ii)* amino acids 1-60 of human galactosyltransferase, or *(iii)* caveolin-1. This approach permitted the visualization of the microtubule network, endoplasmic reticulum (ER), Golgi, and transport vesicles. Mander's overlap coefficient was used to quantify co-localization as the overlap between corresponding fluorescent signals contributed by Cx36 and cell organelles. Cx36Δ279-292 displayed less co-localization to the ER (WT: 0.69 ± 0.04, n = 30; Δ279-292: 0.57 ±0.01, n=25, $p<0.01x10^{-1}$), and Golgi organelles (WT: 0.65 ± 0.03, n = 30; Δ279-292: 0.46±0.04, n= 15, $p<0.01x10^{-1}$), indicating that Cx36 vesicles were not primarily associated with the ER-Golgi complex. A marked reduction in co-localization to the tubulin-cytoskeleton was observed for the Cx36 mutant expression in comparison to the wild-type protein (WT: 0.55±0.02, n=34; Δ279-292: 0.45±0.02, n=36, $p=0.20x10^{-1}$). Co-localization of Cx36Δ279-292 to caveolin-1 was indistinguishable from wild-type (WT: 0.59±0.03, n=40; Δ279-292: 0.58±0.03, n=33, $p=4.09x10^{-1}$) (**Figure 2.2F, Figure S2.4**), however, Cx36Δ279-292 intracellular vesicles were significantly larger (*Vesicular Diameter*, WT: 605±39nm; Δ279-292: 802±50nm, n =50, $p<0.01x10^{-1}$) (**Figure 2.2G**). Our results suggest that the tubulin mediates the transport of Cx36 starting at the ER. Whether the vesicular accumulation of Cx36Δ279-292, following release from the ER-Golgi complex, represents the activation of the unfolded protein stress response or related cellular responses to misfolded or unfolded Cx36 mutant proteins was not investigated.

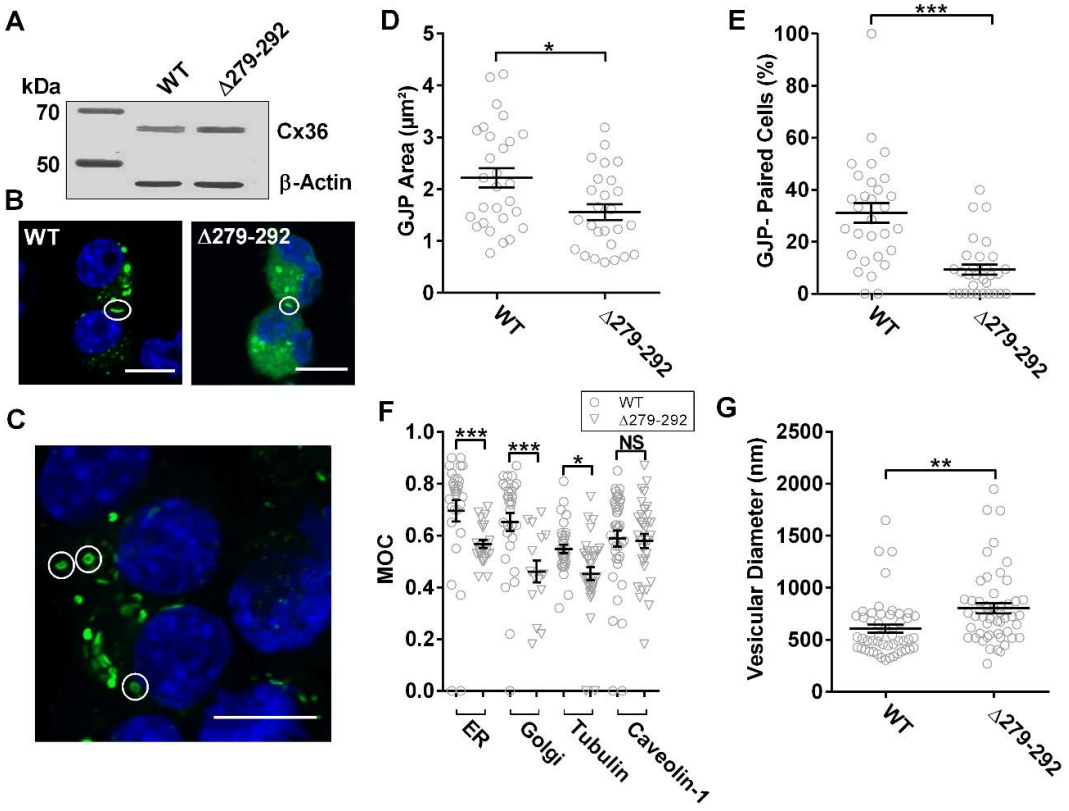

Figure 2.2. Loss of Interaction between Tubulin and Cx36 Promotes Intracellular Localization.

*(**A**) Immunoblot analysis of Neuro-2a cells transiently transfected to express EGFP-tagged wild-type and Δ279-292 Cx36 constructs. Fusion proteins were detected using an anti-EGFP antibody confirming expression. An anti-β-actin antibody served as the loading control; the protein standard is denoted in kDa. (**B-C**) Neuro-2a cells were fixed with formaldehyde and mounted onto slides with DAPI containing media 48hr post-transfection. Cx36 proteins are shown in green. (B) Examples of Cx36 gap junction plaques are indicated by circles. (C) Examples of annular junctions formed in Cx36-Δ279-292 expressing cells, as indicated by circles. Scale bar: 10 μm, Nuclear DAPI staining in blue. (**D-E**) Quantification of GJP size (D) and incidences of GJP-pairings (E) demonstrated a significant reduction in connexon recruitment in cells expressing the tubulin-binding deficient mutant Cx36Δ279-292, indicative of trafficking impairments. Data are mean ± SEM, for GJP area, sample size (n) was 28 and 26 for Cx36 WT and Δ279-292 proteins, respectively. For GJP-paired cells, n = 30 where 10 images were collected in 3 independent experiments. *, p < 0.05, ***, p < 0.0001, Kruskal-Wallis test. (**F**) Co-localization of Cx36 vesicles to organelles was quantified by Mander's overlap coefficient to decipher its intracellular localization. Relative to the wild-type, expression of the tubulin-binding deficient protein resulted in a reduction in ER, Golgi, and tubulin co-localization; caveolin co-localization remained unaffected. Data are mean ± SEM, sample size (n) of WT Cx36 was n = 30 for the ER, n = 30 for the Golgi, n = 34 for tubulin and n = 40 Caveolin-1. Sample size of Cx36-Δ279-292 was n = 35, n = 15, n = 36, and n = 33 for colocalization of the ER, Golgi, tubulin and Caveolin-1 proteins respectively. *, p < 0.05, ***, p < 0.0001, Kruskal-Wallis test, each sample was compared to its corresponding wild-type values. (**G**) Cx36 vesicular diameter of cells co-transfected with caveolin-1 demonstrated an increase in size with mutant expression over wild-type. Data are mean ± SEM, sample size (n) of WT Cx36 was n = 50 vesicles. **, p < 0.001, Kruskal-Wallis test, data was collected from 3 independent experiments.*

The next goal was to elucidate the dynamics of vesicular trafficking of individual vesicles *in vivo* using TIRF microscopy (**Figure 2.3A**). Vesicles with Cx36Δ279-292-EGFP cargo were illuminated in the submembrane space by the evanescent wave known as the TIRF field. These vesicles were less mobile than wild-type controls, demonstrating impairments in both displacement length (WT: 8.70±0.53 μm, n= 475; Δ279-292: 6.36±0.47 μm, n= 304, p= $0.26x10^{-1}$), and mean speed (WT: 0.10±0.01 μm/s; Δ279-292: 0.08±0.01 μm/s, p<$0.01x10^{-1}$) (**Figure 2.3B)**. We concluded that both temporal and spatial mechanisms of trafficking of Cx36 were impacted by the loss of the tubulin binding region.

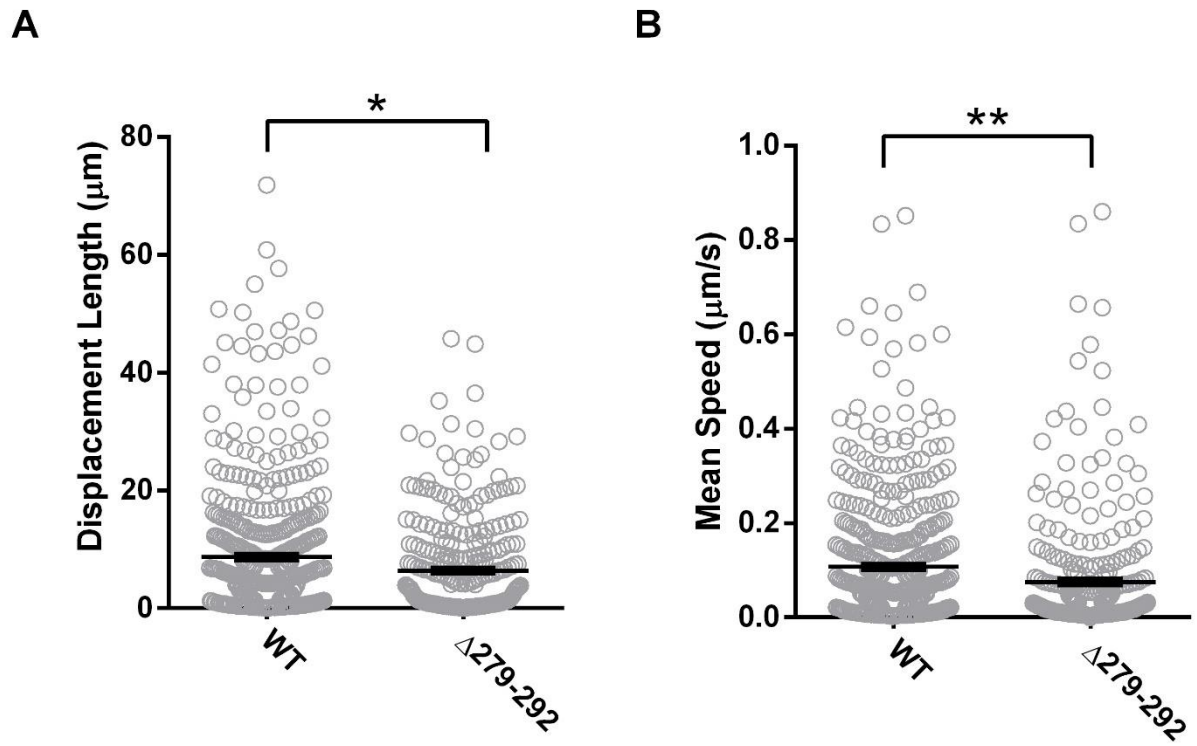

Figure 2.3. Tubulin Interaction Mediates the Spatio-Temporal Delivery of Cx36 Vesicles within the Sub-Membrane.

*(**A-B**) In Cx36-EGFP and tubulin-mCherry co-transfected cells, submembrane vesicular transport was monitored using TIRF microscopy. Mutant expression reduced trafficking as determined by the reduction in (A) displacement (μm) and (B) mean speed (μm/s). Data are mean ± SEM, sample size (n) of WT Cx36 was n = 475 and n= 304 for Cx36 Δ279-292 vesicles. *, p < 0.05, **, p < 0.001, Kruskal-Wallis test.*

How were Cx36 connexons delivered to GJPs in the absence of tubulin binding? In general, connexons can replenish GJPs by two distinct pathways. Targeted direct delivery of connexons to the GJP relies on a complex of cytoskeletal and adherence-junction proteins (Shaw *et al.*, 2007). Alternatively, connexons are routed to the plasma membrane and subsequently recruited into the GJP at the lateral ends (Jordan *et al.*, 1999; Lauf *et al.*, 2002; Thomas *et al.*, 2005). This process occurs despite the ability of microtubules to anchor directly at the GJP (Giepmans, Verlaan and Moolenaar, 2001).

To answer this question, fluorescence recovery after photobleaching (FRAP) was used to determine recovery kinetics of EGFP-tagged Cx36 wild-type or Δ279-292 proteins imaged at 1.0 s intervals pre- and post-bleach iterations. For visualization and quantification of connexon recovery, the fluorescence intensity of each region of interest (ROI) during the post-bleach recovery phase was corrected for background noise and normalized against the pre-bleached fluorescence intensity values. After bleaching, we observed that the plasma membrane (PM) of wild-type Cx36 recovered more efficiently than at the GJP (*mobile fraction (M_f) in %*, GJP: 25.6±0.6, n=28; PM: 69.6±3.6 n=12, $p<0.01x10^{-2}$; *half time of recovery* ($T_{1/2}$), GJP: 11.5s; PM: 23.5s) (**Figure 2.4A, D**). The higher M_f seen at the PM suggested that under control conditions, Cx36 is initially delivered to the plasma membrane and subsequently routed to the plaque, where it becomes stabilized, supporting the mechanisms previously described (Lauf et al. 2002; Thomas et al. 2005; Jordan et al. 1999). In Cx36Δ279-292-expressing cells, the M_f was again higher at the PM than the GJP (GJP: 50±0.5%, n=22; PM: 97.06±1.90%, n=10, $p<0.01x10^{-2}$;), suggesting that no changes were made to the route of delivery. Cx36Δ279-292 expression also led to a $T_{1/2}$ that was faster at the PM and GJP (GJP: 0.9s; PM: 7.3s) than the WT (**Figure 2.4B, D).** We concluded that the interaction with the tubulin cytoskeleton aided in the temporal aspects of Cx36 incorporation from the PM into the GJP, in addition to the quantity of delivery which was verified by GJP size and formation.

In-depth comparisons of FRAP at the GJP revealed that the mutant GJPs were significantly more mobile ($p<0.01x10^{-2}$). This loss of stability was also accompanied by a large reduction in the $T_{1/2}$, reflecting dynamics that were consistent with diffusion outcomes (**Figure 2.4C-D**). Overall, the results advocate for a mechanism in which tubulin interactions aid in the temporal aspects of GJP coalescence, providing a means of regulating the "when" and "how much" of connexon delivery.

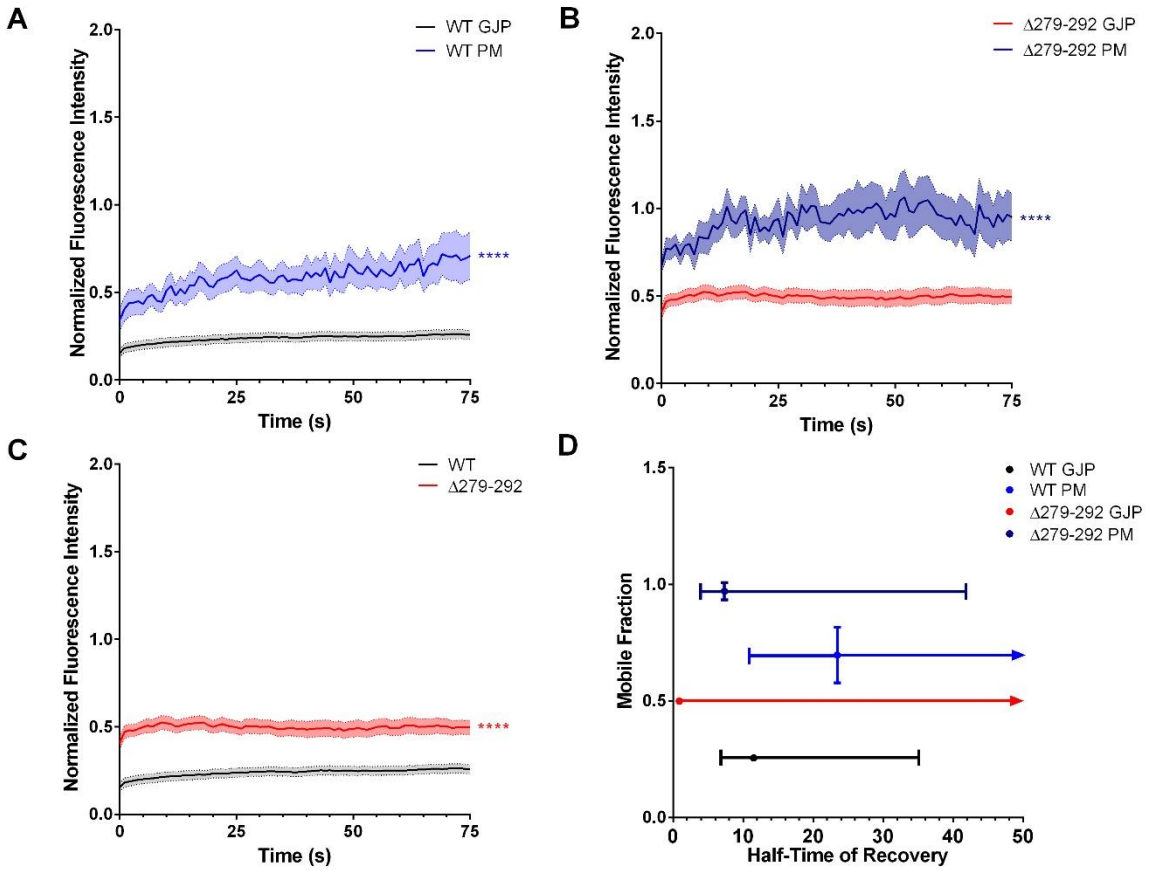

Figure 2.4. Cx36 Connexons are Initially Delivered to the Plasma Membrane via the Tubulin-Cytoskeleton and Diffuse Laterally to the GJP.

*(**A-B**) FRAP microscopy was used to bleach the nonjunctional plasma membrane (PM) and gap junction plaque (GJP) regions of interest (ROI). The averaged fluorescence intensity of each ROI during the recovery phase was normalized to the pre-bleached intensity values and plotted to quantify the relative recovery of fluorescence. In cells expressing Cx36 wild-type (A) and Δ279-292 (B) the plasma membrane (PM) recovered more than at the GJP. Recovery curves are the mean ± SEM. The sample size (n) of WT Cx36 was n = 28 for the GJP and n = 12 for the PM. For Cx36 Δ279-292 the sample size was n = 22 for the GJP and n = 10 for the PM. ****, p < 0.0001, Kruskal-Wallis test. (**C**) An overlap of the GJP curves for the WT (A) and Δ279-292 (B). No significant difference in recovery was found between WT and Δ279-292 at the GJP. (**D**) The plot of the mobile fraction (M_f) against the half-time of recovery ($T_{1/2}$) was extrapolated from the Cx36 WT (A) and Δ279-292 (B) recovery curves. The mobility, as indicated by the M_f, of both WT and Δ279-292 GJPs were lower than their respective PM ROI, suggesting that the GJP was more stable. No differences in mobility were found between the control and mutant protein at the GJPs. However, $T_{1/2}$ for Δ279-292 was faster at the GJP and PM in comparison to the wild-type indicating diffusion was favored over a controlled trafficking mechanism. Data are the mean ± CI.*

2.2.4 Cx36 Transport Correlates to the Modulation of Cytoskeletal Dynamics

Pharmacological manipulation of the microtubule network by bath-application of 100 µM Colchicine, a microtubule destabilizer, or 20 µM Paclitaxel, a microtubule stabilizer, was used to investigate mechanistic details of Cx36 transport to the GJP. Disruption of actin filaments with Cytochalasin D (3 µM)

was included in this investigation since both tubulin, and actin-dependent transport has been found at chemical synapses (Coles and Bradke, 2015), and for the connexin protein Cx43 (Epifantseva and Shaw, 2018). Immunoblot analysis and localization studies 48 h post-transfection confirmed Cx36 expression and recruitment into the GJPs at the juxtamembrane (**Figure 2.5A-B**). Treatments had no impact on the total Cx36 protein expression (**Figure 2.5A**), however, GJP areas were reduced relative to the untreated wild-type (Colchicine: 1.4±0.2µm², n=15, $p=3.00x10^{-3}$; Paclitaxel: 1.4±0.2 µm², n=17, $p=7.00x10^{-3}$; Cytochalasin D: 1.7±0.2µm², n= 26, p=0.01) (**Figure 2.5C**). GJP formation was uniformly reduced in frequency across all treatments in comparison to the untreated wild-type (Colchicine: 6.67±1.42%, $p<0.01x10^{-1}$, Paclitaxel: 10.49±2.21%, $p<0.01x10^{-1}$, Cytochalasin D: 7.34±1.34%, $p<0.01x10^{-1}$) (**Figure 2.5D**). This outcome suggested that an intact and dynamic tubulin-cytoskeleton could facilitate connexon delivery to the cell membrane. Additionally, the reduction in GJP formation by Cytochalasin D treatment suggested that the actin-cytoskeleton contributed to Cx36 delivery, but mechanistic details were not further investigated.

Co-expression of wild-type Cx36-EGFP and tubulin-mCherry, revealed that Cx36 co-localization (overlap coefficient) to the tubulin-cytoskeleton was significantly impaired with both Colchicine (WT: 0.59±0.03, n=40; Colchicine: 0.12±0.07, n= 21, $p<0.01x10^{-1}$) and Paclitaxel treatment (0.44±0.03, n=45, $p=3.00x10^{-3}$). Considering that Paclitaxel stabilizes microtubules, yet less Cx36 interacted with the tubulin-cytoskeleton, we proposed that the binding of paclitaxel creates a steric hindrance for Cx36 binding. In this way, paclitaxel treatment acts as a competitive inhibitor, controlling the quantity of Cx36 able to bind to tubulin. Our results reaffirmed that Cx36 preferentially interacts with an intact and dynamic tubulin-cytoskeleton, promoting transport to the plasma membrane and subsequent coalescence at the GJP. Treatment with Cytochalasin D had no effect on Cx36 co-localization to the tubulin-cytoskeleton (0.58±0.01, n=38, $p=2.43x10^{-1}$) (**Figure 2.5E, Figure S2.5**). This confirmed that the interaction between Cx36 and the tubulin-cytoskeleton was not interdependent on the interactions or stability of the actin-cytoskeleton.

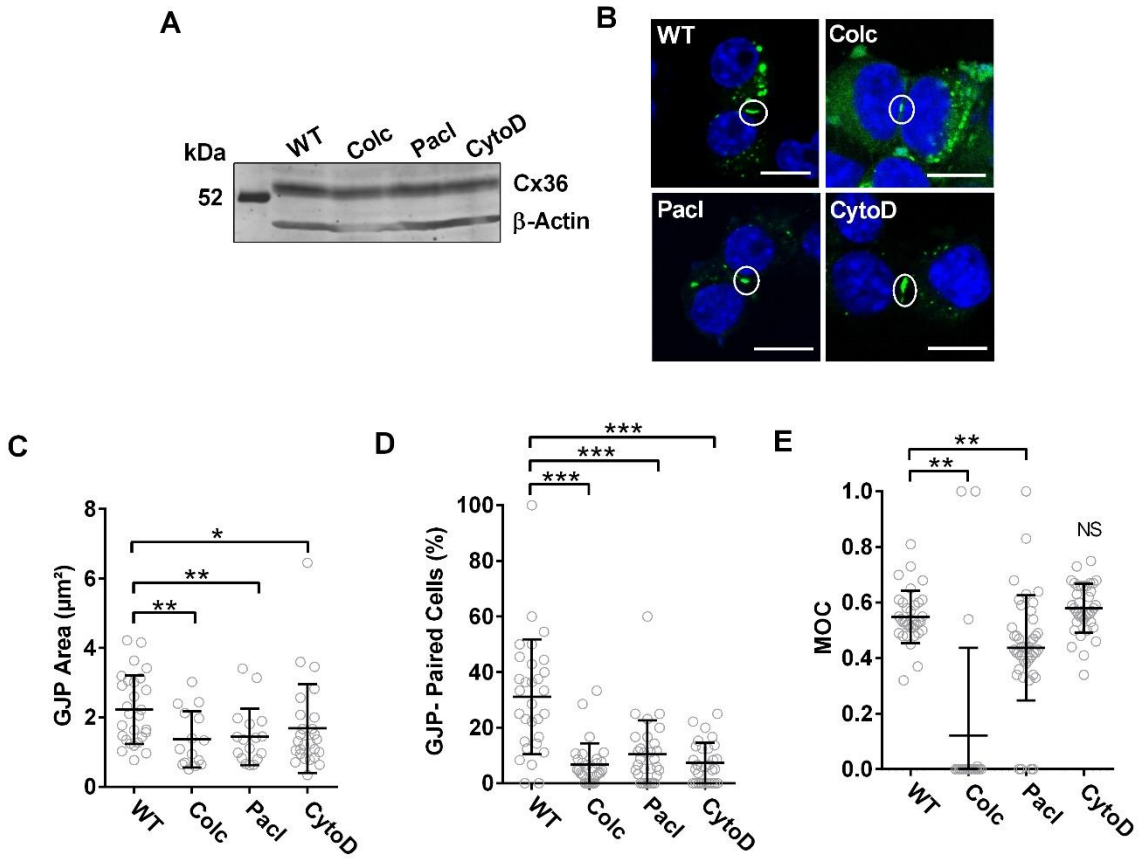

Figure 2.5. Pharmacological Manipulation of the Cytoskeletal-Network Inhibits Cx36 Recruitment.

*(**A**) Immunoblot analysis of Neuro-2a cells transiently transfected to express wild-type Cx36-EGFP and subsequently treated with Colchicine (Colc), Paclitaxel (Pacl), or Cytochalasin D (CytoD). No differences in the expression levels were noted. Cx36 protein was detected using an anti-EGFP antibody, and an anti-β-actin antibody was used to detect actin as the loading control. The protein standard is denoted in kDa. (**B**) Neuro-2a cells were fixed with formaldehyde and mounted onto slides with DAPI containing media 48hr post-transfection. Cx36 proteins are shown in green. Formation of GJPs in vivo under pharmacological manipulation of the tubulin-cytoskeleton (Colchicine and Paclitaxel) or the actin-cytoskeleton (Cytochalasin D). Circles indicate GJPs. Scale bar: 10 µm, nuclear DAPI staining in blue. (**C-D**) Quantification of GJP area (C) and incidences of GJP formation (D) revealed severe impairments under all pharmacological treatments tested. Data are mean ± SEM. For GJP area, sample size (n) was 28 for the WT, n = 15 for Colchicine, n = 17 for Paclitaxel and n = 26 for Cytochalasin D. For GJP-paired cells, n = 30 where 10 images were collected in 3 independent experiments. *, $p < 0.05$, **, $p < 0.001$, ***, $p < 0.0001$, Kruskal-Wallis test, all samples were compared to the WT control. (**E**) Co-localization studies were performed between Cx36 and the tubulin-cytoskeleton; co-localization was expressed using Mander's overlap coefficient. Treatment with Colchicine and Paclitaxel reduced Cx36-tubulin co-localization, suggesting tubulin must be intact to support sufficient Cx36 interaction. Treatment with Cytochalasin D had no impact on the co-localization of Cx36 to the tubulin. Data are mean ± SEM. Sample size (n) indicated the number of cells measured for tubulin co-localization was n = 34 for the WT, n = 21 for the Colchicine, n = 45 for Paclitaxel, and n = 38 for Cytochalasin D. **, $p < 0.001$, Kruskal-Wallis test, all samples were compared to its corresponding WT values.*

TIRF trafficking measurements revealed no significant differences in displacement length (WT: 8.71±0.53 µm n= 475; Colchicine: 6.45±0.43 µm, n= 337, p= $3.01x10^{-1}$) or mean speed (WT: 0.11±0.01 µm/s; Colchicine: 0.07±0.01 µm/s, p<$0.75x10^{-1}$) with Colchicine treatment in comparison to the untreated wild-type. To consider the effectiveness of drug treatment in an over-expression model and the sensitivity of TIRF detection under these circumstances, the experiments were repeated in single transfected cells for Cx36-EGFP. Here, colchicine application significantly impaired the displacement length (WT: 9.86±0.64 µm n= 271; Colchicine: 7.04±0.60 µm, n= 130, p= $0.16x10^{-1}$) and mean speed (WT: 0.09±0.01 µm; Colchicine: 0.05±0.01 µm, p= $0.02x10^{-1}$). In double transfected cells, Paclitaxel treatment also impaired vesicular transport (displacement length: 4.48±0.40 µm, p<$0.01x10^{-1}$; mean speed: 0.05±0.01 µm/s, p<$0.01x10^{-1}$, n=215) emphasizing the importance of a dynamic tubulin-cytoskeleton on trafficking vehicles *in vivo.* Since paclitaxel treatment was sufficient to establish a response in the TIRF field, a single transfected analysis was not further explored. To account for the actin-contribution, Cytochalasin D treatment was also included here. Inhibition of vesicular transport was also apparent with Cytochalasin D treatment (*displacement*, 3.89±0.33 µm, n=237, p<$0.01x10^{-1}$; *mean speed*, 0.06±0.01 µm/s, p<$0.01x10^{-1}$), suggesting that actin can serve as a compensatory modality for Cx36 transport and confirming that Cx36 delivery to the PM is both actin- and tubulin-dependent (**Figure 2.6**).

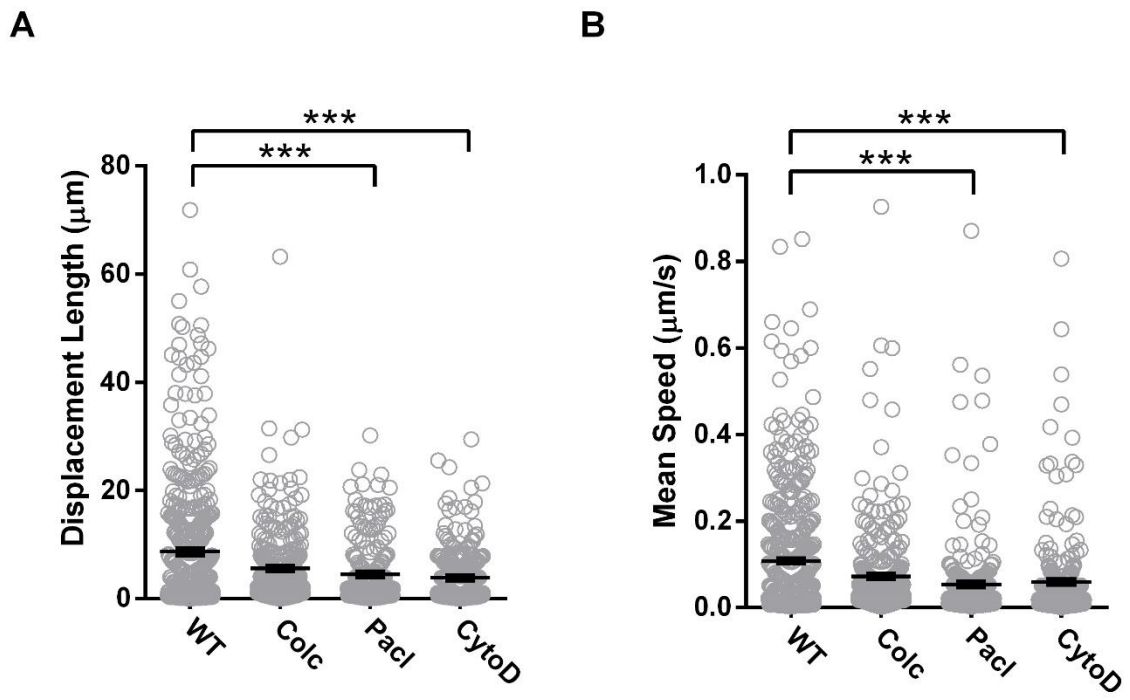

Figure 2.6. Transport and Incorporation of Cx36 into the GJP is Dependent on an Intact Actin- and Tubulin-Cytoskeleton.

*(**A-B**) Vesicular transport within the submembrane region was monitored using TIRF microscopy to determine the (A) displacement (μm) and (B) speed (μm/s) of Cx36 vesicles. Colchicine (Colc) did not significantly affect Cx36 vesicular trafficking. However, both Paclitaxel (Pacl) and Cytochalasin D (CytoD) treatment resulted in a significant reduction in trafficking when administered to Neuro-2a cells. Data are mean ± SEM, sample size (n) was n = 475 for WT, n = 294 for Colchicine, n = 215 for Paclitaxel and n = 237 for Cytochalasin D treated vesicles. ***, p < 0.0001, Kruskal-Wallis test, all samples were compared to the WT control.*

At the GJP, cytoskeletal interference resulted in a $T_{1/2}$ that was uniformly faster across all treatment groups (WT: 11.5s, n=28, Colchicine: 1.3s, n=26; Paclitaxel: 0.6s, n=24; Cytochalasin D: 0.8s, n=22). Here, the incorporation of Cx36 into the GJP after actin- or tubulin-cytoskeletal disruption was consistent with diffusion dynamics (**Figure 2.7**). Similar to results shown earlier (**Figure 2.4**), disruption of the tubulin cytoskeleton with Colchicine increased the M_f at the GJP (WT: 25.59±0.60%, Colchicine: 46.35±0.40%, $p<0.01x10^{-2}$). No significant difference in recovery was found with Paclitaxel treatment (34.70±0.30%, p >0.99), likely attributable to the direct stabilization of the GJP via tubulin stabilization. Although the GJP remained stable under paclitaxel treatment, it is important to highlight that transport into the GJP was impaired, as shown previously (**Figures 2.5 and 2.6**). In this regard, tubulin acts separately, first as a conduit for Cx36 transport and secondly as a GJP stabilizer in the Neuro-2a cell model. Regardless, Cx36 mobility was not completely abolished following tubulin disruption, inferring that the actin-cytoskeleton may provide a secondary transport modality. In support, Cytochalasin D treatment significantly increased

GJP mobility (55.41±0.40%, $p<0.01x10^{-2}$) (**Figure 2.7**), confirming that the actin-cytoskeleton contributes to Cx36 delivery and stabilization at the GJP.

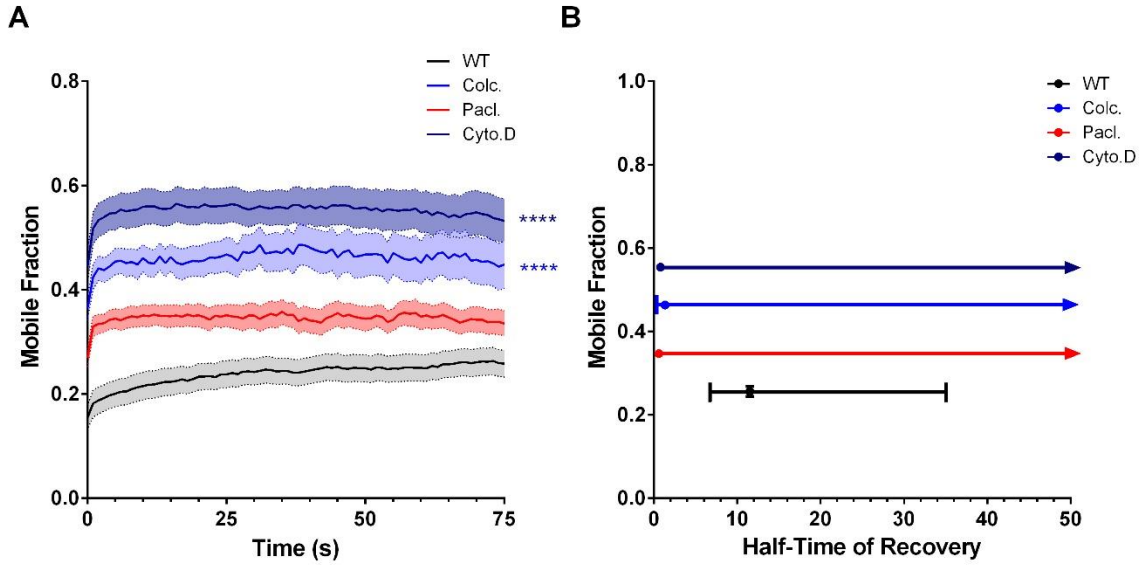

Figure 2.7. Cytoskeletal Manipulation Alters Cx36 Delivery at the GJP.

(A-B) *Recovery of fluorescence curves (A) and corresponding plots for Mf against T1/2 (B) demonstrated the relationship between the mobile fraction and half-time of recovery. The Mf and T1/2 under Colchicine (Colc) and Paclitaxel (Pacl) treatment demonstrated a significant reduction. While the T1/2 remained lower than the untreated wild-type, inhibition of the actin-cytoskeleton with Cytochalasin D (CytoD) resulted in an increase in the mobile fraction, indicating that GJPs became more fluid, suggesting that actin may play a role in fine-tuning Cx36 incorporation at the GJP. Recovery curves are the mean ± SEM and mean ± CI for the XY plots of mobile fraction against half-time of recovery. Sample size (n) was n = 28 for the WT, n = 26 for Colchicine, n = 24 for Paclitaxel, and n = 22 for cytochalasin treated GJPs. ****, p < 0.0001, Kruskal-Wallis test, all samples were compared to the wild-type control.*

2.2.5 Characterization of the Tubulin-Binding Motif

A previous report demonstrated that a 26 amino acid peptide of Cx43 mediates binding to α- and β- tubulin isoforms. This region adopts a helical conformation upon binding to tubulin and is regulated by phosphorylation (Saidi Brikci-Nigassa *et al.*, 2012). Here, we explored whether Cx36 might have a similar binding mechanism using structural modeling of the Cx36 carboxyl-terminal domain. The calmodulin-binding region overlaps the Cx36 CT tubulin-binding region and is known from NMR structural studies to form an amphipathic helix (Siu *et al.*, 2016). With this knowledge, a sequence comparison was made between the Cx36 tubulin-binding region and an engineered helix derived from the stathmin and stathmin-like domain (SLD) family of proteins that were known to prevent microtubule formation by binding multiple α- and β-tubulins (Mignot *et al.*, 2012). From this comparison, we concluded that the Cx36 tubulin-binding region had significant sequence similarity to a portion of the SLD that interacts exclusively with α-

tubulin. A sequence comparison, a helical wheel representation of SLD and Cx36, and a molecular view of the SLD-tubulin interaction are presented in **Figure 2.8**. For both the engineered SLD and Cx36, the contacts made by their respective amphipathic helices appear to favor four hydrophobic amino acids with possibly a bulkier amino acid at first position (L47 in SLD and W277 in Cx36), followed by two basic amino acids that make critical ionic contacts near the tubulin α/β interface. An alternative model for a potential Cx36-tubulin interaction was considered using the structure of a centrosomal-P4.1-associated-protein (CPAP) peptide bound to an alpha-beta tubulin heterodimer (Zheng *et al.*, 2016), but subsequently discounted due to poor sequence and secondary structure similarity.

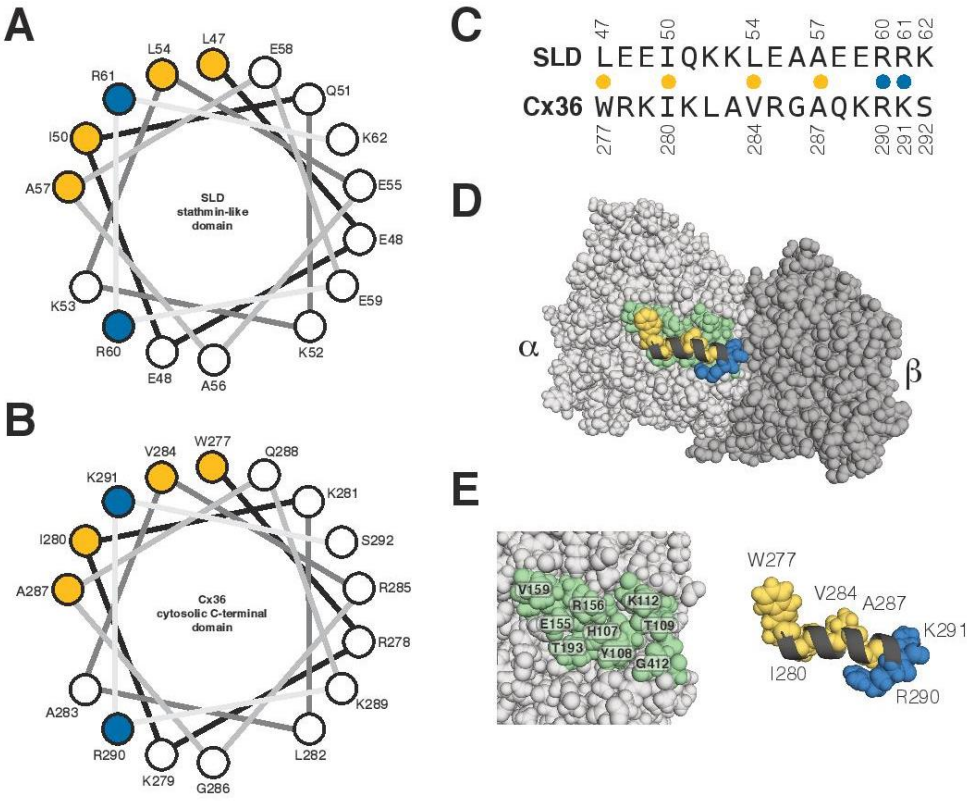

Figure 2.8. Structural Modeling of the CT.

*A model of the interaction between Cx36 and tubulin. When sequence and secondary structure similarity are considered together, the crystal structure of an engineered stathmin-like domain (SLD) and an alpha/beta-tubulin protofilament (PDB: 1Z2B) emerges as a possible template to consider an analogous Cx36 interaction. (**A-B**) Helical wheel representations of the relevant regions of the SLD (47-62) and Cx36 (277-292) with key amino acids colored at the interface according to either hydrophobicity (orange) or charge (blue). **(C)** A sequence comparison following the same scheme as the helical wheel. (**D-E**) Three views of a Cx36/tubulin model highlighting the potential contacts made between Cx36 (black ribbon) and alpha-tubulin (light grey and green). Models were created in PyMOL v1.86.*

Sequential alanine-scanning mutagenesis from K279 to G286 was performed to investigate positional roles of individual amino acids in supporting the binding and physiological mechanisms between Cx36 and tubulin. In contrast to the similar expression observed between Cx36Δ279-292-EGFP and WT Cx36 (**Figure 2.2A**), all point mutants were expressed at lower and variable levels in comparison to the wild-type protein (**Figure 2.9A**). Nonetheless, all mutants formed GJPs at the juxtamembrane (**Figure 2.9B**), with a significant reduction in GJP size (K279A: 0.9±0.2 μm², n=7, $p<0.01x10^{-1}$; I280A: 1.7±0.3 μm², n=19, $p=1.60x10^{-2}$; K281A: 1.1±0.1 μm², n=9, $p=1.00x10^{-3}$; L282A: 1.3±0.1 μm², n=16, $p=3.00x10^{-3}$; V284A: 1.1±0.2 μm², n= 26, $p<0.01x10^{-1}$; R285A: 1.6±0.3 μm², n=12, $p=2.90x10^{-2}$; G286A: 1.1±0.2 μm², n=10, $p=1.00x10^{-3}$) **(Figure 2.9C)**. Specific targeting of the conserved residues, K279A, V284A, and G286A, resulted fewer detected GJPs across cell pairs (n=30, K279A: 8.72±1.57%, $p<0.01x10^{-1}$; V284A: 18.37±3.16%, $p=8.00x10^{-3}$; G286A:12.54±2.67%, $p=0.01x10^{-1}$) **(Figure 2.9D)**, as did most non-conserved residues (I280A: 12.09±2.367%, $p<0.01x10^{-1}$, K281A: 12.26±2.13%, $p<0.01x10^{-1}$, R285A:16.31±2.77%, $p=0.06x10^{-1}$). Cx36-L282A was indistinguishable from the wild-type control (L282A: 24.83±4.90%, $p=0.32x10^{-1}$).

Cells co-expressing mCherry-tubulin with Cx36 I280A had a severe reduction in colocalization (*overlap coefficient*, 0.26±0.05, n=37, $p<0.01x10^{-1}$). Amino acids K279A and K281A also had a marked reduction in co-localization to the tubulin cytoskeleton (*overlap coefficient*, K279A 0.37±0.04, n=36, $p=2.10x10^{-2}$; K281A: 0.41±0.05, n=37, p=0.02), suggesting that amino acids in position 279 to 281 have a significant role in direct binding or anchoring to tubulin. The remaining mutants were indistinguishable from the wild-type (*overlap coefficient*, L282A: 0.41±0.06, n=36, $p=5.30x10^{-2}$; V284A: 0.48±0.04, n=43, $p=3.18x10^{-1}$; R285A: 0.49±0.04, n=26, $p=3.62x10^{-1}$; G285A: 0.44±0.05, n=26, $p=2.19x10^{-1}$) (**Figure 2.9E, Figure S2.6**). Based on the 3D structural model and co-localization results, we propose that Cx36 adopts a similar binding mechanism to SLD; however, *in vivo* the downstream adjacent amino acids K279A, I280, and K281 appear to support most interactions.

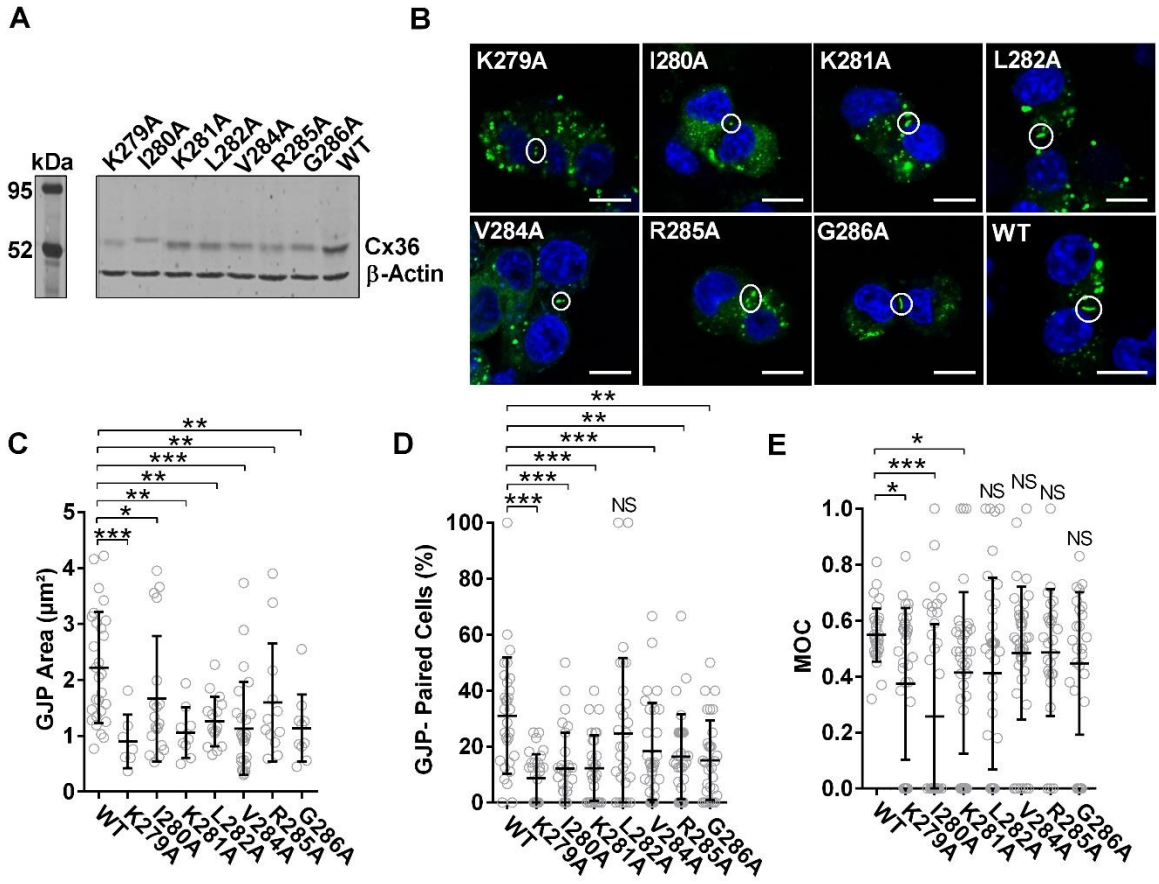

Figure 2.9. The Cx36-Tubulin Protein Interface is Sensitive to Targeting Single Amino Acids.

*(**A**) The tubulin binding motif (corresponding to amino acids Lys279-G286) was targeted by alanine scanning mutagenesis. Immunoblot analysis of Neuro-2a cells transiently transfected to express EGFP-tagged wild-type and mutant constructs reveals variable expression. Proteins were detected using an anti-EGFP antibody. An anti-β-actin antibody was used as the loading control; the protein standard is denoted in kDa. (**B**) Neuro-2a cells were fixed with formaldehyde and mounted onto slides with DAPI containing media 48hr post-transfection. Cx36 proteins are shown in green. The formation of GJPs at the juxtamembrane was confirmed in vivo using confocal microscopy post-mutagenesis. Boxes indicate GJPs. Scale bar: 10 μm, nuclear DAPI staining in blue. (**C**) Quantitatively, a severe reduction in GJP size was observed across all Cx36 mutants. Data are mean ± SEM. Sample size (n) were the following, WT: 28, K279A: 7, I280A: 19, K281A: 9, L282A: 16, V284A: 26, R285A: 12, and G296A: 10 GJPs. *, $p < 0.05$, **, $p < 0.001$, ***, $p < 0.0001$, Kruskal-Wallis test, all samples were compared to the WT control. (**D**) The formation of GJPs between cell-cell contacts was impacted when both the residues conserved between Cx36 and Cx43, Cx36 -K279, -V285, and -G286, and non-conserved residues Cx36-I280, -K281, and G285 were targeted. The sample size for GJP-paired cells was n = 30, where ten images were collected in 3 independent experiments. **, $p < 0.001$, ***, $p < 0.0001$, Kruskal-Wallis test, all samples were compared to the WT control. (**E**) Co-localization to the tubulin cytoskeleton was reduced with Cx36 K279A, I280A, and K281A expression. Sample size (n) were the following, WT: 34, K279A: 36, I280A: 37, K281A: 37, L282A: 36, V284A: 43, R285A: 26, and G296A: 26 cells. *, $p < 0.05$, ***, $p < 0.0001$, Kruskal-Wallis test, all samples were compared to the WT control.*

To investigate the impact of positional amino acid alterations on vesicular transport, displacement length and speed were determined by TIRF microscopy. A reduction in displacement length was observed across select mutants tested (K281A: 5.76±0.47 µm, n=273, $p<0.01x10^{-1}$; R285A: 9.79±0.60 µm, n=302, $p<0.01x10^{-1}$; G286A: 9.64±0.58 µm, n=286, $p=0.02x10^{-1}$). All else were indistinguishable from the WT (K279A: 8.88±0.58 µm, n=390, $p=5.94^{-1}$; I280A: 7.80±0.59 µm, n=237, $p=8.80^{-1}$; L282A: 7.57±0.53 µm, n=244, $p=9.57x10^{-1}$; V284A: 8.69±0.50 µm, n=423, $p=1.11x10^{-1}$) **(Figure 2.10A)**. Similarly, mean speed was reduced exclusively for K281A, R285A and G286A mutations (K281A: 0.08±0.01 µm/s, $p<0.01x10^{-1}$; R285A: 0.11±0.01 µm/s, $p<0.01x10^{-1}$; G286A: 0.01±0.01 µm/s, $p=1.70x10^{-2}$) and all else were indistinguishable from the WT (K279A: 0.01±0.01 µm/s, $p=4.46x10^{-1}$; I280A: 0.11±0.01 µm/s, $p=6.01x10^{-1}$; L282A: 0.10±0.01 µm/s, $p=6.40x10^{-1}$; V284A: 0.10±0.01 µm/s, $p=2.38x10^{-1}$) (**Figure 2.10B**). Together with GJP size, formation and co-localization ability, our results have identified segregated functionality within the binding motif, specific to either the binding or trafficking mechanisms.

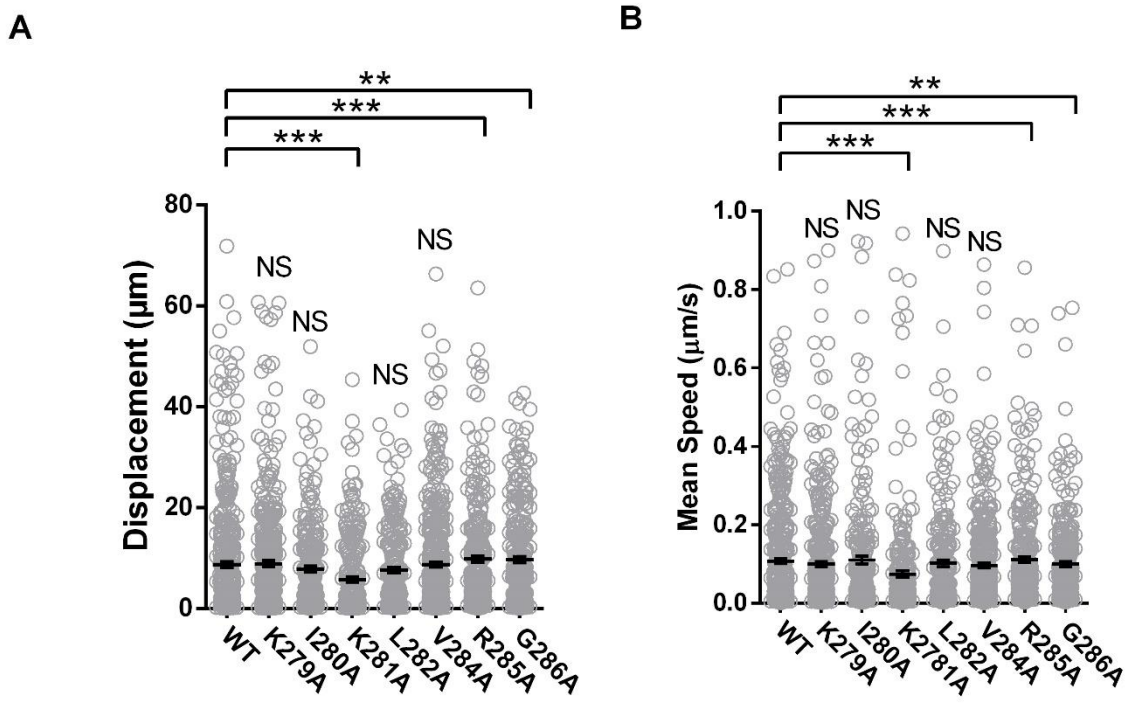

Figure 2.10 Reduced Trafficking of Cx36 Vesicles Post-Alanine Mutagenesis.

*(**A-B**) Submembrane vesicular transport of the point mutant constructs was resolved using TIRF microscopy in Neuro-2A cells. Cx36 K281A, R285A, and G286 mutants significantly disrupted displacement (A) and the mean speed (B). As such, positional interference of the tubulin binding motif was sufficient to disrupt spatiotemporal aspects of protein trafficking. Data are mean ± SEM. Sample size (n) were the following, WT: 475, K279A: 390, I280A: 237, K281A: 273, L282A: 244, V284A: 423, R285A: 302, and G296A: 286 vesicles. **, p < 0.001, ***, p < 0.0001, Kruskal-Wallis test, all samples were compared to the WT control.*

Similar to the deletion mutant Cx36Δ279-292, a faster $T_{1/2}$ was recorded for several mutants in comparison to the wild-type control in FRAP investigations (WT: 11.5s, K279A: 2.2s, n=10; I280A: 0.9s, n=20; L282A: 3.5s, n=23; R285A: 47.8s, n=22). Furthermore, these select mutants displayed a significantly higher M_f (WT: 25.59±0.60%, K279A: 41.50±050%, $p<0.01x10^{-2}$; I280A: 46.16±0.50%, $p<0.01x10^{-2}$; L282A: 40.60±0.60%, $p=0.07x10^{-2}$; R285A: 44.28±13.8, $p<0.01x10^{-2}$). Our results confirmed that single amino acid changes affected the mobility of Cx36, again highlighting the sensitivity of this motif. Amongst these mutants, a less controlled mechanism of GJP incorporation, through the loss of protein-binding partnerships, was promoted. Consistent with our previous model (**Figure 2.8**) outlining K281 as critical in the tubulin-Cx36 binding mechanism, this positional mutation resulted in the highest increase in mobility (60.58±10.40%, n=15, $p<0.01x10^{-2}$), paired with an excessive increase in $T_{1/2}$ (32.18s) (**Figure 2.11**). Please note that a curve fit for V284A and G286A mutations using a monoexponential association equation consistently for all other mutants was not possible, and a detailed analysis of M_f and $T_{1/2}$ could not be provided. However, recovery ability was significantly different from that of the wild-type control (V284A: N= 19, $p<0.01x10^{-2}$; G286A: n=14, $p<0.01x10^{-2}$) (**Figure 2.11**).

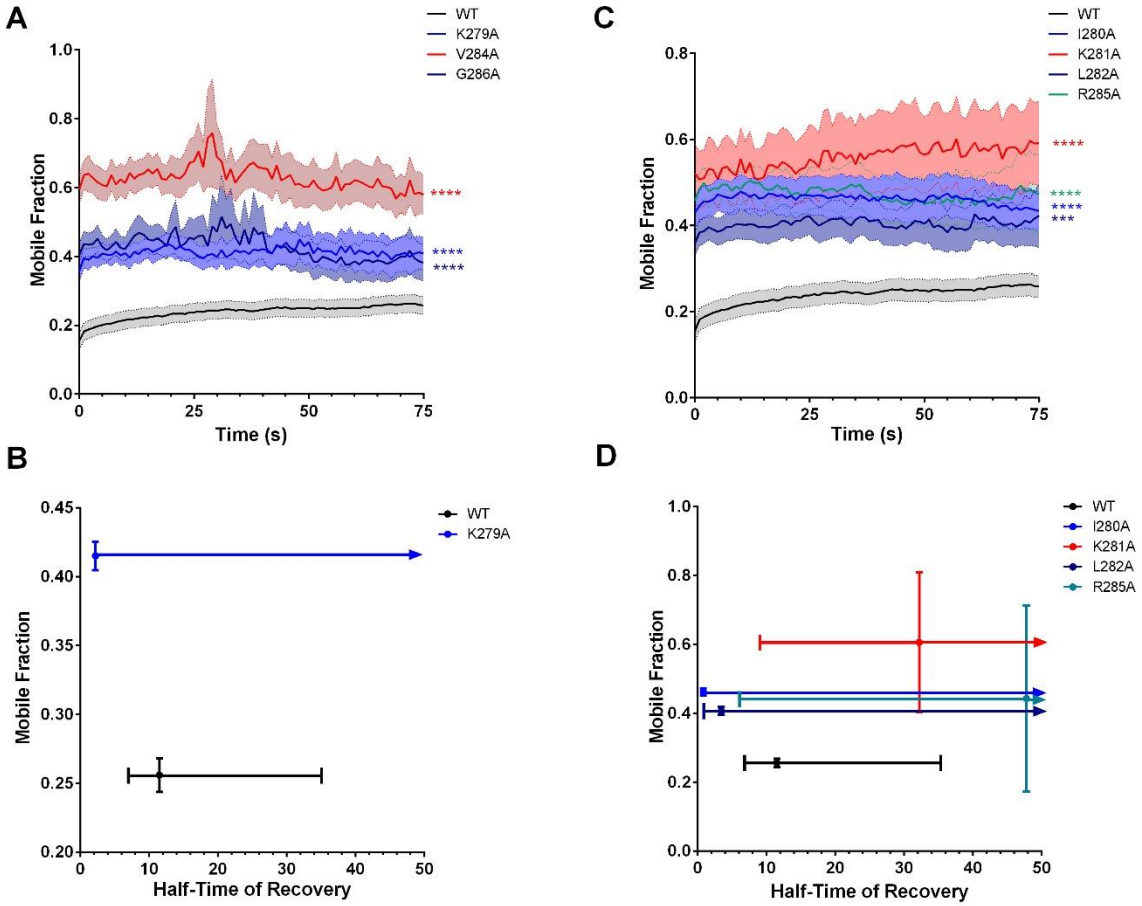

Figure 2.11. Recovery of Cx36 at the GJP was Impaired after Targeting Individual Amino Acids within the Tubulin Binding Motif.

*Repopulation of connexons at the gap junction plaque was significantly impaired in all mutants targeted in the site-directed alanine scan of the tubulin binding motif. (**A-B**) Recovery plot and corresponding XY scatterplot illustrating the relationship between the mobile fraction (%) and half-time of recovery (s) of the residues conserved between Cx36 and Cx43 in the tubulin-binding motif. Recovery curves are the mean ± SEM and mean ± CI for the XY plots of mobile fraction against half-time of recovery. Sample size (n) was n = 28 for the WT, n = 10 for K279A, n = 19 for V284A and n = 14 for G286A GJPs. ****, p < 0.0001, Kruskal-Wallis test, all samples were compared to the wild-type control. Please note that curve fitting for V284A and G286A was not possible; therefore, neither are diagramed here. (**C-D**) Recovery plot of the corresponding M_f vs. $T_{1/2}$ plot non-conserved residues. Since curve fitting was unsuccessful for Cx36-R285A, it was not reported in the M_f vs. $T_{1/2}$ scatterplot. Deviations in the M_f and $T_{1/2}$ suggest that alternations to the tubulin-binding motif were sufficient to provoke phenotypes similar to the complete ablation of the tubulin-binding motif. Recovery curves are the mean ± SEM and mean ± CI for the XY plots of mobile fraction against half-time of recovery. Sample size (n) was n = 28 for the WT, n = 20 for I280A, n = 15 K281A, n = 23 for L282A, and n = 22 for R285A GJPs. **, p < 0.001, ****, p < 0.0001, Kruskal-Wallis test, all samples were compared to the wild-type control.*

2.2.6 Discussion

This research uses a neuroblastoma model of synaptic plasticity to explore the interactions between Cx36 and tubulin. By sequence similarity to Cx43 (Giepmans *et al.*, 2001), a tubulin-binding motif was identified in the carboxy-terminal tail of Cx36. In experimental support, the previously reported binding of

tubulin with the carboxyl-terminal tail of Cx36 (Alev, Zoidl and Dermietzel, 2013) was confirmed independently here using a BioID assay. The Cx36 binding motif is highly conserved and unique among connexin isoforms as it shares its interaction surface amongst tubulin, CaM, and CaMKII binding partners. Typically, CaM binding motifs in other connexins are located in different positions in the amino-terminus (Cx32), cytoplasmic loop (Cx43, Cx44, Cx50), or in a non-overlapping region within the CT domain (Cx32) (Zhou *et al.*, 2007, 2009; Dodd *et al.*, 2008; Myllykoski, Kuczera and Kursula, 2009; Xu *et al.*, 2012; Mruk *et al.*, 2014). Binding of CaMKII to other connexins than Cx36 has not been reported.

2.2.6.1 In-depth Analysis of the Cx36-Tubulin Binding Domain Reveals its Uniqueness

The Cx36 tubulin-binding motif differs from other microtubule-binding motifs found in proline-rich regions of several microtubule-associated proteins (MAPs) or the motor proteins kinesin and dynein. For example, the microtubule-binding motif in both motor proteins has a P-X_6-E-X_4-L core consensus sequence, surrounded by several conserved polar, hydrophobic, and charged amino acids (Witman, 1992; Wilkerson, King and Witman, 1994). Similarly, the tubulin-binding motif of Cx36 is enriched in hydrophobic (isoleucine, leucine, arginine, and valine) and electrically charged basic (arginine and lysine) amino acids. However, the absence of a proline-rich region appears to be a significant and unique property of the Cx36-tubulin motif.

Three-dimensional structural modeling of the Cx36-tubulin binding site to the engineered stathmin-like domain (SLD) predicted similarities between Cx36 and SLD. The Cx36 carboxyl terminus is likely to adopt a helical structure upon binding with tubulin, similar to previous reports on Cx43-tubulin interaction (Saidi Brikci-Nigassa *et al.*, 2012). The previously resolved NMR structure of the Cx36-CaM binding complex suggests that a helical structure is formed as early as interaction with calcium-activated CaM occurs in the ER-Golgi complex (Siu *et al.*, 2016). Siu et al. (2016) have also shown that CaM binding strongly relies on access to W277 and intracellular calcium. The new experimental evidence supports the roles of individual amino acids downstream of W277, with I280 and adjacent amino acids K279 and K281 critical in the Cx36-tubulin binding mechanism as demonstrated by co-localization studies and consistent with the structural model. Noteworthy, phosphorylation of S293 (Urschel *et al.*, 2006; Li *et al.*, 2013; Helen Yanran Wang *et al.*, 2015) downstream of the overlapping tubulin/CaM/CaMKII binding site decreases GJ communication suggesting that competitive and cooperative mechanisms exist side-by-side in a protein domain encompassing less than 20 amino acids (Bazzigaluppi *et al.*, 2017). Consistent with other studies (Hendsch and Tidor, 1994; Sindelar, Hendsch and Tidor, 1998; Zeroka, Jensen and Samuels, 1998; Lombardi *et al.*, 2000; Kumar and Nussinov, 2002; Calhoun *et al.*, 2005), we anticipate that salt bridges formed by the lysine residues contribute to protein stability and specificity driving molecular recognition and catalysis between protein interfaces. We also found that site-directed alanine mutagenesis produced

variability in protein expression levels which were not previously observed with the expression of Cx36Δ279-292. Since large amino acid deletions in the loop, helix, and terminal positions are generally more tolerated than substitutions (Simm *et al.*, 2007; Arpino *et al.*, 2014), we concluded that the Cx36 tertiary structure and functionality were likely compromised, leading to expression variability. Again, we believe this advocated for the significance of positional non-covalent interactions to sustain both the protein itself and protein-protein interfaces.

Expression of Cx36Δ279-292 reduced co-localization to the ER-Golgi complex yet increased co-localization to caveolin-1 vesicles. Although the ER stress response was not further explored in this study, considering that the protein expression between wildtype and mutant was equivalent, it is unlikely that the endoplasmic reticulum-associated degradation (ERAD) pathway was activated. Instead, it is more likely that the mutant protein is prematurely released from the ER-Golgi prior to its packaging into vesicles. Alternatively, since we have demonstrated that Cx36Δ279-292 is still transport-competent, a faster mechanism of transport may be favored. It is currently unclear whether oligomerization of the mutant protein is impacted once packaged into vesicles, as this would need to be resolved via super-resolution microscopy. Nevertheless, we observed an increase in the association between Cx36Δ279-292 and caveolin-1 vesicles. Since we acknowledge that tubulin-transport umbrellas both forward and reverse aspects of trafficking, this accumulation of protein in vesicles reflects the defects in transport following ER-Golgi release, enhanced internalization from the PM, and/or a combination of both.

2.2.6.2 Exploring the Mechanisms and Kinetics of Cx36 Transport into the GJP

The pharmacological manipulation of the microtubule network and genetic manipulation of the tubulin-binding motif confirmed that the trafficking of Cx36-carrying vesicles and the formation of GJPs were critically dependent on an intact and functionally dynamic cytoskeleton. The processes observed appear to follow the generally accepted chain of events in which hemichannels packaged in vesicles emerge from the Golgi and reach the cell membrane via microtubules, which have multiple insertion sites all over the cell surface (Jordan *et al.*, 1999; Lauf *et al.*, 2002; Thomas *et al.*, 2005). After that, hemichannels form clusters of gap junctions known as plaques at cell-cell borders. In addition to the modest similarities in the binding motif, the aforementioned transport mechanism parallels the reports for Cx43 (Lauf *et al.*, 2002; Thomas *et al.*, 2005).

Lauf et al. (2002) previously described the directed transport of Cx43 to the plasma membrane, demonstrating mobility of approximately 70%, before incorporation into GJPs. At GJPs, Cx43 has been described as exhibiting either low or high mobility states at the lateral ends. Categorization of the mobility state was found to be independent of GJP size but rather determined by the C-terminal domain influencing channel density, protein interaction candidates, or both (Simek *et al.*, 2009). Our studies have confirmed

unique differences between Cx43 and Cx36 kinetics both at the plasma membrane and GJP. In this research, we report mobility of wild-type Cx36 as approximately 70% at the plasma membrane, comparable to Lauf et al. (2002), and 25% at the GJP. We suspect that mobility in the PM contributes to the fine-tuning of Cx36 incorporation, especially under activity-dependent circumstances. In a related study (H. Y. Wang *et al.*, 2015), FRAP microscopy of GJPs formed by Cx36-HaloTag fusion proteins was studied in HeLa cells. Here, the initial M_f was reported to be 56% and subsequently decreased to 41% after sequential bleaching. Wang et al. (2015) also found half-time of recovery to be 1.55±0.22s. In this study, the carboxyl terminus of Cx36 was fused with the GFP protein tag, increasing the molecular mass by 27 kDa. We anticipate that the lower mobile fraction and longer half-time of recovery differences observed between our wild-type protein and the Cx36-HaloTag can be attributed to the large C-terminal GFP tag, decreasing the mobility potential of Cx36. Nevertheless, we consistently reported considerably short half-time of recoveries upon manipulation to the tubulin cytoskeleton or interaction thereof. Since a faster $T_{1/2}$ is typically reflective of weaker binding mechanisms, incorporation of Cx36 at the GJP under these circumstances were likely mediated by diffusion rather than a controlled transport mechanism.

2.2.6.3 Actin Serves as a Secondary Conduit to Cx36 Transport to the GJP

Theoretical and practical considerations suggest that other transport mechanisms must exist alongside tubulin-dependent transport. In neurons, microtubules participate in axonal vesicular transport, and tubulin entry into dendritic spines is activity-dependent or associated with development (Hu *et al.*, 2008). Lateral diffusion in the membrane as mechanisms for transport of Cx36 into dendritic spines cannot explain temporal aspects of the plasticity of electrical synapses. Here, experimental evidence showed that treatment conditions targeting tubulin or the tubulin-binding motif reduced the GJP area and formation, but the formation of GJPs at the juxtamembrane was not wholly abolished. We propose a second, actin-dependent transport and GJP formation process, as suggested by (Lynn, Li and Nagy, 2012), similar to the actin-dependent transport of receptor and channel proteins into synaptic spines (Ligon and Steward, 2000; Osterweil, Wells and Mooseker, 2005; Wang *et al.*, 2008; Bär *et al.*, 2016). The binding of Cx36 to actin directly or indirectly through adaptor proteins has not been addressed in this study. Although previous reports indicated that interaction with the actin cytoskeleton was involved in the turnover and invagination endocytosis of gap junctions (Watanabe, Washioka and Tonosaki, 1988), a more recent study on Cx30 proposed that actin is involved in the anchoring of connexons and short-distance transport rather than the facilitation of GJ internalization (Qu, Gardner and Schrijver, 2009). Follow-up studies resolving details of this second transport mechanism will help to understand how molecular and functional asymmetry is created at a vertebrate electrical synapse.

2.2.6.4 Limitations and Critical Considerations

Wayakanon et al. (2012) investigated the consequences of GJ transport and internalization of various CT truncated Cx43 mutants. Of these, deleting amino acids spanning 235-242, which corresponds to the tubulin-binding motif, resulted in the absence of GJPs and thus communication (Wayakanon *et al.*, 2012). In contrast, our results have demonstrated the retention of GJP formation and communication following the deletion of the tubulin-binding motif in Cx36, albeit at reduced efficiencies. These findings do, however, parallel the CT deletion of the N2RB subunit of NMDA receptors in that communication (EPSPs) and targeting to neuronal synapses was drastically reduced rather than abolished (Mohrmann *et al.*, 2002). In addition to protein specificity, we must also consider that cell type plays a role in the transport and internalization of both electrical and chemical modalities. As such, it a reasonable to presume that neurons may have developed a specialized defense mechanism to help retain a fraction of functionality in CT-deleted proteins critical to maintaining cell homeostasis and communication. Considering our results eluded to actin as a secondary conduit for Cx36 transport, and knowledge that NMDA interacts with actin filaments (Lei *et al.*, 2001), this neuronal defense mechanism may involve an increase in actin interaction when mutations that inhibit interaction with the tubulin cytoskeleton are present. Further investigations would be required to determine the efficiency of actin binding under tubulin inhibition.

What is the physiological relevance of Cx36 interaction with microtubules? Cx36 has one of the lowest voltage sensitivities (half-inactivation voltage ±75 mV) and single-channel conductance (10-15 pS), among other connexin isoforms (Srinivas *et al.*, 1999). The detection of Cx36 GJP in the nervous system had been elusive for a long time due to the small size (Rash *et al.*, 2001, 2007). Arguably, the small GJP size and Cx36-specific gating properties suggest that a precise electrical coupling can be achieved through the tight regulation of the number of channels present in the gap junction plaque (Srinivas *et al.*, 1999). This mechanism was attributed to tubulin-dependent trafficking and complemented by the phosphorylation via CaM/CaMKII (Alev *et al.*, 2008) and PKA (Walton, 1999; Ouyang *et al.*, 2005; Kothmann *et al.*, 2007; Helen Yanran Wang *et al.*, 2015; Bazzigaluppi *et al.*, 2017). We acknowledge that such a refined transport mechanism could serve both to enhance neuronal plasticity and/or reduce excitotoxicity and subsequent neuronal cell death, both of which are influenced by Cx36 GJ coupling. Our results point to the significance of the Cx36-tubulin interaction; tubulin is a fundamental component in the modulation of neuronal synapses via channel abundance and stability.

Our investigation sheds insight on a critical step towards molecular and functional asymmetry at a vertebrate electrical synapse. Tubulin-dependent transport connects two major bookends of the life cycle of Cx36. Before interaction with tubulin, direct interaction with CaM occurs primarily at the ER/Golgi complex (Siu *et al.*, 2016). Vesicular transport to the GJP involves tubulin and most likely another transport

system accounting for the structural and functional specialization of pre- and postsynaptic compartments of soma-somatic, dendro-dendritic, dendro-somatic, and axon-dendritic contact sites in mature neurons where Cx36 is expressed (Hamzei-sichani *et al.*, 2007; Bautisa and Nagy, 2014). Outcomes of this research extend to previously recognized similarities of both NMDA receptors and Cx36 interaction with CaM/CaMKII. Similar to Cx36, NMDA receptor channel subunit CTs bind tubulin dimers or soluble forms of tubulin. The efficient modulation of microtubule dynamics by the NR1 and NR2 cytoplasmic domains suggests an interaction of the receptor and the subsynaptic cytoskeletal network that may play a role during morphological and functional adaptations, as observed during synaptogenesis and in adult CNS plasticity. Importantly, results have shown that tubulin-dependent trafficking of Cx36 is part of the molecular machinery potentiating electrical synaptic strength. In this regard, the activity-dependent modulation of the cytoskeleton controls the formation and plasticity of electrical synapses.

2.2.7 Supplementary Figures

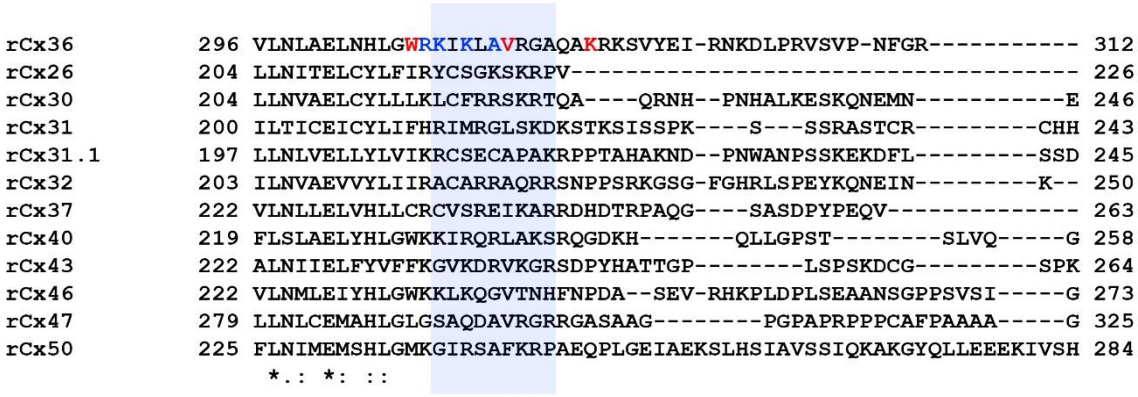

Figure S 2.1. Carboxyl terminal sequence alignment across connexin isoforms.

Sequence alignment of the carboxyl-terminal of Cx36 to several connexin isoforms. The putative tubulin binding motif of Cx36 is shaded in blue. Conserved residues within the Cx36 CT are indicated by the asterisks. Both CaM and CaMKII binding sites appeared to share some overlap with the tubulin-binding motif in the Cx36 protein; however, this signature motif is absent in the other isoforms. The CaMKII binding motif is outlined in blue, and the CaM motif is in red.

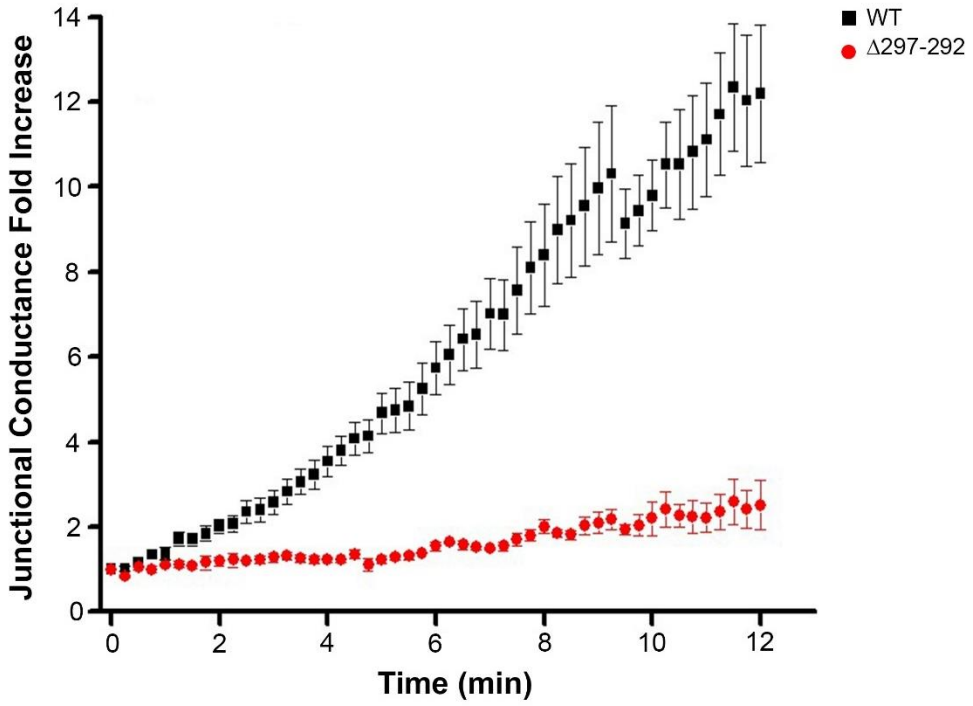

Figure S 2.2. Run-up is abolished in the absence of the tubulin binding motif.

Electrical coupling was measured using the dual whole-cell patch-clamp technique in N2a cell pairs transiently transfected to express Cx36-EGFP. Expression of Cx36Δ279-292-EGFP abolished the run-up suggesting that the identified CT binding motif potentiates electrical plasticity.

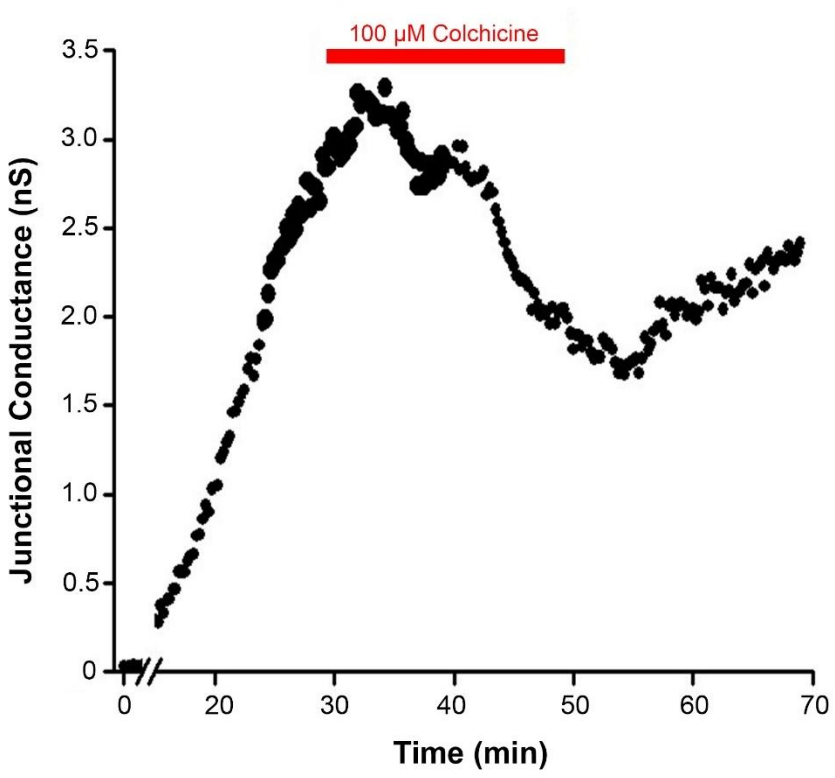

Figure S 2.3. Run-up is reversibly abolished with colchicine application.

A 20 min application of Colchicine was potent enough to impair Cx36-mediated GJ conductance; this effect was reversible upon removal of the Colchicine-supplemented bathing solution.

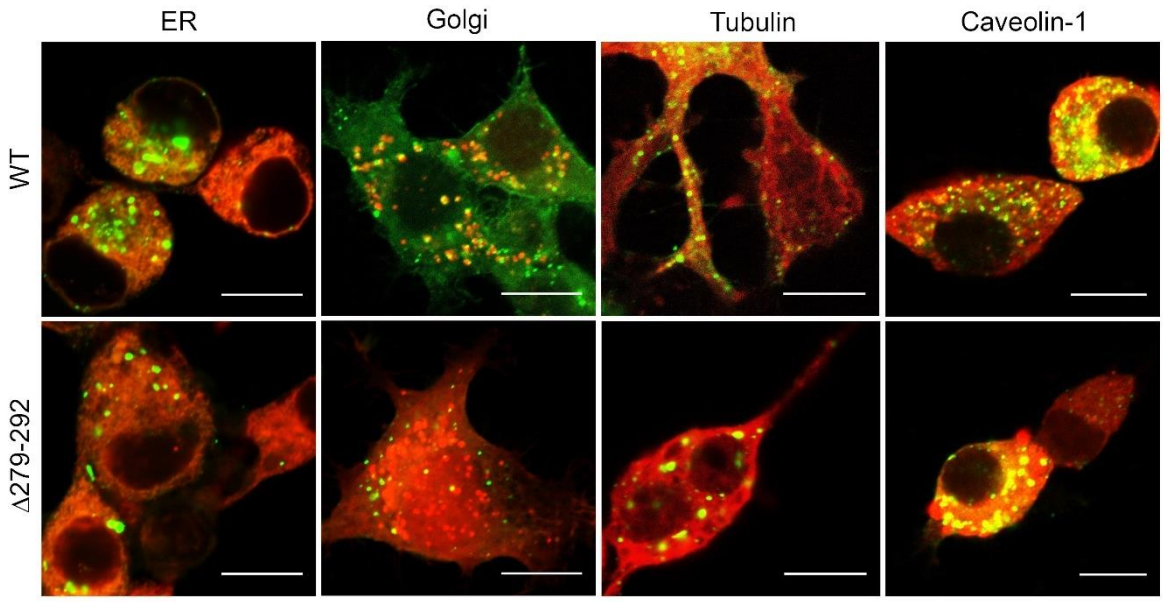

Figure S 2.4. Colocalization image examples of Cx36 to various organelles.

Co-localization was determined by Mander's overlap coefficient. Cells were co-transfected with wildtype or mutant (Δ279-292) Cx36-EGFP and mCherry-tagged tubulin or the DsRed-monomeric protein tagged with the ER retention signal KDEL, amino acids 1-60 of human galactosyltransferase, or caveolin-1.

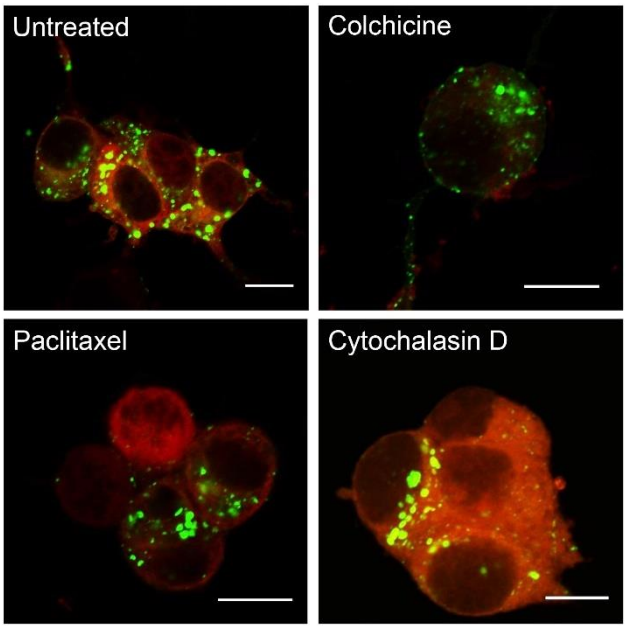

Figure S 2.5. Colocalization image examples of Cx36 to the tubulin-cytoskeleton under pharmacological manipulation.

Co-localization was determined by Mander's overlap coefficient. Cells were co-transfected with wildtype Cx36-EGFP and mCherry-tagged tubulin and subsequently treated with colchicine, paclitaxel, or cytochalasin D. Untreated cells were reserved as a control.

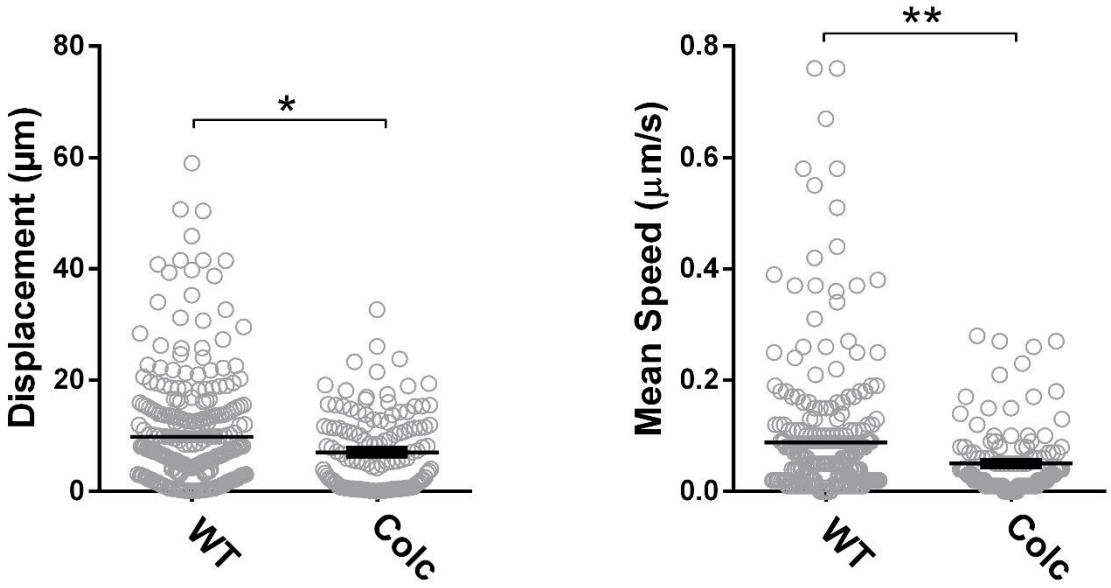

Figure S 2.6. TIRF analysis of transport in single transfected N2a cells.

N2a cells were transfected to express wild-type Cx36-EGFP and subsequently treated with colchicine to inhibit tubulin polymerization. Untreated cells served as the control.

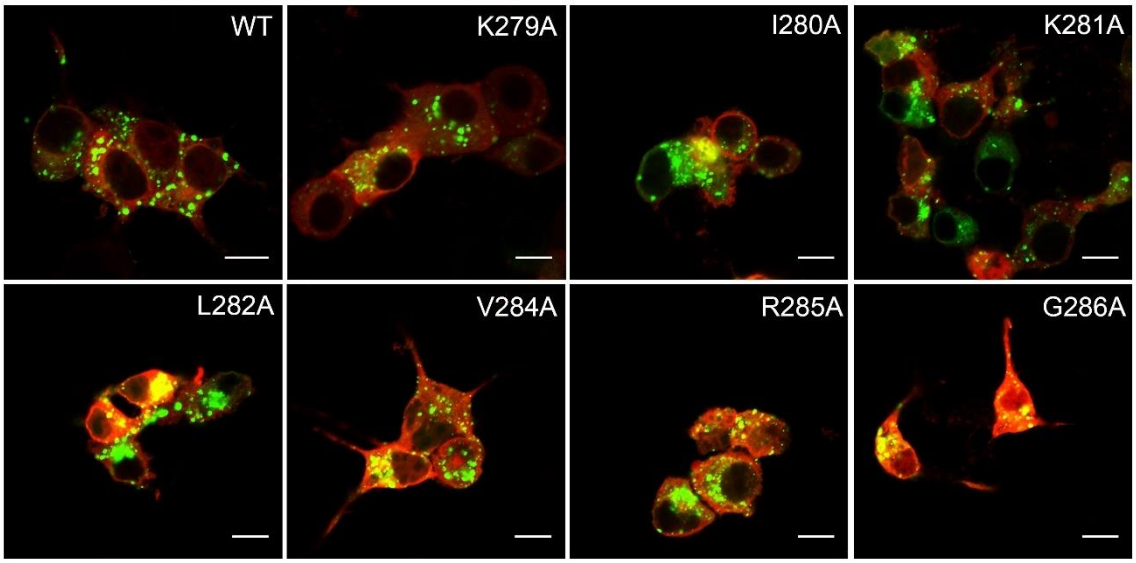

Figure S 2.7. Colocalization image examples of various Cx36 mutants to the tubulin-cytoskeleton.

Co-localization was determined by Mander's overlap coefficient. Cells were co-transfected with wildtype or Cx36-EGFP and mCherry-tagged tubulin.

2.3

Trafficking of Connexin-36 via Microtubules During a Run-Up Model Occurs Independently of CaM-CaMKII Activity

Cherie A. Brown[1], Georg Zoidl[1,2]

[1] Department of Biology, York University, Toronto, ON M3J 1P3, Canada, [2] Department of Psychology, York University, Toronto, ON M3J 1P3, Canada

Author Contributions: Conceptualization, G.Z.; investigation, C.A.B.; writing—original draft preparation, C.A.B.; writing—review and editing, C.A.B. and G.Z.; supervision, G.Z.; funding acquisition, G.Z.

2.3.1 Abstract

The previously eluded tubulin-binding motif within the C-terminal domain of Connexin-36 (Cx36) is near the CaM and CaMKII binding sites suggesting an interplay of competitive or complementary mechanisms between the trio. As such, we hypothesized that CaM-CaMKII activity was a key modulator in the interaction between Cx36 and tubulin. In this way, we predicted that activating this pathway via an elevation in intracellular calcium concentrations would regulate the transport of Cx36 to the gap junction plaque (GJP) during the run-up model of electrical plasticity. We used a combination of co-localization studies, total internal reflection fluorescence (TIRF), and fluorescence recovery after photobleaching (FRAP) microscopy in conjunction with pharmacological interference to decipher the contribution of calcium, CaM, and CaMKII activity individually. Here, we determined that CaM and CaMKII do not play a significant role in the transport of Cx36 during conditions mimicking neuronal plasticity. In contrast, a role in modulating Cx36 vesicular transport was found during basal conditions suggesting that the actions of CaM and CaMKII change depending on the activity state of cells. Nevertheless, activation of both proteins is critical in mediating the stability of the GJP. Moreover, high intracellular calcium concentrations aided in the translocation of Cx36 to the tubulin-cytoskeleton. Taken together, we concluded that the run-up phenomenon is mediated by (1) the channel open probability and turnover via CaM-CaMKII activity at the GJP and (2) the transport of Cx36 via the tubulin cytoskeleton independent of CaM-CaMKII activity.

2.3.2 Cx36 Expression and GJP Size is Maintained by CaMKII Activity

In follow-up to our previous studies (Siu *et al.*, 2016; Brown *et al.*, 2019), the role(s) of calcium homeostasis in modulating Cx36-tubulin interactions and subsequent transport to the gap junction plaque (GJP) were investigated. Here, intracellular calcium ($[Ca^{2+}]_I$) was increased using the calcium ionophore Ionomycin (IM, 2µM) and decreased with the calcium chelator BAPTA-AM (24µM). To provide a more comprehensive overview of the potential interactions mediated by fluctuations in $[Ca^{2+}]_I$, the roles of

calmodulin (CaM) and CaMKII were also included in our study. Manipulation of CaM and CaMKII activity was achieved using W7 (10μM) and KN-93 (50μM). Simultaneous stimulation with ionomycin while blocking with W7 and/or KN-93 allowed for a greater depth understanding of how the roles of CaM and CaMKII may change throughout the events mediating neuronal plasticity.

Immunoblot analysis confirmed that BAPTA-AM and ionomycin treatment had negligible effects on Cx36 expression in our Neuro-2a (N2a) cell model. However, pharmacological interference with W7 or KN-93 reduced Cx36 protein expression (**Figure 2.12A**). Localization studies were performed 48 h post-transfection and demonstrated the recruitment of Cx36 protein into the GJPs at the juxtamembrane despite treatment conditions (**Supplementary Figure S2.8**). Quantitatively, the GJP area remained unaffected after BAPTA-AM or Ionomycin treatment (*GJP area in μm²*, WT: 2.22±0.19, n=28; BAPTA-AM, 1.37±0.11, n=14, $p=2.90x10^{-1}$, IM: 1.75±0.34, n=15, $p=9.47x10^{-1}$). In contrast, treatment with W7 significantly reduced GJP area (1.61±0.17, n=34, $p=0.36x10^{-1}$), as did KN-93 treatment in comparison to the untreated wild-type control (1.45±0.13, n=40, $p=0.06x10^{-1}$). Targeted inhibition of CaM and CaMKII individually while under simultaneous stimulation with ionomycin also significantly reduced the GJP area (*GJP area in μm²*, W7+IM: 1.38±0.10, n=40, $p=0.10x10^{-1}$; KN-93+IM: 1.42±0.10, n=44, $p=0.20^{-1}$) (**Figure 2.12B**). Taken together, these results suggest that Cx36 expression is, in part, dependent on the CaM-mediated activation of CaMKII. Moreover, coalescence into the GJP was also CaMKII-dependent regardless of cell activity state (i.e., basal vs. stimulated conditions).

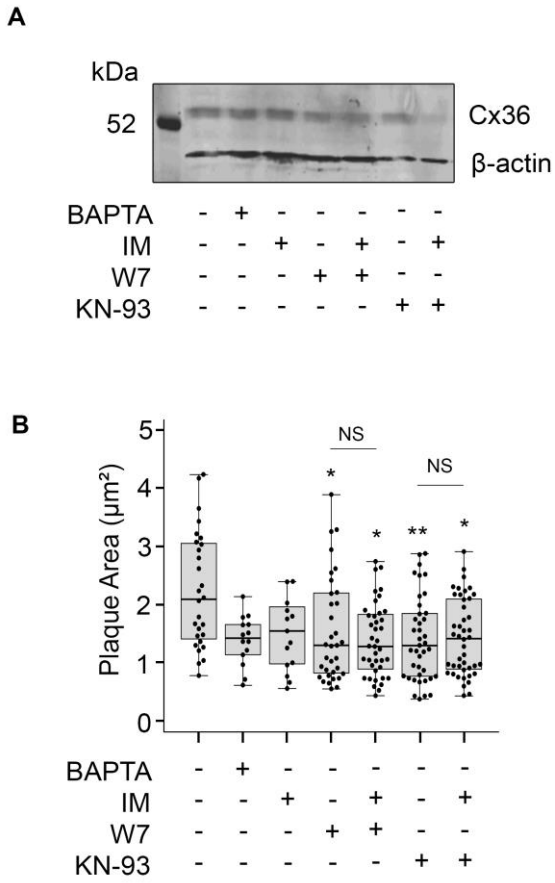

Figure 2.12. Cx36 Expression and Coalescence into the GJP under Pharmacological Manipulation.

***(A)** Immunoblot analysis of N2a cells transiently transfected to express the EGFP-tagged Cx36 wild-type construct. Fusion proteins were detected using an anti-EGFP antibody confirming expression. An anti-β-actin antibody served as the loading control; the protein standard is denoted in kDa. (**B**) Quantification of GJP size demonstrated a significant reduction in connexon recruitment in cells treated with W7 or KN-93. Data are mean ± SEM; for the GJP area, sample size (n) ranged from 14-44 GJPs, as indicated in the text. *, $p < 0.05$, **, $p < 0.001$, Kruskal-Wallis test.*

2.3.3 Cx36 Interaction with the Tubulin-Cytoskeleton is Enhanced with CaM Inhibition

Since CaMKII homeostasis was a determining factor in regulating GJP size, we anticipated that the interaction between Cx36 and tubulin was CaMKII-dependent. To assess this, we performed colocalization studies and quantified protein-protein interaction by significant changes in Mander's overlap coefficient. To visualize the microtubule network, N2a cells were transiently transfected to co-express mCherry-tagged tubulin with Cx36-EGFP, and colocalization was quantified as the overlap between the corresponding fluorescent signals (**Figure 2.13A,** See **Figure S2.4, Section 2.2.7** for WT). Here, we found that neither treatment with BAPTA-AM nor ionomycin had a significant impact on Cx36 co-localization with the tubulin cytoskeleton (*overlap coefficient*, WT: 0.55±0.02, n=34; BAPTA-AM: 0.56±0.03, n=35, $p > 9.99\text{x}10^{-1}$; Ionomycin: 0.54±0.02, n=40, $p > 9.99\text{x}10^{-1}$). While inhibition of CaM with W7 had negligible

effects on Cx36-tubulin co-localization (0.55±0.04, n=29, $p > 9.99x10^{-1}$), simultaneous treatment with W7 and ionomycin resulted in a 128% increase in the Mander's overlap coefficient (0.71±0.03, n=29, $p=0.003x10^{-1}$). Both KN-93 treatment with and without ionomycin stimulation had no impact on colocalization (KN-93: 0.64±0.02, n=37, $p=0.66x10^{-1}$; KN-93+IM: 0.57±0.02, n=37, $p > 9.99x10^{-1}$) (**Figure 2.13B**). Our results suggest the suppression of CaM activation under high intracellular calcium concentrations is complementary to Cx36-tubulin interaction. We recognize that this result was prominent despite the decrease in expression levels and GJP size while under pharmacological inhibition with W7. Nevertheless, ionomycin treatment and KN-93+IM treatment had no impact on Mander's coefficient, suggesting that reducing CaM activity specifically restored co-localization to wild-type levels, confirming the validity of our results.

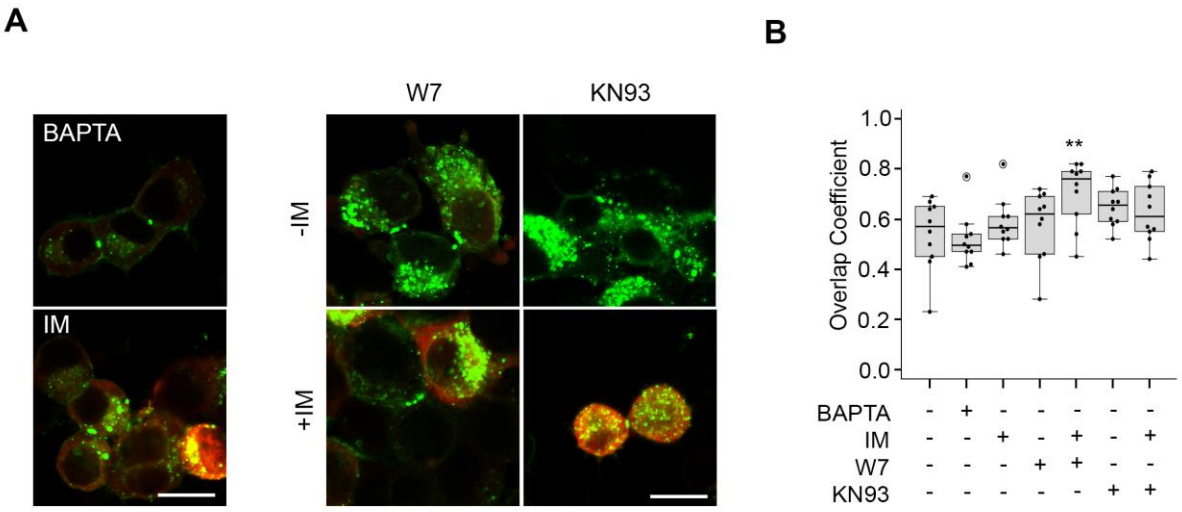

Figure 2.13. Colocalization of Cx36 to the Tubulin Cytoskeleton is Enhanced Under Simultaneous Treatment with W7 and Ionomycin.

*(**A**) Co-localization was determined by Mander's overlap coefficient. Cells were co-transfected with wildtype Cx36-EGFP and mCherry-tagged tubulin. Scale bar 10µm. (**B**) Relative to the untreated wild-type, simultaneously treating N2a cells with ionomycin and W7 resulted in an increase in tubulin co-localization. All else was unaffected. Data are mean ± SEM, the sample size is provided in the text. ***, p < 0.001, Kruskal-Wallis test, each sample was compared to the untreated wild-type values.*

2.3.4 Cx36 Vesicular Trafficking is Mediated Differentially by Calcium, CaM, and CaMKII

We previously quantified the trafficking of wild-type Cx36-EGFP vesicles (displacement length: 8.70±0.53 µm, n= 475; mean speed: 0.10±0.01 µm/s) and demonstrated that both spatial and temporal dynamics of Cx36 transport are manipulated by altering the tubulin-cytoskeleton directly or the corresponding binding motif within the c-terminal domain of Cx36 (Brown *et al.*, 2019). Next, we aimed to understand how calcium, CaM, and CaMKII individually contributed to the tubulin-dependent transport of Cx36. Using TIRF microscopy, we explored the mechanistic consequences of calcium, CaM, and

CaMKII disruption on the vesicular trafficking abilities in N2a cells co-expressing mCherry-tubulin and Cx36-EGFP. Vesicles with Cx36-EGFP cargo were illuminated in the submembrane space by the evanescent wave known as the TIRF field. Here, low $[Ca^{2+}]_I$, achieved with BAPTA-AM treatment, was indistinguishable from the untreated wildtype control in both displacement length and mean speed (*Displacement in µm*, 8.59±0.56, n=314, $p=8.45x10^{-1}$; *Mean Speed in µm/s*, 0.09±0.01, $p > 9.99x10^{-1}$). Similarly, ionomycin treatment had no effect on the displacement or speed of Cx36 vesicles (*Displacement in µm*, 7.43±0.52, n=270, $p > 9.99x10^{-1}$; *Mean Speed in µm/s*: 0.08±0.01, $p > 9.99x10^{-1}$) suggesting that Cx36 vesicular transport was not sensitive to manipulation in calcium concentrations.

Next, we inhibited CaM activity with and without ionomycin stimulation. Under these conditions, we observed negligible effects on the displacement (µm) of Cx36 cargo-carrying vesicles in comparison to the untreated wild-type control (W7: 4.97±0.50, n=148, $p=2.49x10^{-1}$; W7+IM: 8.54±0.66, n=208, $p > 9.99x10^{-1}$). A reduction in the mean speed (µm/s) was observed; however, this was exclusive to W7 treatment alone (W7: 0.05±0.01, $p=0.01x10^{-2}$; W7+IM: 0.09±0.01, $p > 9.99x10^{-1}$). In contrast, inhibiting CaMKII activity resulted in a greater displacement length of Cx36 vesicles under KN-93 treatment alone (10.56 ±0.69, n=319, $p=0.11x10^{-1}$); this increase was restored to wild-type conditions with the simultaneous administration of ionomycin (8.62±0.74, n=213, $p > 9.99x10^{-1}$). No significant changes in mean speed were observed under KN-93 or KN-93+IM treatment conditions (KN-93: 0.10±0.01, $p > 9.99x10^{-1}$, KN-93+IM: 0.01±0.01$p > 9.99x10^{-1}$). Our results suggest that CaM and CaMKII play distinct roles in the transport of Cx36 vesicles. We anticipate that under basal conditions, CaMKII mediates the spatial dynamics of Cx36 transport, whereas CaM mediates the temporal dynamics. Interestingly, elevating calcium concentrations with ionomycin restored the effects of W7 and KN-93 inhibition to wild-type conditions. As such, we propose that high intracellular calcium acts as/or through a compensatory mechanism to maintain Cx36 transport when CaM and CaMKII exhibit a loss of function (**Figure 2.14**).

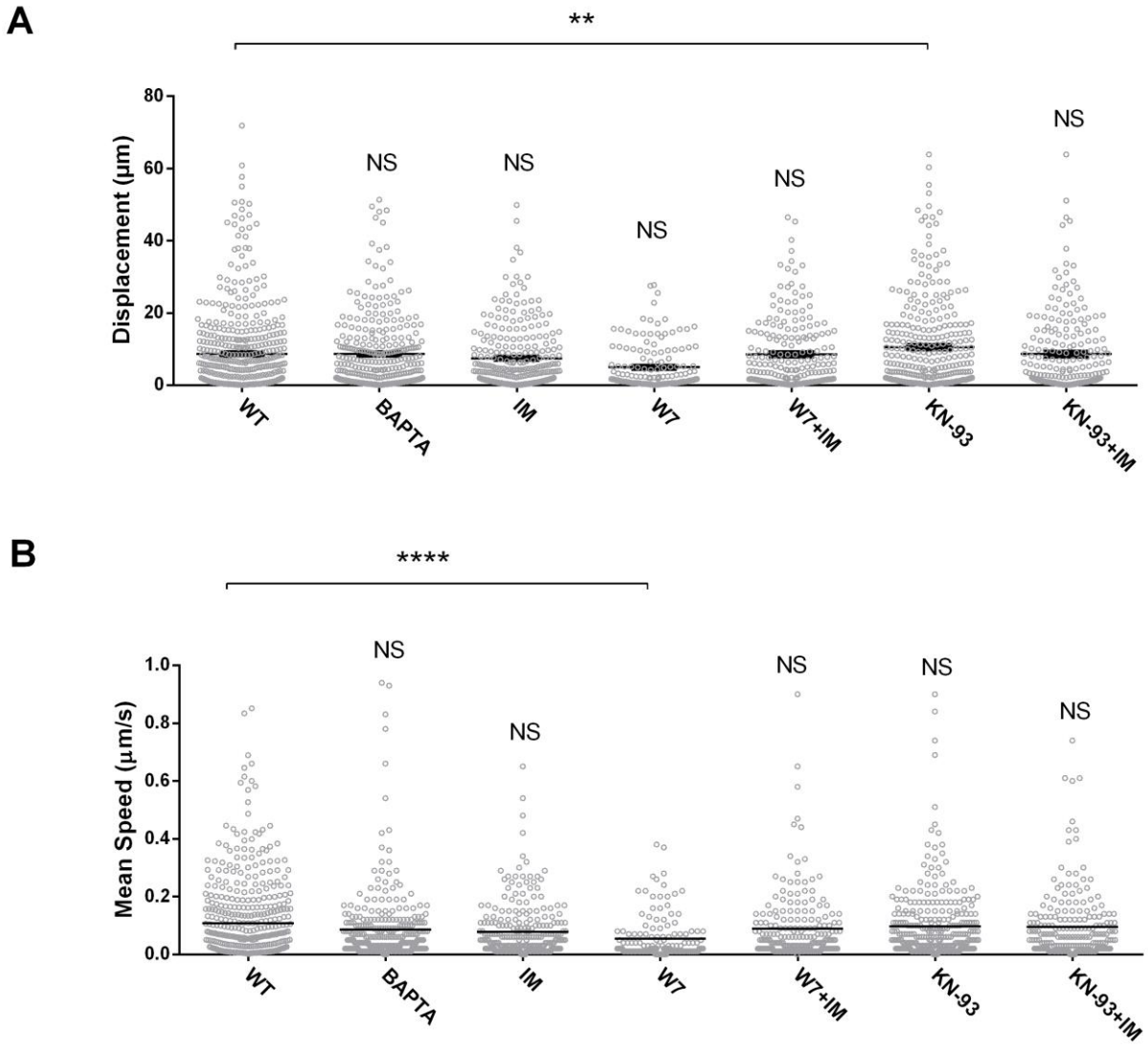

Figure 2.14. Transport Cx36 into the GJP is Dependent on an CaM and CaMKII activity under Basal Conditions.

*(**A-B**) Vesicular transport within the submembrane region was monitored using TIRF microscopy to determine the (A) displacement (µm) and (B) speed (µm/s) of Cx36 vesicles. Our results suggest that CaM and CaMKII control the temporal and spatial dynamics of Cx36 trafficking under basal conditions. Data are mean ± SEM, and the sample size (n) is described throughout the text. **, p < 0.001, ****, p < 0.00001, Kruskal-Wallis test, all samples were compared to the WT control.*

2.3.5 Influence of Calcium on Cx36 incorporation into the GJP

Collectively, our results suggested unique consequences of Ca^{2+}, CaM, and CaMKII on Cx36 trafficking and incorporation into the GJP. Next, we used fluorescence recovery after photobleaching (FRAP) microscopy to resolve the dynamics of connexon coalescence further. Recovery kinetics of EGFP-

tagged Cx36 wild-type proteins were imaged at 1.0 s intervals pre- and post-bleach. For visualization and quantification of connexon delivery into the GJP, the fluorescence intensity at the lateral ends of the GJP were targeted. Wild-type recovery kinetics were previously described (M_f (%): 25.59±0.60%; $T_{1/2}$ (s): 11.5s, n=28) (Brown *et al.*, 2019). Here, we observed an increase in cells treated with BAPTA-AM and ionomycin relative to the untreated controls; however, mobile fraction and half-time of recovery were not reported here due to the high variability causing non-converged data.

As before, we pharmacologically inhibited CaM or CaMKII activity in the presence and absence of ionomycin. Alone, W7 treatment largely increased the mobility at the GJP in comparison to the untreated wild-type (M_f (%): 63.62±1.33). Moreover, half-time of recovery was significantly reduced, suggesting that incorporation of connexons into the GJP was primarily mediated by diffusion kinetics rather than a signaling pathway that involved precise protein-protein interactions ($T_{1/2}$: 0.70s); these results were exacerbated in the presence of Ionomycin (W7+IM, M_f : 472.62±11.64%; $T_{1/2}$: 0.22s). In contrast, blocking CaMKII activity increased both connexon mobilization (M_f : 49.30±30.00%) and recovery at the GJP ($T_{1/2}$: 65.22s). While the mobile fraction remained elevated with the simultaneous treatment of KN-93 with ionomycin (52.23±0.51%), half-time of recovery was again reduced (1.56s), favoring diffusion kinetics for connexon coalescence (**Figure 2.15**).

All of the above let us conclude that elevated $[Ca^{2+}]_I$, while CaM and CaMKII are inhibited, reduced GJP stability, causing a reduction in the GJP area. Moreover, the role of CaM and CaMKII changed depending on the level of cell activity (i.e., intracellular calcium concentrations). Nevertheless, we propose that calcium-dependent CaMKII activation at the GJP is critical in maintaining the quantity and quality of connexon delivery, consistent with our most recent model of Cx36 plasticity (Siu *et al.*, 2016).

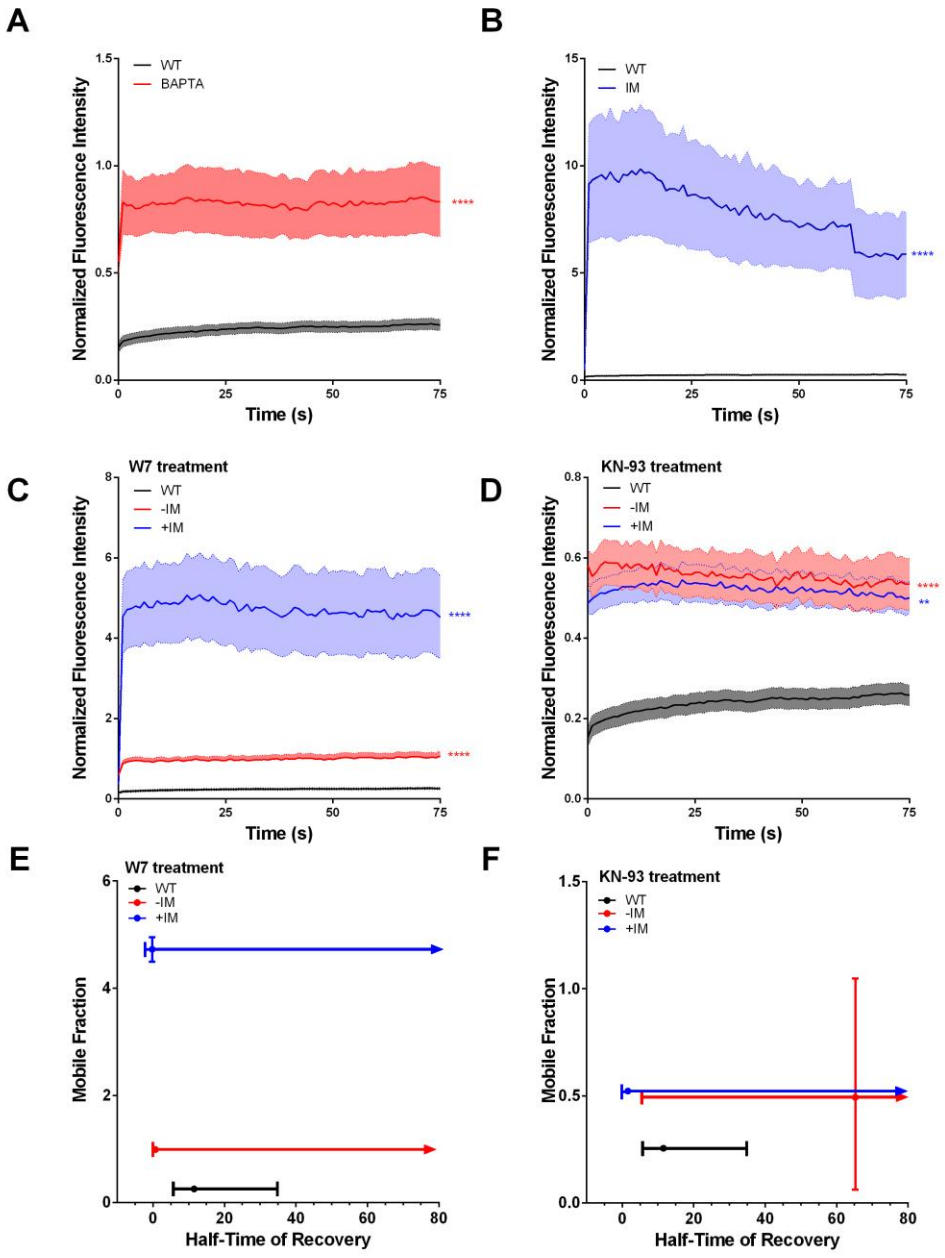

Figure 2.15. Cx36 GJP Stability is Sensitive to Pharmacological Manipulations of the Ca^{2+}/CaM/CaMKII Pathway.

*Repopulation of connexons at the gap junction plaque for N2a cells treated with (**A**) Ionomycin, (**B**) BAPTA-AM, (**C**) the CaM antagonist W7 and (**D**) the CaMKII antagonist KN-93. The corresponding XY scatterplot illustrating the relationship between the mobile fraction and half-time of recovery (s) was included for (**E**) W7 and (**F**) KN93 inhibition. Please note that curve fitting for BAPTA and IM was not possible; therefore, neither is diagramed here. GJP repopulation displayed significant deviances from the untreated wild-type control under all pharmacological conditions. Recovery curves are the mean ± SEM. Sample size (n) is detailed throughout the text. **, $p < 0.001$, ****, $p < 0.0001$, Kruskal-Wallis test, all samples were compared to the wild-type control.*

2.3.6 Discussion

In the present study, we utilized a neuroblastoma cell model of synaptic plasticity to explore the consequences of calcium, CaM, and CaMKII manipulation on Cx36 transport and incorporation into the gap junction plaque. Our experimental design was based on previous work demonstrating that the C-terminal tail of Cx36 contains a highly conserved overlapping region for tubulin, CaM, and CaMKII binding motifs. Typically, CaM binding motifs in other connexins are located in different positions in the amino-terminus (Cx32), cytoplasmic loop (Cx43, Cx44, Cx50), or in a non-overlapping region within the CT domain (Cx32) (Zhou *et al.*, 2007, 2009; Dodd *et al.*, 2008; Myllykoski, Kuczera and Kursula, 2009; Xu *et al.*, 2012; Mruk *et al.*, 2014). Binding of CaMKII to other connexins than Cx36 has not been reported. Since we previously demonstrated that transport of Cx36 is tubulin-dependent, we hypothesized that calcium manipulation, and thus CaM and CaMKII manipulation, was critical in mediating this process.

Cells undergoing neuroplasticity follow a cascade of events leading to the elevation of intracellular calcium, which in turn binds to calmodulin (Ca^{2+}-CaM). This cascade serves as the prerequisite to activating calmodulin kinase II (CaMKII), a critical mediating step in modulating plasticity. Previous studies have demonstrated that inhibition of CaMKII with KN-93 was sufficient to impair the run-up phenomenon, where gap junctional conductance increases 10-fold, specifically at Cx36 GJPs. As such, CaMKII activation is critical in mediating electrical plasticity; however, it is unclear whether this is due to alterations in transport, channel opening probability, or a combination of them both. Nevertheless, due to the inter-dependency of the calcium/CaM/CaMKII cascade, the pharmacological intervention of these pathways needs careful consideration. While the calcium chelator BAPTA-AM is expected to work in opposition to neuronal plasticity by decreasing intracellular calcium concentrations, ionomycin treatment is understood to complement this process by initiating the elevation in intracellular concentrations, thus activating CaM and CaMKII activity. While inhibition of CaMKII activity is achieved specifically with the addition of KN-93, W7 indirectly inhibits CaMKII activation by preventing calcium from binding to CaM. As such, CaM remains in its inactive form, unable to activate CaMKII. Under simultaneous stimulation with ionomycin, W7 inhibition would allow for the actions of intracellular calcium to be elucidated independently of CaM-CaMKII activation. Similarly, inhibiting CaMKII activity while elevating intracellular calcium concentrations would provide insight into how CaM activation affects Cx36 transport and incorporation into the GJP.

2.3.6.1 Pharmacological Inhibition Promoted Differential Expression Levels

Our results demonstrated a reduction in GJP area in N2a cells treated with the CaM and CaMKII blockers W7 and KN-93, which remained poignant despite an elevation in calcium concentrations. However, we attribute this reduction, in part, to lower expression levels as confirmed by immunoblot analysis in the

presence of pharmacological inhibition. Since this effect was observed with both CaM and CaMKII inhibition, we suspected that activation of CaMKII was a critical mediator of Cx36 expression. Of the various CaMKII isoforms expressed in mammals, γCaMKII is known to indirectly influence gene transcription by serving as a conduit to shuttle Ca^{2+}-CaM into the nucleus, activating CaMKIV. This nuclear CaMK activity allows for the rapid phosphorylation of CREB and subsequent gene transcription (Wheeler *et al.*, 2008; Ma *et al.*, 2014; Wang *et al.*, 2017). Interestingly, the promoter region of Cx36 contains a CREB binding motif; however, Arumugam et al. (2005) demonstrated an inverse relationship between CREB and Cx36 where increasing CREB attenuated Cx36 expression and thus gap junctional coupling in a rat animal model (Arumugam *et al.*, 2005). In this regard, we would have expected that inhibition of γCaMKII via W7 and/or KN-93 would indirectly reduce CREB activity and result in more Cx36 expression.

This led us to question what other CaMKII isoforms may be at play, causing the discrepancy in Cx36 protein expression levels when treated with W7 and KN-93? Previously, Bazzigaluppi et al. (2017) demonstrated that GJP length and density were mediated by CaMKII activity via KN-93 inhibition. To further this, they demonstrated that βCaMKII knock-out mice had a significantly reduced number of puncta in the inferior olive (IO), suggesting an important role in mediating junctional conductance rather than the remaining isoforms in the CaMKII family (Bazzigaluppi *et al.*, 2017). Moreover, this was consistent with other findings (Pereda *et al.*, 1998; Kothmann *et al.*, 2012). As such, we suspect that our observed reduction in GJP size and protein expression was due to the inhibition of βCaMKII. However, the mechanism responsible for this has yet to be elucidated. Nevertheless, we hypothesize that the reduction in Cx36 protein expression via βCaMKII inhibition was caused by an increase in gap junction turnover and degradation rather than a reduction in gene transcription. How could this be achieved? βCaMKII has a known role in regulating actin cytoskeletal dynamics and stability at the post synaptic density (PSD). Since we previously demonstrated that Cx36 GJP size, stability, and coalescence were compromised in the presence of Cytochalasin D (Brown *et al.*, 2019), we anticipate that inhibition of βCaMKII reduces actin stability, causing an increase in Cx36 turnover and thus degradation. However, this would require further exploration.

2.3.6.2 Calcium Manipulation Impacts Cx36-Tubulin Co-localization

While we previously provided an in-depth characterization of the interaction between Cx36 and the tubulin cytoskeleton, we did not address how the CT domain, encompassing the tubulin, CaM, and CaMKII binding motifs, may involve complementary or inhibitory roles between the trio. As such, we posed the question: How does altering calcium concentrations, and thus CaM/CaMKII activity, impact the ability of Cx36 to interact with the tubulin cytoskeleton? We addressed this question by analyzing colocalization data under various treatment conditions. Interestingly, only cells treated with ionomycin while simultaneously inhibited with W7 showed any response to Cx36-tubulin co-localization. Our result suggested that high

intracellular concentrations, independent of CaM activity, were sufficient to enhance the interaction between Cx36 and tubulin. Interestingly, CaM and CaMKII activity seemed to have little impact on the binding of Cx36 to tubulin. This finding was unexpected considering the close proximity of the binding motifs relative to the size of the binding proteins. As such, we concluded that tubulin, CaM, and CaMKII interact with Cx36 independently of each other; however, they work in unison to prevent competitive interference. We anticipate that this would involve a precise medley to successfully navigate the temporal and spatial dynamics involved in the trafficking and turnover of Cx36.

2.3.6.3 Segregated Functionality for Transport and Incorporation Mechanisms

We wanted to explore how the transport and incorporation into the gap junction plaque were influenced by changes in calcium, CaM, and CaMKII activity. Using a combination of TIRF and FRAP microscopy, we found that CaM and CaMKII inhibition under basal conditions influenced transport uniquely. Here, W7 treatment impaired temporal dynamics of Cx36 vesicular transport while KN-93 enhanced spatial dynamics, exclusively when intrinsic calcium concentrations were not manipulated. Taken together, this would suggest that CaM and CaMKII are involved in cellular homeostasis by mediating Cx36 transport; however, they are not involved in vesicular transport during neuroplasticity. Our FRAP microscopy investigations, in contrast, revealed that manipulation of any sort reduced GJP stability as reflected by an increase in the mobile fraction (M_f) and variability in half-time of recovery ($T_{1/2}$). As such, we propose a larger influence of CaM/CaMKII activity at the GJP by mediating Cx36 incorporation and turnover. These findings are complementary to our previous investigations characterizing the interaction between Cx36 and CaM/CaMKII, where a larger role of CaMKII activity at the Cx36 GJP was elucidated (Siu *et al.*, 2016). In this way, we concluded that the run-up phenomenon is mediated by both transport and channel opening probability via a non-competitive medley of tubulin, CaM, and CaMKII molecular machinery.

2.3.6.4 Limitations and Critical Considerations

An important limitation to consider when utilizing the application of pharmacological agents is the selectivity and range of off-target effects. Although KN-93 is reasonably selective to the CaMKII family of proteins, off-target effects have been described for voltage-gated K^+ channels (Ledoux, Chartier and Leblanc, 1999; Rezazadeh, Claydon and Fedida, 2006; Hegyi *et al.*, 2015), L-type Ca^{2+} channels (Anderson *et al.*, 1998; Lipscombe, Helton and Xu, 2004), and inositol trisphosphate receptor Ca^{2+} release (Smyth *et al.*, 2002). More recently, Johnson et al. (2019) found that CaM was capable of binding to KN-93, thus inhibiting its interaction with its physiological targets such as the voltage-gated sodium channel $Na_V1.5$ (Johnson *et al.*, 2019). Moreover, W7 is the competitive inhibitor to CaM but is also known to inhibit voltage-gated K^+ channels, particularly Kv4.3 channels (Qu *et al.*, 2007). As such, these additional targets

need consideration when evaluating data using W7 or KN-93. Voltage-gated K^+ channels detect changes in neuronal membrane potential and play a crucial role in returning depolarized cells to the resting state following an action potential. Consequently, inhibition of voltage-gated K^+ channels causes K^+ ions to accumulate intracellularly, thus preventing or slowing repolarization and enhancing neuronal excitability. L-type Ca^{2+} channels are characterized by their large range of activation kinetics and are known to mediate neuronal functions such as gene expression and neurotransmitter release during subthreshold depolarizing events (Lipscombe, Helton and Xu, 2004). Similarly, inositol trisphosphate receptors allow for the release of Ca^{2+} from the endoplasmic reticulum in response to hormones, growth factors, and neurotransmitters (Mikoshiba, 2007). How might inhibition of these ion channels have affected our results? In this regard, an increase in potassium and a decrease in calcium concentrations intracellularly would disrupt the ionic balance, though it is unclear which would have higher precedence. Nevertheless, we would expect two outcomes. (1) Disrupting ionic balance is known to influence trafficking dynamics by modulating cytoskeletal polymerization/depolymerization states (Berkowitz and Wolff, 1981; Wales *et al.*, 2016). As such, W7 and KN-93 may reduce Cx36 transport and incorporation into the GJP by indirectly influencing the cytoskeleton. Though we did not focus on changes in membrane potential via Cx36, we favor the former interpretation rather than an increase in channel opening probability since Cx36 is known to have a low voltage sensitivity (Srinivas *et al.*, 1999). (2) Ionic balance is also critical in maintaining neuronal functions. As such, a disruption in intracellular ion concentrations may influence the expression of genes critical in supporting Cx36-driven neuronal communication. However, this would require a more in-depth analysis.

We demonstrated that tubulin-Cx36 co-localization increased under simultaneous W7 inhibition and ionomycin stimulation. As such, our results suggested that elevated calcium levels alone (i.e., in the absence of CaM activity) are sufficient to enhance Cx36-tubulin interaction. Interestingly, calcium is known to destabilize the tubulin cytoskeleton (Berkowitz and Wolff, 1981), which would inherently inhibit Cx36 vesicular transport, as previously mentioned. However, our studies demonstrated that the dynamics of Cx36 transport remained unaffected. As such, we propose a model where the fast elevation of intracellular calcium concentrations assists in translocating vesicular Cx36 to the tubulin-cytoskeleton where a CaM/CaMKII independent process then mediates its transport to the plasma membrane. Persistent calcium stimulation, resulting in microtubule destabilization, may then be a means of regulating the quantity of Cx36 at the synapse. Here we consider two possibilities: (1) calcium-mediated destabilization of the tubulin-cytoskeleton would serve as a neuroprotective mechanism during overstimulation, or (2) limit the amount of Cx36 at the GJP to fine-tune neuronal communication. We acknowledge that both these mechanisms may work complementary to each other.

Due to the ability of calcium, CaM, and CaMKII to interact with a variety of proteins, it is unclear if the enhanced Cx36-tubulin interaction during W7 and ionomycin treatment were due to calcium alone or through a downstream mechanism activated during elevated calcium concentrations. Moreover, our FRAP studies demonstrated a reduction in GJP stability when the calcium, CaM, and CaMKII pathway were manipulated. However, whether this was due to its impact of calcium/CaM/CaMKII activity on the cytoskeletal dynamics (both tubulin and actin) had yet to be established and would require further investigation.

2.3.7 Supplementary Figures

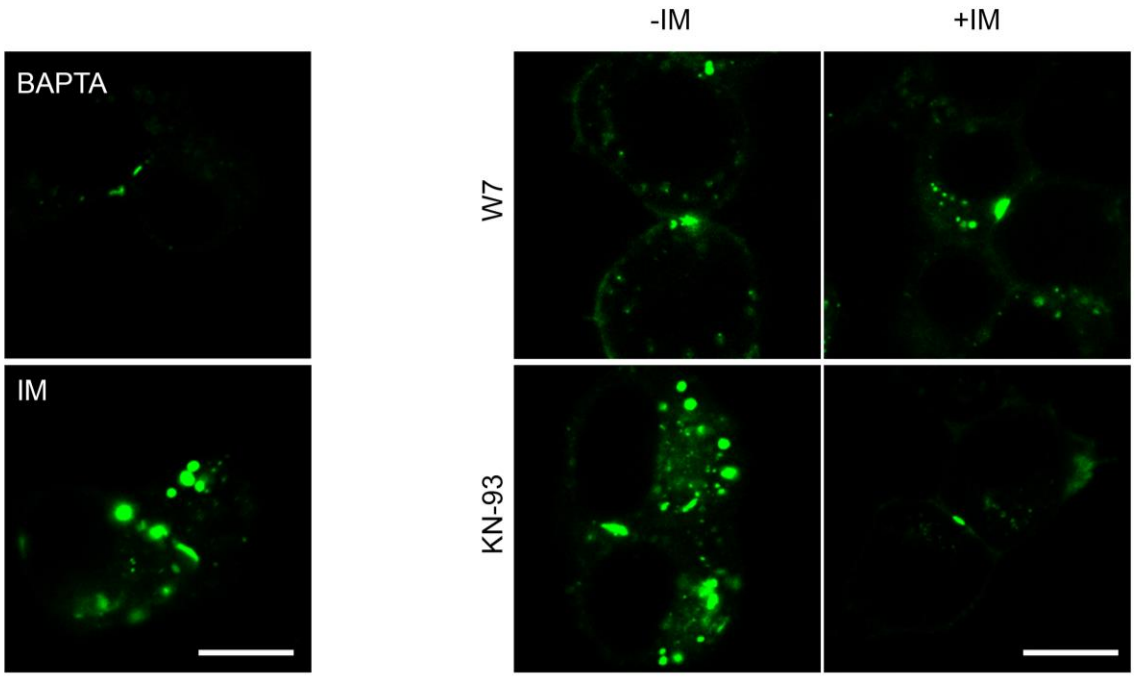

Figure S 2.8. Gap Junction Plaque Formation while under Pharmacological Inhibition.

N2a cells were transiently transfected to express Cx36-EGFP and subsequently treated with BAPTA, IM, W7, and/or KN-93 as indicated. The GJPs that formed at the juxtamembrane were measured using ImageJ. Scale bar, 10µm.

3

EXPLORING THE CELLULAR, SYSTEMS & BEHAVIORAL CONSEQUENCES OF A CX35B KNOCKOUT IN ZEBRAFISH

3.1 Materials & Methods

3.1.1 Zebrafish Lines and Husbandry

Zebrafish (*Danio rerio*) of the Tupfel longfin (TL) strain were utilized. The Cx35b$^{-/-}$ transgenic line was generated in-house using the CRISPR-Cas9 system (Jinek *et al.*, 2012) by targeting exon 1, and transgenic fish were verified by Sanger sequencing. Zebrafish lines of mixed sex were maintained in a recirculating system (Aquaneering Inc., San Diego, CA) at 28.5°C with a 14:10 hour light:dark cycle. Population sizes in tanks were matched and kept on a regular feeding schedule to minimize environmental and other exogenous influences. Water quality was monitored and dosed to maintain conductivity at approximately 600 ms and pH levels between 6-8. Zebrafish were raised, maintained, and handled in compliance with the guidelines of York University and the Animal Care Committee, standard protocols, and local regulations (GZ#2019-7-R2).

3.1.2 Generation of Cx35b$^{-/-}$ Transgenic Fish

Potential CRISPR target sites of *gjd2b* were identified using the E-CRISP tool (www.e-crisp.org). CRISPR sgRNA (Synthego, Redwood City, CA, USA) was designed to target exon 1 of *gjd2b* as follows: 5'-CUCUUAACAGGUAAGGGGGU-3'. CRISPR gRNA/Cas9 injection material was supplemented with 0.05% phenol red prior to microinjections. Delivery of the Cas9:sgRNA duplexes was performed at a 1:2 ratio. Wild-type zebrafish embryos were placed in a chilled chamber (2% agarose supplemented with E2 embryo medium) and subsequently injected with 2nl of the Cas9:sgRNA duplex (400 pg) at the one-cell stage. At 3dpf, a sample of 12 injected larvae was genotyped using PCR in combination with restriction digest for XhoI resilience (Thermo Fisher Scientific; Burlington, ON, Canada) and Sanger sequencing (IDT, Coralville, IA, USA). The remaining embryos of the founding generation were raised to adulthood and outcrossed to wild-type fish for two subsequent generations; this ensured germline transmission and eliminated CRISPR off-target effects. Heterozygous progeny were raised to adulthood and in-crossed to generate the homozygous Cx35b$^{-/-}$ mutant transgenic zebrafish line.

3.1.3 DNA Extraction, PCR Amplification, and Genotyping

Either zebrafish larvae (3-6 dpf) or adult caudal fins were used for genotyping purposes. Zebrafish were anesthetized in pH buffered 0.2 mg/ml tricaine methanesulfonate (MS-222) (Sigma-Aldrich, St. Louis, MO, USA) prior to caudal amputations with surgical scissors. Total DNA was extracted by incubation at 95°C using 100 mM NaOH for 15 minutes with vigorous agitation. DNA samples were diluted in a 1:2 ratio with TE buffer (pH 8.0) prior to use in polymerase chain reaction (PCR) analysis. The *gjd2b* exon 1 region was amplified in a Mastercycler Nexus X1 (Eppendorf, Mississauga, ON, CA) using the primer information as follows: forward primer: 5'-GGTTCTCTGTGTTACATTCGCCTCC-3' and reverse primer: 5'-CAATCATAGTAGAGTGCTGTTGGACAGC-3'. PCR primer pairs were ordered from IDT (Coralville, IA, USA) and optimized at an annealing temperature of 58°C. The PCR reaction was carried out using the Q5 High Fidelity DNA Polymerase PCR Kit (New England BioLabs, Ipswich, MA, USA) in a final volume of 20 µl consisting of 1 µl DNA-template and 19 µl Taq master mix. PCR thermal cycling conditions were initiated at 94°C for 15 min, followed by 38 cycles of denaturing at 94°C for 15 s, annealing at 58°C for 15 s, and extension at 72°C for 30 s. The final extension was carried out at 72°C for 10 min. To determine the presence of indel mutations, PCR amplicons were digested with XhoI using the Fast Digestion Top Fermentas Kit (Thermo Fisher Scientific; Burlington, ON, Canada) as per the manufacturer's protocol. Amplicons were subsequently fractionated and visualized on a 2% agarose gel supplemented with 0.005% ethidium bromide using the Alpha Imager HP System (Thermo Fisher Scientific; Burlington, ON, Canada). For Sanger sequencing, PCR amplicons were blunted and cloned into pJET1.2 using the CloneJET™ PCR Cloning Kit (Thermo Fisher Scientific; Burlington, ON, Canada) as per the manufacturer's protocols. Constructs were transformed into DH5α competent E. coli cells. Plasmids were purified using the QIACube in combination with the QIAPrep spin miniprep kit (Qiagen, Germantown, MD, USA). Sequencing was performed by IDT (Coralville, IA, USA).

3.1.4 RNA Extraction and Quantitative Real-Time PCR (RT-qPCR) Analysis

Total RNA (1 µg) was extracted and purified from approximately 30 zebrafish larvae at 7- or 8-dpf using the RNeasy Plus Mini Kit (Qiagen, Germantown, MD, USA) as per the manufacturer's protocols. When appropriate, larvae were collected immediately following exposure to behavioral tasks, and the tissue was frozen at -80°C until further analysis. Fish were homogenized by bead beating in TE buffer (pH 8.0). RNAs were reverse transcribed into cDNA using the iScript Reverse Transcription Supermix (Bio-Rad, Mississauga, ON, Canada) as per the manufacturer's instructions. Gene expression was analyzed by RT-qPCR using the SsoAdvanced Universal SYBR Green Supermix (Bio-Rad, Mississauga, ON, Canada) in the CFX96™ Real-Time PCR Detection System (Bio-Rad, Mississauga, ON, Canada). Thermal cycling was carried out as 17 cycles of the following: 94°C for 30s, 52°C for 30s, and 72°C for 1min. Three

housekeeping genes (*18S*, *tuba1a*, *actb2*) were used to determine the quality of the samples and for normalization purposes. CT values were averaged and exported from the CFX Manager Software (Bio-Rad, Mississauga, ON, Canada). The fold-difference for the relative gene expression was calculated in the Relative Expression Software Tool (2009) (Pfaffl, 2002) using the $\Delta\Delta C_T$ method as previously described (Livak and Schmittgen, 2001; Schmittgen and Livak, 2008). Three technical replicates per gene were performed from 2-3 biological replicates. Primers for each gene are listed in Appendixes A-C.

3.1.5 Immunohistochemistry

Adult zebrafish were humanely euthanized, and their heads were fixed in 4% paraformaldehyde (PFA) in 1xPBS overnight at 4ºC, followed by cryoprotection in 30% sucrose in 1xPBS. After embedding in Tissue-Tek O.C.T, 15µm sections were cut on a cryotome (Thermofisher Scientific, Burlington, ON, Canada). Samples were washed three times for 5 min with 1xPBS containing 0.1% Tween-20 (PBST) at RT. Unspecific binding sites were blocked with freshly prepared 5% normal goat serum (NGS, Sigma-Aldrich) in PBS-T for 1hr at 4. Following blocking, samples were incubated with primary antibodies (all 1:100, anti-parvalbumin (MAB1572, Sigma-Aldrich, Oakville, ON, Canada), anti-Connexin 36 (#36-4600, Thermofisher, Burlington, ON, Canada), anti-zpr-1 (ZBD-ATB-081002-43, ab-cam, Toronto, ON, Canada)) overnight at 4°C. Subsequent washes with PBS-T were for one hour at 4°C. Alexa 488 and Alexa 546 goat anti-rabbit/mouse secondary antibodies (1:3000 in 1% NGS PBS-T, Life Technologies, Burlington, ON, Canada) were applied for 1 hr at RT. After three washes with PBS-T followed by one wash with PBS, specimens were mounted on microscope slides using ProLong Antifade with DAPI (Thermofisher, Burlington, ON, Canada). Confocal images were collected using LSM-ZEN2 software (Zeiss LSM700 system; Carl Zeiss MicroImaging, Oberkochen, Germany) with a Plan-Apochromat 20x/0.8 or Plan-Apochromat 63x/1.3 oil DIC M27 objectives. The software optimized pixel resolution, line averaging, gain, and digital offset. Post image collection composite figures were created using Adobe Photoshop 2021.

3.1.6 Zebrafish Body Length and Head Measurements

Zebrafish embryos were raised in population-matched Petri dishes as per standard protocol. At 7dpf, individual larvae were collected in a drop of egg water to limit mobility during morphological analyses. Larvae were imaged under a light microscope (CKKX41; Olympus, Toronto, ON, Canada). To minimize human experimental error, two measurements for body length, head length, and midbrain diameter were acquired for each image using ImageJ. Measurements for each image were subsequently averaged before reporting.

3.1.7 Behavioral Assays

At 6dpf, larvae were acclimated to the behavioral room for 24h. On the morning of testing (7dpf), individual larvae were transferred into 6- or 24- well plates (for thigmotaxis studies) or 48- or 96-well plates (for free-swim, VMR, threshold, light-dark, and habituation studies) filled with pH 8.0 egg water. Transparent plates were utilized for all experiments except the free swim assay utilizing black/white well surround plates as indicated and the cross-maze to assess color vision. Unless otherwise stated, larvae underwent a dark- adaptation period for two hours prior to behavioral analyses. Behavioral assays were performed using the Zebrabox® system in conjunction with the Zebralab program (Viewpoint Life Technology, Lyon, Fr) to obtain automated tracking data and video files. Activity was categorized by inactivity (0.0 mm/s), coast swimming (between 0.0 mm/s and 20.0 mm/s) and burst swimming (> 20 mm/s). The recording chamber was equipped with a water heating and flow system to maintain the temperature at 28°C and illuminated from the bottom with LED lights. Dark conditions were monitored in infrared. All experiments utilizing light were performed at 30% light intensity unless otherwise stated. Data was acquisitioned in 1s, 10s, 1 min, or 5min intervals for time periods ranging from 5 minutes to 4.5 hours as outlined in figures. The experimental designs for VMR (Emran, Rihel and Dowling, 2008), Color vision (Park *et al.*, 2016), light-dark stimulation (Irons *et al.*, 2010), thigmotaxis (Schnörr *et al.*, 2012), and habituation (Hinz *et al.*, 2013) assays were adapted from previous reports. Where applicable, results were normalized three-fold to account for larval activity caused by (1) variation in light-intensity received by each well, (2) the batch effect from the inclusion of experimental replicates and (3) variation in the baseline activity measured during the final 5 minutes of light or dark adaptation based on a previous report (Xie *et al.*, 2019).

3.1.7.1 Spontaneous/Free Swim Assay

Spontaneous zebrafish larval locomotor activity was measured under constant illumination or darkness. For constant illumination, larvae were acclimated under ambient light for 2h prior to behavioral analysis. Locomotor activity was tracked for 5 minutes or 1 hour, depending on the type of data acquisition. Studies utilizing the black/white well plates, as indicated in the results text, had a clear bottom to allow for consistent illumination. Here, zebrafish larvae were dark-adapted to avoid pre-exposure biases in activity in response to the wells. Locomotor activity was tracked for 35 minutes (30 minutes of illumination and 5 minutes prior to illumination). Locomotor activity while under ambient light was normalized accordingly.

3.1.7.2 Visual-Motor Response (VMR) Assay

Responsiveness to light changes was measured as described (Emran, Rihel and Dowling, 2008) and under mesopic conditions. Larvae were dark-adapted for 2 hours prior to the experiment commencing. Locomotor activity was tracked for 3.5 hours (3 hrs of the experimental protocol and 30 mins prior to

illumination) for the standard set-up. For mesopic VMR, locomotor activity was tracked for 4.5 hours (4 hrs of the experimental protocol and 30 mins prior to illuminations). For both assays, 3-4 trials of alternating lighting conditions (30 min Light-ON; 30 MIN Light-OFF) were utilized. Light-ON intensity for scotopic VMR was set at 5% or 10%, as indicated in the results text. Mean activity, quantified by the burst duration (s), was measured 1s following light transition. Data were normalized accordingly.

3.1.7.3 Innate Color Preference Test

The innate color preference test allowed for color bias and color-blindness to be assessed in zebrafish larvae. Here, a custom-made cross maze was built using 5mm transparent acrylic sheets. Each arm of the maze was of equal dimensions (15×35×10 mm, W × L ×H) and could accommodate removable sleeves of different colors (B-blue, G-green, Y-yellow, R-red, Null-no color). Up to 20 larvae of the same genotype were placed in the open lid cross maze. Larvae were dark-adapted to avoid pre-exposure to the colors, and sleeves were rotated to avoid location bias. Locomotor activity was tracked for 40 mins (35 minutes of illumination and 5 minutes prior to illumination). Data was measured manually by counting the number of fish in each arm every 2 minutes for the duration of the experiment.

3.1.7.4 Flash Stimuli Threshold Response (FSTR) Assay

Responsiveness to light or dark flashes was assessed with the FSTR assay. For dark flash experiments, larvae were light-adapted prior to investigations. Various stimulus lengths were tested, ranging from 10ms to 1000ms, were tested; however, the final analysis utilized these experimental endpoints. To avoid habituation to the stimuli, cue lengths were presented in forward and reverse order. Larval locomotor activity was tracked for 2.5hrs, including 5 minutes of adaptation for use in normalization calculations. Mean responsiveness, quantified as burst duration (s), 1 s following each stimulus was measured. Data were normalized accordingly.

3.1.7.5 Light-Dark Locomotion Assay

Similar to the standard VMR protocol, zebrafish larvae were exposed to alternating Light-ON and Light-OFF conditions for the duration of 70min. Each lighting condition was presented for 10 mins. Baseline activity was recorded 5min prior to the initial light transition. Mean activity, quantified by the burst duration (s), was measured for the duration of the stimuli presented. Data were normalized accordingly.

3.1.7.6 Thigmotaxis Assay

Thigmotaxis assays were carried out using the light-dark locomotion assay or a variation of the FSTR assay protocols. In the latter case, only a 1 s stimulus was presented once. For experimental data with dark flashes, larvae were acclimated under ambient light. Locomotor activity was measured as the

percentage (%) of time (s) and/or distance (mm) spent in the center of the well (with an approximate diameter of 11.6mm) vs. the outer boundaries proximal to the wall.

3.1.7.7 Habituation

Habituation experiments were carried out utilizing dark flashes or light flashes. For dark flash habituation, larvae were light-adapted prior to the commencement of the experiment. Zebrafish larvae were initially trained in three 30 min blocks followed by a 30 min rest period. Each training block consisted of 60 flashes at 30s interstimulus intervals (ISIs). Rest periods were carried out in light or darkness, depending on their adaptation protocol. Following the third training block, a 2 hr and/or 24 hr retention period was tested to mimic short-term or long-term memory capacity, respectively. Habituation was measured as the mean responsiveness (burst duration, s) during the initial 5 minutes of the testing block. Percent habituation was calculated as follows: % Habituation = $(1st\ Trial - Final\ Trial \div 1st\ Trial) \times 100$. Percent Memory Retention was calculated as follows: % Memory Retention = $(3rd\ Trial - Retest \div 3rd\ Trial) \times 100$.

3.1.8 Pharmacology

Both MS-222 and Buspirone were purchased from Sigma-Aldrich (Mississauga, ON, CA). Where applicable, working concentrations were reported in figure captions and in text.

3.1.9 Program Scripting

Creation of the in-house zebrafish tracking module *DanioReReader v2.0* was created in MATLAB (MathWorks®). The program was designed based on a video file obtained from the Zebrabox tracking system. Here, wild-type zebrafish larvae were tracked in a 48-well plate configuration under ambient light. The generalized algorithm of the script was as follows: (1) select video file input, (2) detect well boundaries, (3) detect larvae via background subtraction, (4) perform video analysis to compute speed (mm/sec) or time (s) variables as appropriate, (5) generate a figure output. Refer to section 3.2 for an in-depth description of the program design.

3.1.10 Statistical analyses

Unless otherwise stated, all data is presented as the mean ± SEM. The sample size for behavioral studies varied from n = 48 to n = 144 across a minimum of two experimental replicates; sample sizes are indicated in the figures. Statistical significance was determined by using a two-tailed unpaired Student's t-test or its nonparametric equivalent Mann-Whitney, one-way ANOVA, or its nonparametric equivalent or Kruskal-Wallis, or two-way ANOVA with a Tukey *post hoc* test where appropriate. Normality was tested with the Shapiro-Wilk normality test. Statistical significance was defined by a p-value of ≤ 0.05. When applicable, data were normalized as previously described (Xie *et al.*, 2019). Statistical analyses were

performed in GraphPad Prism 6 (GraphPad Software, La Jolla, CA, USA). Gardner-Altman estimation plots were created in the R-statistical program (The R Foundation, Aukland, New Zealand) or on www.estimationstats.com (Ho *et al.*, 2019) and show the mean difference between groups is shown. Both groups are plotted on the left or top axes; the mean difference is plotted on floating axes on the right or bottom as a bootstrap sampling distribution. The mean difference is depicted as a dot; the 95% confidence interval is indicated by the ends of the vertical error bar. All remaining figures were created in GraphPad Prism 6.

3.2

Development of the Zebrafish Tracking Module DanioReReader v2.0 using MATLAB®

C.A. Brown[1], G. Zoidl[1,2]

[1] Department of Biology, York University, Toronto, ON M3J 1P3, Canada, [2] Department of Psychology, York University, Toronto, ON M3J 1P3, Canada

Author Contributions: Program design and script, C.A.B.; writing—original draft preparation, C.A.B.; writing—review and editing, C.A.B., and G.Z.; supervision, G.Z.; funding acquisition, G.Z

3.2.1 Abstract

Zebrafish (*Danio rerio*) have been brought to the forefront of alternative animal models since breeding, and animal housing is compatible with high-throughput assessments and large stock maintenance, respectively; a challenge otherwise faced with murine animal models. Larval locomotor activity is essential to zebrafish hunting, predator defense, and social interaction. Subsequently, this behavior is also a direct reflection of neural activity of the CNS and is modulated by external stimuli targeting various sensory systems. As such, tracking zebrafish larval movement is fundamental to modern research; however, the accuracy of detecting larval movement is challenging due to their small size and the presence of background artifacts. Moreover, most commercial high-end software designed to track larval locomotion is costly and is unable to be manipulated without the purchase of additional plug-ins or programs. Here, we aimed to create a program serving as an in-house, open-source alternative for tracking zebrafish locomotion. *DanioReReader v2.0* was created in MATLAB® based on a 48-well plate configuration. The generalized algorithm of the MATLAB® script was as follows: (1) select video file input, (2) detect well boundaries, (3) detect larvae via background subtraction, (4) perform video analysis to compute speed (mm/sec) or time (s) variables as appropriate, (5) generate a figure output. While the *DanioReReader v2.0* program is promising, we faced challenges with well and/or larval detection in various video files. As such, we propose implementing machine learning codes into the *DanioReReader v2.0* script to strengthen its tracking abilities.

3.2.2 Stage I: Well Threshold Detection

We developed a MATLAB® script entitled *DanioReReader v2.0* that tracks and analyses zebrafish locomotor activity. The program was designed to read video files of zebrafish larvae in a 48-well plate format and is compatible with various file extensions (Audio Video Interleave, *.avi; Motion JPEG 2000, *.mj2; Moving Pictures Experts Group, *.mpg; Windows Media Video, *.wmv; MPEG-4, *.mp4., and

MOV, *.mov). To initiate the program, the user selects “New Project” under the file menu and chooses an appropriate video file (**Figure 3.1**). Here, *DanioReReader v2.0* performs background analysis to calculate the frame rate, video duration, and the number of frames of the video file. The first frame of the video file is converted from a color RBG image to grayscale and previewed using the *imshow* function. The file name and path are displayed for confirmation. The *VideoReader* function reads the video files for the purpose.

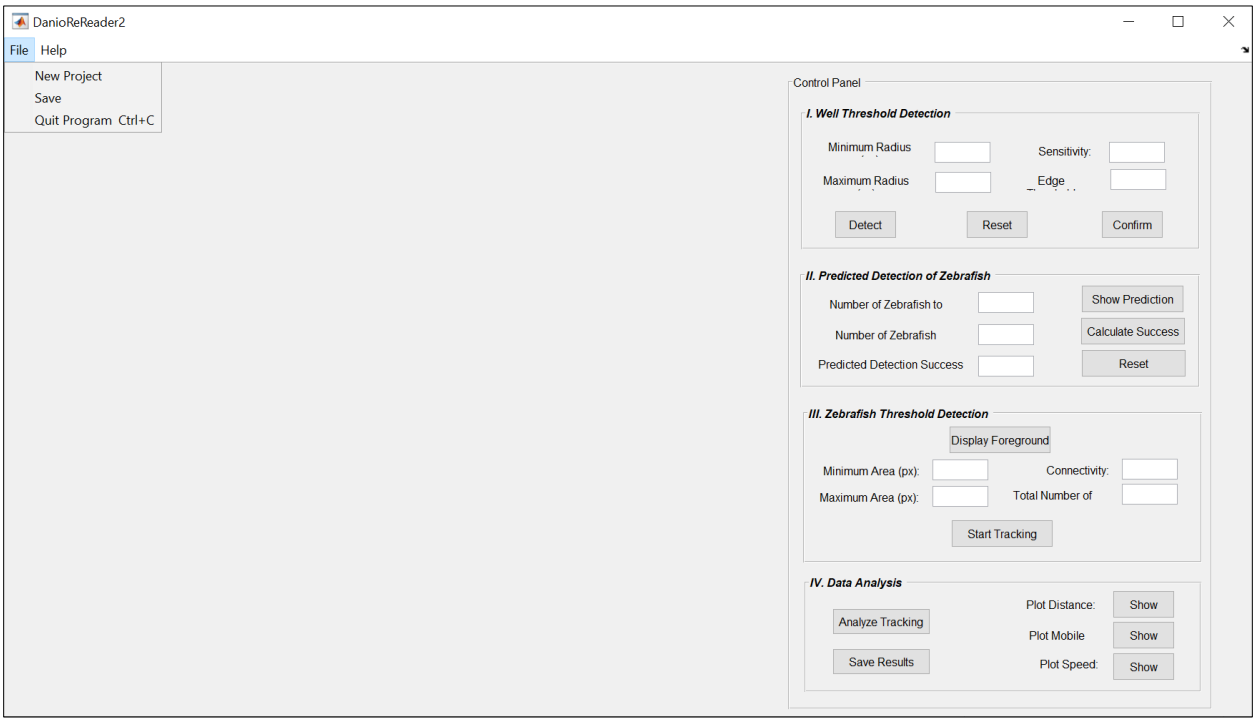

Figure 3.1. DanioReReader v2.0 Initial Interface.

The initial interface of the DanioReReader v2.0 program. User selects ‘New Project’ from the File drop-down menu to begin analyzing video data of zebrafish larvae in a 48-well plate configuration.

Since larval behavioral data is commonly performed in a multi-well format, our program design needed to account for the location restrictions of individual wells. As such, we scripted *DanioReReader v2.0* to identify the 48-well plate format using the first frame of the video file. Here, stage *I. Well Threshold Detection* identifies the wells using the *imfindcircles* command and subsequently stores the centroid x- and y- coordinates and the radius for later processing. All 48 wells must be detected here, or else MATLAB® is unable to complete running the program. The *imfindcircles* command requires the minimum radius, maximum radius, sensitivity, and edge threshold variables to be defined by the user. In this way, the program script can be modified to suit various multi-well plate formats. The minimum and maximum radius of the wells are reported in pixels where the minimum value must not exceed the maximum. Pixel dimensions are scaled to millimeters in the final data analysis based on the known standard measurements

of the 48-well plate. The sensitivity variable specifies the sensitivity factor in the range [0 1] for finding circles. High sensitivity values lead to the detection of more circles, including weak or partially obscured ones; however, this was at the risk of a higher false detection rate. Lastly, a scalar K in the range [0 1] specifies the gradient threshold for determining edge pixels. K = 0 sets the threshold at the zero-gradient magnitude, and K = 1 sets the threshold at the maximum gradient magnitude in the image. As such, a high edge threshold value detects wells with visibly strong and well-defined edges. In contrast, a low edge threshold value detects circles with faint edges. **Table 3.1** outlines the parameters we found to be sufficient for our test video file.

Protocol: To use stage *I. Well Threshold Detection* in the control panel, the user must complete all fields and select the detect button. Troubleshooting may be required; reset if several attempts are needed. Test detections are shown in red and automatically generate within twenty seconds (**Figure 3.2**). Upon the successful detection of all 48-wells, the user selects confirm. DanioReReader v2.0 will automatically store the centroid coordinates and well radius for future processing. Once the circles detected appear in blue, the process is complete (**Figure 3.3**).

Table 3.1. Recommended Parameters for Well Detection in DanioReReader v2.0.

Parameter	Value
Minimum Radius (pixel)	47
Maximum Radius (pixel)	64
Sensitivity	0.973
Edge Threshold	0.09

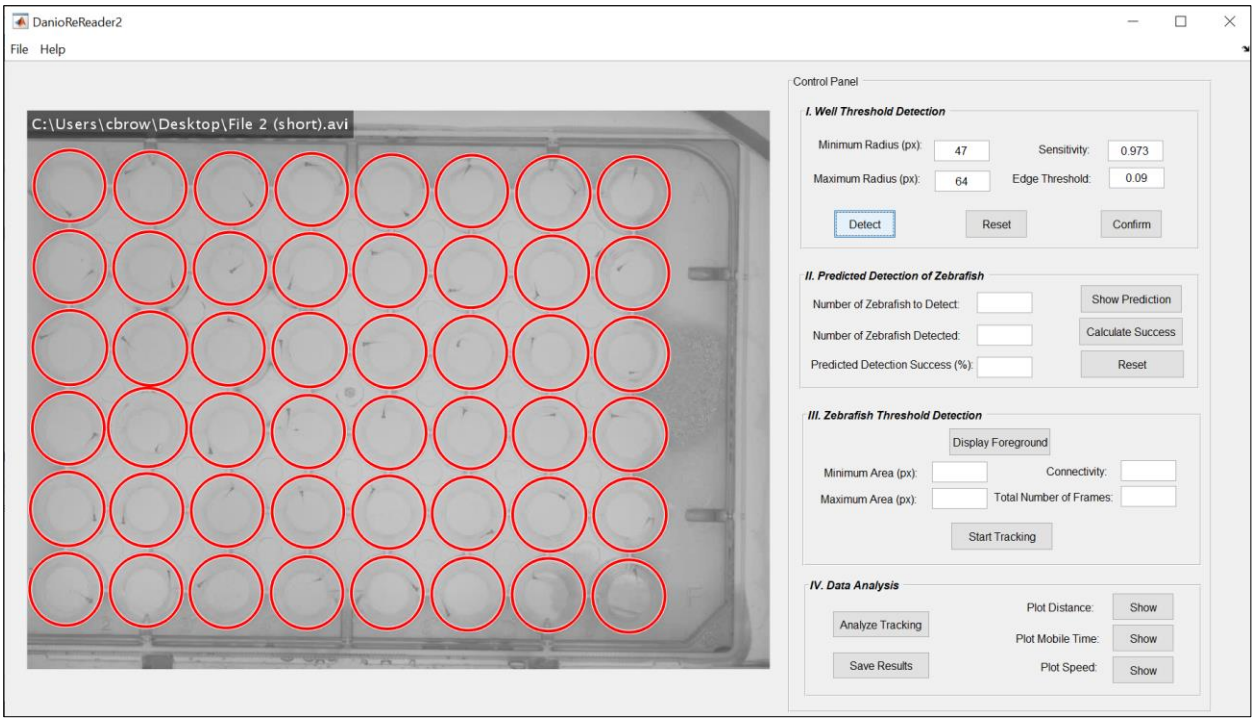

Figure 3.2. Stage I – Well Threshold Detection Initialization.

Well Threshold Detection utilizes the imfindcircles command in MATLAB® and stores the coordinates of each detected well for future calculations. Detected wells are displayed in red.

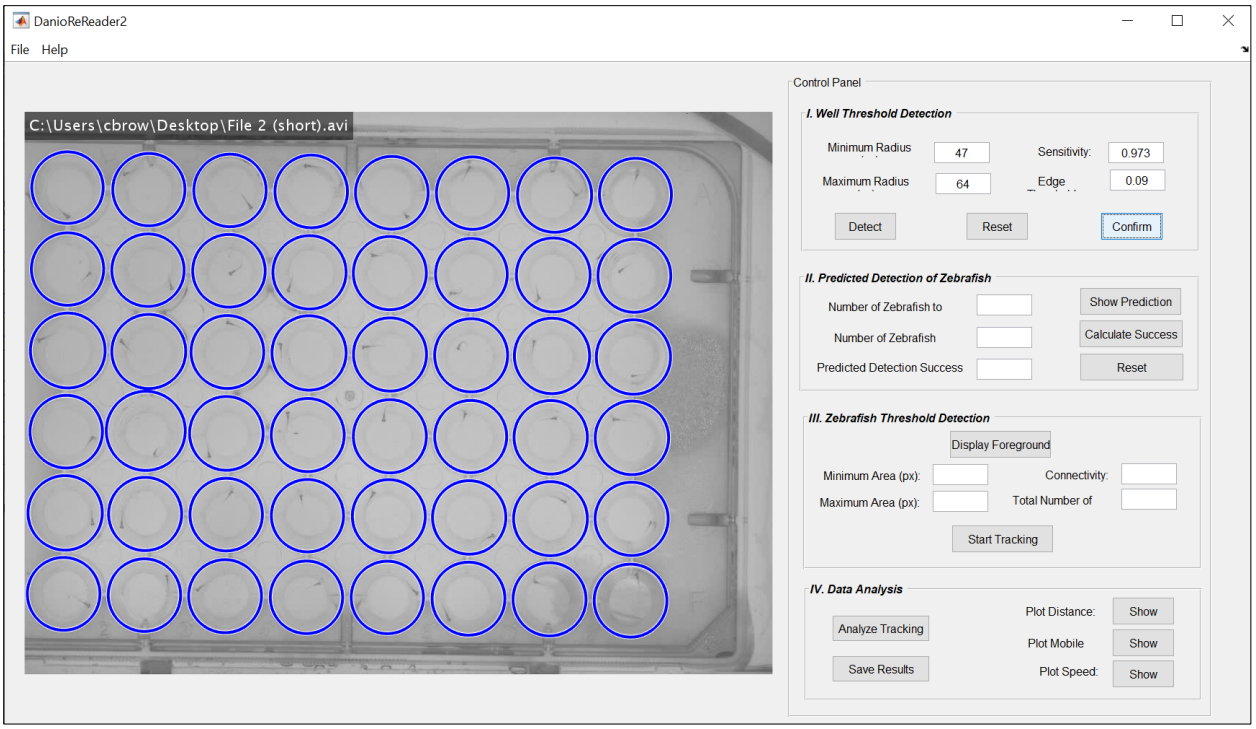

Figure 3.3. Stage I – Well Threshold Detection Confirmation.

Once all 48 wells are successfully detected, the user confirms the well location to store the coordinates. The processing is complete once the detected wells are highlighted in blue.

3.2.3 Stage II: Predicted Detection of Zebrafish

We recognized that zebrafish larval tracking tools were limited by the sharpness of the camera recording the video, the level of contrast between the zebrafish larvae, and the background of the multi-well plate. As such, we included stage *II. Predicted Detection of Zebrafish* as an optional parameter to estimate the quality of video files for zebrafish larval detection using the *detectBRISKFeatures* function. Here, the most dominant features were detected in the first frame preview of the video file. We defined the *detectBRISKFeatures* variables minimum intensity difference (MinContrast) and the number of octaves (NumOctaves) within the script. MinContrast specifies the contrast between the target feature and its surrounding background within a range of [0 1]. NumOctaves determines the size of the target feature detected; although an integer ≥ 0 could be used, the recommended range was defined as [0 4]. Based on the quality of our test video file, we set MinConstrast as 0.2 and the NumOctaves as 1 for the detection of zebrafish larvae. The predicted success of larval detection (%) was calculated by comparing the number of fish detected using the *detectBRISKFeatures* function to the actual number of zebrafish larvae in the multi-well plate.

Protocol: To initiate the predicted detection of zebrafish, the number of larvae in the multi-well plate is defined in the appropriate field. Once the user selects show prediction, the detected larvae are highlighted in green. An estimate of detection accuracy is calculated by counting the amount of successfully captured fish and entering the value in the *Number of Fish Detected* field. Here, we found that *detectBRISKFeatures* may detect distinct differences in the body morphology and highlight larvae more than once. In such cases, only one detection is to be counted. A reset button was also included in the case of an error. The estimated success, measured in percentage (%), is calculated once calculate success is selected (**Figure 3.4**). We acknowledge that while this serves as an estimation tool, the unselected larvae are still eligible for successful detection in the next stage of *DanioReReader v2.0.*

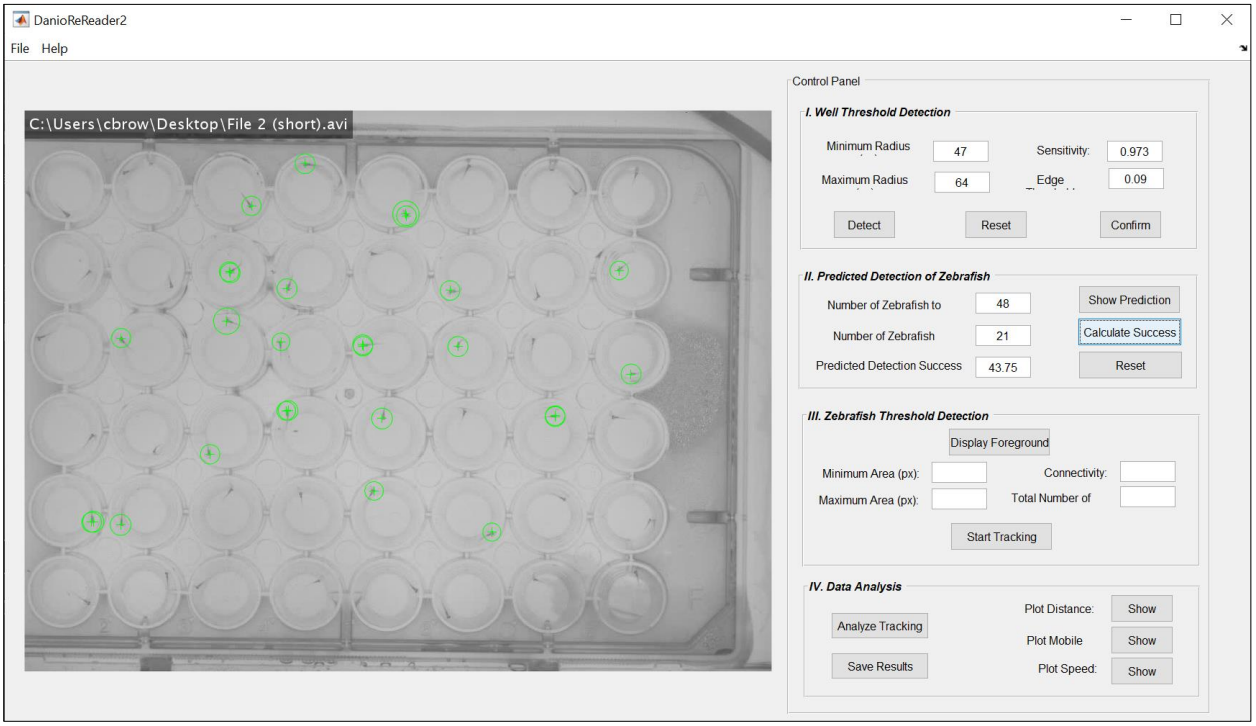

Figure 3.4. Stage II – Predicted Detection of Zebrafish.

As an optional feature, the predicted detection of zebrafish was included. Here, the detectBRISKFeatures command in MATLAB® was utilized to offer the user an estimation of the larvae to be detected. The command detects zebrafish larvae based on the initial video frame.

3.2.4 Stage III: Zebrafish Threshold Detection

The overarching objective of *DanioReReader v2.0* was to provide functionality as a zebrafish larval tracking tool. Here, we tracked larval activity using a background subtraction method via the Computer Vision Toolbox™ provided by MathWorks. The video file is read by *vision.VideoFileReader* and plays using the *vision.VideoPlayer* function. We used the *vision.ForegroundDetector* function to segment the

pixels associated with the multi-well plate background or part of the foreground. As such, background subtraction allowed for the discrimination of zebrafish larvae in the foreground. We specified the number of Gaussian modes in the mixture model (NumGaussians) and the number of training frames (NumTrainingFrames), which are standard variables of the *vision.ForegroundDetector*. The NumGaussians algorithm models each pixel in the frame to allow for the removal of the stationary background. NumGaussians is defined by a positive integer, although typically within the range of [3 5]. We optimized the number of training frames to be appropriate for tracking accuracy while remaining time-efficient. Here, a NumGaussians of 3, and a NumTrainingFrames of 50, were sufficient to create a foreground overlay to discriminate larvae from the multi-well plate background. Pixels in the foreground, representing the zebrafish larvae, were then grouped by the maximum area, minimum area, and connectivity of the pixels defined by the user. **Table 3.2** outlines the parameters we found to be sufficient in our test video file.

Protocol: In this stage, the user initially selects display foreground to overlay the foreground image pixels (outlined in white), representing the larvae (**Figure 3.5**). The pixels are grouped by estimating the minimum and maximum area (in pixels) of the zebrafish. The minimum must not exceed the maximum. Here, we found a minimum area of 50px and a maximum area of 90px were sufficient to detect larvae for tracking. Lastly, the connectivity parameter indicates which pixels are connected and can only hold a value of 4 or 8, although we recommend choosing the higher connectivity. Start tracking initiates the tracking protocol. The video will display red circles tracking larvae movement. Processing time may vary depending on the length of the video file. The MATLAB® command window will be unavailable until the tracking is complete and the user is prompted with a confirmation message (**Figure 3.6**).

Table 3.2. Recommended parameters for Larval Detection in DanioReReader v2.0

Parameter	Value
Minimum Area (pixel)	50
Maximum Area (pixel)	90
Connectivity	8

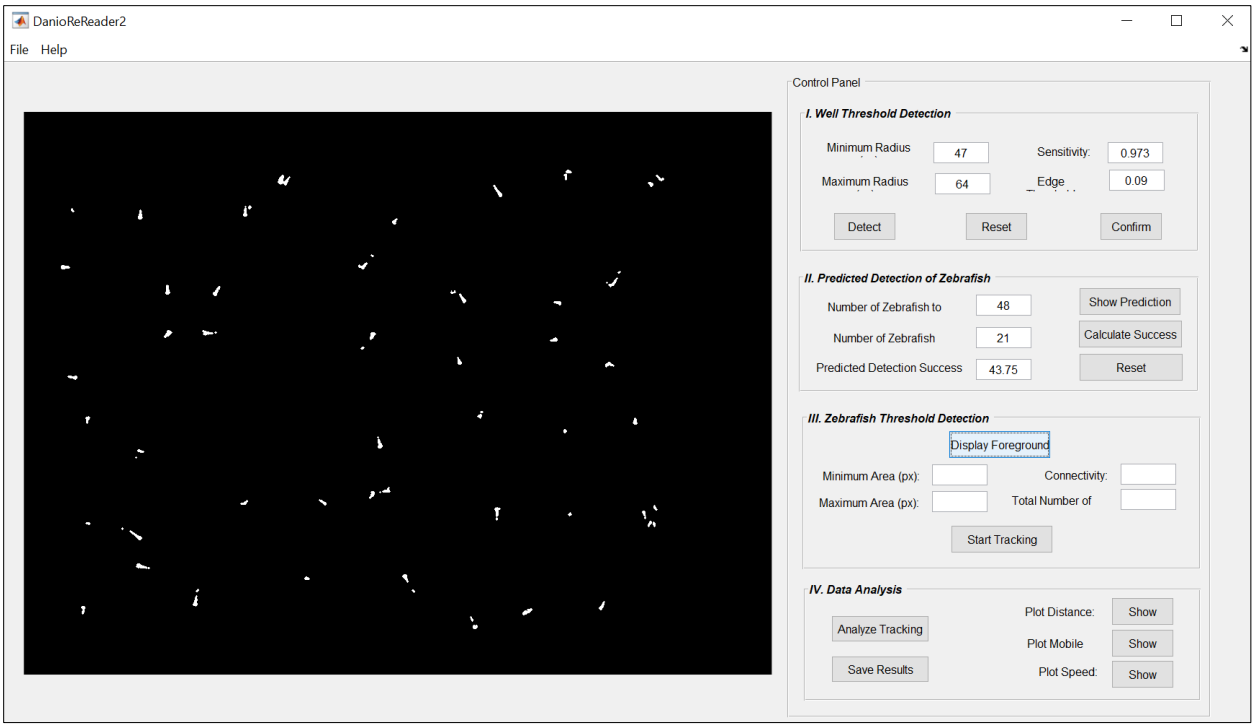

Figure 3.5. Stage III – Zebrafish Threshold Detection Foreground Display.

To avoid the detection of artifacts, a background subtraction method was implemented. The display foreground function removes the background and displays zebrafish larvae in white, where the user can select the size range and connectivity of pixels to track.

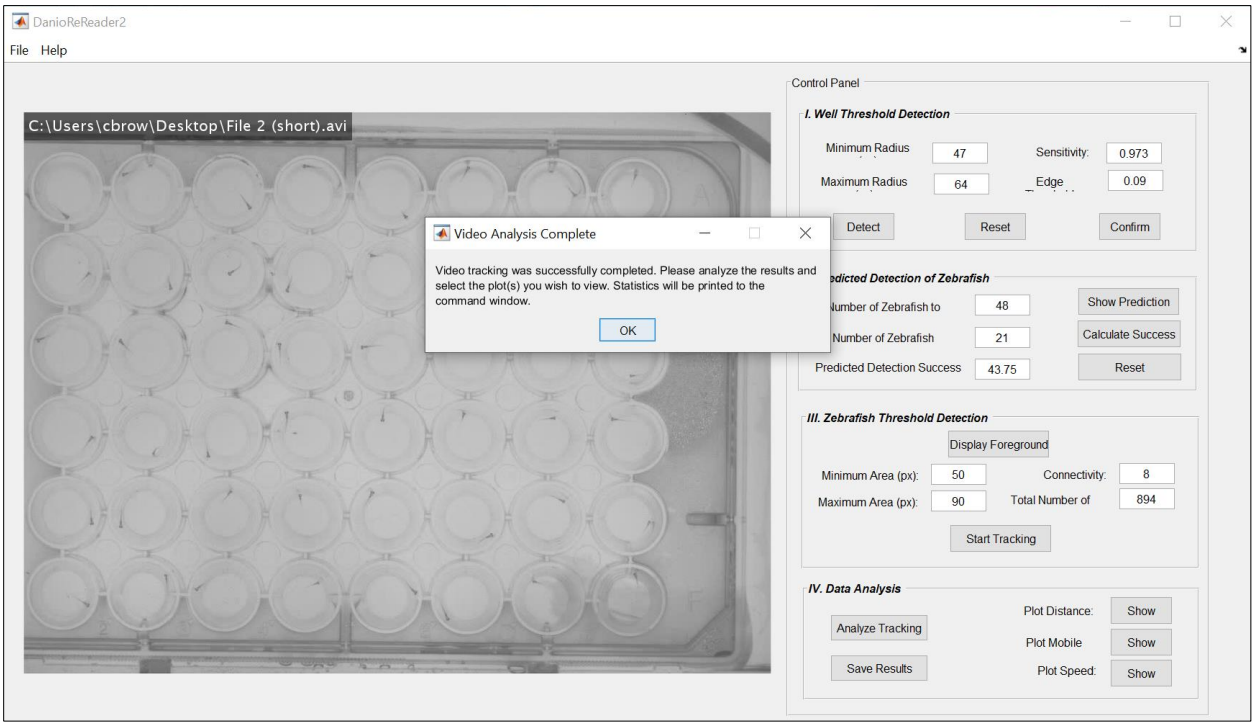

Figure 3.6. Stage III – Zebrafish Threshold Detection Completed Analysis Prompt.

Once video tracking is complete, the user is prompted with a command window to confirm the successful analysis of tracking.

3.2.5 Stage IV: Data Analysis

In the final stage of the program design, we scripted output arguments to provide various options for locomotor data analysis. Upon completion of larval tracking, *DanioReReader v2.0* sorts the x- and y-coordinates of the well's centroid and radius (see section 2.6.1) and assigns a number corresponding to the standard 48-well plate configuration. Similarly, the x- and y- coordinates of the zebrafish larvae are sorted by their respective well location per video frame. *DanioReReader v2.0* performs simple calculations to return the descriptive statistics and heatmaps of the (1) distance traveled (mm), (2) mobility duration (s), and (3) swim speed (mm/s). The heatmap output provided a graphical illustration to account for individual larva differences and location bias. Here, heatmaps of the larval activity were created using the *microplateplot* function available from MATLAB®'s Bioinformatics Toolbox™. Finally, *DanioReReader v2.0* prints the summary of the mean, standard deviation (SD), and standard error of the mean (SEM) for each variable into the command window and enters the results into a spreadsheet for further analysis.

Protocol: To begin the data analysis, the user selects analyze tracking. *DanioReReader v2.0* performs background calculations, and a prompt appears when this step is complete (**Figure 3.7**). The data files are saved to an excel spreadsheet using save result or by clicking "Save" under the file menu. Additionally,

heatmaps of the multi-well plate illustrations are generated by selecting show. The user may manually save the figure under the available formats in the pop-up figure window. The respective statistics (mean, SD, and SEM) are printed to the command window.

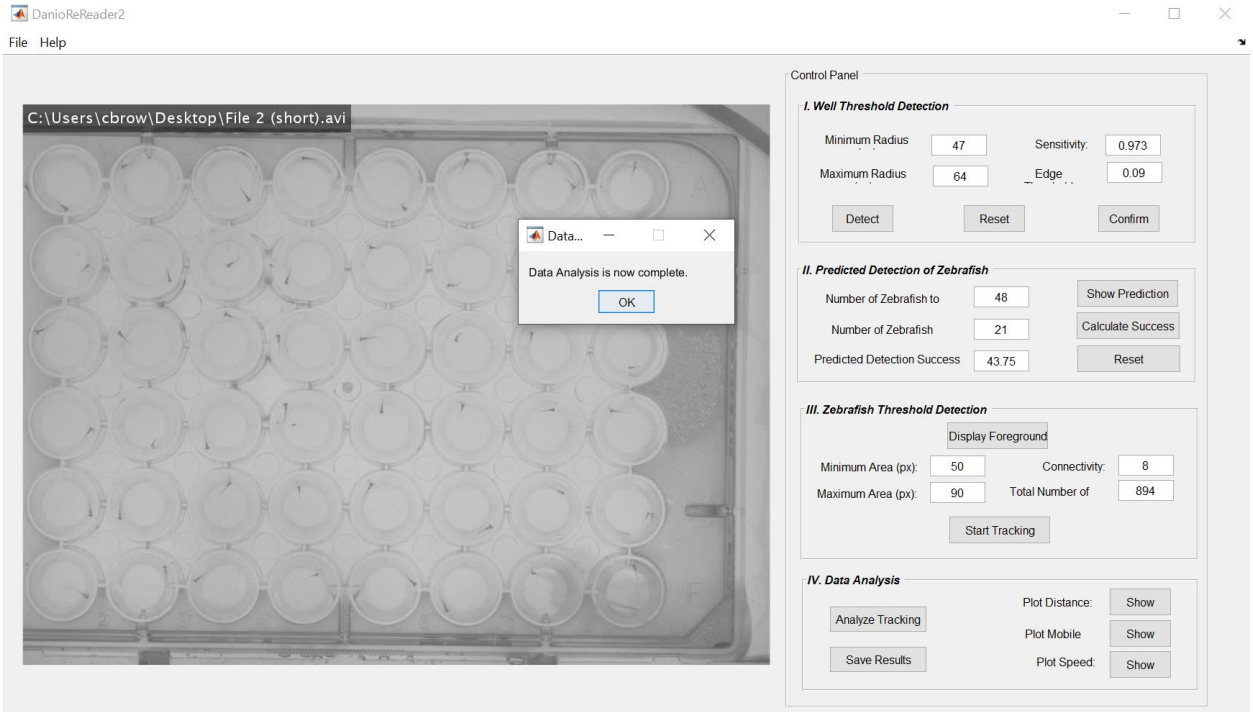

Figure 3.7. Stage IV – Data Analysis.

Data analysis is initiated by the selection of 'Analyze Tracking.' Various heat map plots are then generated and can be visualized using the 'show' button for the appropriate parameter; the Bioinformatics toolbox in MATLAB® was utilized for this purpose. All calculations are exported and saved into an excel spreadsheet upon the selection of 'Save Results.'

3.2.6 Discussion

DanioReReader v2.0 initiates a user-friendly interface for the tracking of zebrafish larvae (*Danio rerio*) in a multi-well plate. Currently, the program supports a 48-well plate configuration and assumes each well has one larva. The program also assumes that each multi-well plate contains genetically indistinguishable zebrafish larvae, although the data output (.xls) allows for segregation and analysis in other programs. Detection and analysis of zebrafish behaviors are completed in a four-stage manner which is modifiable in the control panel. Upon completion, statistics are printed to the command window, and multi-well plots are made available for visualization.

3.2.6.1 Applications of the program

We designed *DanioReReader v2.0* to provide a tracking and data analysis tool for the study of zebrafish larval locomotor activity. Here, the distance traveled (mm), mobility duration (s), and swim speed (mm/s) are reported to the user. While we acknowledge that these are the most common parameters measured in behavioral studies, additional analysis may be required. Moreover, the mean, STD, and SEM are reported for graphing convenience, although additional descriptive statistics may be useful depending on the plot choice. For this reason, we allowed the source code to remain open for additional modifications and customizable algorithms to be added.

To build the program script, we utilized a test video that featured the spontaneous swimming activity of wild-type larvae under ambient light. However, we anticipate *DanioReReader v2.0* to have much broader applications. A catalog of well-described zebrafish behaviors allows for the measurement of a variety of phenotypes, including fear, anxiety, and cognition. As such, *DanioReReader v2.0* is compatible with experimental designs targeting sensorimotor activity (olfaction, auditory, vision) to delineate the changes in swimming activity as it relates to behavioral phenotypes. Moreover, genetic and pharmacological manipulation can be applied while recording spontaneous or sensorimotor-induced behaviors. We believe that *DanioReReader v2.0* will be a useful tool to address fundamental questions in neuronal communication while adding to the cognitive and sensorimotor analysis toolbox currently available.

3.2.6.2 Comparison with other Programs

Tracking zebrafish locomotion is commonly achieved with commercial packages made available by *Zebralab*® designed by ViewPoint (Montreal, QC) and *Ethovision*® designed by Noldus Information Technology (Leesburg, VA). The advantages of such packages are that they have been optimized to the hardware utilized for the video recording of larvae locomotion. Moreover, the user-friendly interface allows for customizable multi-well plate selections. However, such programs are costly and are restricted to the initial computer the package was installed on. As such, computer software upgrades are often incompatible with the current version of commercial zebrafish tracking packages installed and thus quickly become outdated. To address these problems, zebrafish larvae tracking programs designed in open-source programming software, such as MATLAB®, allow for versatility in computer software upgrades and custom-designed experimental apparatuses.

Cario et al. (2011) published the MATLAB® open-source codes *LSRTrack* and *LSRanalyze* for tracking and analyzing zebrafish larvae locomotion (Cario *et al.*, 2011). Similar to *DanioReReader v2.0*, *LSRTrack* records locomotion by executing the generalized protocol where the program i) identifies the multi-well plate coordinates, ii) performs background subtraction, and iii) subsequently tracks the

coordinates of larvae corresponding to the multi-well plate coordinates. However, *LSRTrack* provides additional versatility by accepting a wider variety of multi-well plate configurations (6-, 12-, 24-, 48-, and 96-well plates). The assumption here is that the multi-well plate contains round wells. Moreover, the *LSRanalyze* provides additional measurements not currently available in *DanioReReader v2.0*, such as positional preference, acceleration, frequency of movement events, and rest periods (Zhou *et al.*, 2014); although this could be easily scripted. *DanioReReader v2.0* is unique in that it provides an estimate of the video quality before initiating the tracking protocol. In this way, the user can optimize the experimental apparatus and camera quality before lengthy data analysis. Both programs, however, cannot discriminate the kinematics of larval locomotion. Such analysis would require a more complex algorithm as previously described (Fontaine *et al.*, 2008). Taken together, both *DanioReReader v2.0* and *LSRTrack* are open-source code platforms designed to measure zebrafish larval locomotor activity, whereas *LSRTrack* provides additional multi-well plate formats and descriptive statistics should such analyses be required. For the analysis of larval locomotor kinematics, we propose alternative software or subsequent MATLAB® scripting.

3.2.6.3 Limitations & Critical Considerations

DanioReReader v2.0 was created with MATLAB® and enables data extraction from video files. While MATLAB® supports various video file extensions, the video input must be a format read by MATLAB®. Here, we scripted *DanioReReader v2.0* to read *.avi; *.mj2, *.mpg, *.wmv, *.mp4., and, *.mov file extensions. Video file extensions not currently included in *DanioReReader v2.0*, but supported by MATLAB®, may be written into the script for additional versatility. For unsupported video files, file conversion is necessary. However, the caveat is that file conversion may compromise the file and thus impact the quality of discrimination between larvae and the background necessary for accurate tracking. Alternatively, the user may complete data analysis in comparable programs (see section 3.2.6.2) to preserve video integrity.

High-speed video recordings of zebrafish larvae in a 48-well configuration are read by *DanioReReader v2.0* for the high-throughput analysis of locomotor activity. However, behavioral studies employing 6-, 12-, 24-, or 96-well configuration, commonly used for thigmotaxic and visual-motor response assays, are not currently supported and would need to be scripted for use in *DanioReReader v2.0*. Nevertheless, we acknowledge that video files that meet the basic configuration requirements of *DanioReReader v2.0* are limited by the program assumptions. Firstly, the wells must be round since the multi-well detection protocol utilized the *imfindcircles* function to detect the round edges of the well. While square multi-well formats are less common, to achieve multi-well detection in such cases, one would need to script a shape recognition protocol typically achieved with the *regionprops* command. Secondly,

DanioReReader v2.0 assumes that only one larva is present per well. This allowed for i) unequivocal larval detection and ii) the sorting of larvae to expose location or individual bias. As such, experimental designs targeting social behavior, such as shoaling, would require analysis in a different program. Additionally, the experimental design must account for the combination of the visibility of larva in the multi-well plate and the camera quality. Transparent larvae, known as Casper zebrafish, do not provide a high enough contrast with the multi-well plate. As such, zebrafish larvae must appear dark against a light background to be detected in the foreground. Moreover, a consistent illumination across the multi-well plate is ideal so that zebrafish can be discriminated against the darker pixels; this also limits the potential for location bias. The last consideration accounts for the quality of the camera. High-speed cameras are typically employed for tracking zebrafish larvae locomotion since burst activity, and tail bends require this level of competence. For recording purposes, the camera needs to be placed directly above the plate and at a sufficient distance to limit the visibility of the well's wall so that the surface of each well is displayed equally.

As previously mentioned, our test video used to build the *DanioReReader v2.0* script featured the spontaneous swimming activity of wild-type larvae under ambient light. However, we occasionally found that other video files that meet the configuration requirements and program assumptions produced errors in well-detection and tracking. As such, this would need to be addressed in the future. We suspect that applying a higher-level machine learning protocol would eliminate the challenges in video files with slight variability. Nevertheless, we believe that the *DanioReReader v2.0* script will be advantageous for building subsequent program designs and has great potential to develop into an interface for advanced zebrafish behavioral analysis.

3.3

Zebrafish Lacking the Gap Junction Delta-2b (Cx35b) Gene Exhibit Deficits in Cranial Development and Swimming Competence

Cherie A. Brown[1], Christiane Zoidl[1], Georg Zoidl[1,2]

[1] Department of Biology, York University, Toronto, ON M3J 1P3, Canada, [2] Department of Psychology, York University, Toronto, ON M3J 1P3, Canada

Author Contributions: Conceptualization, C.A.B., and G.Z.; investigation-, C.Z. (immunohistochemistry and RT-qPCR) and C.A.B. (Genome engineering of knock-out animals and all else); data analysis, G.Z. (RT-qPCR), C.A.B. (all else); data interpretation, C.A.B.; writing—original draft preparation, C.A.B.; writing—review and editing, C.A.B., and G.Z.; supervision, G.Z.; funding acquisition, G.Z.

3.3.1 Abstract

In mammals, connexin-36 (Cx36) is the major component of electrical synapses, also found alongside chemical synapses in mixed synapses throughout the vertebrate brain. However, it is unclear how homotypic Cx36 aggregations are capable of neuronal rectification, supporting higher-order brain processing. As such, we utilized the zebrafish animal model that expresses the Cx36 ortholog, Cx35b, presynaptically. Although previous studies have demonstrated that Cx35b is highly expressed in the CNS, current literature has yet to explicitly explore its contributions to circuitry or behavioral phenotypes. We hypothesized that complex alterations to neuronal circuitry via Cx35b knock-out (KO, $Cx35b^{-/-}$) would affect vision, sensorimotor gating, and plasticity-dependent cognitive processing. Targeted ablation of Cx35b was achieved using Cas9/CRISPR technology. Adult homozygous $Cx35b^{-/-}$ fish showed no morphological abnormalities and bred normally; however, progeny (7dpf) displayed larger body sizes and smaller midbrain diameters suggestive of cranial deficits. Alterations in neuronal circuitry were determined by tracking larval locomotion in age-matched larvae. We found that the circuitry underlying spontaneous (i.e., unprovoked) dominant swimming competence was impacted in a light-dependent manner in $Cx35b^{-/-}$ animals; larvae reduced coast swimming bouts in darkness. However, the Mauthner-driven burst swimming was significantly enhanced in Cx35b KOs when exposed to a white- or black-surround well. We suspect that the evolutionary divergence of the *GJD2* gene has led to unique morphological and physiological properties of each Cx36 ortholog. As such, zebrafish could serve as an ideal model organism to investigate the functionality of Cx35b *in vivo* and to better elucidate the multiple cellular roles of mammalian Cx36.

3.3.2 Cx35b$^{-/-}$ Transgenic Line was Established via the CRISPR-Cas9 Genome Engineering Strategy.

We created a Cx35b knock-out (Cx35b$^{-/-}$) model utilizing the CRISPR-Cas9 genome engineering strategy and screened for knock-out candidates produced via idel mutations of the erroneous non-homologous end joining (NHEJ) repair system. Here, exon 1 of the *gjd2b* gene was targeted by designing proximal sgRNAs upstream of the start codon, directed against the sense or antisense DNA strand. Since this method was utilized as an alternative to the TALEN strategy, various protocols for optimization were implemented (data not shown). In the final approach, the sgRNA directed against the antisense strand was successful, and assembly of the RNP complex was carried out in a 1:2 Cas9:gRNA ratio. DNA sequencing verified the specific indel mutation produced. Our founding transgenic line was derived from a heterozygous animal with a 1bp substitution (G12 →A); when translated, this corresponded to amino acid 4 (Tryptophan 4) in wild-type animals but an aberrant early stop codon in knock-out animals (**Figure 3.8**). The knock-out genotype was germline transmissible and outbred for two generations before establishing the homozygous transgenic line.

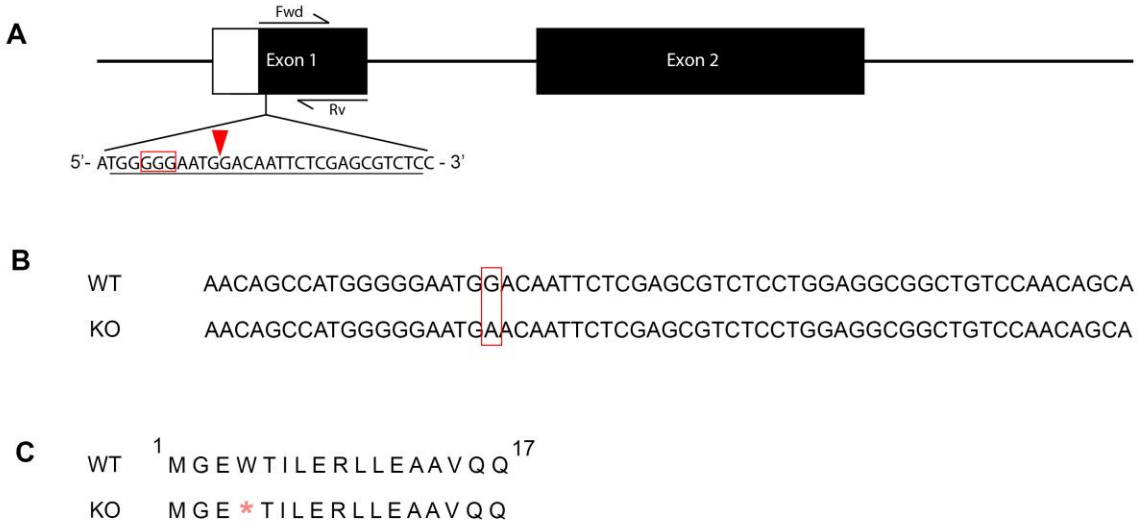

Figure 3.8. CRISPR-Cas9 Targeting Strategy for the gjd2b Gene.

(A) General overview of the Cx35b gene topology. Forward and reverse primers that targeted exon 1 were designed to determine successful CRISPR mutations. PAM sequence is outlined by the red box; CRISPR-Cas9 cut sight is outlined by the red arrow. (B) Cx35b partial DNA sequence. The CRISPR-Cas9 genome engineering strategy produced a 1bp substitution at position 12 of exon 1, resulting in the conversion of G to A in Cx35b$^{-/-}$ (KO) animals. The mutation is outlined with a red box. (C) The mutation produced by CRISPR-Cas9 resulted in the coding of an early stop codon in KO animals, as indicated by the red asterisk (*).

3.3.3 Loss of Cx35b Expression was Confirmed by Pronounced Alterations in the Retina

Previous reports have demonstrated robust expression of Cx35b within the zebrafish retina; however, these results are typically confounded due to the unavailability of antibodies specifically targeting the Cx35b ortholog. As such, to confirm the Cx35b$^{-/-}$ phenotype, we performed immunohistochemistry on wild-type and Cx35b$^{-/-}$ adult zebrafish retinal tissues and screened for changes in expression patterns. Here, a significant reduction in the fluorescence signal was observed in the inner plexiform layer (IPL) of Cx35b$^{-/-}$ larvae. Moreover, we observed greater spacing between photoreceptor cells (PRCs) in Cx35b$^{-/-}$ larvae suggesting that the knock-out phenotype affected PRCs in a cell-type-specific manner. The residual signaling prominent in the remaining PRCs and throughout the retina was attributed to the expression of the remaining Cx36 orthologs known to be expressed in this tissue (O'Brien, Al-Ubaidi and Ripps, 1996; O'Brien *et al.*, 1998; Quint *et al.*, 2021) (**Figure 3.9**).

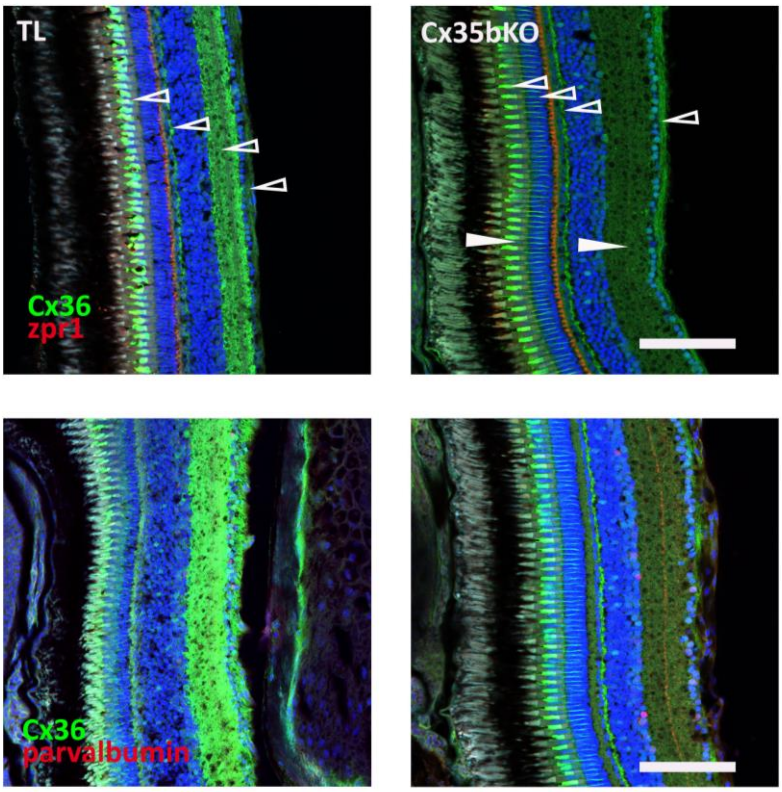

Figure 3.9. Comparison of Adult Retinal Tissue in Wild-type (TL) and Cx35b$^{-/-}$ (KO) animals.

Immunohistochemistry was performed on the retinal tissues derived from adult zebrafish. The monoclonal Cx36 primary antibody was applied to wild-type (TL) (right panel) and Cx35b$^{-/-}$ (KO) tissues (left panel) to determine any deviations in expression patterns. The polyclonal antibodies zpr1 (top panel) and parvalbumin (bottom panel) were used to detect red/green double cones and the calcium-binding protein parvalbumin, respectively. In animals lacking the gdj2b gene, a significant reduction in fluorescence was noted in the IPL layer and between select photoreceptor cells. Scale bar 50µm.

3.3.4 Cx35b$^{-/-}$ Larvae Exhibit Compensatory Regulation Within the Same Gene Family.

Jacobson et al. (2010) previously demonstrated that the regulation of various connexin and pannexin genes remained unchanged in a murine Cx36 knock-out model (Jacobson *et al.*, 2010). However, these results measured Cx30.2, Cx37, Cx43, and Cx45 exclusively and thus provided a limited interpretation of whether a potential connexin-specific compensatory expression mechanism exists in Cx35b$^{-/-}$ animals. Following the genotypic and phenotypic confirmation of our Cx35b$^{-/-}$ model, we explored the consequences of targeted ablation of the *gjd2b* gene on electrical synapses throughout the CNS of zebrafish larvae. To achieve this, we performed quantitative real-time PCR (RT-qPCR) to measure RNA transcript levels as an indication of gene expression. Here, we targeted several genes expressed in neurons (*gjd2b*-Cx35b, *gjd1b*-Cx34.7, *panx1a*-Panx1a, *panx1b*-Panx1b), astrocytes (*gjb8*-Cx30.3, *gja1b*-Cx43), oligodendrocytes (*gjb1a*-Cx27.5, *gjc4a*-Cx44.2, *gjc2*-Cx47.1), microglia (*gjb1a*-Cx27.5, *gjd1b*-*Cx34.7*, *gja1b*-Cx43), and endothelial cells (*gja1b*-Cx43, *gja2*-Cx39.9), to elucidate the underlying gene regulation mechanisms in our Cx35b$^{-/-}$ model. In comparison to the wild-type, Cx39.9 expression levels downregulated 1.87-fold ($p = 0.003$). Our results also demonstrated an upregulation in both Cx47.1 (1.90-fold, $p = 0.009$) and Cx52.9 (1.70-fold, $p = 0.002$). Expression levels of the remaining transcripts in knock-out animals were indistinguishable from the wild-type (**Figure 3.10**). As such, our RT-qPCR data suggest genetic compensatory mechanisms through the regulation of Cx39.9, Cx47.1, and Cx52.9 gap junctions, corresponding to Cx46, Cx45, and Cx59 in human and murine models.

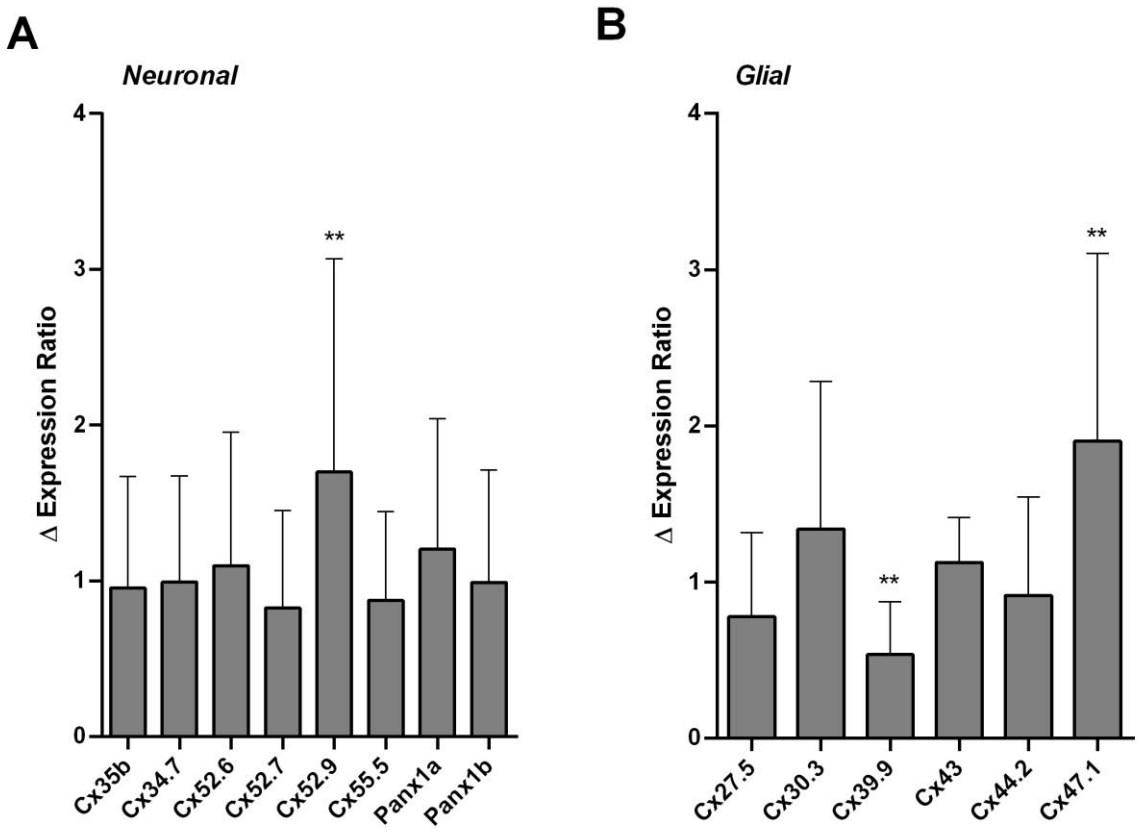

Figure 3.10. Expression Ratios of Connexin/Pannexin Neuronal and Glial Genes via RT-qPCR Analysis.

*RNA transcript levels of several connexin and pannexin genes expressed in (**A**) neurons and (**B**) glial cells, were analyzed by RT-qPCR to determine the relative expression changes in Cx35b$^{-/-}$ larvae. A significant reduction in Cx39.9 expression and upregulation in both Cx47.1 and Cx52.9 expression was observed, suggesting that loss of gjd2b provokes compensatory gene regulation mechanisms. Statistical significance was determined by the One-Way ANOVA test, $p \leq 0.05$, **, $p < 0.001$.*

3.3.5 Dysmorphic Features of the Cx35b$^{-/-}$ Larvae Suggest a Role for *gjd2b* in Growth and Development

We detected developmental deviances in larval morphology by measuring the head-to-tail (body) length, head length, and midbrain diameter (MD) seven days post fertilization (7pdf) (**Figure 3.11A-B**). Here, we found that Cx35b$^{-/-}$ larvae were longer in both body length and head length in comparison to the wild-type (in mm, *Body Length* - WT: 3.84 ± 0.06, n = 19, Cx35b$^{-/-}$: 4.12 ± 0.03, n = 19, p = 0.0003; *Head Length* - WT: 0.70 ± 0.01, Cx35b$^{-/-}$: 0.75 ± 0.01, p = 0.0038, *Mann-Whitney*). However, the MD was indistinguishable between the two genotypes (in mm, WT: 0.52 ± 0.003, Cx35b$^{-/-}$: 0.52 ± 0.004, p = 0.9528) (**Figure 3.11C-E**). These findings lead us to investigate whether the differences in size were proportionate by measuring the head-to-body and head-to-midbrain ratios. Here, we reported no significant differences

in the head-to-body ratio, suggesting that the Cx35b$^{-/-}$ larvae were proportionately larger in their body and head length (WT: 0.18 ± 0.003, Cx35b$^{-/-}$: 0.18 ± 0.002, p = 0.8337) (**Figure 3.11F**). In contrast, the head-to-midbrain ratio revealed that the MD in Cx35b$^{-/-}$ larvae was smaller for their expected head size (WT: 0.74 ± 0.71, Cx35b KO: 0.69 ± 0.01, p = 0.0082) (**Figure 3.11G**). Our results demonstrated that Cx35b expression was involved in driving body and head size trajectories and thus played a role in larval growth and development. Although this was a novel finding, how Cx35b contributes to the signaling mechanisms regulating development was not further explored. Nevertheless, we speculated that the reduction in the midbrain diameter correlated to the loss of Cx35b expression, specifically within this brain region. As such, we expected to observe a loss of functionality in visual sensory integration and motor output pathways in knock-out larvae.

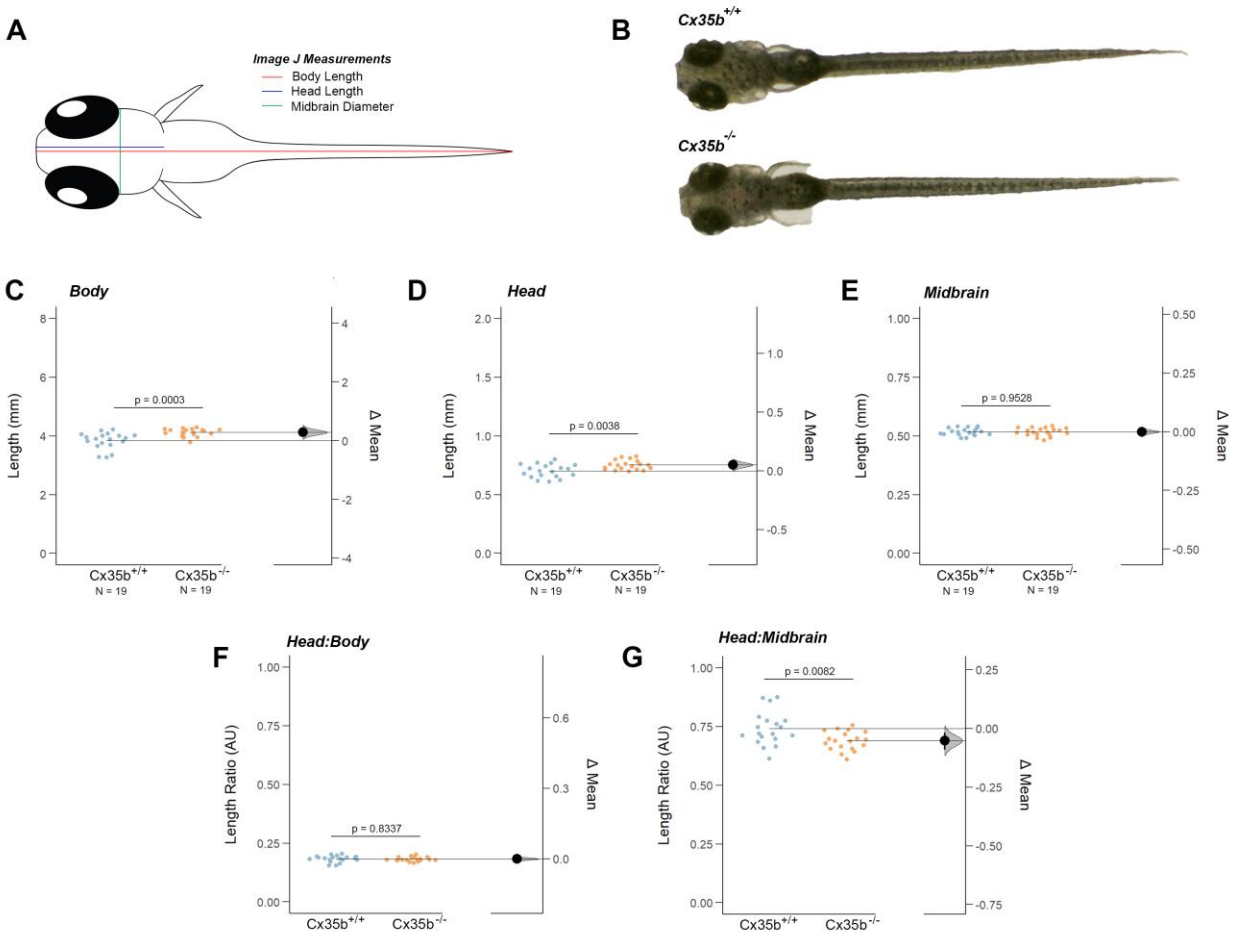

Figure 3.11. Morphological Characterization of Cx35b$^{-/-}$ Larvae Reveal Cranial Defects.

*(**A**) Illustration of the zebrafish measurements taken in Image J. (**B**) A comparison of wild-type (Cx35b$^{+/+}$) and KO (Cx35b$^{-/-}$) zebrafish larva taken under light microscopy. Quantification of the (**C**) body length, (**D**) head length, and (**E**) Midbrain diameter. Cx35b$^{-/-}$ larvae were larger in both body and head length in comparison to the age-matched wild-type larvae. (**F**) Head-to-Body ratio and (**G**) Head-to-Midbrain ratios demonstrated a reduction in the midbrain diameter in Cx35b$^{-/-}$ larvae relative to their body size, suggestive of a cranial defect. Statistical significance was determined by the Mann-Whitney test, $p \leq 0.05$. The sample size (n) was 19 for wild-type and Cx35b$^{-/-}$ larvae.*

3.3.6 Loss of Cx35b Alters Larval Dominant Swimming Competence in Darkness

Given previous reports on Cx35b expression patterns (Jabeen and Thirumalai, 2013) along with our results, we suspected visual-motor deficiencies to be a prominent behavioral phenotype of Cx35b$^{-/-}$ larvae via the loss of Cx35b electrical synapses. To address this, we measured spontaneous locomotor activity in 7dpf zebrafish as an indication of the changes in neuronal circuitry in the presence and absence of light. While both wild-type and Cx35b$^{-/-}$ larvae increased their swimming activity under light conditions (WT: n = 72, $p < 0.0001$; Cx35b$^{-/-}$: n = 72, $p < 0.0001$), Cx35b$^{-/-}$ larvae were indistinguishable from the wild-type

in their distance swam despite lighting conditions (in mm per 10s, *Dark* - WT: 28.49 ± 0.56, n = 72, Cx35b$^{-/-}$: 27.76 ± 0.52, n = 72, p = 0.8578, *Light* - WT: 33.85 ± 0.78, Cx35b$^{-/-}$: 35.19 ± 0.71, p = 0.4706, *Two-Way ANOVA*) (**Figure 3.12A-D**).

We took into consideration that larval swimming distance does not discriminate between the type of bout; larvae typically utilize a combination of slow rhythmic and fast burst bouts, known as the burst-coast behavior, during free swim. Since the signaling pathways underlying slow rhythmic and fast burst bouts are segregated, they provide a more accurate indication of the changes in circuitry involving motor neurons and subsequent muscle recruitment. As such, both dominant and subordinate swimming competence, mediated by slow motor neurons and Mauthner neurons, respectively, were accounted for to assess the changes in neuronal circuitry affecting motor abilities while larvae were unprovoked.

To assess dominant swimming competence, we first measured the coast swimming duration in which swim speeds were less than 20mm/s. In doing so, this allowed us to quantify the activity related to slow motor neurons while excluding burst hyperactivity. Here, we found a significant reduction in the coast duration in Cx35b$^{-/-}$ larvae when exposed to darkness (*in s*, WT: 35.07 ± 0.30, Cx35b$^{-/-}$: 27.86 ± 0.32, p < 0.0001). In contrast, knock-out larvae were indistinguishable from the wild-type under ambient light (in s, WT: 30.90 ± 0.25, Cx35b$^{-/-}$: 30.82 ± 0.30, p = 0.9976). In a similar manner, subordinate swimming competence was measured by the duration larvae spent in burst swim at speeds ≥ 20 mm/s. In comparison to the wild-type, no significant differences in the burst swimming duration were found in darkness (in s, WT: 2.53 ± 0.07, Cx35b$^{-/-}$: 2.54 ± 0.04, p > 0.9999) or under ambient light conditions (in s, WT: 2.58 ± 0.20, Cx35b$^{-/-}$: 2.33 ± 0.09, p = 0.4161) (**Figure 3.12E-H**). Taken together, our results suggest that the circuitry underlying spontaneous (i.e., unprovoked) dominant swimming competence was impacted in a light-dependent manner in Cx35b$^{-/-}$ animals. However, since distance swam was unaffected, we suspect that loss of the *gjd2b* gene alters the larval stride length during coast bouts in darkness.

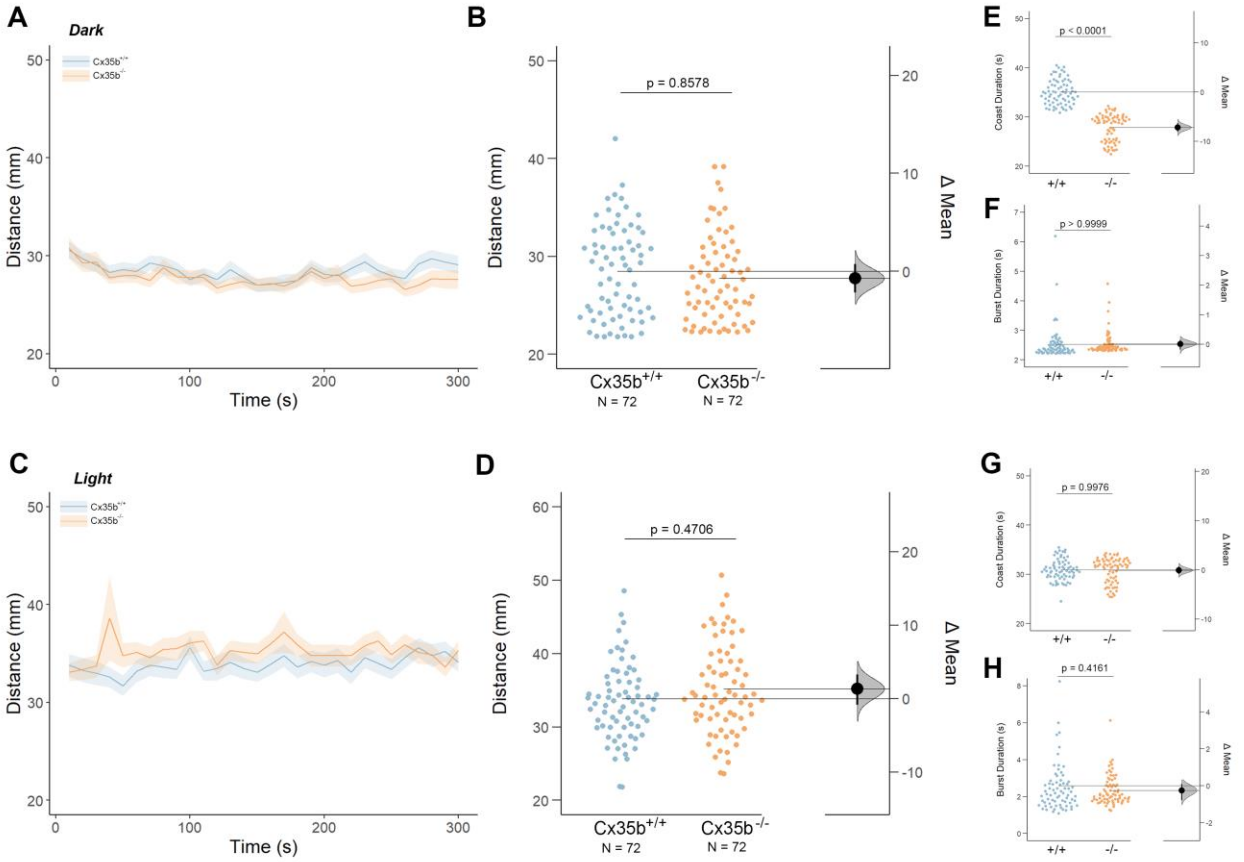

Figure 3.12. Assessment of the Spontaneous Locomotor Activity of Zebrafish Larvae in Continuous Darkness or Light.

*(**A-D**) Spontaneous larval locomotor activity was assessed in a free-swim assay under (**A-B**) dark and (**C-D**) light conditions for a duration of 5 minutes. The distance swam (mm) in larvae lacking the gjd2b gene was indistinguishable from the wild-type. (**E-H**) The duration (s) of larval swimming bouts was assessed by analyzing the burst and coast swimming modalities separately. Cx35b$^{-/-}$ larvae demonstrated a significant reduction in the coast duration under darkness in comparison to the wild-type, suggesting that dominant swimming competence was compromised in a light-dependent manner. All else was indistinguishable from the wild-type. Statistical significance was determined by the Two-Way ANOVA test, $p \leq 0.05$. The sample size (n) was 72 for wild-type and Cx35b$^{-/-}$ larvae.*

3.3.7 Cx35b KO Alters the Visual Subordinate Swimming Competence

Our previous results demonstrated that the spontaneous subordinate swimming competence of Cx35b$^{-/-}$ larvae were unaffected. However, these results led us to question whether provoked burst activity, achieved via sensory stimulation, was impacted in knock-out animals. Since our immunohistochemistry results confirmed an irregular expression pattern in photoreceptor cells and a severe reduction in the IPL, we followed up on these results by providing zebrafish larvae with a visual stimulus and re-assessed subordinate swimming competence. In our strategy, we measured the burst swimming activity of dark-

adapted larvae when placed in a well featuring a black or white surround to simulate a visual discrepancy (**Figure 3.13A**). Here, we found no significant differences in the distance swam in wells with a black surround (in mm per 10s, *Black* - WT: 62.44± 2.58, n=144, Cx35b$^{-/-}$: 61.31 ± 1.88, n=144 p = 0.9658, *Two-Way ANOVA*), or with white-surround wells (in mm per 10s, *White* - WT: 78.10 ± 1.02, Cx35b$^{-/-}$: 70.67 ± 0.67, p = 0.1120). Both genotypes, however, increased their swimming distance in response to the exposure to white surround (WT: p < 0.0001, Cx35b$^{-/-}$: p = 0.0007). Interestingly, a significant increase in burst duration was observed in Cx35b$^{-/-}$ larvae in comparison to the wild-type when exposed to either the black- (in s, WT: 1.29 ± 0.04, Cx35b KO: 1.68 ± 0.06, p > 0.0079) or white-surround wells (in s, WT: 1.42 ± 0.09, Cx35b$^{-/-}$: 2.12 ± 0.13, p < 0.0001). While well color had no impact on the burst duration in wild-type larvae (p = 0.7002), Cx35b$^{-/-}$ hyperactivity was exacerbated when exposed to the white surround (p = 0.0016) (**Figure 3.13 B-E**). As such, our results are indicative of an alteration in the circuitry underlying Mauthner neuron activity exclusively when the visual system is provoked. Moreover, we propose that Cx35b$^{-/-}$ larvae alter their bout type (i.e., burst bouts are favored) and likely the length of bout strides, though we anticipate stride length to be significantly shorter when knock-out larvae are placed in a white surround well. Taken together, we concluded that the *gjd2b* gene contributes to growth, development, and particularly signaling pathways involving the use of unprovoked dominant swimming in darkness and visually-provoked subordinate swimming behaviors.

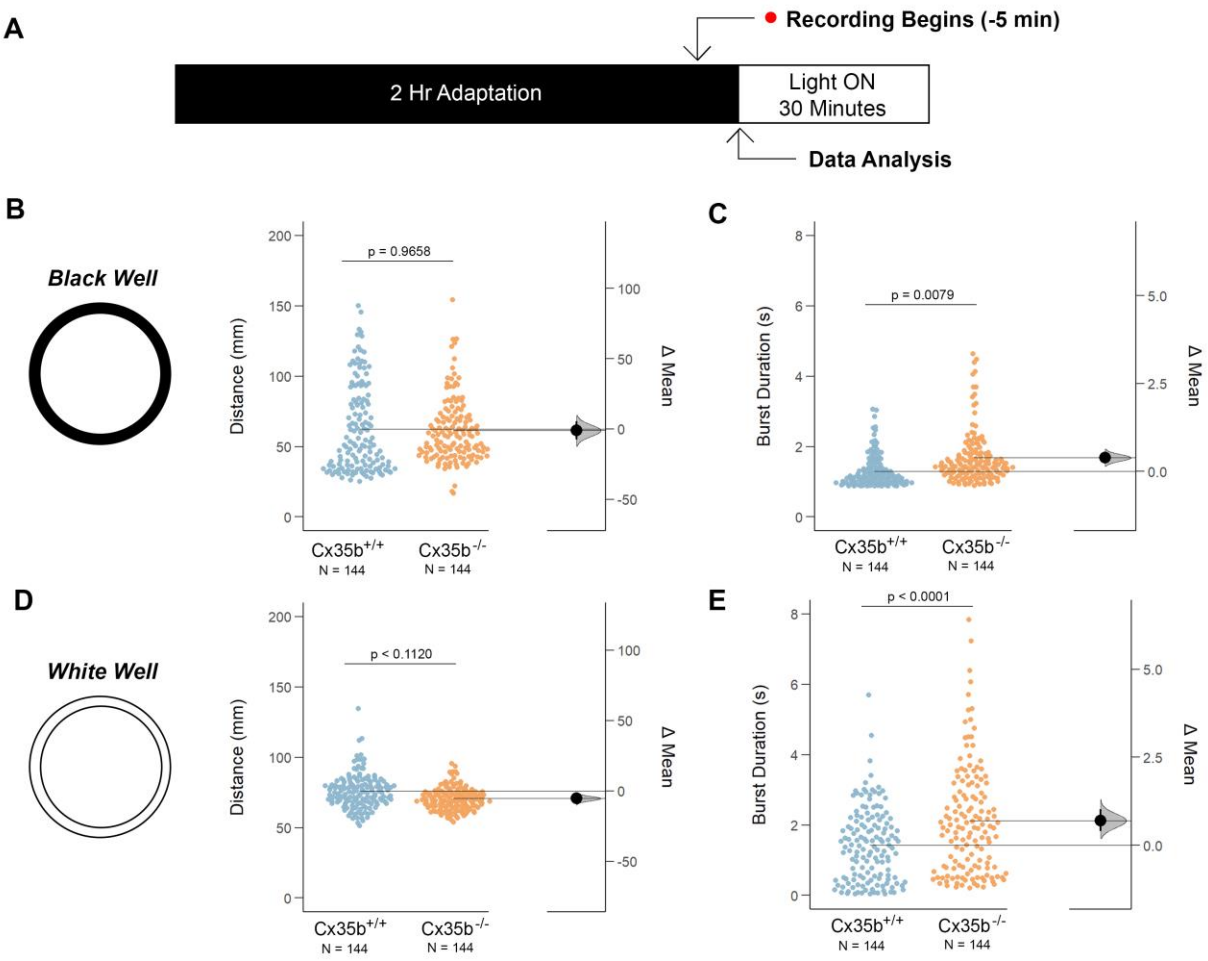

Figure 3.13. Loss of gjd2b Alters Larval Burst Activity Under Visual Stimulation.

*(**A**) Overview of the behavioral protocol. Zebrafish larvae were exposed to either a (**B-C**) black-surround well or a (**D-E**) white-surround well. Larval activity levels were measured by quantifying the distance swam (mm) and the burst duration (s). In comparison to the wild-type, Cx35b$^{-/-}$ larvae exhibited an increase in burst activity under both conditions. No significant difference was found in the distance analysis. Statistical significance was determined by the Two-Way ANOVA test, $p \leq 0.05$. The sample size (n) was 144 for wild-type and Cx35b$^{-/-}$ larvae.*

3.3.8 Discussion

It is widely accepted that genetically modified knock-out animals may be phenotypically distinct from their wild-type counterpart despite provoking compensatory regulation mechanisms in analogous genes. However, current literature has yet to address this in a Cx35b knock-out model. In this study, we aimed to provide a detailed description of the alterations to the genetic profile and protein expression levels in Cx35b$^{-/-}$ zebrafish. The morphological and behavioral phenotypes in zebrafish larvae were investigated at 7dpf when all major brain areas, including sensory organs, were developed. The zebrafish animal model provided a unique opportunity to understand the *GJD2* gene in the context of synaptic asymmetry since

recent reports discovered that Cx35b (*gjd2b*) is expressed presynaptically in Mauthner neurons (A. C. Miller *et al.*, 2017; Marsh *et al.*, 2017). Here, the implication is that presynaptic Cx35b expression drives growth and development, particularly of the midbrain, and its loss impacts neuronal signaling pathways involved in vision-to-motor output. While our results revealed that compensatory mechanisms following the loss of Cx35b exist, they were functionally inadequate to completely compensate for deviances in the vision-to-motor circuitry. To our knowledge, we are the first to describe these cellular and molecular changes to the CNS in a Cx35b$^{-/-}$ model.

3.3.8.1 Compensatory gene regulation in the Cx35b KO larvae & its potential implications.

Although we found no significant differences in the transcript levels of the *gjd2b* gene family, our RT-qPCR data revealed compensatory regulation in several analogous genes. Here, we reported the upregulation of Cx52.9, corresponding to human Cx59 (gap junction alpha 9, *GJA9*), following the loss of Cx35b. Cx52.9 is expressed in the retina, where it localizes in the dendrites of horizontal cells. Typically, Cx52.9 is found alongside the ionotropic glutamate receptor GluR2 and other members of the *gja9* family, Cx55.5 and Cx52.6. Previous studies confirmed that horizontal cells integrate signaling from photoreceptors with a feedback mechanism involving Cx55.5. Loss of Cx55.5 expression resulted in reduced lateral inhibition of the outer retina and decreased contrast sensitivity in Cx55.5 knock-out animals (Klaassen *et al.*, 2011). However, since there was residual feedback from horizontal cells to photoreceptors, the authors hypothesized that Cx52.9 was also involved. In follow-up, Klaassen et al. (2016) found that Cx52.9 was expressed in the H1 horizontal cell subtype and only contacted cone photoreceptor cells in a *Xenopus laevis* oocytes model. Surprisingly, contrast sensitivity was not addressed here (Klaassen *et al.*, 2016). Nevertheless, we suspect that the upregulation in Cx52.9 in Cx35b$^{-/-}$ larvae would allow for greater feedback between H1 horizontal cells and cone photoreceptors, suggestive of greater contrast sensitivity. In support of this, we found that Cx35b$^{-/-}$ larvae were hyperactive (increased burst duration) when placed in black- or white-surround well plates, an effect which may be due to enhanced contrast sensitivity. A detailed investigation into the visual capabilities, typically achieved through optokinetic/optomotor studies, was not further explored in this investigation.

We also observed an upregulation of Cx47.1 transcripts in knock-out larvae; however, current literature has seldom explored the protein functionality in the zebrafish animal model. As a further complication, phylogenetic analysis of the Cx47.1 protein has revealed discrepancies in identifying the appropriate mammalian ortholog. Mikalsen et al. (2020) recognized Cx47.1 as a member of the *gjc2* gene family, along with the mammalian ortholog Cx47 (Mikalsen, Tausen and í Kongsstovu, 2020). Watanabe (2017) places Cx47.1 as a member of the gap junction gamma 1 (*gjc1*), also known as *gja7*, gene family along with several other teleost proteins (Cx52.8, Cx43.4, Cx44.2a, and Cx44.2b) and mammalian Cx45

(Watanabe, 2017). As such, the potential implication of its upregulation needs to take both possible mammalian orthologs into account.

drCx47.1 as an ortholog to mCx47: Cx47 and Cx32 are the primary isoforms expressed in oligodendrocytes in heavily myelinated regions of the CNS. However, Cx47 expression precedes Cx32 developmentally and aids in oligodendrocyte progenitor differentiation and myelinogenesis (Parenti *et al.*, 2010). Mouse Cx47 knock-out models displayed vacuolization of nerve fibers, primarily at the region where myelination begins along the optic nerve. The severity of vacuolization directly correlated with the expression levels of both connexins as Cx47/Cx32 double knock-out (DKO) animals had higher incidences of vacuolization and died prematurely after birth (Odermatt *et al.*, 2003). Therefore, we suspect that the upregulation of Cx47.1 could serve as a neuroprotective mechanism to prevent degeneration and premature aging of the CNS while permitting information processing. In this regard, we anticipated that its upregulation would aid in visual signaling prorogation specifically, though, from our results, this is unlikely. A counter-proposal to this would recognize that abnormal development in white matter and myelination is typically a marker for autistic spectrum disorder in human and animal models (Meikle *et al.*, 2007; Noriuchi *et al.*, 2010; Pacey *et al.*, 2013; Cartocci *et al.*, 2018; Zikopoulos, García-Cabezas and Barbas, 2018; Graciarena *et al.*, 2019; Khanbabaei *et al.*, 2019). As such, an upregulation in Cx47.1 may be indicative of an ASD phenotype, marked by measurable traits such as hyperactivity and social impairments.

drCx47.1 as an ortholog to mCx45: In contrast, Cx45 expression is found in the heart, retina, and throughout the neuronal population of the brain, where it plays a key role in embryonic and postnatal neurogenesis (Beyer *et al.*, 1989; Gourdie *et al.*, 1993; Elias *et al.*, 2010; Khodosevich *et al.*, 2012). Considering that the localization of Cx36 aligns closely to that of Cx45 in the brain and retina, we suspect that the observed upregulation of Cx47.1 in knock-out animals serves as a comparable mechanism in place of Cx35b expression. In support of this hypothesis, previous studies determined that spontaneous firing patterns in retinal ganglion cells elevated similarly in Cx45 knock-out and Cx36 knock-out animals (Hansen *et al.*, 2005; Torborg and Feller, 2005). Double knock-out of Cx36/Cx45 displayed an additive effect on spontaneous firing patterns in a spatial-dependent manner (Blankenship *et al.*, 2011). Taken together, these results suggest that there are phenotypic similarities between Cx36 and Cx45 in mammals. As such, we speculated that teleost Cx35b and Cx47.1 could be, in part, functionally redundant.

Lastly, our RT-qPCR data analysis demonstrated a downregulation of Cx39.9, encoded by the *gja3* gene, in Cx35b$^{-/-}$ larvae. The *gja3* gene family includes both teleost Cx39.9 and Cx48.5 homologs and the mammalian ortholog Cx46. Interestingly, Cx48.5 and mammalian Cx46 are more closely related than Cx39.9 and Cx46. In support, Cx48.5 and Cx46 display similar expression patterns in the lens and heart tissues of human and murine models. Although Cx39.9 expression was identified in several tissues, it is

most notably known as a regulator of slow-twitch muscles in zebrafish larvae. Previously, Hirata et al. (2012) demonstrated Cx39.9-mediated electrical coupling of slow-twitch muscle fibers. Subsequently, larval touch-evoked coiling responses diminished in Cx39.9mi264 animals, which carried a missense mutation in the gene. However, burst swimming remained unaffected in Cx39.9mi264 mutant animals. Since Cx46 and Cx48.5 are not expressed in muscle tissue, the authors suggested that Cx39.9 has diverged to adopt a novel role apart from its original gene family functionality (Hirata *et al.*, 2012). Nevertheless, we suspected that the observed downregulation of Cx39.9 in Cx35b$^{-/-}$ larvae would alter their unprovoked swimming activity due to a reduction in slow-twitch muscle recruitment. However, our results demonstrated that Cx35b$^{-/-}$ larvae were indistinguishable from their age-matched wildtype controls in the distance traveled. Typically, spontaneous zebrafish larval swimming behavior oscillates between fast burst and slow rhythmic swimming bouts, utilizing both fast-twitch and slow-twitch muscle fibers. Therefore, it was possible that measuring distance was insufficient as an exclusive indication of slow-twitch muscle recruitment. To overcome this limitation, we measured the coast duration to account for slow-motor neuron activity and thus slow-twitch muscle recruitment. Indeed, we found a reduction in Cx35b$^{-/-}$ coast duration; however, this was exclusive to darkness. As such, we suspect that the impairment in slow motor neurons, and thus slow-twitch muscle recruitment mediated through Cx39.9, was initiated by alteration in rod photoreceptor cells signaling in Cx35b$^{-/-}$ larvae. How this effect was rescued under photopic conditions remains unclear.

3.3.8.2 Loss of Cx35b Expression in the Retina

Since we found no significant differences in mRNA transcript levels of Cx35b from our RT-qPCR data, the confirmation of the loss of Cx35b expression was achieved by performing immunohistochemistry on retinal tissues, known for its abundant expression of Cx36 in mammals and Cx35b in teleosts. Here we found a significant reduction in expression in the IPL and select photoreceptor cells, which we attributed to the loss of *gjd2b*. The IPL houses the synaptic connections between ganglion cells and amacrine and bipolar cells and is thought to be the region in which motion, brightness, contrast, and hue are processed (Wassle and Boycott, 1991; Calkins and Sterling, 1999). Pan et al. (2010) reported a partial or complete loss of ganglion-to-amacrine cell coupling in Cx36 knock-out mouse models concluding that Cx36 expression was critical in driving the connectivity between most ganglion cell subtypes (Pan *et al.*, 2010). As such, we speculated that the loss in synaptic connectivity of ganglion cells typically achieved through Cx35b expression would impair visual processing of motion, brightness, contrast, and hue. Moreover, the atypical pattern of fluorescence observed at the PRC layer suggests that Cx35b is localized to a specific PRC subtype(s). This may prove to be relevant when we consider Cx35b as a presynaptic gap junction. Nevertheless, a more detailed description of the visual changes in our Cx35b$^{-/-}$ model would aid in

determining which PRCs Cx35b is restricted to and how its expression impacts key components involved in visual processing.

3.3.8.3 Cx35b$^{-/-}$ fish demonstrated unique macroscopic morphological traits.

Our study confirmed the morphological differences at the level of the whole animal, suggesting that Cx35b expression contributes to controlled growth and development; lack thereof resulted in early accelerated growth trajectories. Growth is mainly regulated by the cross-talk between the hypothalamus and pituitary gland, serving as the junction linking the nervous and endocrine systems. The cascade of signaling events initiates at the hypothalamus through the secretion of growth hormone-releasing hormone (GHRH). GHRH, in turn, stimulates the production and release of growth hormone (GH) from the somatotropes of the pituitary gland into the bloodstream. In the mammalian brain, the hypothalamus and pituitary gland are located in the midbrain region and are known to express a variety of connexins, including Cx43, Cx26, Cx32, and Cx36. More specifically, Cx36 mRNA transcripts and protein were reported in the anterior pituitary and exclusively in gonadotropin-releasing hormone (GnRH)-secreting cells of the hypothalamus (Condorelli *et al.*, 1998, 2000; Belluardo *et al.*, 2000; Westberg *et al.*, 2009; Hodson *et al.*, 2015). Jabeen and Thirumalai (2013) reported Cx35b expression throughout the midbrain region, particularly in the ventral diencephalon known to encompass the hypothalamus and pituitary gland (Jabeen and Thirumalai, 2013). Taken together, we suspect that the increase in body and head length observed in knock-out animals may correlate to the anterior pituitary gland functionality and respective signaling cascades rather than upstream mechanisms involving the hypothalamus. While the link between Cx36/Cx35b expression, pituitary gland functionality, and GH secretion has seldomly been explored, one plausible explanation for the increased head and body size would be an enlarged pituitary gland, resulting in the upregulation of GH release. An alternative explanation would account for the disruption of the ion/metabolite homeostasis in the pituitary gland somatotropes resulting in more secretion of GH, which we deem more likely. The latter of these could be achieved through compensatory mechanisms such as the upregulation of voltage-gated calcium (Ca^{2+}) and/or sodium (Na^{+}) channels which are known to control GH exocytosis. However, this study did not aim to address Cx35b in the context of pituitary functionality and thus remains an area for further exploration.

Although growth appeared to be accelerated in Cx35b knock-outs, the head size was disproportionate. Here, we reported a reduction in the midbrain diameter in Cx35b$^{-/-}$ larvae compared to the age-matched controls, thus linking Cx35b expression to microencephaly. Microencephaly is typically associated with intellectual disabilities ranging in severity. Perez et al. (2019) demonstrated that mutations in microtubule-associated protein 11 (MAP11) provoked microencephaly in humans and zebrafish. The reduction was attributed to an impairment in cell survival, either by an increase in apoptotic pathways or by the

suppression of neural stem cell proliferation, thus causing an insufficient population of neurons. Likewise, we suspect the loss of Cx35b provoked cell survival impairments resulting in the reduction in midbrain diameter, though Cx35b expression was not explored throughout the brain in this study. Interestingly, a reduction in midbrain diameter has been consistent with findings on the neurodegenerative disease progressive supranuclear palsy (PSP) in humans. PSP is characterized by the impairment of movement, particularly gait freezing, difficulty swallowing, visual disturbances, and mild dementia, commonly misdiagnosed as Parkinson's disease (PD). Utilizing magnetic resonance imaging, Warmuth-Metz et al. (2001) compared the midbrain diameter in various parkinsonism syndromes, including PSP and PD. While PSP individuals displayed a significant reduction in midbrain diameter, PD patients were indistinguishable from the controls confirming that the midbrain diameter can be utilized as a diagnostic phenotype to distinguish between the two syndromes (Warmuth-Metz *et al.*, 2001). Although we cannot attribute the loss of Cx35b to PSP progression without exploring tau expression levels, the reduction in midbrain diameter may be indicative of impairments in sensory integration and disturbances in motor output that manifest as measurable changes in locomotion, visual acuity, and cognitive span; the former of which was addressed within the scope of this study.

3.3.8.4 Cx35b Contribution to Neuronal Circuitry Underlying Zebrafish Larval Locomotion.

Larval locomotor activity is essential to zebrafish social interaction, hunting, and predator defense. Subsequently, this behavior is also a direct reflection of neural activity of the CNS is modulated by external stimuli targeting various sensory systems. Considering that Cx35b is heavily expressed in the visual system (Kothmann *et al.*, 2007; A. C. Miller *et al.*, 2017; Marsh *et al.*, 2017), we explored changes in locomotion while accounting for signaling cascades mediated by rod and cone photoreceptor cells. Due to the zebrafish's instinctive nature to avoid darkness as a means of predator defense, we anticipated a significant reduction in swimming activity in darkness regardless of genotype. Our results were consistent with this instinctual phenomenon suggesting that Cx35b$^{-/-}$ larvae were able to discriminate the difference between lighting conditions. As such, we deduced that rod and cone photoreceptor cells retained some functionality despite the loss of the *gjd2b* gene.

Altogether, this study demonstrated that Cx35b$^{-/-}$ larvae exhibited a smaller midbrain diameter that correlated with the alterations in locomotion (decreased coast duration during free-swim in darkness and an increase in visually-provoked burst swimming). As such, we propose that Cx35b is critical in i) larval growth and development trajectories, ii) upstream and/or downstream circuitry of slow motor neurons in darkness, and iii) mediating the signaling cascade initiated by cone photoreceptors and terminated downstream on Mauthner neurons.

3.3.8.5 Limitations and Critical Considerations of This Study.

This study utilized coast duration as a measurement of slow motor activity and slow muscle fiber recruitment. However, whether the coast duration is an accurate alternative to the touch-evoked coil response has not been previously addressed. We believe that experiments on the touch-evoked coil responses in Cx35b$^{-/-}$ larvae would provide valuable insight into the compatibility of these measurements. Moreover, it was unclear whether a reduction in coast duration was an effect of Cx35b loss, Cx39.9 downregulation, or a combination of them both. As such, rescue experiments targeting Cx39.9 in Cx35b$^{-/-}$ animals would allow us to delineate the Cx35b-specific contribution to slow motor neurons and subsequent slow-twitch muscle recruitment.

Cx35b expression throughout the CNS had been previously resolved and displayed expression patterns in key areas related to visual-motor integration. As such, we had anticipated that the loss of Cx35b would impact the activity of downstream locomotor pathways resulting in a reduction in the distance swam. However, we were intrigued by our results that distance swam remained unaffected in Cx35b$^{-/-}$ larvae. Nevertheless, the finding that coast duration was reduced in darkness during free swim implied that Cx35b$^{-/-}$ larvae take longer strides with each swimming bout. During provoked swimming, however, burst bouts were favored, and strides were likely shorter. Since the mechanism in which either was achieved remains unknown, we propose additional experiments that address the kinetics of larval locomotion, including intensity and direction of tail bends, in Cx35b$^{-/-}$ larvae. As a second consideration, previous reports have suggested that erratic movements (increased speed and rapid directional changes) combined with an increase in gait freezing are indicative of anxiety-like phenotypes. We reason that thigmotaxis in Cx35b knock-out larvae should also be explored when assessing locomotion kinetics.

Zebrafish larval development typically spans six weeks before transitioning into the juvenile stage. Currently, body length and morphological changes in the fins and pigmentation serve as the standard to assess zebrafish maturation. Here, we reported that Cx35b$^{-/-}$ larvae were significantly larger in body length than their age-matched wild-type counterparts. As such, we must ask ourselves, are Cx35b knock-out fish aging prematurely? The rate of development is influenced partially by external factors such as temperature, fish density, nutrition, and water quality. However, these were accounted for in this study and therefore are unlikely explanations for our results. As such, we suspect that Cx35b$^{-/-}$ larvae growth and development were influenced by intrinsic factors, such as the regulation of the pituitary gland, rather than environmental. Nonetheless, zebrafish aging can be better assessed through behavioral phenotypes, such as cognitive decline and neurobiological changes (measured as changes in gene expression, DNA methylation, proteostasis, telomere attrition, and synaptic regulation) in the brain. We strongly believe that this should be an avenue worth exploring in future investigations.

3.3.9 Supplementary Figures

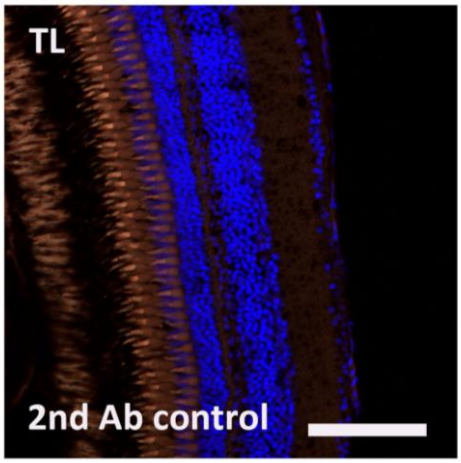

Figure S 3.1. Secondary Antibody Control on Wild-type Zebrafish Retinal Tissue.

A secondary antibody control was included to confirm that Cx36/Cx35b immunofluorescence was due to its protein expression and not due to cross-reactivity.

3.4

Gap Junction Delta-2b (*gjd2b*) Contributes to the Visual Processing of Luminescence Through Cone Photoreceptors

C.A. Brown[1], C. Zoidl[1], G. Zoidl[1,2]

[1] Department of Biology, York University, Toronto, ON M3J 1P3, Canada, [2] Department of Psychology, York University, Toronto, ON M3J 1P3, Canada

Author Contributions: conceptualization, C.A.B. and G.Z.; investigation-, C.Z. (RT-qPCR) and C.A.B. (all else); data analysis, G.Z. (RT-qPCR), C.A.B. (all else); data interpretation, C.A.B.; writing—original draft preparation, C.A.B.; writing—review and editing, C.A.B., and G.Z.; supervision, G.Z.; funding acquisition, G.Z.

3.4.1 Abstract

The loss of *gjd2b* abolished Cx35b expression in the IPL layer (housing the synaptic contacts between ganglion cells and amacrine and bipolar cells) and photoreceptor cells (PRCs) in a subtype-specific manner. As such, we were particularly interested in investigating how Cx35b contributed to various aspects of visual processing and aimed to provide a more detailed description of the visual changes in our Cx35b$^{-/-}$ model. Here, several behavioral paradigms were employed to quantify visual responsiveness, threshold responses, and innate color preference in Cx35b$^{-/-}$ larvae. We found that loss of the *gjd2b* gene caused larvae to display burst hyperactivity to light-ON VMR. Interestingly, Cx35b$^{-/-}$ larvae were also more sensitive to subtle light changes, though this was in a stimulus orientation-dependent manner. While we found no difference in innate color preference, Cx35b$^{-/-}$ did display compensatory mechanisms in the upregulation of the green-detecting opsin and well as pre- and postsynaptic dopaminergic expression. Altogether we concluded that Cx35b contributes to visual processing through the differential discrimination of light stimulus brightness, arrangement, and temporal properties, mediated by cone photoreceptors in an ON- or OFF-signaling dependent manner.

3.4.2 Cx35b Regulates Both Pre- and Postsynaptic Dopaminergic Gene Expression

Previous reports confirmed that the uncoupling of AII amacrine cells in mammals is regulated by dopamine-stimulated dephosphorylation of Cx36 (Kothmann, Massey and O'Brien, 2009). In a similar manner, dopamine co-regulates the phosphorylation state alongside adenosine in photoreceptor cells (PRCs), in turn mediating junctional coupling. (Li *et al.*, 2013). Since both Cx36 and its teleost ortholog Cx35b are highly expressed in the visual system (see section 3.3.3) and a correlation between Cx35b phosphorylation and PRC coupling has been established in zebrafish (Li, Chuang and O'Brien, 2009), we

performed RT-qPCR to determine the consequences of a Cx35b knock-out (Cx35b$^{-/-}$) on dopaminergic gene expression. Here, all homologs of the dopamine receptor (DR) subtypes were measured (*drd1*, *drd2a/b/c*, *drd3*, *drd4a/b*) as well as the dopamine transporter (*dat*) and vesicular monoamine transporter (*vmat*). The tyrosine hydroxylase (*th*) gene was included in the analysis for its role in dopamine production. In comparison to WT animals, we found a significant downregulation in tyrosine hydroxylase gene expression (1.52-fold, p = 0.002, *one-way ANOVA*), indicative of a reduction in dopamine synthesis. Additionally, *Cx35b*$^{-/-}$ larvae also displayed a significant downregulation in *drd4b* expression (1.63-fold, p = 0.016) (**Figure 3.14**). Typically, dopamine-dependent activation of D4R suppresses PKA activity, consequentially inhibiting the phosphorylation of connexins resulting in PRC uncoupling under photopic light conditions. As such, a downregulation in *drd4b* expression would promote junctional coupling by augmenting PKA-dependent phosphorylation of connexins in a similar manner to dim-light conditions. Expression levels of the remaining transcripts analyzed were indistinguishable from the wild-type. Taken together, our results demonstrate that Cx35b expression is required for both the presynaptic dopamine neurotransmitter and postsynaptic dopamine receptor synthesis. These findings are consistent with previous reports (Kothmann *et al.*, 2007; Kothmann, Massey and O'Brien, 2009; Li *et al.*, 2013) demonstrating that dopamine-mediated phosphorylation of Cx35b plays an integral role in modulating the crosstalk between retinal cells. Since dopaminergic signaling to enhance junctional coupling was seemingly being promoted in Cx35b-deficient larvae, we suspected that this was a compensatory mechanism allowing *Cx35b*$^{-/-}$ zebrafish to rectify their visual sensitivity.

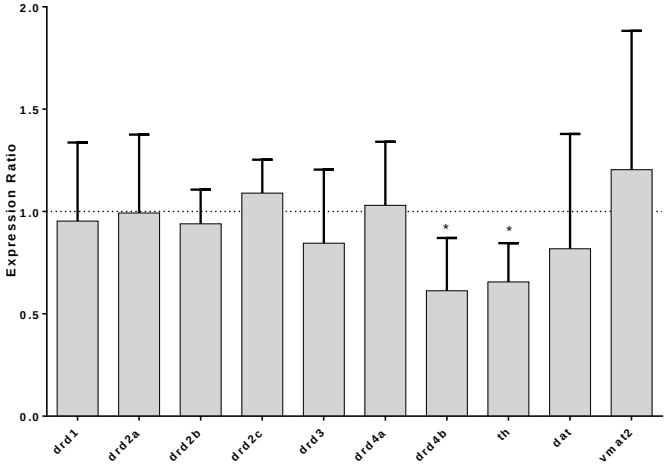

Figure 3.14 Expression Ratios of Dopaminergic Genes in Cx35b$^{-/-}$ larvae via RT-qPCR Analysis.

*RNA transcript levels of several dopaminergic genes were measured by RT-qPCR to determine the relative expression changes in Cx35b$^{-/-}$ larvae. A significant reduction in drd4b and th expression was observed, suggesting that loss of gjd2b inhibits presynaptic and postsynaptic dopamine expression. Statistical significance was determined by the One-Way ANOVA test, $p \leq 0.05$, *, $p < 0.05$.*

3.4.3 Enhanced Cone-Cone Photoreceptor Cell Activity in Cx35b$^{-/-}$ Larvae

We previously demonstrated that *Cx35b*$^{-/-}$ larvae exhibit normal spontaneous burst swim activity despite lighting conditions; however, they significantly increased their burst duration in response to a visual stimulus (see sections 3.3.6 and 3.3.7). As such, we speculated that the visual-to-Mauthner neuronal circuity was altered following the loss of *gjd2b*. Given the Cx35b expression patterns in the retina, we anticipated that this result was initiated upstream at the visual system by the underlying phototransduction pathways. To determine the efficacy and quality of visual responsiveness, we performed VMR on 7dpf larvae (**Figure 3.15A**). For consistency, we measured the burst duration as an indication of the larval primitive startle response behavior mediated by Mauthner neurons. Here, both genotypes demonstrated an immediate and robust increase in burst duration in response to the light-ON VMR stimuli; though, *Cx35b*$^{-/-}$ larvae were hyperactive in comparison to the wild-type (*in s*, WT: 0.16 ± 0.01, Cx35b$^{-/-}$: 0.18 ± 0.01, n = 48, $p < 0.0001$, *Mann-Whitney*). Interestingly, the light-OFF VMRs were indistinguishable between the WT and *Cx35b*$^{-/-}$ larvae (*in s*, WT: 0.28 ± 0.02, Cx35b$^{-/-}$: 0.21 ± 0.01, $p = 0.7542$) (**Figure 3.15B-E**). These results confirmed that *Cx35b*$^{-/-}$ larvae readily detect changes in light but were more sensitive to photopic light stimuli. As such, we suggest that the cone-cone photoreceptor activity and downstream signaling pathways were enhanced in *Cx35b*$^{-/-}$ larvae, while the rod-rod photoreceptor activity was preserved. Moreover, we anticipate that these results correlate with our previous findings on dopaminergic gene expression; however, the changes in dopaminergic synthesis and its impact on junctional conductance were not explored.

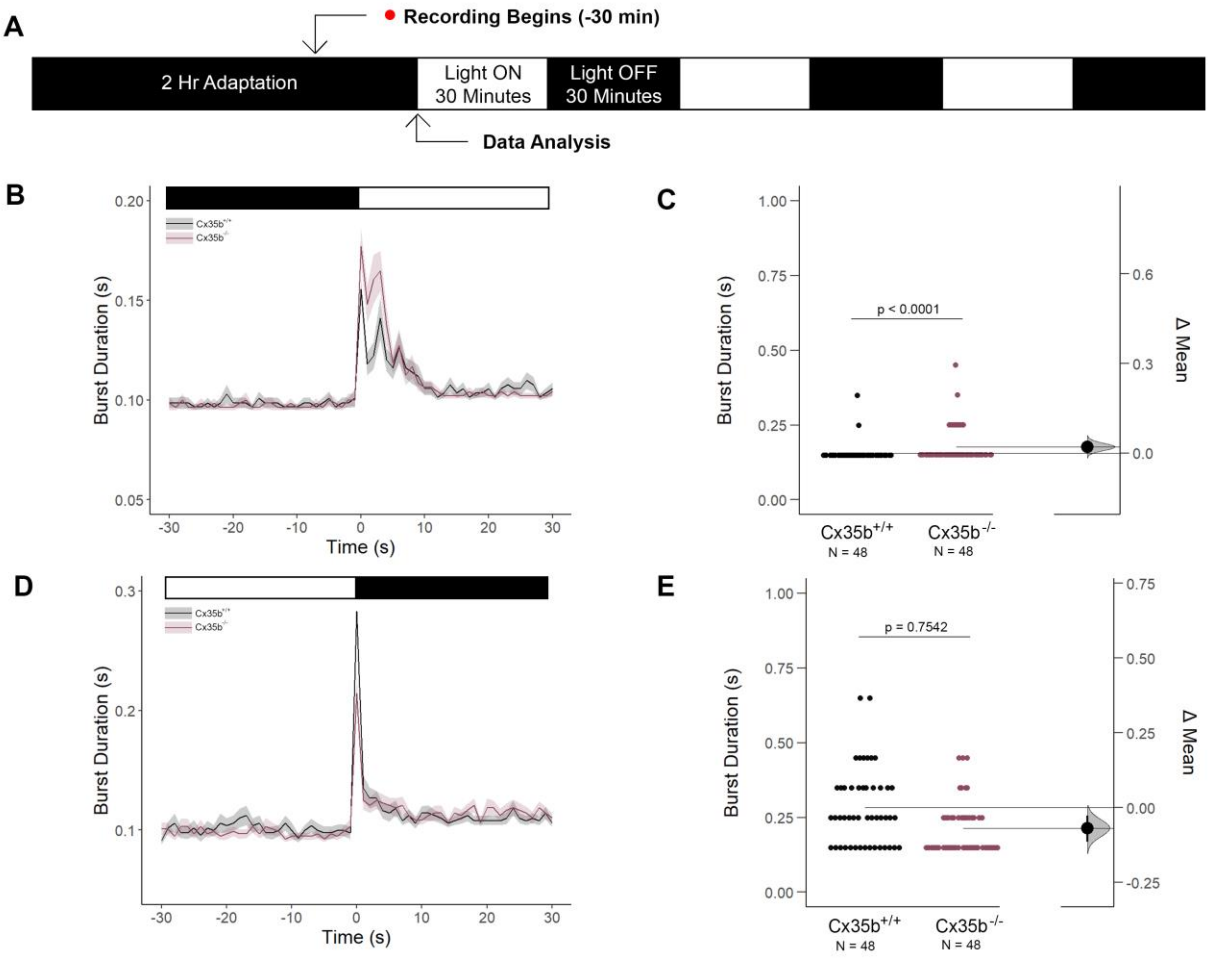

Figure 3.15. Standardized VMR Assay Revealed Cx35b$^{-/-}$ are Hyperactive in response to Light-ON Stimuli.

*(**A**) Overview of the experimental procedure. Burst activity was assessed for (**B-C**) Light-ON responses and (**D-E**) Light-OFF responses. Both wild-type and Cx35b$^{-/-}$ larvae readily detected light transitions indicative of visual functionality. In comparison to the wild-type, Cx35b$^{-/-}$ larvae were hyperactive, suggesting that they were more sensitive to light stimulation. No significant difference was found for Light-OFF responses. Statistical significance was determined by the Mann-Whitney test, $p \leq 0.05$. The sample size (n) was 48 for wild-type and Cx35b$^{-/-}$ larvae.*

3.4.4 Cx35b KO Larvae Have Normal Threshold Responses to Flash Stimuli

Next, we examined whether the light-ON VMR hyperactivity seen in Cx35b-deficient larvae was due to their ability to process visual stimuli faster than their wild-type counterpart. To determine the changes in visual processing speed, we delivered transient light flashes ranging from 1000ms to 10ms to dark-adapted zebrafish and measured their responsiveness (burst duration) 30 seconds prior to and following delivery of the stimuli; the study was termed the flash stimuli threshold response (FSTR) assay (**Figure 3.16A-B**). While the burst activity of WT and Cx35b$^{-/-}$ larvae were indistinguishable prior to the visual

stimuli (*in s*, WT: $0.046 \pm 0.02x10^{-1}$, Cx35b$^{-/-}$: $0.045 \pm 0.02x10^{-1}$, n = 48, p = 0.9827, *Two-Way ANOVA*), in response to a 1000ms light flash we found that both genotypes significantly increased their burst duration (*in s*, WT: $0.082 \pm 0.04x10^{-1}$, p <0.0001, Cx35b$^{-/-}$: $0.062 \pm 0.03x10^{-1}$, p = 0.0003*)*. In contrast to light-ON VMR, here, Cx35b$^{-/-}$ larvae had attenuated responses following the 1000ms light flash; burst activity increased by 178% for the wild-type but only 138% for Cx35b$^{-/-}$ larvae (p < 0.0001) (**Figure 3.16C**). Similar results were obtained when larvae were exposed to a 10ms light flash. Prior to the light stimulus, both WT and Cx35b were indistinguishable in burst activity (*in s*, WT: $0.052 \pm 0.01x10^{-1}$, Cx35b$^{-/-}$: $0.048 \pm 0.01x10^{-1}$, p = 0.0850). Upon stimulation with 10ms of light exposure, WT and Cx35b larvae increased their average burst duration by 112% and 109% respectively (*in s*, WT: $0.058 \pm 0.02x10^{-1}$, p = 0.0005, Cx35b$^{-/-}$: $0.052 \pm 0.01x10^{-1}$, n = 96, p = 0.0363). Cx35b$^{-/-}$ responses following the 10ms flash stimulus were again reduced in comparison to the wild-type (p = 0.0017) (**Figure 3.16D**). Our data suggest that visual processing responses were more robust with longer durations of stimuli. This would support the notion that light-ON VMR hyperactivity was triggered by a sudden change with prolonged light stimuli rather than transient stimuli. Nevertheless, since Cx35b$^{-/-}$ larvae increased their burst activity following the 10ms flash of light, albeit at reduced levels in comparison to the wild-type, we concluded that the threshold for visual processing speed responses was unaffected in Cx35b$^{-/-}$ larvae.

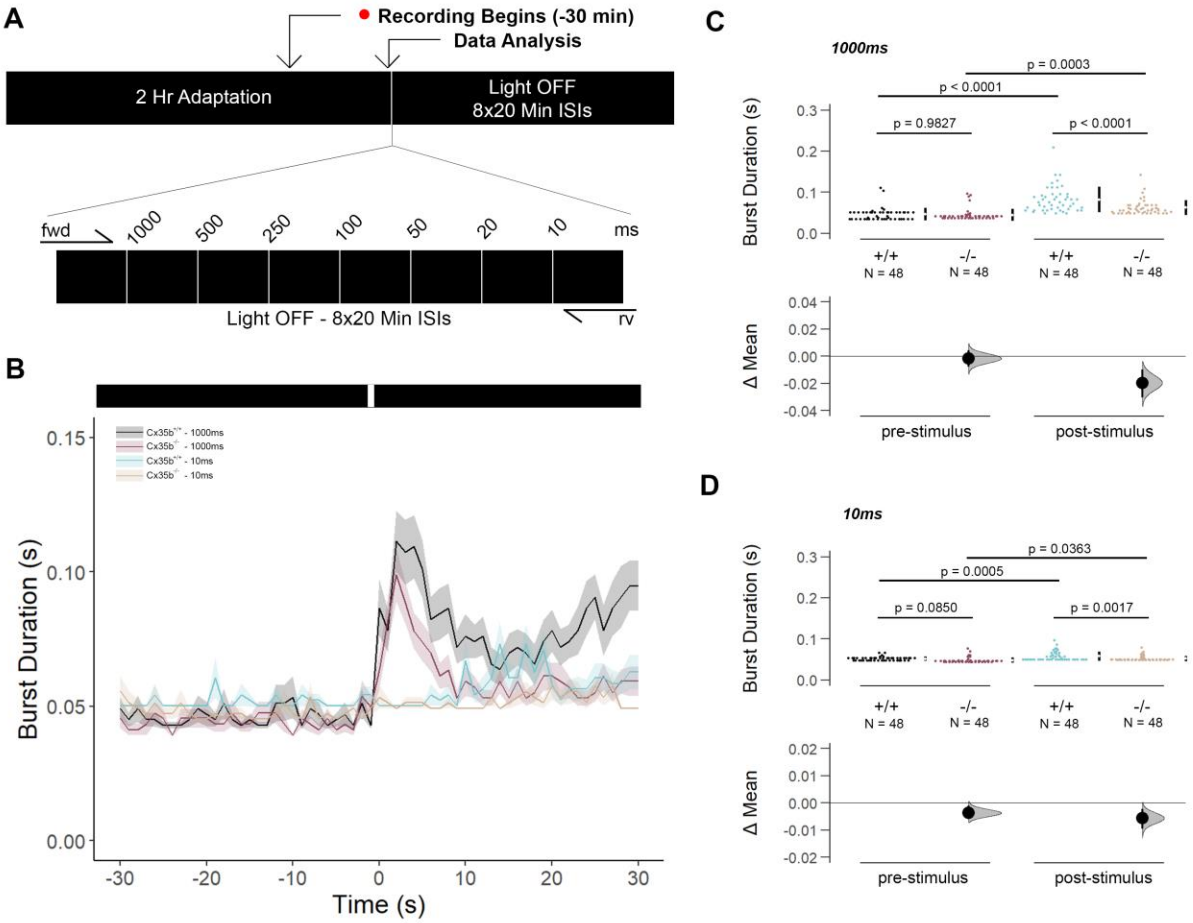

Figure 3.16. Cx35b$^{-/-}$ Larvae Respond Normally in the Flash Stimuli Threshold Response (FSTR) Assay.

*(**A**) Overview of the FSTR assay protocol. Stimuli were presented in both the forward (fwd) and reverse (rv) direction to eliminate attenuation due to habituation. (**B**) Dark-adapted larvae were subject to light stimuli of various lengths. Average responses within 30s of the (**C**) 1000ms and (**D**) 10ms stimuli were plotted. Statistical significance was determined by the Two-Way ANOVA test, $p \leq 0.05$. The sample size (n) was 48 for wild-type and Cx35b$^{-/-}$ larvae.*

3.4.5 Cx35b Mediates Rod-Cone Photoreceptor Signaling During the Transition from Mesopic to Scotopic Vision

Li et al. (2009) previously demonstrated that Cx35 electrical coupling facilitates both cone-cone and rod-cone photoreceptor crosstalk, the latter of which allows for saturated rod signaling to reroute to cones when exposed to the mesopic visual range (Li, Chuang and O'Brien, 2009). As such, we determined how Cx35b expression, or lack thereof, influenced visual responsiveness mediated by rod-cone coupling. For this, we performed VMR under mesopic light conditions allowing for the recruitment of rod PRCs in our analyses while preserving the existing functionality of cone PRCs. Our VMR experiment was designed to also determine whether larvae were able to discriminate between minor changes in illumination as an

assessment of the quality of visual perception under low-light conditions. To achieve this, dark-adapted zebrafish were presented with an initial light-ON stimulus cue of 10% light intensity and a subsequent visual cue of 5% light intensity (**Figure 3.17A**). Here, we found no significant difference in burst duration between genotypes immediately after light-onset when presented with the 10% light-ON visual cue (*in s*, WT: 0.175 ± 0.009, Cx35b$^{-/-}$: 0.185 ± 0.009, n = 96, p = 0.9181, *Two-Way ANOVA*) or the 5% light-ON visual cue (*in s*, WT: 0.209 ± 0.014, Cx35b$^{-/-}$: 0.233 ± 0.014, p = 0.4567). Moreover, wild-type larvae behaved similarly when presented with either the 10% or 5% light-ON visual stimuli (p = 0.1756), suggesting that they were unable to differentiate between the change in light intensity. Interestingly, however, Cx35b$^{-/-}$ larvae were able to discriminate between the two light conditions and increased burst swimming activity in response to the 5% light-ON stimulus (p = 0.0226) (**Figure 3.17B-C**). These results insinuate that rod photoreceptor recruitment was sufficient to rescue the hyperactivity seen with photopic light-ON VMR. Nevertheless, Cx35b$^{-/-}$ larvae were more responsive to subtle changes in low-light illumination mediated by rod-cone signaling.

Next, we assessed the light-OFF VMR responses and found that Cx35b$^{-/-}$ larvae had a significantly lower burst duration in comparison to the wild-type when transitioning from the 10% light intensity (*in s*, WT: 0.259 ± 0.017, Cx35b$^{-/-}$: 0.166 ± 0.009, p < 0.0001). In contrast, burst duration was indistinguishable between wild-type and Cx35b$^{-/-}$ larvae when exposed to the 5% light-OFF stimuli (*in s*, WT: 0.117 ± 0.005, Cx35b$^{-/-}$: 0.116 ± 0.006, p > 0.9999) indicating that there is a narrow range of mesopic luminescence where Cx35b expression contributes to rod-cone mediated light-OFF signaling. Nevertheless, the recruitment of additional rod photoreceptors via the reduction in light intensity rescued the hypoactivity seen at 10% light-OFF VMR. We also found that both wild-type and Cx35b$^{-/-}$ larvae reduced burst activity when exposed to the 5% light-OFF stimulus (WT: p < 0.0001, Cx35b$^{-/-}$: p = 0.0043) (**Figure 3.17D-E**).

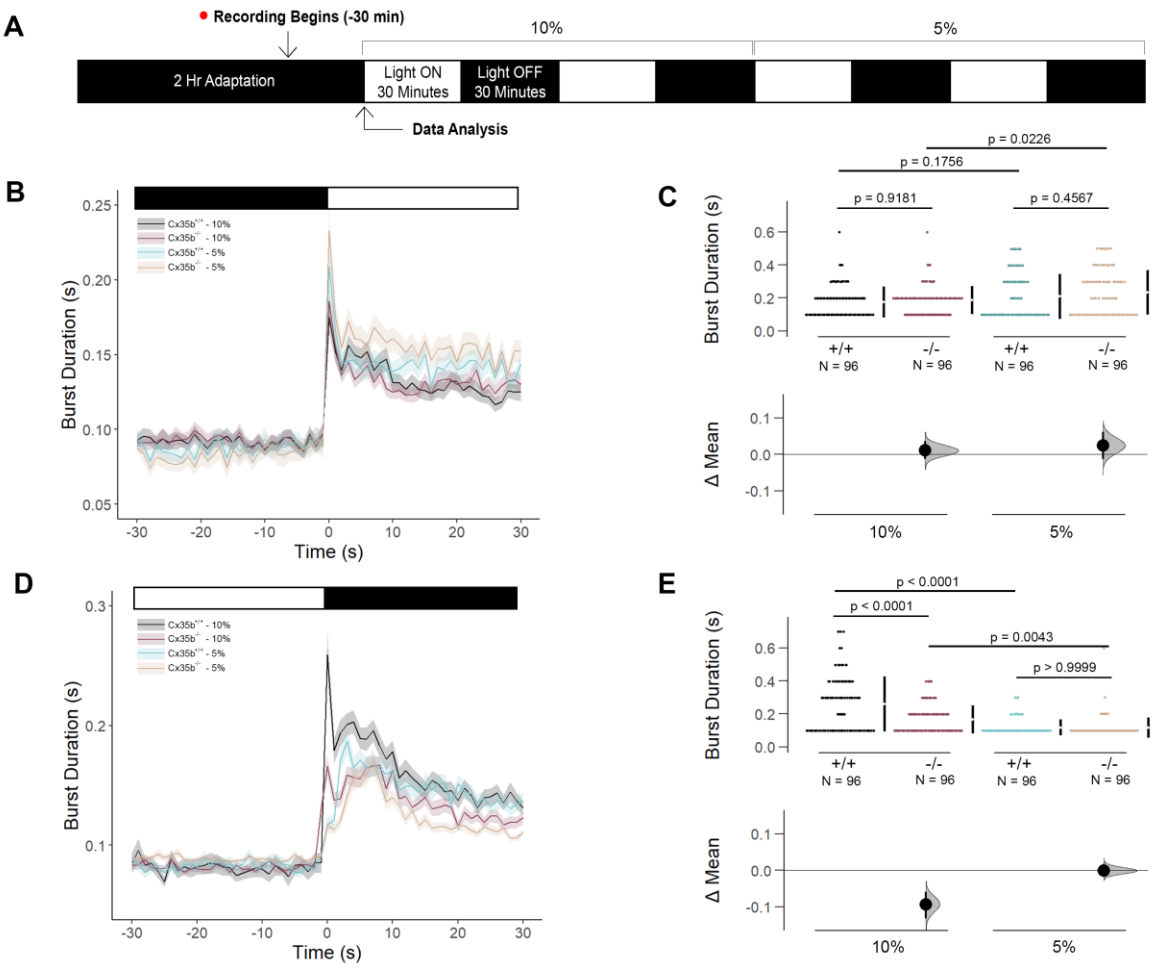

Figure 3.17. Quantification of Burst Activity in Cx35b$^{-/-}$ Larvae While Exposed to the Mesopic VMR Assay.

*(**A**) General overview of the mesopic VMR Assay. Zebrafish larvae were exposed to 10% and 5% light intensity to determine their sensitivity to visual discrepancies. (**B-C**) Light-ON responses revealed that Cx35b$^{-/-}$ were able to discriminate between the two lighting conditions. Nevertheless, the recruitment of rod-PRC activity rescued the burst hyperactivity previously seen in Cx35$^{-/-}$ Light-ON VMR responses. (**D-E**) Light-OFF responses were reduced in Cx35b$^{-/-}$ larvae at the 10% light intensity, suggesting that there is a defined range in luminescence Cx35b$^{-/-}$ expression is functionally significant. Statistical significance was determined by the Two-Way ANOVA test, $p \leq 0.05$. The sample size (n) was 96 for wild-type and Cx35b$^{-/-}$ larvae.*

We recognized the potential that the observed downregulation in burst activity between the 10% and 5% mesopic light-OFF conditions could be due to learning and memory mechanisms and/or physical exhaustion. As such, we validated the authenticity of our results by reversing the order of the light stimuli and repeating burst duration measurements for both light-ON and light-OFF VMR (**Figure 3.18A**). We hypothesized that if the downregulation in burst activity was, in fact, due to learning and memory and/or physical exhaustion, larvae would again downregulate their burst activity when presented with the

subsequent 10% light-OFF cue. Here, WT and Cx35b$^{-/-}$ larvae behaved similarly when exposed to the light-ON cues regardless of light intensity (*in s*, 5% light-ON - WT: 0.117 ± 0.007, Cx35b$^{-/-}$: 0.111 ± 0.005, n= 48, p = 0.9259; 10% light-ON- WT: 0.126 ± 0.008, Cx35b$^{-/-}$: 0.122 ± 0.007, p = 0.9730). Similarly, no significant differences in burst duration were found during light-OFF VMR at 5% light intensity (in s, WT: 0.279 ± 0.017, Cx35b KO: 0.267 ± 0.014, p = 0.9439) or 10% light intensity (WT: 0.281 ± 0.016, Cx35b KO: 0.236 ± 0.013, p = 0.1570). Neither genotype showed any indication of modulating burst activity in response to the 5% and 10% light cues (*Light-ON* - WT: p=0.8265, Cx35b: p=0.7230; *Light-OFF* - WT: p > 0.9999, Cx35b: p=0.4598) confirming that learning and memory and/or physical exhaustion did not play a role in the previous downregulation of mesopic light-OFF VMRs (**Figure 3.18B-E**). Instead, our results revealed that the contribution of Cx35b to rod-cone mediated mesopic vision and discrimination was dependent on light intensity as well as the arrangement of the light stimulus (i.e., the transition from higher-to-lower mesopic vision but not vice versa).

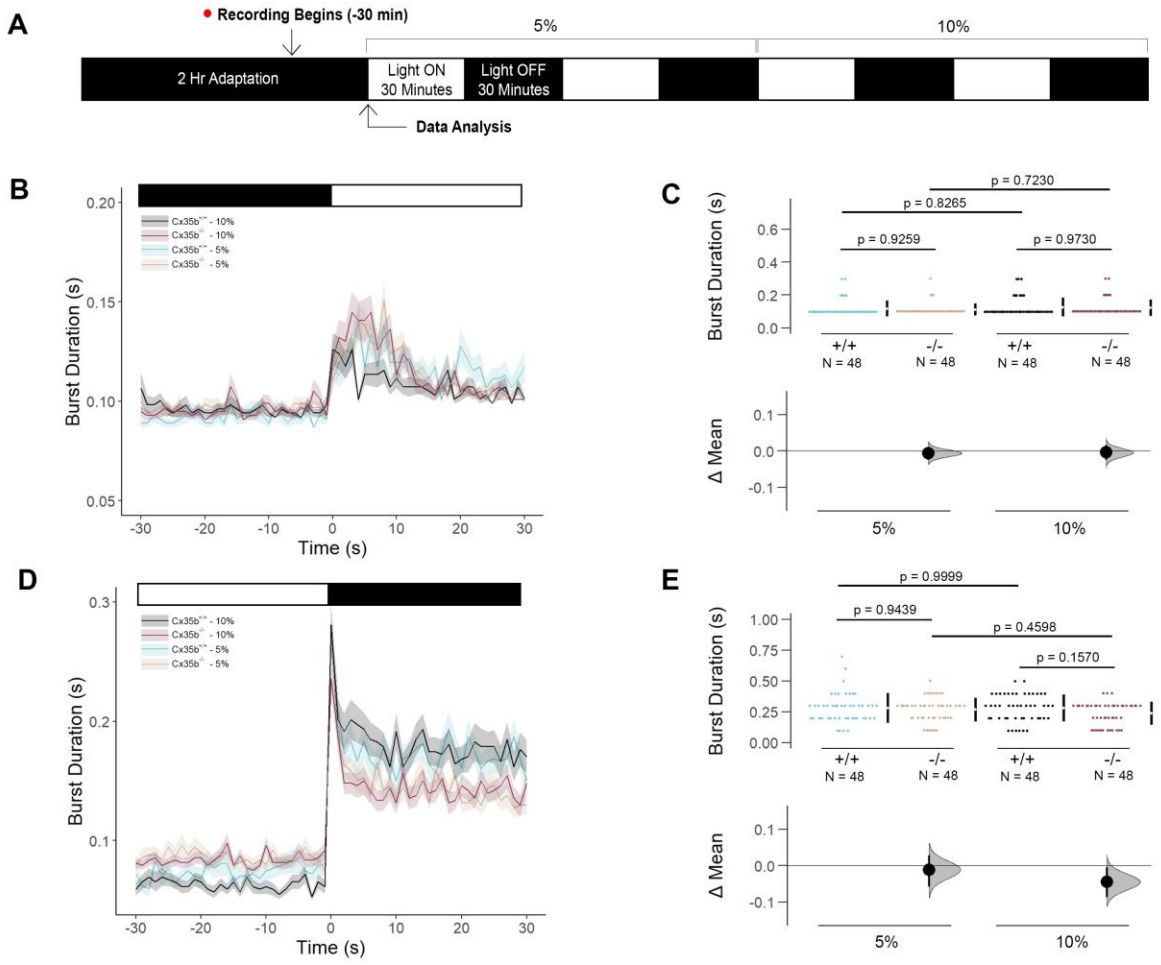

Figure 3.18. Quantification of Burst Activity in Cx35b$^{-/-}$ Larvae While Exposed to the Reversed Mesopic VMR Assay.

*(**A**) General overview of the mesopic VMR Assay with the light intensity in reversed order. Zebrafish larvae were exposed to 5% then 10% light intensity cues to determine their sensitivity to visual discrepancies. (**B-C**) Light-ON responses and (**D-E**) Light-OFF revealed no significant differences between genotypes suggesting that the contribution of Cx35b to rod-cone mediated mesopic vision and discrimination was dependent on the arrangement of the light stimulus. Statistical significance was determined by the Two-Way ANOVA test, $p \leq 0.05$. The sample size (n) was 48 for wild-type and Cx35b$^{-/-}$ larvae.*

3.4.6 Expression of Cone Opsin is Regulated by Cx35b

In follow-up to our VMR studies, we explored whether opsins, the light-absorbing photopigments of PRCs, were directly affected in Cx35b$^{-/-}$ larvae. Although studies to date have confirmed that zebrafish express ten distinct opsin genes (Morrow *et al.*, 2016), we focused our analysis on the six most abundant and well characterized. For this, we performed RT-qPCR on the red (*opn1lw2*), green (*opn1mw1* and *opn1mw2*), ultraviolet (*opn1sw1*), blue (*opn1sw2*), and low-light rhodopsin (*rho*) photopigments. Here, we observed an upregulation in gene expression for *opn1mw2* (1.449-fold, p = 0.046, *one-way ANOVA*),

whereas the remaining transcripts analyzed were indistinguishable from the WT (**Figure 3.19**). These data indicated that Cx35b was involved in modulating green cone-opsin expression. As such, we suspected that Cx35b expression was integral in maintaining spectral vision sensitivity, particularly to green light.

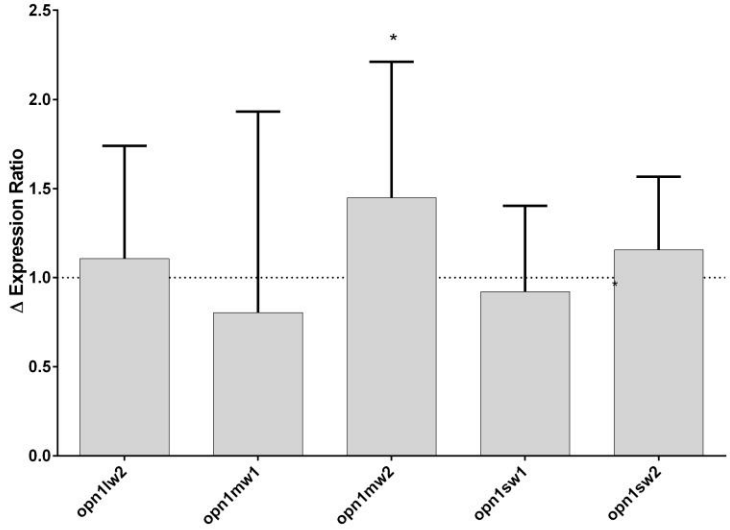

Figure 3.19. Expression Ratios of Opsin Genes in Cx35b$^{-/-}$ larvae via RT-qPCR Analysis.

*RNA transcript levels of several opsin genes were measured by RT-qPCR to determine the relative expression changes in Cx35b$^{-/-}$ larvae. A significant increase in opn1mw2 expression was observed, suggesting that the gjd2b gene modulates spectral sensitivity to green light. Statistical significance was determined by the One-Way ANOVA test, *, $p < 0.05$.*

To determine how the increase in *opn1mw2* expression in Cx35b$^{-/-}$ larvae affected their color vision, we assessed innate color preference using a cross maze as previously described (Park *et al.*, 2016) (**Figure 3.20A**). Our experimental design accounted for potential location bias by implementing (1) a dark adaptation period to confirm an equal distribution throughout the maze prior to the recording stage (**Figure 3.20B**) and (2) experimental repetitions alternating the colors within each arm of the maze. Consistent with previous reports (Avdesh *et al.*, 2012; Park *et al.*, 2016), wild-type larvae demonstrated a robust preference towards blue (*in %*, 41.18 ± 2.13, n = 100, $p < 0.0001$, *two-way ANOVA*), however, were indifferent towards to the red, green, and yellow color exposures (*in %*, Red: 17.35 ± 0.88, Green: 18.94 ± 1.83, Yellow: 18.53 ± 1.43, $p > 0.9999$). Similarly, Cx35b$^{-/-}$ larvae also strongly preferred blue (*in %*, 44.55 ± 2.71, n = 93, $p < 0.0001$) with no distinguishable preference between the remaining colors (*in %*, Red: 19.06 ± 1.10, Green: 17.73 ± 1.25, Yellow: 19.56 ± 0.96, $p > 0.9999$). Two-way ANOVA analysis revealed no significant differences between the genotypes (Blue: $p = 0.8490$, Red: $p = 0.9985$, Green: $p > 0.9999$, Yellow: $p > 0.9999$) suggesting that the loss of Cx35b did not alter color vision despite the upregulation in *opn1mw2* (**Figure 3.20C**).

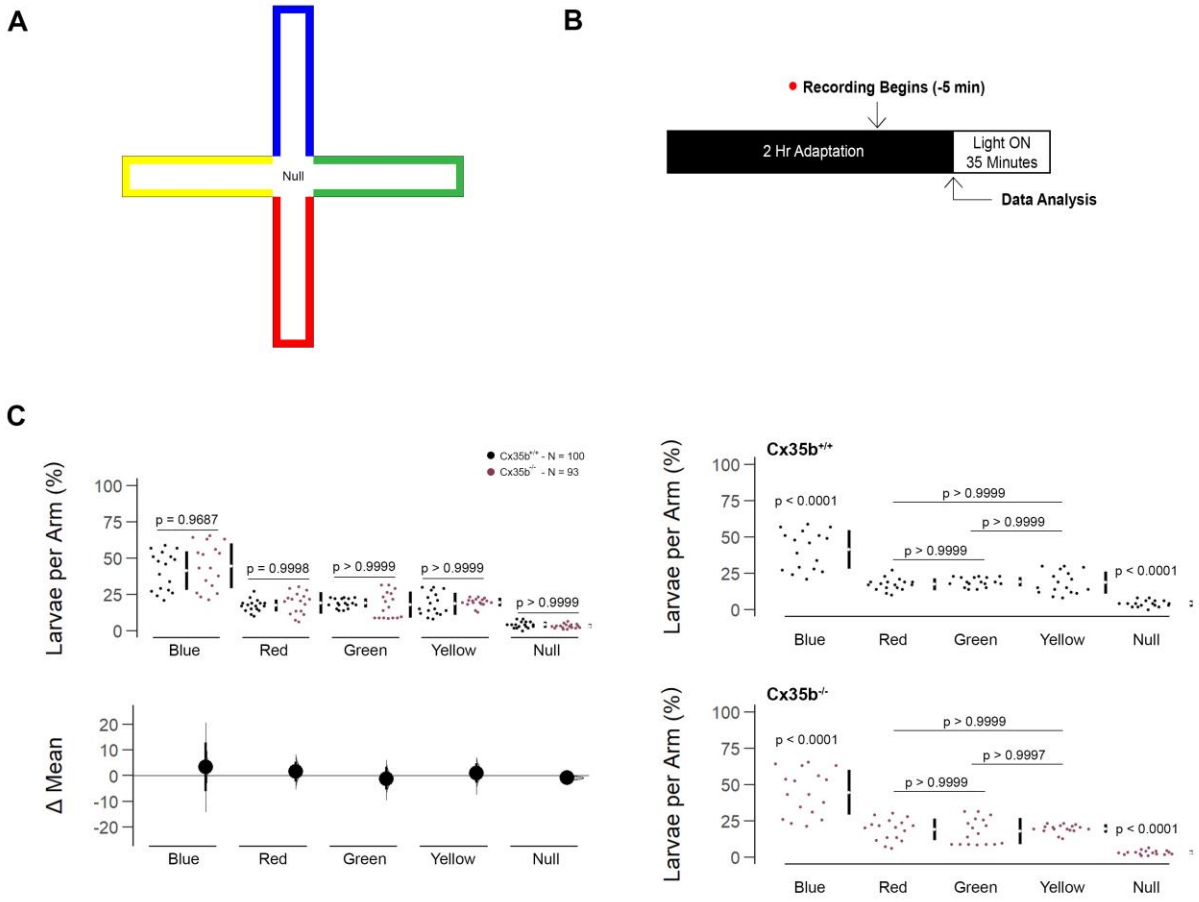

Figure 3.20. Innate Color Preference Assay in Cx35b$^{-/-}$ Larvae Reveals Similarity to Wild-type Larvae.

*Overview of the (**A**) experimental cross-maze and (**B**) protocol design used to assess innate color preference. (C) Summary of the mean larvae per arm. Both genotypes equally preferred the blue arm; however, all else were indistinguishable. Statistical significance was determined by the Two-Way ANOVA test, $p \leq 0.05$. The sample size (n) was 100 for wild-type and 93 Cx35b$^{-/-}$ larvae.*

3.4.7 Discussion

Recent localization studies have coined Cx35b expression as a major contributor to electrical synapses of the retina (A. C. Miller *et al.*, 2017; Marsh *et al.*, 2017; Quint *et al.*, 2021). However, apart from refractive error leading to myopia (Quint *et al.*, 2021), little is known about the aspects of visual processing controlled by Cx35b. In the present study, we assessed the genetic compensation and visual capabilities of *gjd2b*-deficient zebrafish larvae previously generated using the CRISPR-Cas9 genome editing tool (see section 3.3.2). Our results suggest that Cx35b$^{-/-}$ larvae retain visual functionality, although they display hypersensitivity to cone photoreceptor stimulation and subsequent downstream ON-bipolar

cell signaling. This result was rescued by the recruitment of rod photoreceptors via low-light exposure. Since Cx35b$^{-/-}$ larvae demonstrated alterations in dopaminergic gene expression, we suspect that pre- and/or postsynaptic dopamine signaling may contribute to the observed cone-mediated hypersensitivity; however, this requires further study. Cx35b$^{-/-}$ larvae also distinguished between subtle changes in brightness, specifically when transitioning from higher-to-lower mesopic light intensities. Innate color preferences remained intact despite an increase in *opn1mw2* in knock-out animals, although additional studies would allow for further differentiation towards spectral sensitivities. While we found that processing speed remained intact, visuomotor behavior of Cx35b$^{-/-}$ larvae was dampened by flash stimuli (FSTR assay). Altogether we concluded that Cx35b contributes to visual processing through the differential discrimination of light stimulus brightness, arrangement, and temporal properties, mediated by cone photoreceptors in a ON- or OFF-signaling dependent manner.

3.4.7.1 Potential Implications of Dopaminergic Signaling in Cx35b KO Larvae

The relationship between Cx36/Cx35b electrical synapses and dopaminergic signaling has been extensively described in the context of the visual system; this is largely due to the dynamic nature of the synapses in response to light/dark adaptation and the circadian rhythm. Cx35b expression has been observed in cone-cone and rod-cone contacts and is also suspected to be present in rod-rod PRC synapses (Li, Chuang and O'Brien, 2009). In the present study, Cx35b-deficient larvae demonstrated a downregulation in the dopamine precursor tyrosine hydroxylase and the dopamine receptor gene *drd4b*, suggesting that both presynaptic dopamine and postsynaptic dopamine receptor synthesis are impaired, although the latter is isoform-specific.

In mammals, five distinct types of dopamine receptors have been identified and are classified into two families; D_1-like (D1R and D5R), which are stimulatory subsets to adenyl cyclase, and D_2-like (D2R, D3R, and D4R) which inhibit adenyl cyclase. Both D2R and D4R subtypes are expressed in rod and cone PRCs of the outer retina, whereas horizontal cells and cone bipolar cells of the inner retina express D1R. While *drd3* gene transcripts have been found in teleost retinal ganglion cells (Boehmler *et al.*, 2004) and *DRD5* is known to be restricted to the retinal epithelium layer (Guha *et al.*, 2012), current literature provides well-described evidence outlining similar expression patterns of across vertebrates for D1R, D2R and D4R in the retina (Callier *et al.*, 2003; Yamamoto *et al.*, 2013). Typically, bright light (photopic conditions) increases dopamine production (Witkovsky, 2004). The binding of dopamine to the high-affinity D2R and D4R receptor subtypes induces a cascade of signaling events that subsequently prevents the activation of adenyl cyclase and its downstream target PKA. As such, under photopic light conditions, gap junctions are primarily dephosphorylated, resulting in the uncoupling of PRCs; this is critical in supporting high contrast vision. Considering this, a reduction in *th* and *drd4b* gene expression would suggest that phosphorylation

and thus junctional coupling is being favored in Cx35b$^{-/-}$ larvae, an effect typically seen under low-light conditions. Although this provides evidence for a dopaminergic-dependent compensatory mechanism in Cx35b$^{-/-}$ larvae, it remains unclear which Cx36 ortholog(s) would be involved as phosphorylation targets. We previously reported that Cx34.7 (*gjd1b*) and Cx35.5 (*gjd2a*), both of which are expressed in PRCs (Li, Chuang and O'Brien, 2009; Quint *et al.*, 2021), remain intact in Cx35b$^{-/-}$ larvae, however, changes in coupling were not addressed. We propose that these targets may be involved in mediating the dopaminergic-dependent coupling of PRCs in the Cx35b$^{-/-}$ model. Nevertheless, our results confirmed that Cx35b expression regulates dopaminergic gene expression.

3.4.7.2 Cx35b is Involved in Light Intensity Discrimination

The visual-motor response (VMR) assay has been widely used to determine how genetic and/or environmental changes impact neuronal circuitry through the measurement of innate behavioral responses to changes in luminescence. Here, we report that Cx35b$^{-/-}$ larvae demonstrated a robust increase (hyperactivity) in burst duration following light-onset (light-ON responses). Our results suggest that the loss of *gjd2b* alters the sensitivity of cone-cone PRCs under photopic conditions. As such, we can deduce that the neuronal circuitry initiated at cone photoreceptors, routing through ON-bipolar cells and subsequently synapsing downstream on the Mauthner neurons, has been strengthened, although this could cause the signaling to overload and strain the circuit. Light-ON VMR hyperactivity was not observed under low-light conditions (10% and 5% light intensities), indicating that the recruitment of rod photoreceptor cells was able to rescue this effect. As such, our results support previous literature (Li, Chuang and O'Brien, 2009) confirming the role of Cx35b in mediating cone-cone PRC coupling. We propose that Cx35b primarily mediates cone-cone PRCs crosstalk by engaging in a fine-tuning effect.

Although we suspect from our RT-qPCR data that the changes in dopaminergic gene expression (*th* and *drd4b*) may contribute to light-ON VMR hypersensitivity, to date, this remains unclear. Another possibility would take into consideration the upregulation of the opsin gene *op1mw2*. Berry et al. (2019) have found that viral-delivered medium-wave opsin restored visual sensitivity and speed in blind *rd1* mice to allow for spatiotemporal discrimination under dim-light and room-light (photopic) conditions; a result rhodopsin was unable to achieve (Berry *et al.*, 2019). As such, we cannot discount that *op1mw2* upregulation may have provided additional visual sensitivity.

A common misconception is that rod signaling is not functional in zebrafish until 15dpf; however, numerous reports have implicated a role of rod PRCs in visual discrimination tasks as early as 5dpf (Moyano, Porteros and Dowling, 2013; Venkatraman *et al.*, 2020; Ganzen *et al.*, 2021). Considering this, measuring the light-OFF VMR and VMR under mesopic light conditions was a feasible means to assess the contribution of Cx35b to rod-mediated circuitry. Here, we reported no changes to light-OFF VMR when

under photopic light conditions. However, mesopic light produced light-OFF VMR hypoactivity in Cx35b$^{-/-}$ animals in a manner that was dependent on brightness and stimulus arrangement. We anticipate that the modulation of rod PRC crosstalk through Cx35b expression exists but is secondary to cone-cone photoreceptor communication for two main reasons. (1) Rod-rod signaling was unaffected, as confirmed through light-OFF VMR experiments. While scotopic VMR may provide more insight into rod-rod mediated signaling, we do not anticipate any novel finding here. (2) A reduction in rod-cone PRC communication, specifically within a narrow range of brightness, was confirmed by mesopic light-OFF VMR data. Although we provided evidence of Cx35b-dependent rod-cone PRC crosstalk, taken together, we propose that Cx35b is restricted to cone-photoreceptors as the recruitment of rod PRCs rescued both light-ON VMR hyperactivity and mesopic light-OFF VMR hypoactivity. We recognize that our hypothesis conflicts with previous literature detailing Cx35b expression in both cone and rod photoreceptors; more specifically, Cx35b gap junction plaques were found between cone pedicles and rod spherules (Li, Chuang and O'Brien, 2009). However, we found that antibody specificity was a limitation to this study since antibodies against each Cx36 teleost ortholog are currently unavailable commercially. While the antibody used by Li et al. (2009) does not cross-react with Cx34.7, immunoreactivity to Cx35a has yet to be addressed. As such, we believe that rod-mediated signaling is modulated by presynaptic Cx35a and postsynaptic Cx34.7. Our data provided several indications of cone-cone enhancement despite the lack of Cx35b, suggesting that Cx35a and Cx34.7 are also expressed alongside Cx35b in cone PRCs. Nevertheless, since we found that the hypoactive light-OFF response in Cx35b$^{-/-}$ animals under mesopic light was dependent on the sequence that the visual stimuli were presented, we concluded that Cx35b acts in a directional manner, allowing signaling to flow from cone to rod PRCs. Therefore, we suspect that Cx35b plays a role in the gradual transition from day to night, supporting the notion that photoreceptor coupling through phosphorylation is enhanced at under dim-light.

Again, we examined whether larvae were capable of distinguishing minor changes in illumination by measuring the light-ON responses in mesopic light conditions. Here, we found that Cx35b$^{-/-}$ larvae exclusively were capable of this discrimination task depending on the stimulus arrangement. More specifically, Cx35b$^{-/-}$ larvae recognized the change in luminescence when transitioning from higher-to-lower mesopic visual ranges. This led us to question whether gap junctional coupling was being favored in a cell-type-specific manner in Cx35b$^{-/-}$ animals? Considering our results of photopic light-ON VMR enhancement in combination with mesopic light discrimination, we suspect that junctional coupling may be favored amongst cone photoreceptor cells routing to the ON-bipolar cells. While we observed that enhanced coupling was not sufficient to rescue rod-cone mediated cross-talk due to the absence of Cx35b, we propose that it is sufficient to provide illumination discrimination sensitivity. Although the validity of this proposed mechanism remains to be confirmed, previous reports on mice have detailed a similar

observation. Lin et al. (2020) demonstrated that a knock-in phosphomimetic Cx36 mouse line, termed Cx36-DEDD, resulted in increased junctional coupling and disparities in visual acuity, specifically in photopic conditions (Lin *et al.*, 2020). As such, we anticipate a similar mechanism is involved in Cx35b$^{-/-}$ larvae.

3.4.7.3 Spectral Sensitivity and Visual Processing Speed Remained Intact in Cx35b KO Larvae

The quality of visual processing can be quantified by the measurement of several elements, including luminescence, chromaticity, and spatiotemporal properties of light stimuli. Our VMR studies addressed how Cx35b contributes to the discrimination of luminescence; however, it was limited in providing information regarding chromaticity and spatiotemporal detection. To address this, we performed innate color preference tests and visual processing speed experiments. Previous reports have confirmed innate color preferences in adult zebrafish (Spence and Smith, 2008; Avdesh *et al.*, 2012) and larvae as early as 5dpf (Park *et al.*, 2016). Although there is conflicting evidence for red, green, and yellow color preferences, zebrafish consistently presented a robust preference for blue. Here, we reported that both wildtype and Cx35b$^{-/-}$ larvae displayed a color preference towards blue, consistent with the literature. However, we found no other existing color preferences with either genotype. These results led us to conclude that the increase in the green cone opsin gene *op1mw2* seen in Cx35b$^{-/-}$ larvae was insufficient to impact innate color preferences. Nevertheless, we caution the interpretation that color preferences to red, green, and yellow are nonexistent as we recognize the potential that the experimental design may have masked subtle differences in preference. Instead, we suggest a more simplified design, allowing for the discrimination of two colors at a time (for example green vs. yellow), be implemented in future studies.

Our visual processing speed experiments (FSTR assay) revealed that Cx35b$^{-/-}$ larvae modulated their behavior appropriately in response to a 1000ms and 10ms flash of light, suggesting that the threshold of light detection remained intact. In support of this, Quint et al. (2021) demonstrated that electroretinograms measuring the B-wave responses in Cx35b$^{-/-}$ zebrafish were indistinguishable from the wildtype (Quint *et al.*, 2021). As such, visual processing speed remained intact in Cx35b$^{-/-}$ larvae. However, behavioral responses were more robust with longer durations of light flashes. What piqued further interest was the range of behavioral responses across types of visual stimuli. Here, Cx35b larvae were hypoactive in comparison to the wildtype when exposed to a sudden flash of light; this response was similar to our previous report where larvae were exposed to constant light. In contrast, light-ON VMR produced hypersensitivity. As such, Cx35b$^{-/-}$ larval responses to visual stimuli were dependent on the temporal features of the stimuli. To our knowledge, we are the first to describe these behavioral responses in Cx35b-deficient zebrafish.

3.4.7.4 Limitations & Critical Considerations of This Study

We previously detailed the changes in immunofluorescence of wild-type and Cx35b$^{-/-}$ adult retinal tissues using a monoclonal Cx36 primary antibody (see section 3.3.3). While we observed a distinct expression pattern in Cx35b$^{-/-}$ animals where PRC labeling was interspersed, it remains unclear which PRC subtype(s) Cx35b$^{-/-}$ is expressed in. Although we propose that Cx35b$^{-/-}$ is restricted to cone photoreceptors, future immunohistochemistry studies should aim at validating these results.

The Zebrabox® (Viewpoint, Montreal, QC) system used for our behavioral studies is equipped with ambient LED light that provides the user with the option to modify luminescence between 0% (0 lux) and 100% (8000 lux) light power. However, the stability of the light source is lost beyond the light power of 5%. As such, our experimental design utilized a minimum of 5% light intensity; lower light conditions, mimicking mesopic and/or scotopic vision, cannot be assessed with the manufacturer's set-up. To overcome this limitation and to improve the Zebrabox® sensitivity, previous reports (Moyano, Porteros and Dowling, 2013; Venkatraman *et al.*, 2020; Ganzen *et al.*, 2021) have utilized light filters placed in the path of the light source, where each filter accounts for a 40-60% reduction in light intensity. In this way, a luminescence power as low as 0.01 lux can be achieved as an indication of rod-rod PRC signaling under scotopic light conditions.

Our studies led to the proposed mechanism that light-ON hypersensitivity observed in Cx35b$^{-/-}$ larvae under photopic light conditions was mediated by cone-cone photoreceptor signaling. Since higher light intensities were not further explored, the ceiling to this hyperactivity remains unclear. We anticipate that the relationship between Cx35b loss and light-ON VMR hyperactivity will be logarithmic with subsequent increments of brightness since the recruitment of additional cone photoreceptors must reach a point of saturation. However, the following questions arise: Is the point of cone-cone saturation attainable within the visible light spectrum? Does the upregulation in *opn1mw2* provide a broader range of ceiling limits for cone saturation in Cx35b$^{-/-}$ animals? Further investigations into the mechanism of this cone hypersensitivity would provide greater insights.

Visual perception in its entirety encompasses several elements of vision, such as visual discrimination, visual memory, and visuospatial behavior. In the present study, we have addressed how Cx35b contributes to visual function (processing speed and spectral sensitivity) and discrimination towards changes in luminescence. However, visual discrimination in the context of acuity was not addressed here since previous reports have outlined diminished visual acuity in the Cx36-DEDD mouse (Lin *et al.*, 2020) and Cx35b$^{-/-}$ zebrafish models (Quint *et al.*, 2021). Visual acuity is defined as the sharpness or clarity of vision and is measured as the ability to distinguish between two separate objects or visual stimuli at a designated angular distance. In zebrafish, visual acuity is typically measured by the optomotor (OMR)

and/or optokinetic response (OKR), accounting for their visuospatial behavior. Quint et al. (2021) demonstrated that Cx35b$^{-/-}$ mutant zebrafish displayed reduced positive responses at spatial frequencies above 0.25cpd as well as reduced eye tracking movements (Quint *et al.*, 2021).

We found that Cx35b$^{-/-}$ animals had a significant reduction in the dopamine precursor enzyme tyrosine hydroxylase and the dopamine receptor gene *drd4b*, suggesting that Cx35b expression modulates dopaminergic signaling in a manner that supports photopic vision. However, these changes in dopaminergic gene expression were obtained from preparations of the whole larvae and thus are not exclusive to photoreceptor cells. Although dopaminergic signaling was not further explored here, changes in the expression of *drd4b* is of particular interest since its expression profile displays prominence throughout the frontal cortex and hippocampus. In D4R-deficient mice, novel object recognition responses were compromised, suggesting that dopaminergic signaling is involved in modulating working memory (Zhang *et al.*, 2004). Moreover, a global reduction in TH is typically associated with motor impairments such as that seen in parkinsonism disorders (Alam and Richardson, 2020). As such, we anticipate that the downregulation of both *th* and *drd4b* in Cx35b$^{-/-}$ models plays a crucial role in larval movement, learning, and memory paradigms.

Lastly, behavioral assays performed in this report capitalized on the innate fear response of zebrafish larvae to sudden changes in light intensity as a stressor. In this way, the differences seen in activity levels, particularly the VMR-driven hyperactivity in Cx35b$^{-/-}$ larvae, may be accounted for by the innate behavioral response differentiating a state of relaxation vs. anxiety/fear in a way that is Cx35b-dependent. We suggest future studies take this into consideration.

3.5

Cognitive Indexing Following the Genetic Ablation of *gjd2b* Reveals the Relationship Between Electrical Synapses, Visual Functionality, and the Integrity of the CNS

C.A. Brown[1], C. Zoidl[1], G. Zoidl[1,2]

[1] Department of Biology, York University, Toronto, ON M3J 1P3, Canada, [2] Department of Psychology, York University, Toronto, ON M3J 1P3, Canada

Author Contributions: conceptualization, C.A.B and G.Z.; investigation-, CZ (RT-qPCR) and C.A.B. (all else); data analysis, G.Z. (RT-qPCR), C.A.B. (all else); data interpretation, C.A.B.; writing—original draft preparation, C.A.B.; writing—review and editing, C.A.B., and G.Z.; supervision, G.Z.; funding acquisition, G.Z.

3.5.1 Abstract

One of the fundamental questions in neuroscience research is how specific genes, signaling pathways, and the overall architecture of neuronal connectivity influence higher-order behaviors. While the relationship between anxiety and memory is established, the neurobiology of their interplay remains poorly understood. Moreso, only a few studies have addressed the link between anxiety and memory in the zebrafish animal model. Here, we used 7dpf zebrafish larvae to explore the contribution of presynaptic Cx35b expression to anxiety, learning, and memory cognitive indexes. We demonstrated that loss of Cx35b expression provokes elevated levels of anxiety in zebrafish larvae as determined by the increase in thigmotaxic behavior during the light-dark locomotion assay. Although genetic ablation of the *gjd2b* gene had no impact on the learning and memory capacity, we determined that visual-based habituation paradigms are impacted by the type of visual stimuli delivered, establishing a relationship between visual integrity and non-associative learning and memory. Nevertheless, Cx35b$^{-/-}$ larvae demonstrated differential regulation in various genes contributing to anxiety, learning, and memory, suggesting that complementary and inhibitory mechanisms are at play. We concluded that presynaptic Cx35b expression contributes to anxiety phenotypes but does not impact non-associative learning and memory.

3.5.2 Targeted Ablation of *gjd2b* Increases Thigmotaxic Behavior

Several reports (Schnörr *et al.*, 2012; Peng *et al.*, 2016; Basnet *et al.*, 2019; Maeda, Hasumi and Yoshida, 2021) have confirmed that an increase in locomotor activity during light-dark transitions is indicative of elevated levels of stress and anxiety in zebrafish larvae, unifying the mutuality between visual

functionality and the integrity of the nervous system. We previously demonstrated that ablation of *gjd2b* did not cause deficits in distance swam under continuous illumination or darkness (see section 3.3.6) but rather provoked hyper-activity in the innate larval burst swim in response to light-ON VMR (see section 3.4.3) reiterating its importance to visual signaling pathways, particularly those synapsing on Mauthner neurons. This was further supported by our findings demonstrating that a loss of Cx35b expression was evident in the retinal PRC and IPL layers. However, whether the alterations in the visual system and its functionality were also indicative of an underlying change in stress and anxiety levels was not explored. As such, we utilized the previously generated Cx35b$^{-/-}$ (see section 3.3.2) larval model to determine whether the *gjd2b* gene contributes to the neurobehavior of stress and anxiety. For a robust index of aberrant anxiety, we measured thigmotaxic behavior as the percentage of the total distance moved within the outer margins of the well while performing the light-dark locomotion assay (**Figure 3.21A**). Buspirone (5mg/L) was also included in the study for its known effect as an anxiolytic (Jann, 1988).

Thigmotaxic activity measured during dark transitions revealed that untreated Cx35b$^{-/-}$ larvae moved more within the outer zone than the untreated wild-type (*in %*, WT: 71.594±0.411, n=36; Cx35b$^{-/-}$: 74.319±0.703, n=36, $p = 0.0024$, *Two-Way ANOVA*). Surprisingly, pharmacological intervention with Buspirone caused an increase in wild-type larval thigmotaxic behavior in comparison to the untreated control (78.874±0.600%, n=24, $p = 0.0009$); however, Cx35b$^{-/-}$ larvae showed a reduced thigmotaxic behavior in response to Buspirone treatment (71.461±0.504%, n=24, $p = 0.0050$). Since the reduction in the distance moved within the outer zone was indistinguishable between the untreated wild-type and buspirone-treated Cx35b$^{-/-}$ larvae ($p = 0.8208$), our results suggested that the observed anxiety-like behavior was treatable with pharmacological intervention (**Figure 3.21B**). Similarly, during light-ON periods, untreated Cx35b$^{-/-}$ larvae swam longer distances in the outer margin than the untreated wild-type (*in %*, WT: 68.776±0.735, Cx35b$^{-/-}$: 78.219±1.290, $p < 0.0001$) suggesting that Cx35b$^{-/-}$ were also more anxious during light transitions. While treatment with Buspirone again increased the distance that wild-type larvae moved within the outer margin (WT: 75.716±1.080%, $p < 0.0001$), Cx35b$^{-/-}$ larvae reduced their distance traveled in comparison to the untreated counterpart (70.442±1.017%, $p < 0.0001$). Again, Cx35b$^{-/-}$ activity under buspirone treatment was indistinguishable from the untreated wild-type ($p = 0.7037$) (**Figure 3.21C**). Overall, our results suggest that loss of *gjd2b* induces anxiety-like behavior in zebrafish larvae; however, anxiolytic treatment was sufficient to rescue this effect.

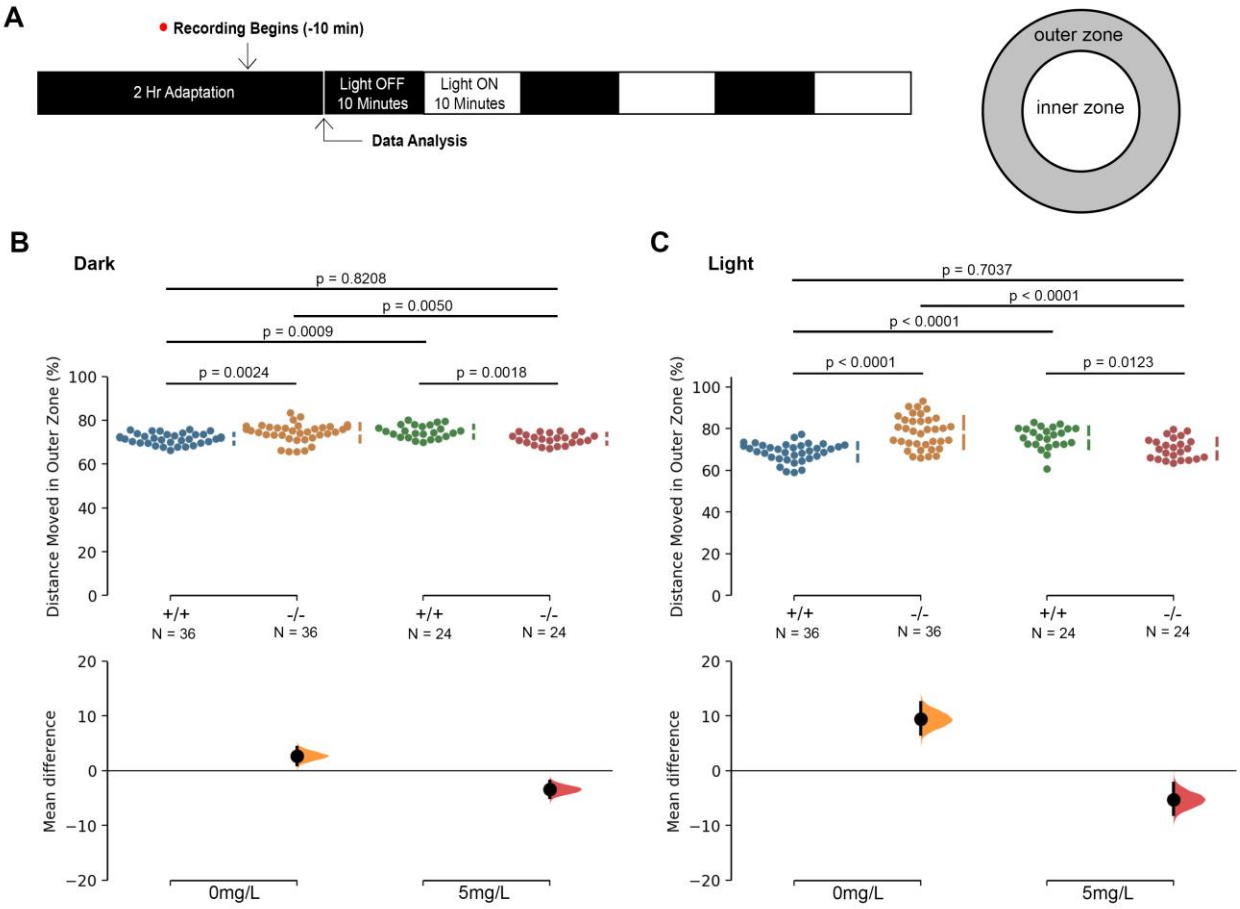

Figure 3.21 Thigmotaxis during Light-Dark Transitions Demonstrates that Cx35b$^{-/-}$ Larvae Display Anxiety-Like Behavior.

*(**A**) General overview of the light-dark locomotion assay used to assess thigmotaxic behavior. Thigmotaxis was measured as the distance moved within the outer zone of the well (%). (**B**) During dark transitions, untreated Cx35b$^{-/-}$ larvae demonstrated an increase in thigmotaxic behavior. This effect was rescued by the application of Buspirone (5mg/L). (**C**) Light transitions provoked elevated anxiety-like behavior in Cx35b$^{-/-}$ larvae which were restored to untreated wild-type conditions upon treatment with buspirone. Statistical significance was determined by the Two-Way ANOVA test, $p \leq 0.05$. The sample size (n) was 36 for untreated wild-type and Cx35b$^{-/-}$ larvae, and n = 24 for the buspirone-treated wild-type and Cx35b$^{-/-}$ larvae.*

3.5.3 Loss of *gjd2b* Increases Expression of Immediate Early Genes

Since the neurobiology between anxiety and memory is poorly understood, we aimed to lessen this knowledge gap by understanding how presynaptic Cx35b expression, or loss thereof, affects learning and memory capacity while also contributing to anxiety-like phenotypes. As such, we explored the

consequences of targeted ablation of the *gjd2b* gene on the expression of key genes that display overlapping involvement in anxiety, learning, and memory. To achieve this, we performed quantitative real-time PCR (RT-qPCR) to measure RNA transcript levels as an indication of gene expression. Here, we targeted several immediate early genes (*fosab*, *egr1*, *egr2a*, *egr2b*, *egr4*, *jun*, *bdnf*), membrane protein genes (*gria2b*, *grin1a*, and *slc6a4*), and the tyrosine-protein kinase gene (*fyna*) known to regulate intracellular calcium concentrations. Here, we found that the loss of Cx35 expression provoked a significant upregulation in *fosab* ($p = 0.023$), *egr1* ($p = 0.006$), *egr2a* ($p = 0.015$), *egr4* ($p = 0.009$) and *jun* ($p = 0.014$) expression profiles. In contrast, membrane protein genes *gria2b* ($p = 0.014$), *grin1a* (0.004), and *slc6a4* (0.019) were significantly downregulated suggesting that Cx35b expression is modulating the expression of NMDA receptors, AMPA receptors, and serotonin transporters. All else was indistinguishable between wild-type and Cx35b$^{-/-}$ larvae (**Figure 3.22**).

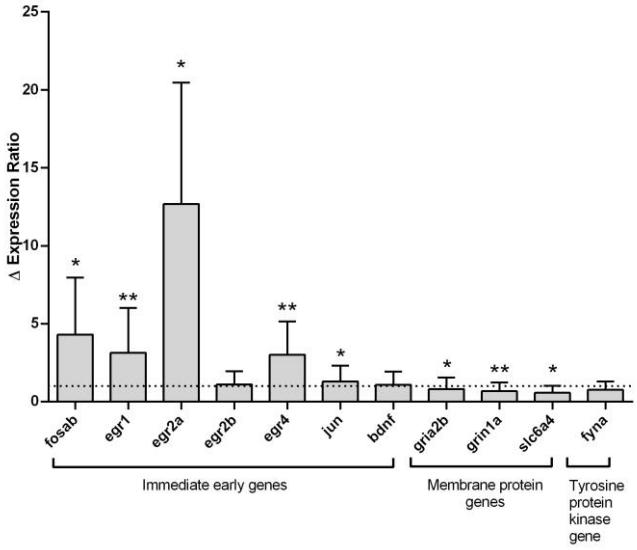

Figure 3.22. Targeted Ablation of the gjd2b Gene Increases Immediate Early Genes Expression and Decreases Membrane Protein Gene Expression.

*RNA transcript levels of several genes implicated in both anxiety and memory were measured by RT-qPCR to determine the relative expression changes in Cx35b$^{-/-}$ larvae. Here, a significant increase in several immediate early genes was observed. Additionally, Cx35b$^{-/-}$ larvae demonstrated a downregulation in membrane protein genes, confirming the relevance of gjd2b gene expression to the genetic modulation of anxiety. Statistical significance was determined by the One-Way ANOVA test, $p \leq 0.05$; *, $p < 0.05$, **, $p < 0.001$.*

3.5.4 Non-Associative/Non-Declarative Learning Through Habitation

Considering the increase in anxiety-like behavior during the light-dark locomotion assay in combination with the modulation of learning and memory genes, we suspected that Cx35b expression contributed to the neurobiology of their interplay. Next, we explored how the loss of the *gjd2b* gene contributed to long- and short-term memory capacity by utilizing the habituation learning and memory paradigm to measure non-associative memory. Since our behavioral assay was visual-based, we accounted for the discrepancies in visual functionality of Cx35b$^{-/-}$ larvae by delivering both light- and dark-flash stimuli. We capitalized on our previous results demonstrating that a one-second stimulus was sufficient for Cx35b$^{-/-}$ larvae to detect while preventing burst hyperactivity (see section 3.4.4). Here, 60 flash stimuli at 30s interspace intervals (ISIs) were delivered to age-matched wild-type and Cx35b$^{-/-}$ larvae. Larvae were trained three times prior to a 2hr or 24hr memory retention period, corresponding to short- and long-term memory, respectively, and habituation responses (%) were subsequently measured (**Figure 3.23A**). When comparing habituation responses between the initial and final training blocks, we found no significant difference between genotypes with dark flash stimuli (in %, WT: 15.912±2.026, n=48; Cx35b$^{-/-}$: 16.310±1.887, n=48, p = 0.9992, *Two-Way ANOVA*) or light flash stimuli (in %, WT: 11.128±1.626, n=72; Cx35b$^{-/-}$: 6.094±2.039, n=72, p = 0.1786). While wild-type larvae demonstrated no change in their learning abilities in response to dark or light flashes (p = 0.3112), Cx35b$^{-/-}$ larvae significantly reduced their habituation response to light flash stimuli (p = 0.0016), suggesting that the type of visual cue impacted the quality of learning. Nevertheless, since both genotypes demonstrated positive habituation (%), we concluded that Cx35b$^{-/-}$ larvae were still capable of learning with reasonable capacity (**Figure 3.23B**).

In follow-up, we explored how both short- and long-term memory was impacted in Cx35b$^{-/-}$ larvae during the light- and dark flash habituation test. Here, we measured memory retention (%) by comparing the activity levels between the final training block and the re-test block following the memory retention period (**Figure 3.23A**). In comparison to the wild-type, Cx35$^{-/-}$ displayed no significant difference in their short-term memory (*in %*, WT: 2.465±1.416; Cx35b$^{-/-}$: 1.901±1.331, p = 0.9971) or long-term memory retention (*in %*, WT: -4.427±2.482; Cx35b$^{-/-}$: -6.618±2.382, p = 0.8617) while exposed to dark flashes. However, Cx35b$^{-/-}$ larvae performed significantly worse on the recall task following a 24hr memory retention period (p = 0.0139), an observation not observed for wild-type larvae (p = 0.0687) (**Figure 3.23C**). Nevertheless, both genotypes displayed similar memory capabilities to dark flashes, where larvae had a positive recall following a 2hr retention period and negative recall following a 24hr retention period, indicative of forgetfulness.

Likewise, light flash stimuli had no impact on short-term or long-term memory capabilities between genotypes (*in %, 2hr* - WT: -138.234±25.309; Cx35b$^{-/-}$: -111.750±20.593, p = 0.7230; *24hr* - WT:

5.608±1.743; Cx35b$^{-/-}$ 10.198±1.450, p = 0.9988). Interestingly, both wild-type ($p < 0.0001$) and Cx35b$^{-/-}$ ($p < 0.0001$) larvae performed better on recalling the light flash stimuli following a 24hr retention period than a 2hr retention period (**Figure 3.23D**). Taken together, we concluded that learning and memory capacities were unaffected following the genetic ablation of the *gjd2b* gene. Interestingly, however, stimulus type played a significant role in memory recall suggesting that visual perception influences learning and memory.

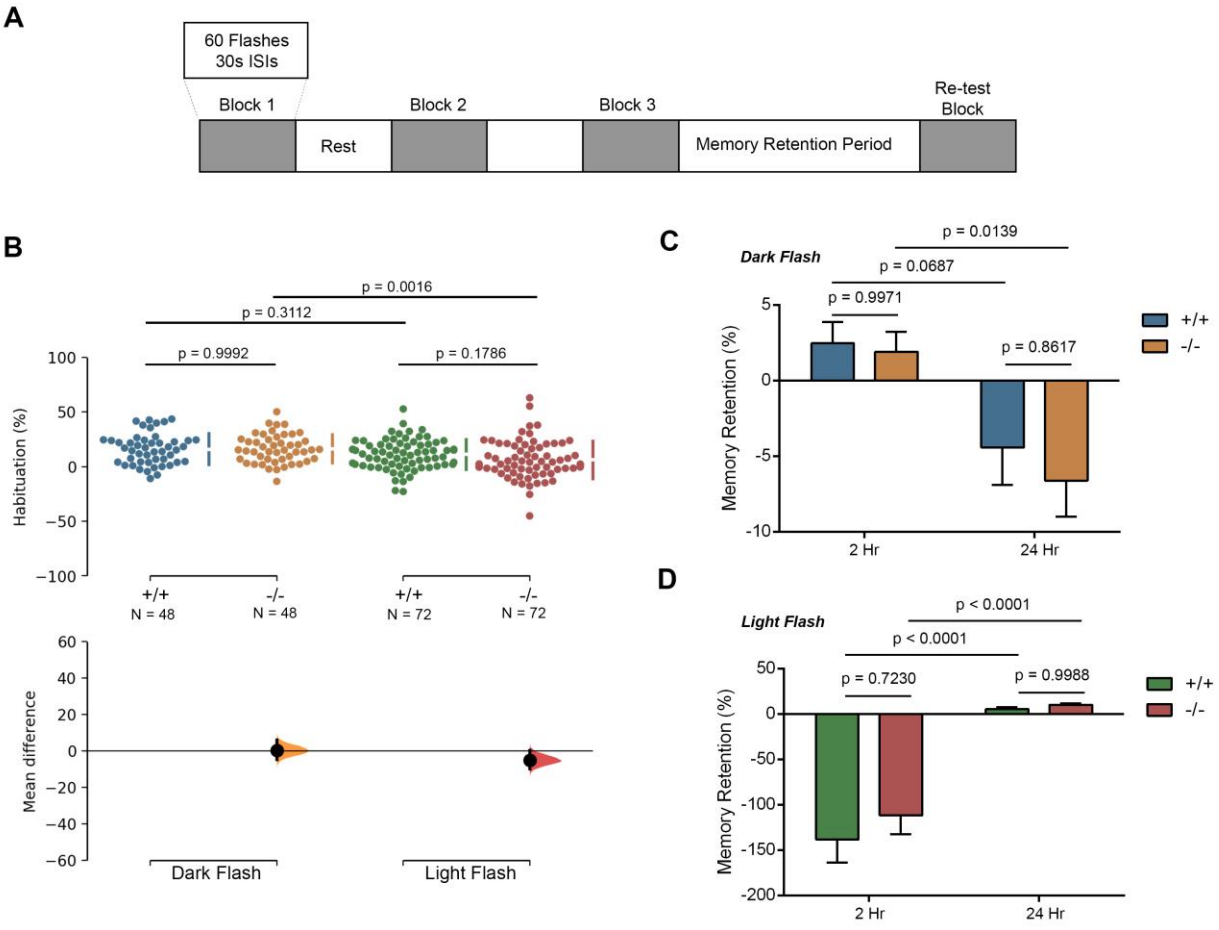

Figure 3.23. Habituation and Memory Retention Responses in Cx35b$^{-/-}$ Larvae are Functionally Intact.

*(**A**) General overview of the habituation assay used to assess learning and memory phenotypes. Flashes of light or darkness were delivered to dark-adapted or light-adapted zebrafish, respectively. Rest periods mimicked the lighting conditions of the adaptation phase. Three training blocks were administered before testing short- and long-term memory recall. (**B**) Habituation (%) was measured by comparing responses of the third training block to the initial training block to determine learning capabilities. Cx35b$^{-/-}$ larvae performed equally as well during the dark- and light-flash training blocks Memory retention for (**C**) dark-flash habituation and (**D**) light-flash habituation was assessed by comparing the third training block responses to the re-test block. While Cx35b$^{-/-}$ larvae performed equally as well despite the recall length or visual stimulus, the type of visual cue impacted the integrity of memory recall. Statistical significance was determined by the Two-Way ANOVA test, $p \leq 0.05$. The sample size (n) was 48 for wild-type and Cx35b$^{-/-}$ larvae under dark flash habituation and n – 72 for wild-type and Cx35b$^{-/-}$ larvae under light flash habituation.*

3.5.5 Differential Regulation of Learning and Memory Genes Following Light- and Dark-Flash Habituation Assay

We were particularly intrigued that Cx35b$^{-/-}$ larvae performed equally as well in comparison to the age-matched wild-type during light- and dark-flash habituation assays. Moreover, since memory retention was differentially regulated based on stimulus type, we explored the genetic changes that may account for the previous results. Again, we performed quantitative real-time PCR (RT-qPCR) to measure RNA transcript levels as an indication of gene expression in critical learning and memory genes following the habituation assay. Here, we targeted several immediate early genes (*fosab*, *egr1*, *egr4*, *bdnf*), cyclic-AMP response element-binding (CREB) genes (*creb1a*, c*reb1b*), the select members of kinase family genes (*dlg4*, *camk2a*, *camk4*). Following dark-flash habituation, most immediate early genes and CaMK genes analyzed were downregulated in both genotype groups in comparison to their respective naïve control (larvae that had not performed the habituation task). In contrast, *creb1b* and *dlg4* were upregulated in both wild-type and Cx35b$^{-/-}$ larvae. However, while only wild-type larvae significantly downregulated *bdnf* following dark-flash habituation ($p = 0.049$), Cx35b$^{-/-}$ larvae displayed an elevation in *creb1a* expression ($p = 0.023$) (**Figure 3.24A-B**). Following light-flash habituation, both wild-type and Cx35b$^{-/-}$ larvae demonstrated upregulation in *egr4* expression and downregulated the expression of kinase family genes, *creb1b*, *fosab*, and *egr1*. Wild-type larvae, however, also displayed a reduction in *creb1b* expression ($p = 0.020$), whereas no changes were observed in Cx35b$^{-/-}$ larvae.

Interestingly, *egr4* was consistently upregulated during light-flash habituation and downregulated during dark flash habituation regardless of genotype. Moreover, *creb1b* and *dlg4* expression showed the opposite effect, where dark-flash habituation caused an upregulation in these genes, and light-flash habituation downregulated expression levels. Taken together, we suspect that the alterations in the genetic expression in *egr4*, *creb1b*, and *dlg4* may account for the discrepancies in visual-based learning and memory paradigms.

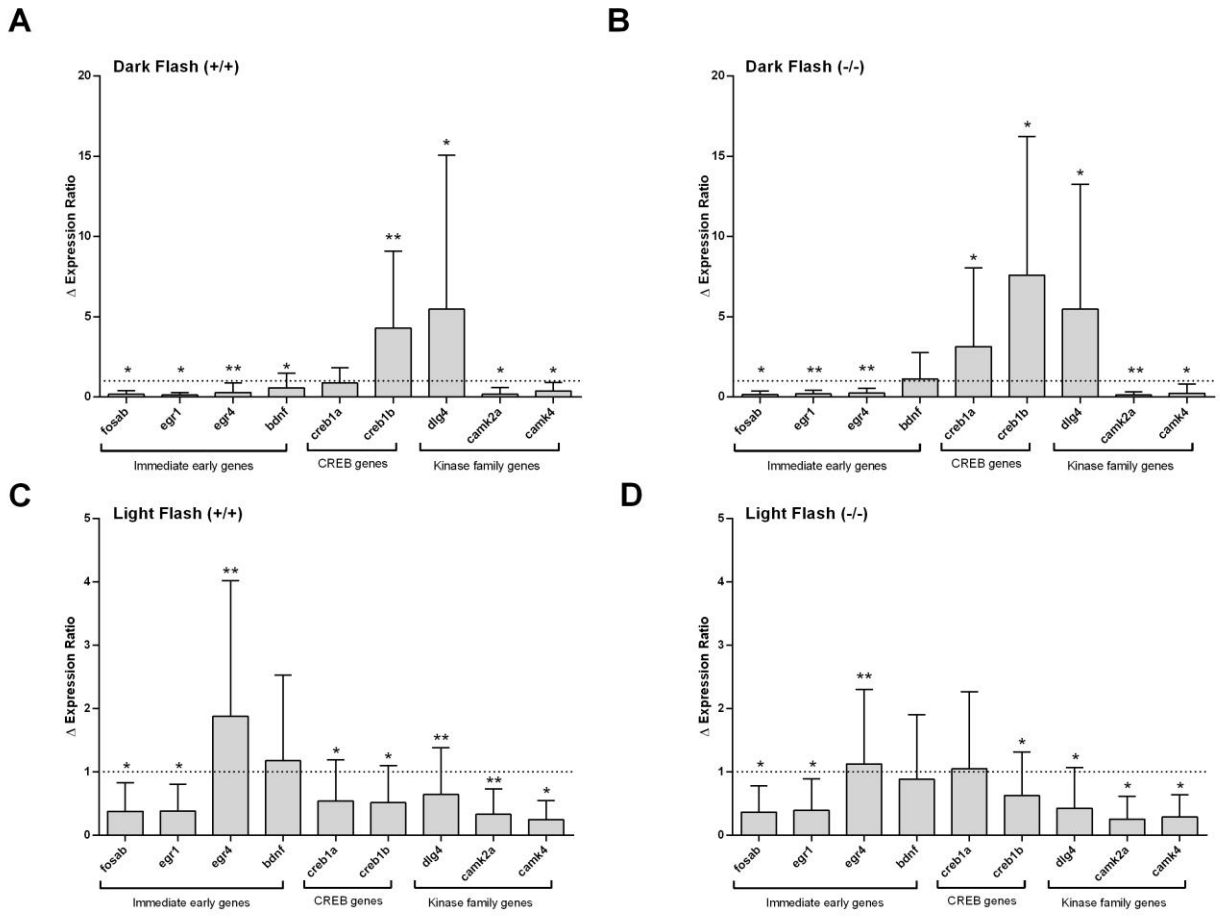

Figure 3.24. Differential Regulation of Learning and Memory Genes Following the Light- and Dark-Flash Habituation Assay.

*RNA transcript levels of several genes implicated in both anxiety and memory were measured by RT-qPCR to determine the relative expression changes in Cx35b$^{-/-}$ larvae. Here, a significant increase in several immediate early genes was observed. Additionally, Cx35b$^{-/-}$ larvae demonstrated a downregulation in membrane protein genes, confirming the relevance of gjd2b gene expression to the genetic modulation of anxiety. Statistical significance was determined by the One-Way ANOVA test, $p \leq 0.05$; *, $p < 0.05$, **, $p < 0.001$.*

3.5.6 Discussion

In the mammalian brain, Cx36 is expressed in a variety of regions, including the cerebral cortex and hippocampus (Condorelli *et al.*, 1998); however, loss of Cx36 eradicates most dendro-dendritic coupling in the hippocampus. At the behavioral level, Cx36$^{-/-}$ mice show impairments in object recognition and in short-term spatial memory (Frisch *et al.*, 2005; Allen *et al.*, 2011). However, little is known about how homotypic Cx36 aggregates modulate learning and memory distinctly from the presynapse to the postsynapse. Moreover, few studies have explored the broader aspects of cognitive indexing in Cx36 knock-out models. As such, while the relationship between anxiety and memory is well established, the

neurobiology of their interplay remains poorly understood. In the present study, we assessed how presynaptic Cx35b expression impacts anxiety, learning, and memory in the zebrafish animal model. Since we previously detailed the contribution of Cx35b to visual functionality, our investigations explored visually-provoked models of anxiety and non-associative memory. Here, we found that loss of the *gjd2b* gene provoked anxiety during light and dark transitions; however, it had no impact on the capacity of learning and memory. Nevertheless, we demonstrated that the type of visual stimuli, and thus visual perception, impact non-associative learning and memory paradigms. We suspect that a compensatory mechanism, via the expression of the remaining Cx36 teleost orthologs and several immediate early genes critical to synaptic plasticity, may account for the similar short- and long-term memory observed. Nevertheless, genetic ablation of the remaining orthologs may provide further insight into the pre- and postsynaptic contribution of various aspects of cognitive indexing.

3.5.6.1 The Agonist/Antagonist Activity of Buspirone Influences its Anxiolytic Properties

In this research investigation, we explored thigmotaxic behavior as a measure of aberrant anxiety during light-dark transitions. Here, Cx35b$^{-/-}$ demonstrated an increase in this wall-hugging behavior indicative of greater anxiety levels. The anxiety phenotype was rescued with the bath application of Buspirone (5mg/L), comparable to the untreated wild-type levels. However, we also found that wild-type larvae responded to Buspirone adversely. Here, Buspirone treatment increased thigmotaxic behavior, indicative of elevated stress and anxiety. As such, we must interpret our results considering the possible off-target effects of Buspirone to account for this result. Buspirone is classified as an azaspirodecanedione anxiolytic that acts as an agonist to the serotonin (5-HT)1A receptor. Serotonin neurotransmission is linked to mood and anxiety disorders in humans (Jans *et al.*, 2007; aan het Rot, Mathew and Charney, 2009; Durant, Christmas and Nutt, 2010; Ganasen and Stein, 2010; Ravindran and Stein, 2010) where increasing available serotonin concentrations via selective serotonin reuptake inhibitors (SSRIs) or serotonergic agents is linked to its therapeutic effect (Gartside, V. Umbers and Sharp, 1995). In contrast, SSRI treatment in early development has been shown to increase anxiety in rodent animal models (Caspi *et al.*, 2003; Lira *et al.*, 2003; Ansorge, Morelli and Gingrich, 2008; Olivier *et al.*, 2008; Oberlander, Gingrich and Ansorge, 2014), suggesting that serotonin impacts the immature and mature-anxiety circuitry differently. Based on our results detailing the impact of Cx35b loss on larval growth and development (see section 3.3.5), we previously raised the question of whether Cx35b$^{-/-}$ larvae are aging prematurely. Though this remains an area of exploration, premature aging or early maturation processes may explain why Buspirone had an anxiolytic effect on Cx35b$^{-/-}$ larvae but an anxiogenic effect on wild-type larvae. As a second consideration, we demonstrated that Cx35b$^{-/-}$ larvae exhibited downregulated expression levels of the serotonin transporter gene *slc6a4*. As such, this down-regulation may have provoked Cx35b$^{-/-}$ to be particularly sensitive to the

therapeutic effects of Buspirone. However, we acknowledge that this may not entirely account for the discrepancy seen with wild-type larvae and predict that premature aging in Cx35b$^{-/-}$ larvae is the more probable explanation. Interestingly, Buspirone is also known to be a mixed agonist/antagonist on postsynaptic dopamine receptors (McMillen *et al.*, 1983; Sumiyoshi *et al.*, 2007). Since we previously demonstrated differential regulation in *th* and *drd4b* expression in Cx35b$^{-/-}$ larvae, this also serves as an alternative explanation to our data.

3.5.6.2 Non-Associative Learning and Memory was Functionally Intact in Cx35b$^{-/-}$ Larvae

Non-associative learning and memory were measured using the classic habituation assay. While habituation responses can be measured by visual, auditory, and tactile stimuli, our investigation implemented visual cues due to our previous report (see section 3.4) and current literature (Quint *et al.*, 2021) detailing the contribution of Cx35b to visual functionality. While we expected to observe impairments in learning and memory based on previous reports in Cx36$^{-/-}$ mice (Frisch *et al.*, 2005; Allen *et al.*, 2011), instead, we found that Cx35$^{-/-}$ larvae performed similarly to the age-matched wild-type. We anticipate that this may be due to the expression of the remaining Cx36 orthologs (Cx35a and Cx34.7) that are still capable of driving signaling cascades from the presynapse to the postsynapse respectively. In this case, Cx35a and Cx34.7 expression could serve as a compensatory mechanism to maintain the integrity of neuronal communication during learning and memory paradigms. This could be achieved by the upregulation in Cx35a and/or Cx34.7 protein expression, though, from our previous report, we believe this is an unlikely explanation (see section 3.3.8.1). Instead, we propose that the enhancement of Cx35a and Cx34.7 junctional coupling could account for the similarity in memory recall between wild-type and Cx35b$^{-/-}$ larvae. This would support our previous findings suggesting that cone-cone coupling was enhanced in Cx35b$^{-/-}$ larvae. In this case, we anticipate that gap junctional coupling would be enhanced throughout the CNS. This also complements the work accomplished by Li et al. (2020), proposing a similar mechanism in a knock-in phosphomimetic Cx36 mouse line, termed Cx36-DEDD, which resulted in increased junctional coupling (Lin *et al.*, 2020). Future studies examining the changes in junctional coupling throughout the brain in Cx35b$^{-/-}$ larvae, particularly in the hippocampus, would be invaluable in confirming this mechanism.

3.5.6.3 Loss of gjd2b Differentially Regulates the Expression of Anxiety, Learning, and Memory Genes in Zebrafish

Our study addressed the genetic footprint of Cx35b$^{-/-}$ larvae by describing the changes in the expression of genes with overlapping functionality in anxiety, learning, and memory. Here, we found that *gria2b*, *grin1a*, and *slc6a4* were downregulated in Cx35b$^{-/-}$ larvae suggesting that Cx35b expression is critical for the expression of NMDA receptors, AMPA receptors, and serotonin transporters. We previously addressed that the downregulation of *slc6a4* likely played a role in establishing the anxiety-like behavior

in Cx35b$^{-/-}$ by reducing the availability of serotonin. However, we found that a reduction in *gria2b* and *grin1a* was consistent with the literature that confirmed electrical synapses are critical for chemical synaptogenesis (Maher, McGinley and Westbrook, 2009). As such, presynaptic Cx35b expression regulates postsynaptic receptors at the chemical synapse. Nevertheless, a reduction in NMDA receptor neurotransmission has been linked to cognitive deficits, anxiety, and depression in mouse models (Li *et al.*, 2014). Similarly, mice models of anxiety and depression showed a reduction in AMPA receptors; however, pharmacological innervation countering the decrease in AMPA receptor neurotransmission was sufficient to alleviate the adverse behavior (Ma *et al.*, 2021). Taken together, a reduction in *gria2b*, *grin1a*, and *slc6a4* in Cx35b$^{-/-}$ larvae was consistent with the literature detailing the involvement of their respective proteins in provoking anxiety-like behavior.

Immediate early genes (IEGs) encode for a variety of transcription factors, cytoskeletal proteins, growth factors, metabolic enzymes, and various signal transduction proteins. Typically, IEGs are activated quickly and transiently in response to a cellular stimulus; neuronal IEGs are known to function at the synapse to influence learning and memory. However, IEGs also have implications for models of anxiety. In Cx35b$^{-/-}$ zebrafish larvae, we observed an increase in *fosab*, *egr1*, *egr2a*, *egr4*, and *jun* neuronal IEG expression. Most notably, upregulation of *fosab* and *fosb*, members of the Fos family of transcription factors, has been previously linked to the stress and anxiety response in zebrafish larvae (Fan *et al.*, 2021). Similarly, the early growth response gene *egr1* is critical for memory consolidation, and its mRNA transcript levels are used as a measure of depressive phenotypes. *Egr1* upregulation has also been linked to anxiety-like behavior in several reports (Schreiber *et al.*, 1991; Watanabe, Stone and McEwen, 1994; Cullinan *et al.*, 1995; Olsson, Håkansson and Seckl, 1997; Knapska and Kaczmarek, 2004; Kozlovsky *et al.*, 2009). Given the well-established roles of *fosab* and *egr1* in anxiety, as well as its role in modulating synaptic plasticity, we explored how the expression of these genes is altered following habituation. Interestingly, both *fosab* and *egr1* were downregulated in following the light- and dark-flash habituation assay suggesting that these genes were sensitive to repetitive stressors. We anticipate that the downregulation of *fosab* and *egr1* following habituation training would cause a reduction in anxiety-like behavior during the re-test block. However, this has yet to be established.

3.5.6.4 Memory Recall is Dependent on both Visual Stimuli and Memory Retention Period

Although Cx35b$^{-/-}$ larvae performed similarly in their memory recall to the age-matched wild-type, we observed that the capacity to recall was dependent on the visual stimulus and memory retention period. Short-term memory recall was positive following dark flash habituation; however, it was impaired during light-flash habituation. In contrast, long-term memory recall impairment was evident following a two-hour memory retention period but displayed a positive response following a twenty-four-hour retention period.

Though this was a novel finding, how the genetic profile of zebrafish larvae changes depending on a short- or long-term memory task was not addressed here. Nevertheless, our RT-qPCR data reveal differential regulation of *dlg4*, *creb1b*, and *egr4* genes in response to the light- or dark-flash visual stimuli. More specifically, *dlg4* and *creb1b* were downregulated, and *egr4* was upregulated in response to light flash habituation regardless of genotype; the opposite was found in response to dark flash habituation. In mammals, the cyclic- adenosine monophosphate response element-binding protein (CREB), encoded by *creb1*, is known to be tightly regulated with suprachiasmatic nuclei (SCN) rhythms modulating the circadian rhythm (Ginty *et al.*, 1993). As such, we anticipate that the differential regulation of habitation responses during light- or dark-flash stimuli to be linked to *creb1b* expression and the circadian rhythm. Current literature has yet to address how light/dark stimuli affect *dlg4* and *egr4* expression, encoding for the proteins PSD95 and early growth response protein 4, respectively.

3.5.6.5 Limitations and Critical Considerations

We recognized that neither wild-type nor Cx35b$^{-/-}$ larvae displayed a significant difference in their learning efficacy when comparing the final training block to the initial training block during the habituation assays. As such, we anticipate that the habituation protocol could be further assessed to determine whether extending or adding additional training blocks would optimize the protocol. We anticipate that larvae would display a significant increase in habituation (%) in comparison to the initial training block if the current protocol was inferior. As a second consideration, our data analysis averaged burst activity; however, whether the total activity responses would have been a more suitable measure was not explored. Lastly, learning measurements could be masked when averaging the entire training or re-test block. Though this is typically how habituation responses are measured in the literature, we propose analyzing a more narrow time window to capture the initial recall responses to improve accuracy.

Although we found that Cx35b$^{-/-}$ did not play a role in non-associative memory, we cannot discount its role in associative memory. Andersson et al. (2015) established a means of measuring associative (declarative) by combining the novel object recognition (NOR) test with brain lateralization, referred to as VLNOR (visual lateralization NOR). In this model, 10dpf zebrafish larvae approach novelty with a left-eye bias and familiarity with a right-eye bias (Andersson, Ek and Olsson, 2015). As such, future studies should still consider the contribution of Cx35b$^{-/-}$ to associative memory by measuring VLNOR. Whether VLNOR is present as early as 7dpf, however, has not been previously addressed and would need to be established first.

The ability to recall a task following training typically follows time peaks where recalling learned information is performed best. While a twenty-four-hour peak has been observed in mice (Loh *et al.*, 2010), some studies suggest that a twelve-hour peak also exists. Interestingly, this twelve-hour peak was dependent

on the time of day training occurred since later training times abolished this effect (Holloway and R. A. Wansley, 1973; Holloway and R. Wansley, 1973; Wansley and Holloway, 1975, 1976; Hunsicker and Mellgren, 1977). Whether the rhythm of recall follows a twelve or twenty-four-hour peak has yet to be addressed in the zebrafish animal model and should be a point of consideration in future learning and memory paradigms.

4 DISCUSSION

4.1 Understanding the Asymmetry of Mixed Synapses from a Cells-to-Systems Approach

4.1.1 Modeling Molecular and Functional Asymmetry of Cx36 using Cx35b

Since the initial discovery of mixed (chemical and electrical) synapses in the mammalian spinal cord (Rash *et al.*, 1996), various studies have confirmed their presence throughout the vertebrate CNS, often coinciding with Cx36/Cx35b expression (Pereda *et al.*, 2003, 2004; Hamzei-Sichani *et al.*, 2012). While Cx36 electrical synapses are abundant in the vertebrate brain, their molecular and functional complexity remains poorly understood. As such, the question arises of **how gap junctions are modulated distinctly pre- and postsynaptically, particularly at homotypic aggregates?** We addressed this question from the cellular and molecular standpoint by investigating the similarities in molecular machinery utilized by both chemical and electrical synapses. Here, we found that Cx36 interacts directly with the tubulin cytoskeleton, and its interaction drives the transport of connexons to modulate channel abundance at the gap junction plaque. This mechanism is reminiscent of that utilized by the NMDA subunit NR2B. Moreover, we found that transport of Cx36, under conditions mimicking synaptic plasticity, occurred independent of CaMKII activity. Our report was consistent with previous investigations by Siu et al. (2016) suggesting that CaMKII activity plays a role at Cx36 aggregates by mediating the opening of channels (Siu *et al.*, 2016). As such, plasticity of Cx36 electrical synapses is modulated by 1) the tubulin-dependent trafficking of Cx36 and 2) the CaMKII-dependent opening of Cx36 gap junction channels.

While the investigations performed in this dissertation begin to paint a picture of how Cx36 is modulated similarly to chemical synapses, particularly at the postsynapse, its functional relevance remains unclear. Moreover, identifying the mechanisms that drive the molecular fingerprint of Cx36 on either side of the GJP is not yet understood. To achieve a better understanding of this, we utilized the zebrafish animal model that is known to express the Cx36 orthologs distinctly at either the presynapse or postsynapse in Mauthner neurons. While the asymmetry seen in Mauthner neurons still needs to be resolved throughout the CNS, studying each ortholog individually will provide clues into the mechanism Cx36 uses to achieve asymmetry at mixed synapses and its functional relevance. Considering this, we then explored how the loss of Cx35b expression impacts tissue organization, system functionality, and behavioral outcomes in zebrafish larvae (7dpf) when all major brain areas and circuitry are developed. Cx35b was chosen for our research investigations since it displays the highest sequence similarity to mammalian Cx36 and is known to be expressed presynaptically. As such, our question then became, **what is the functional relevance, if**

any, of presynaptic Cx35b expression? Our investigations focused primarily on the visual contributions of Cx35b, given that its localization in the retina is well established. Here, we uncovered several potential implications of Cx35b expression, including driving larval growth trajectories, fine-tuning cone-to-cone photoreceptor communication, aiding in the discrimination of the brightness, arrangement, and temporal properties of visual stimuli, and modulating the neurobehavior of anxiety. Interestingly, we also found that Cx35b does not contribute to non-associative learning and memory, though we do not discount its involvement in associative learning and memory paradigms. Moreover, we anticipate that Cx35b expression is restricted to the presynapse of cone-photoreceptors, though this has yet to be confirmed. The results of this dissertation concluded by providing a better understanding of the relevance of presynaptic Cx35b expression in driving systemic and behavioral outcomes.

To advance this area of research, the pertinent question is, **how can we merge the mammalian Cx36 and teleost Cx35b models to further our understanding of the asymmetry of mixed synapses?** The expression of Cx35b in the teleost model is reminiscent of presynaptic Cx36 expression. However, the postsynaptic interacting partner(s) must also be accounted for, particularly when we consider that homotypic Cx36 aggregates can achieve electrical rectification. In Mauthner neurons, molecular asymmetry is achieved with the remaining Cx36 orthologs; both Cx35a and Cx35b have been detailed at the presynaptic terminal, and both Cx34.1 and Cx34.7 have been described at the postsynapse (Rash *et al.*, 2013; A. C. Miller *et al.*, 2017). As such, we wonder whether homotypic Cx36 asymmetry is driven by (1) post-translational modifications, (2) variations of signaling complexes interacting with either side of the gap junction plaque, or (3) the overall asymmetric properties of the pre- and postsynaptic membrane; there is some evidence to suggest that all three possibilities may play a role (Li *et al.*, 2004; Li, Lynn and Nagy, 2012; A. C. Miller *et al.*, 2017; Bazzigaluppi *et al.*, 2017; Nagy and Lynn, 2018; O'Brien, 2019). Firstly, post-translational modifications can amplify the Cx36 proteome and create multiple variants which may compartmentalize Cx36 to the pre- or postsynapse. As such, understanding which post-translational modifications are specific to presynaptic Cx35a/Cx35b and postsynaptic Cx34.1/Cx34.7 may aid in distinguishing those involved with Cx36 asymmetry; this task is typically achieved with Nuclear Magnetic Resonance (NMR) Spectrometry to obtain site-specific resolution. Moreover, since enzymatic reactions can be followed in a time-dependent manner with NMR, observing the change in post-translational modifications during synaptic plasticity will better detail the switch from bi-directional-to-uni-directional communication at mixed synapses expressing Cx36. Secondly, protein interactions unique to presynaptic Cx35a/Cx35b and postsynaptic Cx34.1/Cx34.7 can be elucidated in transient or cell expression lines utilizing the same strategies we employed in Chapter 2 to uncover tubulin as an interacting candidate of Cx36. Investigations utilizing structural modeling would also detail the similarities/differences in presynaptic and postsynaptic protein interaction candidates and their subsequent molecular binding

mechanisms. In doing so, we would unify how post-translational modifications effect the protein-protein interactions differently on either side of the synapse. This work would serve as a basis to further explore protein-protein interactions *in vivo* with the zebrafish animal model to provide a more complex, but accurate depiction of the asymmetric proteome at mixed synapses. For this, the BioID strategy we utilized in Neuro-2a cells (see section 2.2) has now been adapted for proximity-dependent biotinylation in zebrafish *in vivo* (Rosenthal *et al.*, 2021). Moreover, the newly developed technique BLITZ (Biotin Labeling In Tagged Zebrafish) combines BioID with a GFP-binding nanobody to target GFP-tagged transgenic fish lines which offers the versatility of studying the proteome of Cx36 teleost orthologs in a tissue specific manner (Xiong *et al.*, 2021). The caveat to BLITZ, however, would be the establishment of Cx35a/Cx35b/Cx34.1/Cx34.7-GFP-tagged fish lines; this would firstly need to be established with a CRISPR-based knock-out/knock-in genome engineering strategy. Nevertheless, BioID and BLITZ both allow for the protein-protein interactions contributing to the dynamic processes at the synapse to be resolved while visualizing the morphology and physiology of individual cells at higher resolution. This is of particular interest at dendro-dendritic contacts, where Cx36 is primarily found, which can alter shape and spine density to affect functional characteristics and thus behavioral outcomes. Altogether, uncovering unique protein-protein interacting candidates of Cx35b may provide insight into the signaling complexes of the presynapse; likewise for the remaining orthologs (presynaptic Cx35a and postsynaptic Cx34.1 and Cx34.7). Lastly, to address the consequences of the asymmetric expression of Cx36, two strategies can be employed. (1) Cell-specific knock-out models can be generated to limit the confounding effects of systemic cross-talk and overlapping signaling cascades by utilizing the Cre-*loxP* tissue-specific recombination system; though this is limited to the current database of Cre-driver lines available in the zebrafish animal model. (2) Cell-specific rescue experiments with global knockouts can be utilized by targeting cell-specific reporters. Nevertheless, the contribution of Cx35b to specific systems, such as the visual system, should also be studied separately instead of globally.

Much like mixed synapses, Cx35b and Cx36 research should occur in tandem as a complement to each other. This reciprocity could be capitalized on by investigating whether previously established protein-protein interactions of Cx36 are also interacting candidates of Cx35b, such as tubulin. A similar approach of reciprocity was utilized here since our investigations found that non-associative memory was unaffected in a Cx35b$^{-/-}$ teleost model when previous studies found learning and memory impairments in Cx36 knockout mice models. We can now better appreciate the significance of molecular asymmetry in driving behavioral outcomes, particularly in a research model with a similar retinal organization to humans. In this manner, we can aim to solve the contribution of the presynapse and postsynapse to complex higher-order behaviors.

4.1.2 Exploring the Relevance of Cx35b to Clinical Research

It should go without saying that part of understanding the neurophysiology of the brain is to advance research in areas with relevance to neurological dysfunction. As such, whether the collection of behavioral phenotypes displayed by Cx35b$^{-/-}$ larvae was indicative of symptoms of neurodegenerative diseases or disorders was of interest. We considered that Cx35b$^{-/-}$ displayed a smaller midbrain diameter, hyperactivity to light-ON VMR, as well as an increase in anxiety levels, and all of the above satisfied the attention deficit hyperactivity disorder (ADHD) criteria. ADHD is a complex neurodevelopmental disorder characterized by inattention and hyperactivity but is not in itself considered a learning disability. In morphological studies of children and adolescents with ADHD, Sowell et al. (2003) found a significant reduction in brain volume in comparison to healthy controls. More specifically, the distance between the center of the brain and the cortical surface was reduced, as was the bilateral brain surface (measured from the lateral anterior temporal cortices) of ADHD patients (Sowell *et al.*, 2003). ADHD also coincides with optical dysfunctions. Mezer et al. (2012) found that children diagnosed with ADHD were more likely to display myopia and refractive error (Mezer and Wygnanski-Jaffe, 2012), which is also a phenotype of Cx35b$^{-/-}$ larvae (Quint *et al.*, 2021). Moreover, photophobia is a prominent symptom in ADHD patients (Kooij and Bijlenga, 2014). Behaviorally, ADHD often coincides with anxiety (Jacob *et al.*, 2014), and their interplay is demonstrated by numerous reports showing a reduction in anxiety with ADHD treatment (Bouffard *et al.*, 2003; Gabriel, 2010; Gabriel and Violato, 2011; Mattos *et al.*, 2013; Bloch *et al.*, 2017).

In an era of personalized precision medicine, the dopamine receptor DRD4 is commonly used as a biomarker for childhood ADHD susceptibility (Asghari *et al.*, 2002; Faraone, Bonvicini and Scassellati, 2014; Bonvicini *et al.*, 2020). This is due to its high expression in brain regions implicated in attention, such as the orbitofrontal and anterior cingulate (20,21). While *DRD4* polymorphisms are commonly studied in the context of ADHD, Bonvivini et al. (2020) demonstrated a downregulation of DRD4 found in ADHD-specific brain regions based on a recent genome-wide association meta-analysis (Bonvicini *et al.*, 2020). Interestingly, our results also demonstrated a global downregulation in the teleost ortholog *drd4b* following the genetic ablation of *gjd2b*. Not only did this illustrate a relationship between Cx35b expression and dopaminergic signaling, but we anticipate that *drd4b* expression, regulated by presynaptic Cx35b, coincides with the collection of behavioral phenotypes in our knock-out model. Taken together, we propose that the loss of Cx35b$^{-/-}$ may have clinical implications for ADHD.

4.1.3 Limitations & Critical Considerations

Both chemical and electrical modalities of transmission have been well established in the vertebrate CNS, however, research revolving around electrical synapses has only recently evolved to showcase their complexity, diversity, and modifiability, comparable to that found at chemical synapses (Sterling and Matthews, 2005; J.-C. Hervé *et al.*, 2007; Flores *et al.*, 2012; Pereda *et al.*, 2013; Pereda, 2014). While the relationship between chemical and electrical transmission is known to be reciprocal and synergistic (Söhl *et al.*, 1998; Belluardo *et al.*, 2000; Park *et al.*, 2011), this leads us to question (1) to what extent are chemical and electrical synapses found alongside each other in mixed synapses? And (2) how do gap junctions, and Cx36 specifically, influence neuronal circuits where chemical and electrical transmission is paired vs. separate? Reconstructed connectomes of *C. elegans* and the rabbit retina estimate about 20% of synaptic connections are electrical (White *et al.*, 1986; Anderson *et al.*, 2011; Jarrell *et al.*, 2012; Cook *et al.*, 2019). However, estimates of electrical connectivity in the CNS of teleosts, murines, and humans, typically achieved via a combination of freeze-fracture replicas and electron microscopy, have not been established. As such, current literature has yet to address how many synapses are estimated to be mixed, and which circuits rely on this form of transmission. To this end, defining which aspects of cellular functionality, and ultimately behavioral outcomes, depend on mixed transmission should be addressed in the future.

What are the implications of a dual-modality of synaptic transmission? Communication achieved through gap junctions can acutely affect the excitability of neurons receiving multiple inputs within a circuit. The earliest evidence of this preceded the knowledge of gap junctions when Furshapan and Potter (1959) demonstrated that subthreshold electrical stimulation transferred current directly between crayfish nerve cells (Furshpan and Potter, 1959). Nevertheless, the instantaneous transfer of ions and metabolites in the absence of an action potential via gap junction channels promotes the synchronous firing of neuronal groups (Getting, 1974; Getting and Willows, 1974; Galarreta and Hestrin, 2001; Veruki and Hartveit, 2002; Curti *et al.*, 2012). This is of significance in neuronal populations that require high-speed and reliable transmission such as those governing escape behaviors (Korn and Faber, 2005). At mixed-glutamatergic synapses, a dual-modality would increase the sensitivity of the network by (1) priming individual neurons prior to receiving an EPSP, ensuring that a single or sequence of action potentials are initiated, (2) providing a secondary means for glutamate release, (3) synchronizing groups of neurons innervated by a single pre-synaptic terminal and, (4) providing feedback to the presynaptic cell, capitalizing on the bidirectional property unique to gap junctions. Similar mechanisms would be at play at mixed GABAergic synapses receiving IPSPs. Moreover, the presence of mixed synapses could provide a form of neuronal resilience since gap junctions are impartial to short-term synaptic fatigue where synaptic vesicles have been depleted and/or post-synaptic receptors are desensitized (Zhang *et al.*, 2005; Simons-Weidenmaier *et al.*, 2006).

Considering the above, we recognize that gap junction-mediated neuromodulation would precede neuroplasticity temporally and in a spatial-dependent manner. As such, understanding the cellular and molecular changes to chemical transmission at mixed synapses is still a knowledge gap that should be explored in the future.

Due to the multiple genome duplications in teleost species, zebrafish express single or multiple homologs to human connexin genes in addition to several unique connexins (see appendix D) (Volff, 2005; Eastman *et al.*, 2006; Lukowicz-Bedford, Farnsworth and Miller, 2022). More specifically, the zebrafish equivalent to the *GJD2* gene, corresponding to the Cx36 protein, are the two paralogs *gjd1a/b* (corresponding to Cx34.1/Cx34.7) and *gjd2a/b* (corresponding to Cx35a/Cx35b) (McLachlan *et al.*, 2003; A. C. Miller *et al.*, 2017). Conveniently, experiments carried out in zebrafish Mauthner neurons have demonstrated the asymmetric expression of these paralogs whereby *gjd1a/b* are expressed post-synaptically and *gjd2a/b* are expressed presynaptically (A. C. Miller *et al.*, 2017). Though our research study utilized a Cx35b knock-out zebrafish model, data interpretation must take the following into careful consideration. Both pre- and postsynaptic connexin expression retain some redundancy via gene paralogs; since Cx35a expression remained intact following the loss of Cx35b, this may limit the degree to which asymmetry is affected. However, this largely depends on how asymmetry is defined. (1) *Lower potency* - Since our results demonstrated that the expression of the remaining connexin proteins were unaffected, we would anticipate that loss of Cx35b would alter the electrophysiological fingerprint, which we proposed may be regulated by dopaminergic gene expression. While this change may be considered mild in nature, since the loss of Cx35b is restricted to the presynapse, any deviance from the wild-type can be considered as an asymmetric effect. We propose that future investigations incorporate electrophysiological recordings to resolve the changes in gap junction coupling and electrical transmission in the $Cx35b^{-/-}$ zebrafish larvae. (2) *Higher potency* – Targeting the presynaptic connexins, via a Cx35a/Cx35b double knock-out model, would demonstrate the totality of losing presynaptic electrical transmission on tissue organization, system functionality, and behavioral outcomes; however, this has yet to be established. Here, we may suspect more robust changes to the visual system and measurable cognitive indexes, though compensatory gene regulation mechanisms would also need to be addressed if animals are viable. Nevertheless, the emphasis remains that both sides of electrical synapses are not necessarily mirror images of each other and provide a means of molecular asymmetry and functionality similar to chemical synapses.

4.2 Comparing & Troubleshooting with the TALEN and CRISPR Genome Engineering Strategies.

4.2.1 TALENS Failed to Gene Edit Cx35b

The murine model typically used to assess plasticity-dependent behavioral phenotypes is limited by efficiency, cost, and high-throughput accessibility. Moreover, behavioral outcomes largely dependent on visual processing are not fully translatable from murines to humans due to the distinct expression of multiple opsins in the human visual system, which is absent in murines. As such, we utilized the zebrafish (*Danio rerio*) animal model to explore the contribution of Cx35b to cognition and behavior. Initial investigations made use of transcription activator-like effector nuclease (TALEN) technology since our research group previously established knock-out efficiencies of up to 85% with TALENs directed against the drPanx1a, drPanx1b, drPanx2, and drCx27.5 genes. The TALEN genome engineering strategy offers versatility since the DNA-binding sequence is customized for the recognition of specific DNA motifs while minimizing off-target effects. The efficiency of TALENs largely depends on the probability that both TALEN pairs will effectively target adjacent sites for the proximity-based activation of nuclease activity and subsequent double-strand DNA break to occur. For our purposes, however, TALENs were ineffective in engineering indel mutations in the *gjd2* gene at the targeted loci despite rigorous attempts. Typically, when considering troubleshooting options, one must account for both TALEN vectors injecting into the same cell with equal efficiency to provide equal TALEN protein expression. Since microinjections were carried out at the 1- to 2- cell stage, injection into the same cell was accounted for. Additionally, several target sequences were tested. Therefore, the inability to establish Cx35b knockouts with TALEN technology may have been due to technical details which were not identified by troubleshooting.

4.2.2 Utilizing the CRISPR-Cas9 Genome Engineering Strategy

The CRISPR-Cas9 system has been popularized in modern genome engineering strategies as an alternative to TALENs. As such, we continued our investigations by implementing this strategy to achieve genetic ablation of the *gjd2* gene. Multiple Cas9:gRNA ratios were tested, and the final optimization protocol accounted for both efficiency and larvae survivability. Our results suggested that an RNP complex assembled at a 1:2 ratio was sufficient at producing indel mutations with a targeting efficiency of 25%; this was consistent with previous reports with efficiencies yielding up to 50% as determined by the SURVEYOR assay (Mali *et al.*, 2013; Ran *et al.*, 2013). Increasing the ratio of gRNA delivered led to cell toxicity and promoted premature death, thus reducing larvae survivability to 3% 24hrs post-injection (data not shown). While both TALENS and CRISPR-Cas9 can be programmed to target and cleave specific DNA sequences, it is important to acknowledge that the CRISPR-Cas9 system is more susceptible to off-target

effects. Whole exome sequencing can be used to expose such off-target effects; however, this strategy is costly. To overcome this limitation and to eliminate potential off-target effects, our research protocol employed two rounds of outbreeding to wild-type zebrafish before heterozygous fish were inbred to successfully achieve the homozygous knockout.

4.3 Conclusions & Future Directions

Following the research conducted in this dissertation, we've opened new avenues of Cx35b-focused investigations and beyond. Firstly, the relationship between Cx36/Cx35b, pituitary gland functionality, and GH secretion has seldomly been explored. We provided evidence of accelerated growth trajectories, which may be directly linked to the dysregulation of the cross-talk between the nervous and endocrine systems. Moreover, this result, in combination with a reduction in anxiety-like behavior seen with bath application of Buspirone, led us to question whether the loss of Cx35b expression causes pre-mature aging. Zebrafish aging can be better assessed through behavioral phenotypes, such as cognitive decline and neurobiological changes (measured as changes in gene expression, DNA methylation, proteostasis, telomere attrition, and synaptic regulation) in the brain. While we demonstrated that learning and memory were unaffected in habituation paradigms, our research investigations have not yet addressed associative learning paradigms. As such, cognitive decline should still be addressed in future studies. We strongly believe that premature aging versus early maturation processes in a Cx35b$^{-/-}$ model should be an avenue worth exploring in future investigations.

As a second consideration, Cx35b expression in PRC subtypes should be further elucidated. We proposed that Cx35b is localized to cone photoreceptor cells and fine-tunes photoreceptor coupling. As such, additional studies focused on detailing the localization of Cx35b in PRCs would be beneficial in validating this proposal. Alternatively, we recognize that Cx35b could be expressed in both cone and rod PRCs, however, predict that they are predominantly expressed in cone PRCs. This would account for the discrepancy in Cx35b localization previously reported at cone pedicles and rod spherules (Li, Chuang and O'Brien, 2009), though the antibody specificity in this report remains in question. Since our results also led us to conclude that loss of the *gjd2b* gene causes an increase in gap junctional coupling in the visual system, likely mediated through a dopaminergic-dependent pathway acting on Cx35a and Cx34.7, follow-up studies should also investigate dye transfer between retinal photoreceptor cells as a measure of coupling in Cx35b$^{-/-}$ zebrafish. Whether or not coupling is mediated through Cx35a and Cx34.7 explicitly would conclude this study. Although Cx35b has been described throughout the CNS, current literature has seldomly explored the localization or the functional consequences of the remaining isoforms. It is reasonable to suspect that the evolutionary divergence of the *GJD2* gene has led to the unique morphological and physiological

properties of each Cx36 ortholog. Considering that Cx35a and Cx34.7 are both expressed in the visual system, exploring their contributions to visual functionality will help further our understanding of the functional significance of electrical asymmetry to visual integrity.

Though we did not find a Cx35b-dependent effect on dark- or light-flash habituation, how the integrity of the visual system affects the capacity for learning and memory remains a worthy area of exploration. We anticipate that Cx35a and Cx34.7 expression, and subsequent coupling, may be involved in this signaling pathway. Moreover, both orthologs are still candidates to study the interplay of anxiety and memory. Taken together, the zebrafish animal model could serve as an ideal model organism to better elucidate the multiple cellular and functional roles of mammalian Cx36.

5 REFERENCES

aan het Rot, M., Mathew, S. J. and Charney, D. S. (2009) 'Neurobiological mechanisms in major depressive disorder', *CMAJ*, 180(3), pp. 305–313. doi: 10.1503/cmaj.080697.

Abascal, F. and Zardoya, R. (2012) 'Evolutionary analyses of gap junction protein families', *Biochimica et Biophysica Acta (BBA) - Biomembranes*. Elsevier B.V., 1828(1), pp. 4–14. doi: 10.1016/j.bbamem.2012.02.007.

Ahmad, S. *et al.* (1999) 'Synthesis and assembly of connexins in vitro into homomeric and heteromeric functional gap junction hemichannels.', *The Biochemical journal*, 339 (Pt 2, pp. 247–253. doi: 10.1042/0264-6021:3390247.

Alam, G. and Richardson, J. R. (2020) 'Regulation of tyrosine hydroxylase: relevance to Parkinson's disease', in *Genetics, Neurology, Behavior, and Diet in Parkinson's Disease*. Elsevier, pp. 51–66. doi: 10.1016/B978-0-12-815950-7.00004-7.

Alev, C. *et al.* (2008) 'The neuronal connexin36 interacts with and is phosphorylated by CaMKII in a way similar to CaMKII interaction with glutamate receptors.', *Proceedings of the National Academy of Sciences of the United States of America*, 105(52), pp. 20964–9. doi: 10.1073/pnas.0805408105.

Alev, C., Zoidl, G. and Dermietzel, R. (2013) 'The Cytoskeleton'. Edited by R. Dermietzel. Totowa, NJ: Humana Press (Neuromethods), 79, pp. 135–149. doi: 10.1007/978-1-62703-266-7.

Allen, K. *et al.* (2011) 'Gap junctions between interneurons are required for normal spatial coding in the hippocampus and short-term spatial memory.', *The Journal of neuroscience : the official journal of the Society for Neuroscience*, 31(17), pp. 6542–52. doi: 10.1523/JNEUROSCI.6512-10.2011.

Anderson, J. R. *et al.* (2011) 'Exploring the retinal connectome.', *Molecular vision*, 17, pp. 355–79. Available at: http://www.ncbi.nlm.nih.gov/pubmed/21311605.

Anderson, M. E. *et al.* (1998) 'KN-93, an inhibitor of multifunctional Ca++/calmodulin-dependent protein kinase, decreases early afterdepolarizations in rabbit heart.', *The Journal of pharmacology and experimental therapeutics*, 287(3), pp. 996–1006. Available at: http://www.ncbi.nlm.nih.gov/pubmed/9864285.

Andersson, M. Å., Ek, F. and Olsson, R. (2015) 'Using visual lateralization to model learning and memory in zebrafish larvae', *Scientific Reports*, 5, p. 8667. doi: 10.1038/srep08667.

Ansorge, M. S., Morelli, E. and Gingrich, J. A. (2008) 'Inhibition of serotonin but not norepinephrine transport during development produces delayed, persistent perturbations of emotional behaviors in mice', *J Neurosci.*, 28(1), pp. 199–207. doi: 10.1523/JNEUROSCI.3973-07.2008.

Anumonwo, J. M. *et al.* (2001) 'The carboxyl terminal domain regulates the unitary conductance and voltage dependence of connexin40 gap junction channels.', *Circulation research*, 88(7), pp. 666–673. doi: 10.1161/hh0701.088833.

Arpino, J. A. J. *et al.* (2014) 'Random Single Amino Acid Deletion Sampling Unveils Structural Tolerance and the Benefits of Helical Registry Shift on GFP Folding and Structure', *Structure*, 22(6), pp. 889–898. doi: 10.1016/j.str.2014.03.014.

Arumugam, H. *et al.* (2005) 'NMDA receptors regulate developmental gap junction uncoupling via CREB signaling', *Nature Neuroscience*, 8(12), pp. 1720–1726. doi: 10.1038/nn1588.

Aseervatham, J. *et al.* (2020) 'Calmodulin Binding to Connexin 35: Specializations to Function as an Electrical Synapse', *International Journal of Molecular Sciences*, 21(17), p. 6346. doi: 10.3390/ijms21176346.

Asghari, V. *et al.* (2002) 'Modulation of Intracellular Cyclic AMP Levels by Different Human Dopamine D4 Receptor Variants', *Journal of Neurochemistry*, 65(3), pp. 1157–1165. doi: 10.1046/j.1471-4159.1995.65031157.x.

Avdesh, A. *et al.* (2012) 'Evaluation of Color Preference in Zebrafish for Learning and Memory', *Journal of Alzheimer's Disease*, 28(2), pp. 459–469. doi: 10.3233/JAD-2011-110704.

Avila, R. L. *et al.* (2007) 'Myelin structure and composition in zebrafish', *Neurochemical Research*, 32(2), pp. 197–209. doi: 10.1007/s11064-006-9136-5.

Bär, J. *et al.* (2016) 'Periodic F-actin structures shape the neck of dendritic spines.', *Scientific reports*, 6, p. 37136.

doi: 10.1038/srep37136.

Baranova, A. *et al.* (2004) 'The mammalian pannexin family is homologous to the invertebrate innexin gap junction proteins', *Genomics*, 83(4), pp. 706–716. doi: 10.1016/j.ygeno.2003.09.025.

Basnet, R. *et al.* (2019) 'Zebrafish Larvae as a Behavioral Model in Neuropharmacology', *Biomedicines*, 7(1), p. 23. doi: 10.3390/biomedicines7010023.

Bautisa, W. and Nagy, J. (2014) 'Connexin36 in gap junctions forming electrical synapses between motoneurons in sexually dimorphic motor nuclei in spinal cord of rat and mouse.', *European Journal of Neuroscience*, 39(5), pp. 771–87.

Baux, G. *et al.* (1978) 'Uncoupling of electrotonic synapses by calcium.', *Proceedings of the National Academy of Sciences of the United States of America*, 75(9), pp. 4577–4581. doi: 10.1073/pnas.75.9.4577.

Bazzigaluppi, P. *et al.* (2017) 'Modulation of Murine Olivary Connexin 36 Gap Junctions by PKA and CaMKII', *Frontiers in Cellular Neuroscience*, 11. doi: 10.3389/fncel.2017.00397.

Belluardo, N. *et al.* (2000) 'Expression of Connexin36 in the adult and developing rat brain', *Brain Research*, 865(1), pp. 121–138. doi: 10.1016/S0006-8993(00)02300-3.

Belousov, A. B. and Fontes, J. D. (2013) 'Neuronal gap junctions: making and breaking connections during development and injury.', *Trends in neurosciences*. Elsevier Ltd, 36(4), pp. 227–36. doi: 10.1016/j.tins.2012.11.001.

Bennett, M. (1977) 'Electrical transmission:a functional analysis and comparison with chemical transmission', in *Cellular Biology of Neurons, Handbook of Physiology, The Nervous System 1*, pp. 357–416.

Bennett, M. V. L. and Zukin, R. S. (2004) 'Electrical Coupling and Neuronal Synchronization in the Mammalian Brain', *Neuron*, 41(4), pp. 495–511. doi: 10.1016/S0896-6273(04)00043-1.

Berkowitz, S. A. and Wolff, J. (1981) 'Intrinsic calcium sensitivity of tubulin polymerization. The contributions of temperature, tubulin concentration, and associated proteins.', *Journal of Biological Chemistry*, 256(21), pp. 11216–11223. doi: 10.1016/S0021-9258(19)68580-7.

Bernardos, R. L. and Raymond, P. A. (2006) 'GFAP transgenic zebrafish', *Gene Expression Patterns*, 6(8), pp. 1007–1013. doi: 10.1016/j.modgep.2006.04.006.

Berry, M. H. *et al.* (2019) 'Restoration of high-sensitivity and adapting vision with a cone opsin', *Nature Communications*, 10(1), p. 1221. doi: 10.1038/s41467-019-09124-x.

Beyer, E. C. *et al.* (1989) 'Antisera directed against connexin43 peptides react with a 43-kD protein localized to gap junctions in myocardium and other tissues.', *Journal of Cell Biology*, 108(2), pp. 595–605. doi: 10.1083/jcb.108.2.595.

Beyer, E. C. *et al.* (2012) 'Structural organization of intercellular channels II. Amino terminal domain of the connexins: Sequence, functional roles, and structure', *Biochimica et Biophysica Acta - Biomembranes*, pp. 1823–1830. doi: 10.1016/j.bbamem.2011.10.011.

Bhalla-Gehi, R. *et al.* (2010) 'Pannexin1 and pannexin3 delivery, cell surface dynamics, and cytoskeletal interactions', *J. Biol. Chem*, 285, pp. 9147–9160.

Bi, A. . *et al.* (2010) 'Region-specific involvement of actin rearrangement-related synaptic structure alterations in conditioned taste aversion memory', *Learn. Mem.*, 17, pp. 420–27.

Bibliowicz, J., Tittle, R. K. and Gross, J. M. (2011) 'Toward a Better Understanding of Human Eye Disease', in, pp. 287–330. doi: 10.1016/B978-0-12-384878-9.00007-8.

Blankenship, A. G. *et al.* (2011) 'The Role of Neuronal Connexins 36 and 45 in Shaping Spontaneous Firing Patterns in the Developing Retina', *Journal of Neuroscience*, 31(27), pp. 9998–10008. doi: 10.1523/JNEUROSCI.5640-10.2011.

Blaser, R. E., Chadwick, L. and McGinnis, G. C. (2010) 'Behavioral measures of anxiety in zebrafish (Danio rerio)', *Behavioural Brain Research*, 208(1), pp. 56–62. doi: 10.1016/j.bbr.2009.11.009.

Bloch, Y. *et al.* (2017) 'Methylphenidate Reduces State Anxiety During a Continuous Performance Test That Distinguishes Adult ADHD Patients From Controls', *Journal of Attention Disorders*, 21(1), pp. 46–51. doi: 10.1177/1087054712474949.

Boehmler, W. *et al.* (2004) 'Evolution and expression of D2 and D3 dopamine receptor genes in zebrafish',

Developmental Dynamics, 230(3), pp. 481–493. doi: 10.1002/dvdy.20075.

Bonvicini, C. *et al.* (2020) 'DRD4 48 bp multiallelic variants as age-population-specific biomarkers in attention-deficit/hyperactivity disorder', *Translational Psychiatry*, 10(1), p. 70. doi: 10.1038/s41398-020-0755-4.

Bouffard, R. *et al.* (2003) 'The Efficacy of 2 Different Dosages of Methylphenidate in Treating Adults with Attention-Deficit Hyperactivity Disorder', *The Canadian Journal of Psychiatry*, 48(8), pp. 546–554. doi: 10.1177/070674370304800806.

Brocke, L. *et al.* (1999) 'Functional Implications of the Subunit Composition of Neuronal CaM Kinase II', *Journal of Biological Chemistry*, 274(32), pp. 22713–22722. doi: 10.1074/jbc.274.32.22713.

Brown, C. A. *et al.* (2019) 'Tubulin-Dependent Transport of Connexin-36 Potentiates the Size and Strength of Electrical Synapses', *Cells*, 8(10), p. 1146. doi: 10.3390/cells8101146.

Bruzzone, R., White, T. W. and Paul, D. L. (1996) 'Connections with connexins: the molecular basis of direct intercellular signaling.', *European journal of biochemistry / FEBS*, 238(1), pp. 1–27. doi: 10.1007/978-3-642-60659-5.

Buchanan, J. T. and Grillner, S. (1987) 'Newly identified "glutamate interneurons" and their role in locomotion in the lamprey spinal cord.', *Science (New York, N.Y.)*, 236(4799), pp. 312–4. Available at: http://www.ncbi.nlm.nih.gov/pubmed/3563512.

Budick, S. A. and O'Malley, D. M. (2000) 'Locomotor repertoire of the larval zebrafish: swimming, turning and prey capture.', *The Journal of experimental biology*, 203(Pt 17), pp. 2565–79. Available at: http://www.ncbi.nlm.nih.gov/pubmed/10934000.

Bukauskas, F. F. *et al.* (2000) 'Clustering of connexin 43-enhanced green fluorescent protein gap junction channels and functional coupling in living cells.', *Proceedings of the National Academy of Sciences of the United States of America*, 97(6), pp. 2556–61. doi: 10.1073/pnas.050588497.

Burr, G. S. *et al.* (2005a) 'Calcium-dependent binding of calmodulin to neuronal gap junction proteins', *Biochemical and Biophysical Research Communications*, 335(4), pp. 1191–1198. doi: 10.1016/j.bbrc.2005.08.007.

Burr, G. S. *et al.* (2005b) 'Calcium-dependent binding of calmodulin to neuronal gap junction proteins', *Biochemical and Biophysical Research Communications*, 335(4), pp. 1191–1198. doi: 10.1016/j.bbrc.2005.08.007.

Buss, R. R. and Drapeau, P. (2001) 'Synaptic drive to motoneurons during fictive swimming in the developing zebrafish.', *Journal of neurophysiology*, 86(1), pp. 197–210. doi: 10.1152/jn.2001.86.1.197.

Butkevich, E. *et al.* (2004) 'Drebrin is a novel connexin-43 binding partner that links gap junctions to the submembrane cytoskeleton', *Curr. Biol.*, 14, pp. 650–658.

Buzsaki, G. *et al.* (1992) 'High-frequency network oscillation in the hippocampus', *Science*, 256, pp. 1025–1027.

Cahill, G. M. (2002) 'Clock mechanisms in zebrafish', *Cell and Tissue Research*, pp. 27–34. doi: 10.1007/s00441-002-0570-7.

Calhoun, J. R. *et al.* (2005) 'Artificial diiron proteins: From structure to function', *Biopolymers - Peptide Science Section*, pp. 264–278. doi: 10.1002/bip.20230.

Calkins, D. J. and Sterling, P. (1999) 'Evidence that Circuits for Spatial and Color Vision Segregate at the First Retinal Synapse', *Neuron*, 24(2), pp. 313–321. doi: 10.1016/S0896-6273(00)80846-6.

Callier, S. *et al.* (2003) 'Evolution and cell biology of dopamine receptors in vertebrates', *Biology of the Cell*, 95(7), pp. 489–502. doi: 10.1016/S0248-4900(03)00089-3.

Cao, F. *et al.* (1998) 'A quantitative analysis of connexin-specific permeability differences of gap junctions expressed in HeLa transfectants and Xenopus oocytes.', *Journal of cell science*, 111 (Pt 1, pp. 31–43.

Cape, E. . *et al.* (2000) 'Neurotensin-induced bursting of cholinergic basal forebrain tions induced in the rat CA3 region by carbachol in vitro. Eur. J. neurons promotes gamma and theta cortical activity together with Neurosci. 12, 4093–4106. waking and paradoxical sleep.', *Journal of Neuroscience*, 20, pp. 8452–8461.

Cario, C. L. *et al.* (2011) 'Automated measurement of zebrafish larval movement', *The Journal of Physiology*, 589(15), pp. 3703–3708. doi: 10.1113/jphysiol.2011.207308.

Carter-Dawson, L. D. and Lavail, M. M. (1979) 'Rods and cones in the mouse retina. I. Structural analysis using light

and electron microscopy', *The Journal of Comparative Neurology*, 188(2), pp. 245–262. doi: 10.1002/cne.901880204.

Cartocci, V. *et al.* (2018) 'Altered Brain Cholesterol/Isoprenoid Metabolism in a Rat Model of Autism Spectrum Disorders', *Neuroscience*, 372, pp. 27–37. doi: 10.1016/j.neuroscience.2017.12.053.

Caspi, A. *et al.* (2003) 'Influence of life stress on depression: moderation by a polymorphism in the 5-HTT gene', *Science*, 301(5631), pp. 386–9. doi: 10.1126/science.1083968.

de Castro, M. R. *et al.* (2009) 'Behavioral and neurotoxic effects of arsenic exposure in zebrafish (Danio rerio, Teleostei: Cyprinidae)', *Comparative Biochemistry and Physiology Part C: Toxicology & Pharmacology*, 150(3), pp. 337–342. doi: 10.1016/j.cbpc.2009.05.017.

Chao, L. H. *et al.* (2010) 'Intersubunit capture of regulatory segments is a component of cooperative CaMKII activation', *Nature Structural & Molecular Biology*, 17(3), pp. 264–272. doi: 10.1038/nsmb.1751.

Chinen, A. *et al.* (2003) 'Gene Duplication and Spectral Diversification of Cone Visual Pigments of Zebrafish', *Genetics*, 163(2), pp. 663–675. doi: 10.1093/genetics/163.2.663.

Chong, M. and Drapeau, P. (2007) 'Interaction between hindbrain and spinal networks during the development of locomotion in zebrafish', *Developmental Neurobiology*, 67(7), pp. 933–947. doi: 10.1002/dneu.20398.

Coles, C. H. and Bradke, F. (2015) 'Coordinating neuronal actin-microtubule dynamics.', *Current biology : CB*, 25(15), pp. R677-91. doi: 10.1016/j.cub.2015.06.020.

Collingridge, G., Isaac, J. and Wang, Y. (2004) 'Receptor trafficking and synaptic plasticity', *Nature reviews. Neuroscience*, 5, pp. 952–962.

Condorelli, D. F. *et al.* (1998) 'Cloning of a new gap junction gene (Cx36) highly expressed in mammalian brain neurons', *Journal of Neuroscience*, 10(3), pp. 1202–1208.

Condorelli, D. F. *et al.* (2000) 'Expression of Cx36 in mammalian neurons.', *Brain research. Brain research reviews*, 32(1), pp. 72–85. Available at: http://www.ncbi.nlm.nih.gov/pubmed/10751658.

Connors, B., Benardo, L. and Prince, D. (1983) 'Coupling between neurons of the developing rat neocortex', *The Journal of Neuroscience*, 3(4), pp. 773–782. doi: 10.1523/JNEUROSCI.03-04-00773.1983.

Cook, S. J. *et al.* (2019) 'Whole-animal connectomes of both Caenorhabditis elegans sexes', *Nature*, 571(7763), pp. 63–71. doi: 10.1038/s41586-019-1352-7.

del Corsso, C. *et al.* (2006) 'Transfection of mammalian cells with connexins and measurement of voltage sensitivity of their gap junctions.', *Nature protocols*, 1(4), pp. 1799–809. doi: 10.1038/nprot.2006.266.

Del Corsso, C. *et al.* (2012) 'Calmodulin dependent protein kinase increases conductance at gap junctions formed by the neuronal gap junction protein connexin36.', *Brain research*. Elsevier, 1487, pp. 69–77. doi: 10.1016/j.brainres.2012.06.058.

Coulon, P. and Landisman, C. E. (2017) 'The Potential Role of Gap Junctional Plasticity in the Regulation of State', *Neuron*, 93(6), pp. 1275–1295. doi: 10.1016/j.neuron.2017.02.041.

Csicsvari, J. *et al.* (1999) 'Fast network oscillations in the hippocampal CA1 region of Buhl, E.H. (2001). Differential expression of synaptic and nonsynapthe behaving rat', *Journal of Neuroscience*, 19, p. RC20.

Cullinan, W. E. *et al.* (1995) 'Pattern and time course of immediate early gene expression in rat brain following acute stress', *Neuroscience*, 64(2), pp. 477–505. doi: 10.1016/0306-4522(94)00355-9.

Curti, S. *et al.* (2012) 'Synergy between Electrical Coupling and Membrane Properties Promotes Strong Synchronization of Neurons of the Mesencephalic Trigeminal Nucleus', *Journal of Neuroscience*, 32(13), pp. 4341–4359. doi: 10.1523/JNEUROSCI.6216-11.2012.

Deans, M. R. *et al.* (2001) 'Synchronous Activity of Inhibitory Networks in Neocortex Requires Electrical Synapses Containing Connexin36', *Neuron*, 31, pp. 477–485.

Deans, M. R. *et al.* (2002) 'Connexin36 Is Essential for Transmission of Rod-Mediated Visual Signals in the Mammalian Retina', 36(4), pp. 703–712.

Deliagina, T. G., Zelenin, P. V and Orlovsky, G. N. (2002) 'Encoding and decoding of reticulospinal commands.', *Brain research. Brain research reviews*, 40(1–3), pp. 166–77. Available at: http://www.ncbi.nlm.nih.gov/pubmed/12589915.

Derkach, V. *et al.* (2007) 'Regulatory mechanisms of AMPA receptors in synaptic plasticity', *Nature reviews. Neuroscience*, 8, pp. 101–113.

Dermietzel, R. and Spray, D. C. (1993) 'Gap junctions in the brain: where, what type, how many and why?', *Trends in neurosciences*, 16(5), pp. 186–192. doi: 10.1016/0166-2236(93)90151-B.

Diez, J. A., Ahmad, S. and Evans, W. H. (1999) 'Assembly of heteromeric connexons in guinea-pig liver en route to the Golgi apparatus, plasma membrane and gap junctions', *European Journal of Biochemistry*, 262(1), pp. 142–148. doi: 10.1046/j.1432-1327.1999.00343.x.

Dillon, C. and Goda, Y. (2005) 'The actin cytoskeleton: integrating form and function at the synapse.', *Annual review of neuroscience*, 28, pp. 25–55. doi: 10.1146/annurev.neuro.28.061604.135757.

Dodd, R. *et al.* (2008) 'Calmodulin Association with Connexin32-derived Peptides Suggests trans -Domain Interaction in Chemical Gating of Gap Junction Channels', *Journal of Biological Chemistry*, 283(40), pp. 26911–26920. doi: 10.1074/jbc.M801434200.

Durant, C., Christmas, D. and Nutt, D. (2010) 'The pharmacology of anxiety', *Curr Top Behav Neurosci.*, 2, pp. 303–330. doi: 10.1007/7854_2009_8.

Eastman, S. D. *et al.* (2006) 'Phylogenetic analysis of three complete gap junction gene families reveals lineage-specific duplications and highly supported gene classes.', *Genomics*, 87(2), pp. 265–74. doi: 10.1016/j.ygeno.2005.10.005.

Eaton, R. C. *et al.* (1977) 'Functional development in the mauthner cell system of embryos and larvae of the zebra fish', *Journal of Neurobiology*, 8(2), pp. 151–172. doi: 10.1002/neu.480080207.

Eaton, R. C., DiDomenico, R. and Nissanov, J. (1991) 'Role of the Mauthner Cell in Sensorimotor Integration by the Brain Stem Escape Network', *Brain, Behavior and Evolution*, 37(5), pp. 272–285. doi: 10.1159/000114365.

Eaton, R. C., Lavender, W. A. and Wieland, C. M. (1981) 'Identification of Mauthner-initiated response patterns in goldfish: Evidence from simultaneous cinematography and electrophysiology', *Journal of Comparative Physiology ? A*, 144(4), pp. 521–531. doi: 10.1007/BF01326837.

Eaton, R. C., Lee, R. K. K. and Foreman, M. B. (2001) 'The Mauthner cell and other identified neurons of the brainstem escape network of fish', *Progress in Neurobiology*, 63(4), pp. 467–485. doi: 10.1016/S0301-0082(00)00047-2.

Eaton, R. C., Nissanov, J. and Wieland, C. M. (1984) 'Differential activation of Mauthner and non-Mauthner startle circuits in the zebrafish: Implications for functional substitution', *Journal of Comparative Physiology A*, 155(6), pp. 813–820. doi: 10.1007/BF00611598.

Elias, L. A. B. *et al.* (2010) 'Connexin 43 Mediates the Tangential to Radial Migratory Switch in Ventrally Derived Cortical Interneurons', *Journal of Neuroscience*, 30(20), pp. 7072–7077. doi: 10.1523/JNEUROSCI.5728-09.2010.

Ellis, L. D., Seibert, J. and Soanes, K. H. (2012) 'Distinct models of induced hyperactivity in zebrafish larvae', *Brain Research*, 1449, pp. 46–59. doi: 10.1016/j.brainres.2012.02.022.

Emran, F., Rihel, J. and Dowling, J. E. (2008) 'A Behavioral Assay to Measure Responsiveness of Zebrafish to Changes in Light Intensities', *Journal of Visualized Experiments*, (20). doi: 10.3791/923.

Endo, M. (2006) 'Calcium Ion as a Second Messenger With Special Reference to Excitation-Contraction Coupling', *Journal of Pharmacological Sciences*, 100(5), pp. 519–524. doi: 10.1254/jphs.CPJ06004X.

Epifantseva, I. and Shaw, R. M. (2018) 'Intracellular trafficking pathways of Cx43 gap junction channels.', *Biochimica et biophysica acta*, 1860(1), pp. 40–47. doi: 10.1016/j.bbamem.2017.05.018.

Essenfelder, G. M. *et al.* (2004) 'Connexin30 mutations responsible for hidrotic ectodermal dysplasia cause abnormal hemichannel activity', *Human Molecular Genetics*, 13(16), pp. 1703–1714. doi: 10.1093/hmg/ddh191.

Faber, D. S., Fetcho, J. R. and Korn, H. (1989) 'Neuronal networks underlying the escape response in goldfish. General implications for motor control.', *Annals of the New York Academy of Sciences*, 563, pp. 11–33. Available at: http://www.ncbi.nlm.nih.gov/pubmed/2672948.

Fadool, J. M. (2003) 'Rod genesis in the teleost retina as a model of neural stem cells', *Experimental Neurology*, 184(1), pp. 14–19. doi: 10.1016/S0014-4886(03)00309-1.

Falk, M. M. *et al.* (1997) 'Cell-free synthesis and assembly of connexins into functional gap junction membrane channels', *EMBO Journal*, 16(10), pp. 2703–2716. doi: 10.1093/emboj/16.10.2703.

Fan, E. *et al.* (2021) 'Acute exposure to N-Ethylpentylone induces developmental toxicity and dopaminergic receptor-regulated aberrances in zebrafish larvae', *Toxicology and Applied Pharmacology*, 417, p. 115477. doi: 10.1016/j.taap.2021.115477.

Faraone, S. V., Bonvicini, C. and Scassellati, C. (2014) 'Biomarkers in the Diagnosis of ADHD – Promising Directions', *Current Psychiatry Reports*, 16(11), p. 497. doi: 10.1007/s11920-014-0497-1.

Faught, E. and Vijayan, M. M. (2022) 'Coordinated Action of Corticotropin-Releasing Hormone and Cortisol Shapes the Acute Stress-Induced Behavioural Response in Zebrafish', *Neuroendocrinology*, 112(1), pp. 74–87. doi: 10.1159/000514778.

Feigenspan, A. *et al.* (2004) 'Expression of connexin36 in cone pedicles and OFF-cone bipolar cells of the mouse retina.', *The Journal of neuroscience : the official journal of the Society for Neuroscience*, 24(13), pp. 3325–34. doi: 10.1523/JNEUROSCI.5598-03.2004.

Fischbach, G. D. (1972) 'Synapse formation between dissociated nerve and muscle cells in low density cell cultures', *Developmental Biology*, 28(2), pp. 407–429. doi: 10.1016/0012-1606(72)90023-1.

Fischer, A. *et al.* (2004) 'Distinct roles of hippocampal de novo protein synthesis and actin rearrangement in extinction of contextual fear', *Journal of Neuroscience*, 24, pp. 1962–1966.

Fletcher, D. A. and Mullins, R. D. (2010) 'Cell mechanics and the cytoskeleton', *NIH*, 463(7280), pp. 485–492. doi: 10.1038/nature08908.Cell.

Flores, C. E. *et al.* (2012) 'Trafficking of gap junction channels at a vertebrate electrical synapse in vivo', *Proceedings of the National Academy of Sciences*, pp. E573–E582. doi: 10.1073/pnas.1121557109.

Fontaine, E. *et al.* (2008) 'Automated visual tracking for studying the ontogeny of zebrafish swimming', *Journal of Experimental Biology*, 211(8), pp. 1305–1316. doi: 10.1242/jeb.010272.

Frisch, C. *et al.* (2005) 'Stimulus complexity dependent memory impairment and changes in motor performance after deletion of the neuronal gap junction protein connexin36 in mice.', *Behavioural brain research*, 157(1), pp. 177–85. doi: 10.1016/j.bbr.2004.06.023.

Fukunaga, K. *et al.* (1993) 'Long-term potentiation is associated with an increased activity of Ca2+/calmodulin-dependent protein kinase', *Biol Chem*, 268, pp. 7863–7867.

Furshpan, E. J. and Potter, D. D. (1959) 'Transmission at the giant motor synapses of the crayfish', *The Journal of Physiology*, 145(2), pp. 289–325. doi: 10.1113/jphysiol.1959.sp006143.

Gabriel, A. (2010) 'The mixed amphetamine salt extended release (Adderall XR, Max-XR) as an adjunctive to SSRIS or SNRIS in the treatment of adult ADHD patients with comorbid partially responsive generalized anxiety: an open-label study', *ADHD Attention Deficit and Hyperactivity Disorders*, 2(2), pp. 87–92. doi: 10.1007/s12402-010-0025-z.

Gabriel, A. and Violato, C. (2011) 'Adjunctive atomoxetine to SSRIs or SNRIs in the treatment of adult ADHD patients with comorbid partially responsive generalized anxiety (GA): an open-label study', *ADHD Attention Deficit and Hyperactivity Disorders*, 3(4), pp. 319–326. doi: 10.1007/s12402-011-0063-1.

Gaikwad, S. *et al.* (2011) 'Acute stress disrupts performance of zebrafish in the cued and spatial memory tests: The utility of fish models to study stress–memory interplay', *Behavioural Processes*, 87(2), pp. 224–230. doi: 10.1016/j.beproc.2011.04.004.

Galarreta, M. and Hestrin, S. (2001) 'Spike Transmission and Synchrony Detection in Networks of GABAergic Interneurons', *Science*, 292(5525), pp. 2295–2299. doi: 10.1126/science.1061395.

Ganasen, K. A. and Stein, D. J. (2010) 'Pharmacotherapy of social anxiety disorder', *Curr Top Behav Neurosci.*, 2, pp. 487–503. doi: 10.1007/7854_2009_1.

Ganzen, L. *et al.* (2021) 'Drug screening with zebrafish visual behavior identifies carvedilol as a potential treatment for an autosomal dominant form of retinitis pigmentosa', *Scientific Reports*, 11(1), p. 11432. doi: 10.1038/s41598-021-89482-z.

Gartside, S. E., V. Umbers, M. H. and Sharp, T. (1995) 'Interaction between a selective 5-HT1A receptor antagonist

and an SSRI in vivo: effects on 5-HT cell firing and extracellular 5-HT.', *Br J Pharmacol.*, 115(6), pp. 1064–1070. doi: 10.1111/j.1476-5381.1995.tb15919.x.

Gendron, T. F. and Petrucelli, L. (2009) 'The role of tau in neurodegeneration.', *Molecular neurodegeneration*, 4, p. 13. doi: 10.1186/1750-1326-4-13.

Getting, P. A. (1974) 'Modification of neuron properties by electrotonic synapses. I. Input resistance, time constant, and integration.', *Journal of Neurophysiology*, 37(5), pp. 846–857. doi: 10.1152/jn.1974.37.5.846.

Getting, P. A. and Willows, A. O. (1974) 'Modification of neuron properties by electrotonic synapses. II. Burst formation by electrotonic synapses.', *Journal of Neurophysiology*, 37(5), pp. 858–868. doi: 10.1152/jn.1974.37.5.858.

Giepmans, B. N. *et al.* (2001) 'Gap junction protein connexin-43 interacts directly with microtubules.', *Current biology : CB*, 11(17), pp. 1364–8. Available at: http://www.ncbi.nlm.nih.gov/pubmed/11553331.

Giepmans, B. N., Verlaan, I. and Moolenaar, W. H. (2001) 'Connexin-43 interactions with ZO-1 and alpha- and beta-tubulin', *Cell communication & adhesion*, 8, pp. 219–223.

Gigant, B. *et al.* (2005) 'Structural basis for the regulation of tubulin by vinblastine.', *Nature*, 435(7041), pp. 519–22. doi: 10.1038/nature03566.

Ginty, D. D. *et al.* (1993) 'Regulation of CREB Phosphorylation in the Suprachiasmatic Nucleus by Light and a Circadian Clock', *Science*, 260(5105), pp. 238–241. doi: 10.1126/science.8097062.

Gollisch, T. and Meister, M. (2010) 'Eye Smarter than Scientists Believed: Neural Computations in Circuits of the Retina', *Neuron*, 65(2), pp. 150–164. doi: 10.1016/j.neuron.2009.12.009.

González-Nieto, D. *et al.* (2008) 'Regulation of neuronal connexin-36 channels by pH.', *Proceedings of the National Academy of Sciences of the United States of America*, 105(44), pp. 17169–17174. doi: 10.1073/pnas.0804189105.

González, D., Gómez-Hernández, J. M. and Barrio, L. C. (2007) 'Molecular basis of voltage dependence of connexin channels: An integrative appraisal', *Progress in Biophysics and Molecular Biology*, pp. 66–106. doi: 10.1016/j.pbiomolbio.2007.03.007.

Goodenough, D. a. (1974) 'Bulk isolation of mouse hepatocyte gap junctions. Characterization of the principal protein, connexin', *Journal of Cell Biology*, 61(2), pp. 557–563. doi: 10.1083/jcb.61.2.557.

Gourdie, R. G. *et al.* (1993) 'The spatial distribution and relative abundance of gap-junctional connexin40 and connexin43 correlate to functional properties of components of the cardiac atrioventricular conduction system', *Journal of Cell Science*, 105(4), pp. 985–991. doi: 10.1242/jcs.105.4.985.

Graciarena, M. *et al.* (2019) 'Hypomyelination and Oligodendroglial Alterations in a Mouse Model of Autism Spectrum Disorder', *Frontiers in Cellular Neuroscience*, 12. doi: 10.3389/fncel.2018.00517.

Grillner, S., Robertson, B. and Stephenson-Jones, M. (2013) 'The evolutionary origin of the vertebrate basal ganglia and its role in action selection', *The Journal of Physiology*, 591(22), pp. 5425–5431. doi: 10.1113/jphysiol.2012.246660.

Gu, J., Firestein, B. L. and Zheng, J. Q. (2008) 'Microtubules in dendritic spine development.', *The Journal of Neuroscience*, 28(46), pp. 12120–4. doi: 10.1523/JNEUROSCI.2509-08.2008.

Guha, S. *et al.* (2012) 'Stimulation of the D5 dopamine receptor acidifies the lysosomal pH of retinal pigmented epithelial cells and decreases accumulation of autofluorescent photoreceptor debris', *Journal of Neurochemistry*, 122(4), pp. 823–833. doi: 10.1111/j.1471-4159.2012.07804.x.

Güldenagel, M. *et al.* (2001) 'Visual transmission deficits in mice with targeted disruption of the gap junction gene connexin36.', *The Journal of neuroscience : the official journal of the Society for Neuroscience*, 21(16), pp. 6036–44. Available at: http://www.ncbi.nlm.nih.gov/pubmed/11487627.

Guo, S. (2004) 'Linking genes to brain, behavior and neurological diseases: What can we learn from zebrafish?', *Genes, Brain and Behavior*, pp. 63–74. doi: 10.1046/j.1601-183X.2003.00053.x.

Haas, J. S., Greenwald, C. M. and Pereda, A. E. (2016) 'Activity-dependent plasticity of electrical synapses: increasing evidence for its presence and functional roles in the mammalian brain', *BMC Cell Biology*, 17(S1), p. 14. doi: 10.1186/s12860-016-0090-z.

Haehnel, M., Taguchi, M. and Liao, J. C. (2012) 'Heterogeneity and dynamics of lateral line afferent innervation

during development in zebrafish (Danio rerio)', *The Journal of Comparative Neurology*, 520(7), pp. 1376–1386. doi: 10.1002/cne.22798.

Hale, M. E. *et al.* (2016) 'Neural circuits that drive startle behavior, with a focus on the Mauthner cells and spiral fiber neurons of fishes', *Journal of Neurogenetics*, 30(2), pp. 89–100. doi: 10.1080/01677063.2016.1182526.

Hamzei-sichani, F. *et al.* (2007) 'Gap junctions on hippocampal mossy fiber axons demonstrated by thin-section electron microscopy and freeze – fracture replica immunogold labeling', *PNAS*, 104(30), pp. 12548–12553.

Hamzei-Sichani, F. *et al.* (2012) 'Mixed Electrical–Chemical Synapses in Adult Rat Hippocampus are Primarily Glutamatergic and Coupled by Connexin-36', *Frontiers in Neuroanatomy*, 6. doi: 10.3389/fnana.2012.00013.

Hansen, K. A. *et al.* (2005) 'Expression and function of the neuronal gap junction protein connexin 36 in developing mammalian retina', *The Journal of Comparative Neurology*, 493(2), pp. 309–320. doi: 10.1002/cne.20759.

Hegyi, B. *et al.* (2015) 'KN-93 inhibits IKr in mammalian cardiomyocytes', *Journal of Molecular and Cellular Cardiology*, 89, pp. 173–176. doi: 10.1016/j.yjmcc.2015.10.012.

Hendsch, Z. S. and Tidor, B. (1994) 'Do salt bridges stablize proteins - a continuum electrostatic analysis', *Prot. Sci.*, 3(2), pp. 211–226. doi: 10.1002/pro.5560030206.

Hervé, J.-C. *et al.* (2007) 'The Connexin Turnover, an Important Modulating Factor of the Level of Cell-to-Cell Junctional Communication: Comparison with Other Integral Membrane Proteins', *Journal of Membrane Biology*, 217(1–3), pp. 21–33. doi: 10.1007/s00232-007-9054-8.

Hervé, J. C. *et al.* (2007) 'The connexin turnover, an important modulating factor of the level of cell-to-cell junctional communication: Comparison with other integral membrane proteins', in *Journal of Membrane Biology*, pp. 21–33. doi: 10.1007/s00232-007-9054-8.

Hinz, F. I. *et al.* (2013) 'Protein Synthesis-Dependent Associative Long-Term Memory in Larval Zebrafish', *The Journal of Neuroscience*, 33(39), pp. 15382–15387. doi: 10.1523/JNEUROSCI.0560-13.2013.

Hirata, H. *et al.* (2012) 'Connexin 39.9 Protein Is Necessary for Coordinated Activation of Slow-twitch Muscle and Normal Behavior in Zebrafish', *Journal of Biological Chemistry*, 287(2), pp. 1080–1089. doi: 10.1074/jbc.M111.308205.

Ho, J. *et al.* (2019) 'Moving beyond P values: data analysis with estimation graphics', *Nature Methods*, 16(7), pp. 565–566. doi: 10.1038/s41592-019-0470-3.

Hodson, D. J. *et al.* (2015) 'Roles of connexins and pannexins in (neuro)endocrine physiology', *Cellular and Molecular Life Sciences*, 72(15), pp. 2911–2928. doi: 10.1007/s00018-015-1967-2.

Holland, N. D. (2005) 'Chordates.', *Current biology : CB*, 15(22), pp. R911–R914. doi: 10.1016/j.cub.2005.11.008.

Holloway, F. A. and Wansley, R. (1973) 'Multiphasic Retention Deficits at Periodic Intervals after Passive-Avoidance Learning', *Science*, 180(4082), pp. 208–210. doi: 10.1126/science.180.4082.208.

Holloway, F. A. and Wansley, R. A. (1973) 'Multiple retention deficits at periodic intervals after active and passive avoidance learning', *Behavioral Biology*, 9(1), pp. 1–14. doi: 10.1016/S0091-6773(73)80164-6.

Hormuzdi, S. G. *et al.* (2001) 'Impaired Electrical Signaling Disrupts Gamma Frequency Oscillations in Connexin 36-Deficient Mice', 31, pp. 487–495.

Hormuzdi, S. G. *et al.* (2004) 'Electrical synapses: a dynamic signaling system that shapes the activity of neuronal networks.', *Biochimica et biophysica acta*, 1662(1–2), pp. 113–37. doi: 10.1016/j.bbamem.2003.10.023.

Hotulainen, P. and Hoogenraad, C. C. (2010) 'Actin in dendritic spines: connecting dynamics to function', *Journal of Cellular Biology*, 189, pp. 619–629.

Hou, Y. . *et al.* (2009) 'Involvement of actin rearrangements within the amygdala and the dorsal hippocampus in aversive memories of drug withdrawal in acute morphine-dependent rats', *Journal of Neuroscience*, 29, pp. 12244–12254.

Hu, X. *et al.* (2008) 'Activity-dependent dynamic microtubule invasion of dendritic spines.', *The Journal of neuroscience : the official journal of the Society for Neuroscience*, 28(49), pp. 13094–13105. doi: 10.1523/JNEUROSCI.3074-08.2008.

Hudmon, A. and Schulman, H. (2002) 'Structure–function of the multifunctional Ca2+/calmodulin-dependent protein

kinase II', *Biochemical Journal*, 364(3), pp. 593–611. doi: 10.1042/bj20020228.

Hughes, J. R. (1958) 'Post-tetanic potentiation.', *Physiological reviews*, 38(1), pp. 91–113.

Hunsicker, J. P. and Mellgren, R. L. (1977) 'Multiple deficits in the retention of an appetitively motivated behavior across a 24-h period in rats', *Animal Learning & Behavior*, 5(1), pp. 14–16. doi: 10.3758/BF03209124.

Irons, T. D. *et al.* (2010) 'Acute neuroactive drug exposures alter locomotor activity in larval zebrafish', *Neurotoxicology and Teratology*, 32(1), pp. 84–90. doi: 10.1016/j.ntt.2009.04.066.

Jabeen, S. and Thirumalai, V. (2013) 'Distribution of the gap junction protein connexin 35 in the central nervous system of developing zebrafish larvae.', *Frontiers in neural circuits*, 7(May), p. 91. doi: 10.3389/fncir.2013.00091.

Jacob, C. *et al.* (2014) 'Internalizing and externalizing behavior in adult ADHD', *ADHD Attention Deficit and Hyperactivity Disorders*, 6(2), pp. 101–110. doi: 10.1007/s12402-014-0128-z.

Jacobson, G. M. *et al.* (2010) 'Connexin36 knockout mice display increased sensitivity to pentylenetetrazol-induced seizure-like behaviors', *Brain Research*, 1360, pp. 198–204. doi: 10.1016/j.brainres.2010.09.006.

Jann, M. W. (1988) 'Buspirone: An Update on a Unique Anxiolytic Agent', *Pharmacotherapy: The Journal of Human Pharmacology and Drug Therapy*, 8(2), pp. 100–116. doi: 10.1002/j.1875-9114.1988.tb03543.x.

Jans, L. A. W. *et al.* (2007) 'Serotonergic vulnerability and depression: assumptions, experimental evidence and implications', *Mol Psychiatry*, 12(6), pp. 522–543. doi: 10.1038/sj.mp.4001920.

Jarrell, T. A. *et al.* (2012) 'The Connectome of a Decision-Making Neural Network', *Science*, 337(6093), pp. 437–444. doi: 10.1126/science.1221762.

Jaworski, J. *et al.* (2009) 'Dynamic Microtubules Regulate Dendritic Spine Morphology and Synaptic Plasticity', *Neuron*, 61(1), pp. 85–100. doi: 10.1016/j.neuron.2008.11.013.

Jinek, M. *et al.* (2012) 'A Programmable Dual-RNA – Guided DNA Endonuclease in Adaptice Bacterial Immunity', *Science (New York, N.Y.)*, 337(August), pp. 816–822. doi: 10.1126/science.1225829.

Johnson, C. N. *et al.* (2019) 'The CaMKII inhibitor KN93-calmodulin interaction and implications for calmodulin tuning of NaV1.5 and RyR2 function', *Cell Calcium*, 82, p. 102063. doi: 10.1016/j.ceca.2019.102063.

Jongen, W. M. F. *et al.* (1991) 'Regulation of connexin 43-mediated gap junctional intercellular communication by CA2+ in mouse epidermal cells is controlled by E-cadherin', *Journal of Cell Biology*, 114(3), pp. 545–555.

Jordan, K. *et al.* (1999) 'Trafficking, assembly, and function of a connexin43-green fluorescent protein chimera in live mammalian cells.', *Molecular biology of the cell*, 10(6), pp. 2033–50. doi: 10.1091/mbc.10.6.2033.

Jordan, L. M. (1998) 'Initiation of locomotion in mammals.', *Annals of the New York Academy of Sciences*, 860, pp. 83–93. Available at: http://www.ncbi.nlm.nih.gov/pubmed/9928303.

Kalueff, A. V. *et al.* (2013) 'Towards a Comprehensive Catalog of Zebrafish Behavior 1.0 and Beyond', *Zebrafish*, 10(1), pp. 70–86. doi: 10.1089/zeb.2012.0861.

Kamermans, M. *et al.* (2001) 'Hemichannel-mediated inhibition in the outer retina.', *Science (New York, N.Y.)*, 292(5519), pp. 1178–1180. doi: 10.1126/science.1060101.

Kapitein, L. C. *et al.* (2011) 'NMDA receptor activation suppresses microtubule growth and spine entry.', *The Journal of neuroscience : the official journal of the Society for Neuroscience*, 31(22), pp. 8194–209. doi: 10.1523/JNEUROSCI.6215-10.2011.

Kats, B. and Miledi, R. (1965) 'The measurement of synaptic delay, and the time course of acetylcholine release at the neuromuscular junction', *Proceedings of the Royal Society of London. Series B. Biological Sciences*, 161(985), pp. 483–495. doi: 10.1098/rspb.1965.0016.

Kawakami, K. *et al.* (2004) 'A transposon-mediated gene trap approach identifies developmentally regulated genes in zebrafish', *Developmental Cell*, 7(1), pp. 133–144. doi: 10.1016/j.devcel.2004.06.005.

Khanbabaei, M. *et al.* (2019) 'Precocious myelination in a mouse model of autism', *Translational Psychiatry*, 9(1), p. 251. doi: 10.1038/s41398-019-0590-7.

Khodosevich, K. *et al.* (2012) 'Connexin45 modulates the proliferation of transit-amplifying precursor cells in the mouse subventricular zone', *Proceedings of the National Academy of Sciences*, 109(49), pp. 20107–20112. doi:

10.1073/pnas.1217103109.

Kimmel, C. B., Eaton, R. C. and Powell, S. L. (1980) 'Decreased fast-start performance of zebrafish larvae lacking mauthner neurons', *Journal of Comparative Physiology ? A*, 140(4), pp. 343–350. doi: 10.1007/BF00606274.

Kirby, B. B. *et al.* (2006) 'In vivo time-lapse imaging shows dynamic oligodendrocyte progenitor behavior during zebrafish development.', *Nature neuroscience*, 9(12), pp. 1506–1511. doi: 10.1038/nn1803.

Klaassen, L. J. *et al.* (2011) 'Synaptic Transmission from Horizontal Cells to Cones Is Impaired by Loss of Connexin Hemichannels', *PLoS Biology*. Edited by R. O. L. Wong, 9(7), p. e1001107. doi: 10.1371/journal.pbio.1001107.

Klaassen, L. J. *et al.* (2016) 'Specific connectivity between photoreceptors and horizontal cells in the zebrafish retina', *Journal of Neurophysiology*, 116(6), pp. 2799–2814. doi: 10.1152/jn.00449.2016.

Knapska, E. and Kaczmarek, L. (2004) 'A gene for neuronal plasticity in the mammalian brain: Zif268/Egr-1/NGFI-A/Krox-24/TIS8/ZENK?', *Progress in Neurobiology*, 74(4), pp. 183–211. doi: 10.1016/j.pneurobio.2004.05.007.

Kohashi, T. and Oda, Y. (2008) 'Initiation of Mauthner- or Non-Mauthner-Mediated Fast Escape Evoked by Different Modes of Sensory Input', *Journal of Neuroscience*, 28(42), pp. 10641–10653. doi: 10.1523/JNEUROSCI.1435-08.2008.

Kooij, J. J. S. and Bijlenga, D. (2014) 'High Prevalence of Self-Reported Photophobia in Adult ADHD', *Frontiers in Neurology*, 5. doi: 10.3389/fneur.2014.00256.

Korn, H. and Faber, D. S. (2005) 'The Mauthner Cell Half a Century Later: A Neurobiological Model for Decision-Making?', *Neuron*, 47(1), pp. 13–28. doi: 10.1016/j.neuron.2005.05.019.

Kothmann, W. W. *et al.* (2007) 'Connexin 35/36 is phosphorylated at regulatory sites in the retina', *Visual Neuroscience*, 24(03), pp. 363–375. doi: 10.1017/S095252380707037X.

Kothmann, W. W. *et al.* (2012) 'Nonsynaptic NMDA Receptors Mediate Activity-Dependent Plasticity of Gap Junctional Coupling in the AII Amacrine Cell Network', *Journal of Neuroscience*, 32(20), pp. 6747–6759. doi: 10.1523/JNEUROSCI.5087-11.2012.

Kothmann, W. W., Massey, S. C. and O'Brien, J. (2009) 'Dopamine-Stimulated Dephosphorylation of Connexin 36 Mediates AII Amacrine Cell Uncoupling', *Journal of Neuroscience*, 29(47), pp. 14903–14911. doi: 10.1523/JNEUROSCI.3436-09.2009.

Kozlovsky, N. *et al.* (2009) 'A distinct pattern of intracellular glucocorticoid-related responses is associated with extreme behavioral response to stress in an animal model of post-traumatic stress disorder', *European Neuropsychopharmacology*, 19(11), pp. 759–771. doi: 10.1016/j.euroneuro.2009.04.009.

Kumar, N. M. and Gilula, N. B. (1996) 'The gap junction communication channel', *Cell*, 84, pp. 381–388.

Kumar, S. and Nussinov, R. (2002) 'Close-range electrostatic interactions in proteins', *ChemBioChem*, pp. 604–617. doi: 10.1002/1439-7633(20020703)3:7<604::AID-CBIC604>3.0.CO;2-X.

Kyriakatos, A. *et al.* (2011) 'Initiation of Locomotion in Adult Zebrafish', *Journal of Neuroscience*, 31(23), pp. 8422–8431. doi: 10.1523/JNEUROSCI.1012-11.2011.

Laird, D. W. (2010) 'The gap junction proteome and its relationship to disease.', *Trends in cell biology*, 20(2), pp. 92–101. doi: 10.1016/j.tcb.2009.11.001.

LaPointe, N. E. *et al.* (2009) 'The amino terminus of tau inhibits kinesin-dependent axonal transport: Implications for filament toxicity', *Journal of Neuroscience Research*, 87(2), pp. 440–451. doi: 10.1002/jnr.21850.

Lauf, U. *et al.* (2002) 'Dynamic trafficking and delivery of connexons to the plasma membrane and accretion to gap junctions in living cells.', *Proceedings of the National Academy of Sciences of the United States of America*, 99(16), pp. 10446–10451. doi: 10.1073/pnas.162055899.

Ledoux, J., Chartier, D. and Leblanc, N. (1999) 'Inhibitors of calmodulin-dependent protein kinase are nonspecific blockers of voltage-dependent K+ channels in vascular myocytes.', *The Journal of pharmacology and experimental therapeutics*, 290(3), pp. 1165–74. Available at: http://www.ncbi.nlm.nih.gov/pubmed/10454491.

Lei, S. *et al.* (2001) 'Regulation of NMDA Receptor Activity by F-Actin and Myosin Light Chain Kinase', *The Journal of Neuroscience*, 21(21), pp. 8464–8472. doi: 10.1523/JNEUROSCI.21-21-08464.2001.

Li, H. *et al.* (2013) 'Adenosine and Dopamine Receptors Coregulate Photoreceptor Coupling via Gap Junction

Phosphorylation in Mouse Retina', *Journal of Neuroscience*, 33(7), pp. 3135–3150. doi: 10.1523/JNEUROSCI.2807-12.2013.

Li, H., Chuang, A. Z. and O'Brien, J. (2009) 'Photoreceptor Coupling Is Controlled by Connexin 35 Phosphorylation in Zebrafish Retina', *Journal of Neuroscience*, 29(48), pp. 15178–15186. doi: 10.1523/JNEUROSCI.3517-09.2009.

Li, H., Chuang, A. Z. and O'Brien, J. (2014) 'Regulation of photoreceptor gap junction phosphorylation by adenosine in zebrafish retina.', *Visual neuroscience*, 31(3), pp. 237–43. doi: 10.1017/S095252381300062X.

Li, S.-X. *et al.* (2014) 'Role of the NMDA receptor in cognitive deficits, anxiety and depressive-like behavior in juvenile and adult mice after neonatal dexamethasone exposure', *Neurobiology of Disease*, 62, pp. 124–134. doi: 10.1016/j.nbd.2013.09.004.

Li, X. *et al.* (2004) 'Neuronal connexin36 association with zonula occludens-1 protein (ZO-1) in mouse brain and interaction with the first PDZ domain of ZO-1', *European Journal of Neuroscience*, 19(8), pp. 2132–2146. doi: 10.1111/j.0953-816X.2004.03283.x.

Li, X. *et al.* (2008) 'Connexin45-Containing Neuronal Gap Junctions in Rodent Retina Also Contain Connexin36 in Both Apposing Hemiplaques, Forming Bihomotypic Gap Junctions, with Scaffolding Contributed by Zonula Occludens-1', *Journal of Neuroscience*, 28(39), pp. 9769–9789. doi: 10.1523/JNEUROSCI.2137-08.2008.

Li, X., Lynn, B. D. and Nagy, J. I. (2012) 'The effector and scaffolding proteins AF6 and MUPP1 interact with connexin36 and localize at gap junctions that form electrical synapses in rodent brain', *European Journal of Neuroscience*, 35(2), pp. 166–181. doi: 10.1111/j.1460-9568.2011.07947.x.

Ligon, L. A. and Steward, O. (2000) 'Role of microtubules and actin filaments in the movement of mitochondria in the axons and dendrites of cultured hippocampal neurons.', *The Journal of comparative neurology*, 427(3), pp. 351–61. Available at: http://www.ncbi.nlm.nih.gov/pubmed/11054698.

Lin, Y.-P. *et al.* (2020) 'A phosphomimetic Cx36 mutant mouse displays excess neuronal coupling and photopic visual deficits', *Investigative Ophthalmology & Visual Science*, 61.

Lipscombe, D., Helton, T. D. and Xu, W. (2004) 'L-Type Calcium Channels: The Low Down', *Journal of Neurophysiology*, 92(5), pp. 2633–2641. doi: 10.1152/jn.00486.2004.

Lira, A. *et al.* (2003) 'Altered depression-related behaviors and functional changes in the dorsal raphe nucleus of serotonin transporter-deficient mice', *Biol Psychiatry.*, 54(10), pp. 960–71. doi: 10.1016/s0006-3223(03)00696-6.

Liu, K. S. and Fetcho, J. R. (1999) 'Laser Ablations Reveal Functional Relationships of Segmental Hindbrain Neurons in Zebrafish', *Neuron*, 23(2), pp. 325–335. doi: 10.1016/S0896-6273(00)80783-7.

Livak, K. J. and Schmittgen, T. D. (2001) 'Analysis of Relative Gene Expression Data Using Real-Time Quantitative PCR and the 2−ΔΔCT Method', *Methods*, 25(4), pp. 402–408. doi: 10.1006/meth.2001.1262.

Loewi, O. (1924) 'Über humorale Übertragbarkeit der Herznervenwirkung', *Pflügers Archiv für die Gesamte Physiologie des Menschen und der Tiere*, 204(1), pp. 629–640. doi: 10.1007/BF01731235.

Loh, D. H. *et al.* (2010) 'Rapid Changes in the Light/Dark Cycle Disrupt Memory of Conditioned Fear in Mice', *PLoS ONE*. Edited by C. T. Dickson, 5(9), p. e12546. doi: 10.1371/journal.pone.0012546.

Lombardi, A. *et al.* (2000) 'Retrostructural analysis of metalloproteins: Application to the design of a minimal model for diiron proteins', *Proceedings of the National Academy of Sciences*, 97(12), pp. 6298–6305. doi: 10.1073/pnas.97.12.6298.

Long, M. a *et al.* (2005) 'Electrical synapses coordinate activity in the suprachiasmatic nucleus.', *Nature neuroscience*, 8(1), pp. 61–6. doi: 10.1038/nn1361.

Lopresti, V., Macagno, E. R. and Levinthal, C. (1974) 'Structure and Development of Neuronal Connections in Isogenic Organisms: Transient Gap Junctions between Growing Optic Axons and Lamina Neuroblasts', *Proceedings of the National Academy of Sciences*, 71(4), pp. 1098–1102. doi: 10.1073/pnas.71.4.1098.

Luchtenburg, F. J., Schaaf, M. J. M. and Richardson, M. K. (2019) 'Functional characterization of the cannabinoid receptors 1 and 2 in zebrafish larvae using behavioral analysis', *Psychopharmacology*, 236(7), pp. 2049–2058. doi: 10.1007/s00213-019-05193-4.

Lukowicz-Bedford, R. M., Farnsworth, D. R. and Miller, A. C. (2022) 'Connexinplexity: the spatial and temporal expression of connexin genes during vertebrate organogenesis', *G3 Genes|Genomes|Genetics*. Edited by A.

McCallion, 12(5). doi: 10.1093/g3journal/jkac062.

Lynn, B. D., Li, X. and Nagy, J. I. (2012) 'Under Construction: Building the Macromolecular Superstructure and Signaling Components of an Electrical Synapse', *The Journal of Membrane Biology*, 245(5–6), pp. 303–317. doi: 10.1007/s00232-012-9451-5.

Ma, H. *et al.* (2014) 'γCaMKII Shuttles Ca2+/CaM to the Nucleus to Trigger CREB Phosphorylation and Gene Expression', *Cell*, 159(2), pp. 281–294. doi: 10.1016/j.cell.2014.09.019.

Ma, H. *et al.* (2021) 'Amygdala-hippocampal innervation modulates stress-induced depressive-like behaviors through AMPA receptors', *Proceedings of the National Academy of Sciences*, 118(6). doi: 10.1073/pnas.2019409118.

Maeda, H., Hasumi, A. and Yoshida, K. (2021) 'Caffeine-induced bradycardia, death, and anxiety-like behavior in zebrafish larvae', *Forensic Toxicology*, 39(2), pp. 427–436. doi: 10.1007/s11419-021-00577-8.

Maher, B. J., McGinley, M. J. and Westbrook, G. L. (2009) 'Experience-dependent maturation of the glomerular microcircuit', *Proceedings of the National Academy of Sciences*, 106(39), pp. 16865–16870. doi: 10.1073/pnas.0808946106.

Mali, P. *et al.* (2013) 'RNA-guided human genome engineering via Cas9', *Science*, 339(6121), pp. 823–826. doi: 10.1126/science.1232033.

Marsh, A. J. *et al.* (2017) 'Asymmetry of an Intracellular Scaffold at Vertebrate Electrical Synapses', *Current Biology*, 27(22), p. 3561–3567.e4. doi: 10.1016/j.cub.2017.10.011.

Mattos, P. *et al.* (2013) 'A Multicenter, Open-Label Trial to Evaluate the Quality of Life in Adults With ADHD Treated With Long-Acting Methylphenidate (OROS MPH)', *Journal of Attention Disorders*, 17(5), pp. 444–448. doi: 10.1177/1087054711434772.

McLachlan, E. *et al.* (2003) 'Zebrafish Cx35: cloning and characterization of a gap junction gene highly expressed in the retina.', *Journal of neuroscience research*, 73(6), pp. 753–764.

McLean, D. L. and Fetcho, J. R. (2008) 'Using imaging and genetics in zebrafish to study developing spinal circuits in vivo', *Developmental Neurobiology*, pp. 817–834. doi: 10.1002/dneu.20617.

McMillen, B. *et al.* (1983) 'Dopamine receptor antagonism by the novel antianxiety drug, buspirone', *The Journal of Neuroscience*, 3(4), pp. 733–738. doi: 10.1523/JNEUROSCI.03-04-00733.1983.

Mcvicker, D. P., Millette, M. M. and Dent, E. W. (2015) 'Signaling to the microtubule cytoskeleton: An unconventional role for CaMKII', *Developmental Neurobiology*, 75(4), pp. 423–434. doi: 10.1002/dneu.22227.

Meikle, L. *et al.* (2007) 'A mouse model of tuberous sclerosis: neuronal loss of Tsc1 causes dysplastic and ectopic neurons, reduced myelination, seizure activity, and limited survival.', *The Journal of neuroscience : the official journal of the Society for Neuroscience*, 27(21), pp. 5546–58. doi: 10.1523/JNEUROSCI.5540-06.2007.

Merriam, E. B. *et al.* (2011) 'Dynamic microtubules promote synaptic NMDA receptor-dependent spine enlargement', *PLoS ONE*, 6(11). doi: 10.1371/journal.pone.0027688.

Merriam, E. B. *et al.* (2013) 'Synaptic regulation of microtubule dynamics in dendritic spines by calcium, F-actin, and drebrin.', *The Journal of neuroscience : the official journal of the Society for Neuroscience*, 33(42), pp. 16471–82. doi: 10.1523/JNEUROSCI.0661-13.2013.

Meyer, R. A. *et al.* (1992) 'Inhibition of gap junction and adherens junction assembly by connexin and A-CAM antibodies', *Journal of Cell Biology*, 119(1), pp. 179–189. doi: 10.1083/jcb.119.1.179.

Mezer, E. and Wygnanski-Jaffe, T. (2012) 'Do Children and Adolescents with Attention Deficit Hyperactivity Disorder have Ocular Abnormalities?', *European Journal of Ophthalmology*, 22(6), pp. 931–935. doi: 10.5301/ejo.5000145.

Mignot, I. *et al.* (2012) 'Design and Characterization of Modular Scaffolds for Tubulin Assembly', *Journal of Biological Chemistry*, 287(37), pp. 31085–31094. doi: 10.1074/jbc.M112.383869.

Mikalsen, S.-O., Tausen, M. and í Kongsstovu, S. (2020) 'Phylogeny of teleost connexins reveals highly inconsistent intra- and interspecies use of nomenclature and misassemblies in recent teleost chromosome assemblies', *BMC Genomics*, 21(1), p. 223. doi: 10.1186/s12864-020-6620-2.

Mikoshiba, K. (2007) 'IP 3 receptor/Ca 2+ channel: from discovery to new signaling concepts', *Journal of*

Neurochemistry, 102(5), pp. 1426–1446. doi: 10.1111/j.1471-4159.2007.04825.x.

Miller, A. C. *et al.* (2017) 'A genetic basis for molecular asymmetry at vertebrate electrical synapses', *eLife*, 6. doi: 10.7554/eLife.25364.

Miller, T. H. *et al.* (2017) 'Social Status–Dependent Shift in Neural Circuit Activation Affects Decision Making', *The Journal of Neuroscience*, 37(8), pp. 2137–2148. doi: 10.1523/JNEUROSCI.1548-16.2017.

Mohrmann, R. *et al.* (2002) 'Deletion of the C-terminal domain of the NR2B subunit alters channel properties and synaptic targeting of N-methyl-D-aspartate receptors in nascent neocortical synapses', *Journal of Neuroscience Research*, 68(3), pp. 265–275. doi: 10.1002/jnr.10219.

Moreno, A. P. *et al.* (2002) 'Role of the carboxyl terminal of connexin43 in transjunctional fast voltage gating', *Circulation Research*, 90(4), pp. 450–457. doi: 10.1161/hh0402.105667.

Morrow, J. M. *et al.* (2016) 'A second visual rhodopsin gene, rh1-2 , is expressed in zebrafish photoreceptors and found in other ray-finned fishes', *Journal of Experimental Biology*. doi: 10.1242/jeb.145953.

Moyano, M., Porteros, Á. and Dowling, J. E. (2013) 'The effects of nicotine on cone and rod b-wave responses in larval zebrafish', *Visual Neuroscience*, 30(4), pp. 141–145. doi: 10.1017/S0952523813000187.

Mruk, K. *et al.* (2014) 'Calmodulation meta-analysis: predicting calmodulin binding via canonical motif clustering.', *The Journal of general physiology*, 144(1), pp. 105–14. doi: 10.1085/jgp.201311140.

Müller, U. K. and van Leeuwen, J. L. (2004) 'Swimming of larval zebrafish: ontogeny of body waves and implications for locomotory development.', *The Journal of experimental biology*, 207(Pt 5), pp. 853–68. Available at: http://www.ncbi.nlm.nih.gov/pubmed/14747416.

Musil, L. S. and Goodenough, D. A. (1993) 'Multisubunit assembly of an integral plasma membrane channel protein, gap junction connexin43, occurs after exit from the ER.', *Cell*, 74(6), pp. 1065–1077. doi: 10.1016/0092-8674(93)90728-9.

Myllykoski, M., Kuczera, K. and Kursula, P. (2009) 'Complex formation between calmodulin and a peptide from the intracellular loop of the gap junction protein connexin43: Molecular conformation and energetics of binding.', *Biophysical chemistry*, 144(3), pp. 130–5. doi: 10.1016/j.bpc.2009.08.001.

Nagy, J. I. and Lynn, B. D. (2018) 'Structural and Intermolecular Associations Between Connexin36 and Protein Components of the Adherens Junction–Neuronal Gap Junction Complex', *Neuroscience*, 384, pp. 241–261. doi: 10.1016/j.neuroscience.2018.05.026.

Nasevicius, a and Ekker, S. C. (2000) 'Effective targeted gene "knockdown" in zebrafish.', *Nature genetics*, 26(2), pp. 216–20. doi: 10.1038/79951.

Nelson, B. . *et al.* (2012) 'A role for hippocampal actin rearrangement in object placement memory in female rats', *Neurobiol. Learn. Mem.*, 98, pp. 284–290.

Ninkovic, J. and Bally-Cuif, L. (2006) 'The zebrafish as a model system for assessing the reinforcing properties of drugs of abuse', *Methods*, 39(3), pp. 262–274. doi: 10.1016/j.ymeth.2005.12.007.

Noriuchi, M. *et al.* (2010) 'Altered white matter fractional anisotropy and social impairment in children with autism spectrum disorder', *Brain Research*, 1362, pp. 141–149. doi: 10.1016/j.brainres.2010.09.051.

O'Brien, J. *et al.* (1998) 'Cloning and Expression of Two Related Connexins from the Perch Retina Define a Distinct Subgroup of the Connexin Family', *The Journal of Neuroscience*, 18(19), pp. 7625–7637. doi: 10.1523/JNEUROSCI.18-19-07625.1998.

O'Brien, J. (2019) 'Design principles of electrical synaptic plasticity', *Neuroscience Letters*, 695, pp. 4–11. doi: 10.1016/j.neulet.2017.09.003.

O'Brien, J., Al-Ubaidi, M. R. and Ripps, H. (1996) 'Connexin 35: Cloning of a cap junctional protein expressed preferentially in the skate retina', *Investigative Ophthalmology and Visual Science*, 37(3).

O'Malley, D. M., Kao, Y. H. and Fetcho, J. R. (1996) 'Imaging the functional organization of zebrafish hindbrain segments during escape behaviors.', *Neuron*, 17(6), pp. 1145–55. Available at: http://www.ncbi.nlm.nih.gov/pubmed/8982162.

Oberlander, T., Gingrich, J. and Ansorge, M. (2014) 'Sustained Neurobehavioral Effects of Exposure to SSRI

Antidepressants During Development: Molecular to Clinical Evidence', *Clin Pharmacol Ther.*, 86(6), pp. 672–77. doi: 10.1038/clpt.2009.201.

Odermatt, B. *et al.* (2003) 'Connexin 47 (Cx47)-Deficient Mice with Enhanced Green Fluorescent Protein Reporter Gene Reveal Predominant Oligodendrocytic Expression of Cx47 and Display Vacuolized Myelin in the CNS', *The Journal of Neuroscience*, 23(11), pp. 4549–4559. doi: 10.1523/JNEUROSCI.23-11-04549.2003.

Olivier, J. D. A. *et al.* (2008) 'A study in male and female 5-HT transporter knockout rats: an animal model for anxiety and depression disorders', *Neuroscience*, 152(3), pp. 573–84. doi: 10.1016/j.neuroscience.2007.12.032.

Olsson, T., Håkansson, Å. and Seckl, J. R. (1997) 'Ketanserin selectively blocks acute stress-induced changes in NGFI-A and mineralocorticoid receptor gene expression in hippocampal neurons', *Neuroscience*, 76(2), pp. 441–448. doi: 10.1016/S0306-4522(96)00432-0.

Orger, M. B. *et al.* (2004) 'Behavioral Screening Assays in Zebrafish', *Methods in Cell Biology*, 77, pp. 53–68. doi: 10.1016/S0091-679X(04)77003-X.

Orger, M. B. *et al.* (2008) 'Control of visually guided behavior by distinct populations of spinal projection neurons.', *Nature neuroscience*, 11(3), pp. 327–333. doi: 10.1038/nn2048.

Orthmann-Murphy, J. L. *et al.* (2007) 'Two Distinct Heterotypic Channels Mediate Gap Junction Coupling between Astrocyte and Oligodendrocyte Connexins', *Journal of Neuroscience*, 27(51), pp. 13949–13957. doi: 10.1523/JNEUROSCI.3395-07.2007.

Osterweil, E., Wells, D. G. and Mooseker, M. S. (2005) 'A role for myosin VI in postsynaptic structure and glutamate receptor endocytosis.', *The Journal of cell biology*, 168(2), pp. 329–38. doi: 10.1083/jcb.200410091.

Ouyang, X. *et al.* (2005) 'Protein kinase A mediates regulation of gap junctions containing connexin35 through a complex pathway.', *Brain research. Molecular brain research*, 135(1–2), pp. 1–11. doi: 10.1016/j.molbrainres.2004.10.045.

Pacey, L. K. K. *et al.* (2013) 'Delayed myelination in a mouse model of fragile X syndrome', *Human Molecular Genetics*, 22(19), pp. 3920–3930. doi: 10.1093/hmg/ddt246.

Palacios-Prado, N. *et al.* (2012) 'Intracellular Magnesium-Dependent Modulation of Gap Junction Channels Formed by Neuronal Connexin36', *Journal of Neuroscience*, 33(11), pp. 4741–4753. doi: 10.1523/JNEUROSCI.2825-12.

Pan, F. *et al.* (2010) 'Connexin36 is required for gap junctional coupling of most ganglion cell subtypes in the mouse retina', *The Journal of Comparative Neurology*, 518(6), pp. 911–927. doi: 10.1002/cne.22254.

Parenti, R. *et al.* (2010) 'Dynamic expression of Cx47 in mouse brain development and in the cuprizone model of myelin plasticity', *Glia*, 58(13), pp. 1594–1609. doi: 10.1002/glia.21032.

Park, J.-S. *et al.* (2016) 'Innate Color Preference of Zebrafish and Its Use in Behavioral Analyses', *Molecules and Cells*, 39(10), pp. 750–755. doi: 10.14348/molcells.2016.0173.

Park, W.-M. *et al.* (2011) 'Interplay of Chemical Neurotransmitters Regulates Developmental Increase in Electrical Synapses', *Journal of Neuroscience*, 31(16), pp. 5909–5920. doi: 10.1523/JNEUROSCI.6787-10.2011.

Paul, D. L. *et al.* (1991) 'Connexin46, a novel lens gap junction protein, induces voltage-gated currents in nonjunctional plasma membrane of Xenopus oocytes', *Journal of Cell Biology*, 115(4), pp. 1077–1089. doi: 10.1083/jcb.115.4.1077.

Paul, D. L. (1995) 'New functions for gap junctions', *Current Opinion in Cell Biology*, pp. 665–672. doi: 10.1016/0955-0674(95)80108-1.

Peng, X. *et al.* (2016) 'Anxiety-related behavioral responses of pentylenetetrazole-treated zebrafish larvae to light-dark transitions', *Pharmacology Biochemistry and Behavior*, 145, pp. 55–65. doi: 10.1016/j.pbb.2016.03.010.

Pereda, a E. *et al.* (1998) 'Ca2+/calmodulin-dependent kinase II mediates simultaneous enhancement of gap-junctional conductance and glutamatergic transmission.', *Proceedings of the National Academy of Sciences of the United States of America*, 95(22), pp. 13272–7.

Pereda, A. *et al.* (2003) 'Connexin35 Mediates Electrical Transmission at Mixed Synapses on Mauthner Cells', *The Journal of Neuroscience*, 23(20), pp. 7489–7503. doi: 10.1523/JNEUROSCI.23-20-07489.2003.

Pereda, A. E. *et al.* (2004) 'Dynamics of electrical transmission at club endings on the Mauthner cells.', *Brain research.*

Brain research reviews, 47(1–3), pp. 227–44. doi: 10.1016/j.brainresrev.2004.06.010.

Pereda, A. E. *et al.* (2013) 'Gap junction-mediated electrical transmission: Regulatory mechanisms and plasticity', *Biochimica et Biophysica Acta - Biomembranes*, pp. 134–146. doi: 10.1016/j.bbamem.2012.05.026.

Pereda, A. E. (2014) 'Electrical synapses and their functional interactions with chemical synapses.', *Nature reviews. Neuroscience*. Nature Publishing Group, 15(4), pp. 250–63. doi: 10.1038/nrn3708.

Peri, F. and Nüsslein-Volhard, C. (2008) 'Live Imaging of Neuronal Degradation by Microglia Reveals a Role for v0-ATPase a1 in Phagosomal Fusion In Vivo', *Cell*, 133(5), pp. 916–927. doi: 10.1016/j.cell.2008.04.037.

Peters, K. G. *et al.* (1995) 'Green fluorescent fusion proteins: powerful tools for monitoring protein expression in live zebrafish embryos.', *Developmental biology*, pp. 252–257. doi: 10.1006/dbio.1995.1276.

Pfaffl, M. W. (2002) 'Relative expression software tool (REST(C)) for group-wise comparison and statistical analysis of relative expression results in real-time PCR', *Nucleic Acids Research*, 30(9), p. 36e–36. doi: 10.1093/nar/30.9.e36.

Phelan, P. *et al.* (1998) 'Innexins: A family of invertebrate gap-junction proteins', *Trends in Genetics*, pp. 348–349. doi: 10.1016/S0168-9525(98)01547-9.

Piato, Â. L. *et al.* (2011) 'Unpredictable chronic stress model in zebrafish (Danio rerio): Behavioral and physiological responses', *Progress in Neuro-Psychopharmacology and Biological Psychiatry*, 35(2), pp. 561–567. doi: 10.1016/j.pnpbp.2010.12.018.

Postlethwait, J. H. *et al.* (2000) 'Zebrafish comparative genomics and the origins of vertebrate chromosomes', *Genome Research*, 10(12), pp. 1890–1902. doi: 10.1101/gr.164800.

Postma, F. *et al.* (2011) 'Electrical synapses formed by connexin36 regulate inhibition- and experience-dependent plasticity'. doi: 10.1073/pnas.1100166108/-/DCSupplemental.www.pnas.org/cgi/doi/10.1073/pnas.1100166108.

Qu, C., Gardner, P. and Schrijver, I. (2009) 'The role of the cytoskeleton in the formation of gap junctions by Connexin 30', *Exp. Cell Res.*, 215, pp. 1683–1692.

Qu, Y.-J. *et al.* (2007) 'W-7 modulates K v 4.3: pore block and Ca 2+ -calmodulin inhibition', *American Journal of Physiology-Heart and Circulatory Physiology*, 292(5), pp. H2364–H2377. doi: 10.1152/ajpheart.00409.2005.

Quint, W. H. *et al.* (2021) 'Loss of Gap Junction Delta-2 (GJD2) gene orthologs leads to refractive error in zebrafish', *Communications Biology*, 4(1), p. 676. doi: 10.1038/s42003-021-02185-z.

Ran, F. A. *et al.* (2013) 'Genome engineering using the CRISPR-Cas9 system.', *Nat Protoc*, 8(11), pp. 2281–2308. doi: 10.1038/nprot.2013.143.

Rankin, C. H. *et al.* (2009) 'Habituation revisited: An updated and revised description of the behavioral characteristics of habituation', *Neurobiology of Learning and Memory*, 92(2), pp. 135–138. doi: 10.1016/j.nlm.2008.09.012.

Rao, G., Barnes, C. A. and McNaughton, B. L. (1987) 'Occlusion of hippocampal electrical junctions by intracellular calcium injection.', *Brain research*, 408(1–2), pp. 267–270. doi: 10.1016/0006-8993(87)90385-4.

Rash, J. E. *et al.* (1996) 'Mixed synapses discovered and mapped throughout mammalian spinal cord.', *Proceedings of the National Academy of Sciences*, 93(9), pp. 4235–4239. doi: 10.1073/pnas.93.9.4235.

Rash, J. E. *et al.* (2001) 'Identification of cells expressing Cx43, Cx30, Cx26, Cx32 and Cx36 in gap junctions of rat brain and spinal cord.', *Cell communication & adhesion*, 8(4–6), pp. 315–20. Available at: http://www.ncbi.nlm.nih.gov/pubmed/12064610.

Rash, J. E. *et al.* (2004) 'High-resolution proteomic mapping in the vertebrate central nervous system: Close proximity of connexin35 to NMDA glutamate receptor clusters and co-localization of connexin36 with immunoreactivity for zonula occludens protein-1 (ZO-1)', *Journal of Neurocytology*, 33(1), pp. 131–151. doi: 10.1023/B:NEUR.0000029653.34094.0b.

Rash, J. E. *et al.* (2007) 'Connexin36 vs. connexin32, "miniature" neuronal gap junctions, and limited electrotonic coupling in rodent suprachiasmatic nucleus.', *Neuroscience*, 149(2), pp. 350–71. doi: 10.1016/j.neuroscience.2007.06.052.

Rash, J. E. *et al.* (2013) 'Molecular and Functional Asymmetry at a Vertebrate Electrical Synapse', *Neuron*, 79(5), pp. 957–969. doi: 10.1016/j.neuron.2013.06.037.

Raveh, B., London, N. and Schueler-Furman, O. (2010) 'Sub-angstrom modeling of complexes between flexible

peptides and globular proteins.', *Proteins*, 78(9), pp. 2029–40. doi: 10.1002/prot.22716.

Ravindran, L. N. and Stein, M. B. (2010) 'The pharmacologic treatment of anxiety disorders: a review of progress', *J Clin Psychiatry*, 71(7), pp. 839–854. doi: 10.4088/JCP.10r06218blu.

Revel, J. P. and Karnovsky, M. J. (1967) 'Hexagonal array of subunits in intercellular junctions of the mouse heart and liver.', *Journal of Cell Biology*, 33(3). doi: 10.1083/jcb.33.3.C7.

Rezazadeh, S., Claydon, T. W. and Fedida, D. (2006) 'KN-93 (2-[N -(2-Hydroxyethyl)]- N -(4-methoxybenzenesulfonyl)]amino- N -(4-chlorocinnamyl)- N -methylbenzylamine), a Calcium/Calmodulin-Dependent Protein Kinase II Inhibitor, Is a Direct Extracellular Blocker of Voltage-Gated Potassium Channels', *Journal of Pharmacology and Experimental Therapeutics*, 317(1), pp. 292–299. doi: 10.1124/jpet.105.097618.

Rosenberg, O. S. *et al.* (2005) 'Structure of the Autoinhibited Kinase Domain of CaMKII and SAXS Analysis of the Holoenzyme', *Cell*, 123(5), pp. 849–860. doi: 10.1016/j.cell.2005.10.029.

Rosenthal, S. M. *et al.* (2021) 'A Toolbox for Efficient Proximity-Dependent Biotinylation in Zebrafish Embryos', *Molecular & Cellular Proteomics*, 20, p. 100128. doi: 10.1016/j.mcpro.2021.100128.

Roux, K. J. *et al.* (2012) 'A promiscuous biotin ligase fusion protein identifies proximal and interacting proteins in mammalian cells.', *The Journal of cell biology*, 196(6), pp. 801–10. doi: 10.1083/jcb.201112098.

Saidi Brikci-Nigassa, A. *et al.* (2012) 'Phosphorylation controls the interaction of the connexin43 C-terminal domain with tubulin and microtubules', *Biochemistry*, 51(21), pp. 4331–4342. doi: 10.1021/bi201806j.

Saillour, Y. *et al.* (2014) 'Beta tubulin isoforms are not interchangeable for rescuing impaired radial migration due to Tubb3 knockdown', *Human Molecular Genetics*, 23(6), pp. 1516–1526. doi: 10.1093/hmg/ddt538.

Sanhueza, M. *et al.* (2011) 'Role of the CaMKII/NMDA receptor complex in the maintenance of synaptic strength', *Journal of Neuroscience*, 31(9170–8).

Sarma, J. Das, Wang, F. and Koval, M. (2002) 'Targeted gap junction protein constructs reveal connexin-specific differences in oligomerization', *Journal of Biological Chemistry*, 277(23), pp. 20911–20918. doi: 10.1074/jbc.M111498200.

Sato, T. *et al.* (2007) 'Genetic single-cell mosaic analysis implicates ephrinB2 reverse signaling in projections from the posterior tectum to the hindbrain in zebrafish.', *The Journal of neuroscience : the official journal of the Society for Neuroscience*, 27(20), pp. 5271–9. doi: 10.1523/JNEUROSCI.0883-07.2007.

Scemes, E., Spray, D. C. and Meda, P. (2009) 'Connexins, pannexins, innexins: Novel roles of "hemi-channels"', *Pflugers Archiv European Journal of Physiology*, pp. 1207–1226. doi: 10.1007/s00424-008-0591-5.

Schmittgen, T. D. and Livak, K. J. (2008) 'Analyzing real-time PCR data by the comparative CT method', *Nature Protocols*, 3(6), pp. 1101–1108. doi: 10.1038/nprot.2008.73.

Schnörr, S. J. *et al.* (2012) 'Measuring thigmotaxis in larval zebrafish', *Behavioural Brain Research*, 228(2), pp. 367–374. doi: 10.1016/j.bbr.2011.12.016.

Schreiber, S. S. *et al.* (1991) 'Activation of immediate early genes after acute stress', *NeuroReport*, 2(1), pp. 17–20. doi: 10.1097/00001756-199101000-00004.

Schweitzer, J. *et al.* (2006) 'Evolution of myelin proteolipid proteins: Gene duplication in teleosts and expression pattern divergence', *Molecular and Cellular Neuroscience*, 31(1), pp. 161–177. doi: 10.1016/j.mcn.2005.10.007.

Severi, K. E. *et al.* (2014) 'Neural Control and Modulation of Swimming Speed in the Larval Zebrafish', *Neuron*, 83(3), pp. 692–707. doi: 10.1016/j.neuron.2014.06.032.

Sevetson, J. *et al.* (2017) 'A calcium-dependent pathway underlies activity-dependent plasticity of electrical synapses in the thalamic reticular nucleus', *The Journal of Physiology*, 595(13), pp. 4417–4430. doi: 10.1113/JP274049.

Shaw, R. M. *et al.* (2007) 'Microtubule plus-end-tracking proteins target gap junctions directly from the cell interior to adherens junctions.', *Cell*, 128(3), pp. 547–60. doi: 10.1016/j.cell.2006.12.037.

Sheng, M. and Hoogenraad, C. C. (2007) 'The postsynaptic architecture of excitatory synapses: a more quantitative view', *Annu. Rev. Biochem.*, 76, pp. 823–847.

Sheng, M., Sabatini, B. . and Sudhof, T. . (2012) 'The Synapse', *Cold Spring Harbor Laboratory*.

Shik, M. L., Orlovskiĭ, G. N. and Severin, F. V (1966) '[Organization of locomotor synergism].', *Biofizika*, 11(5), pp. 879–86. Available at: http://www.ncbi.nlm.nih.gov/pubmed/6000596.

Shik, M. L., Severin, F. V and Orlovskiĭ, G. N. (1966) '[Control of walking and running by means of electric stimulation of the midbrain].', *Biofizika*, 11(4), pp. 659–66. Available at: http://www.ncbi.nlm.nih.gov/pubmed/6000625.

Shimizu, K. and Stopfer, M. (2013) 'Gap junctions', *Current Biology*, 23(23). doi: 10.1016/j.cub.2013.10.067.

Simek, J. *et al.* (2009) 'Cx43 has distinct mobility within plasma-membrane domains, indicative of progressive formation of gap-junction plaques', *Journal of Cell Science*, 122(4), pp. 554–562. doi: 10.1242/jcs.036970.

Simm, A. M. *et al.* (2007) 'Investigating protein structural plasticity by surveying the consequence of an amino acid deletion from TEM-1 β-lactamase', *FEBS Letters*, 581(21), pp. 3904–3908. doi: 10.1016/j.febslet.2007.07.018.

Simon, A. M. and Goodenough, D. A. (1998) 'Diverse functions of vertebrate gap junctions', *Trends in Cell Biology*, pp. 477–482. doi: 10.1016/S0962-8924(98)01372-5.

Simons-Weidenmaier, N. S. *et al.* (2006) 'Synaptic depression and short-term habituation are located in the sensory part of the mammalian startle pathway', *BMC Neuroscience*, 7(1), p. 38. doi: 10.1186/1471-2202-7-38.

Sindelar, C. V, Hendsch, Z. S. and Tidor, B. (1998) 'Effects of salt bridges on protein structure and design.', *Protein science : a publication of the Protein Society*, 7(9), pp. 1898–1914. doi: 10.1002/pro.5560070906.

Siu, R. C. F. *et al.* (2016) 'Structural and Functional Consequences of Connexin 36 (Cx36) Interaction with Calmodulin', *Frontiers in Molecular Neuroscience*, 9, p. 120. doi: 10.3389/fnmol.2016.00120.

Smyth, J. T. *et al.* (2002) 'Inhibition of the Inositol Trisphosphate Receptor of Mouse Eggs and A7r5 Cells by KN-93 via a Mechanism Unrelated to Ca2+/Calmodulin-dependent Protein Kinase II Antagonism', *Journal of Biological Chemistry*, 277(38), pp. 35061–35070. doi: 10.1074/jbc.M202928200.

Söhl, G. *et al.* (1998) 'The murine gap junction gene connexin36 is highly expressed in mouse retina and regulated during brain development', *FEBS Letters*, 428(1–2), pp. 27–31. doi: 10.1016/S0014-5793(98)00479-7.

Söhl, G. *et al.* (2004) 'New insights into the expression and function of neural connexins with transgenic mouse mutants', in *Brain Research Reviews*, pp. 245–259. doi: 10.1016/j.brainresrev.2004.05.006.

Söhl, G., Maxeiner, S. and Willecke, K. (2005) 'Expression and functions of neuronal gap junctions.', *Nature reviews. Neuroscience*, 6(3), pp. 191–200. doi: 10.1038/nrn1627.

Söhl, G. and Willecke, K. (2003) 'An update on connexin genes and their nomenclature in mouse and man.', *Cell communication & adhesion*, 10(4–6), pp. 173–180. doi: 10.1080/15419060390262877.

Soroldoni, D., Hogan, B. M. and Oates, A. C. (2009) 'Simple and efficient transgenesis with meganuclease constructs in zebrafish.', *Methods in molecular biology (Clifton, N.J.)*, 546, pp. 117–130. doi: 10.1007/978-1-60327-977-2_8.

Sowell, E. R. *et al.* (2003) 'Cortical abnormalities in children and adolescents with attention-deficit hyperactivity disorder', *The Lancet*, 362(9397), pp. 1699–1707. doi: 10.1016/S0140-6736(03)14842-8.

Spence, R. and Smith, C. (2008) 'Innate and Learned Colour Preference in the Zebrafish, Danio rerio', *Ethology*, 114(6), pp. 582–588. doi: 10.1111/j.1439-0310.2008.01515.x.

Srinivas, M. *et al.* (1999) 'Functional properties of channels formed by the neuronal gap junction protein connexin36.', *The Journal of neuroscience : the official journal of the Society for Neuroscience*, 19(22), pp. 9848–9855.

Stauch, K., Kieken, F. and Sorgen, P. (2012) 'Characterization of the Structure and Intermolecular Interactions between the Connexin 32 Carboxyl-terminal Domain and the Protein Partners Synapse-associated Protein 97 and Calmodulin', *Journal of Biological Chemistry*, 287(33), pp. 27771–27788. doi: 10.1074/jbc.M112.382572.

Stenkamp, D. L. (2015) 'Development of the Vertebrate Eye and Retina', in, pp. 397–414. doi: 10.1016/bs.pmbts.2015.06.006.

Sterling, P. and Matthews, G. (2005) 'Structure and function of ribbon synapses', *Trends in Neurosciences*, 28(1), pp. 20–29. doi: 10.1016/j.tins.2004.11.009.

Sumiyoshi, T. *et al.* (2007) 'Effect of buspirone, a serotonin1A partial agonist, on cognitive function in schizophrenia: A randomized, double-blind, placebo-controlled study', *Schizophrenia Research*, 95(1–3), pp. 158–168. doi: 10.1016/j.schres.2007.06.008.

Svoboda, K. R. and Fetcho, J. R. (1996) 'Interactions between the neural networks for escape and swimming in goldfish.', *The Journal of neuroscience : the official journal of the Society for Neuroscience*, 16(2), pp. 843–52. Available at: http://www.ncbi.nlm.nih.gov/pubmed/8551364.

Teubner, B. *et al.* (2000) 'Functional Expression of the Murine Connexin 36 Gene Coding for a Neuron-Specific Gap Junctional Protein', *The Journal of Membrane Biology*, 176(3), pp. 249–262. doi: 10.1007/s00232001094.

Thaler, C. *et al.* (2009) 'Structural rearrangement of CaMKIIα catalytic domains encodes activation', *Proceedings of the National Academy of Sciences*, 106(15), pp. 6369–6374. doi: 10.1073/pnas.0901913106.

Thomas, T. *et al.* (2005) 'Mechanisms of Cx43 and Cx26 transport to the plasma membrane and gap junction regeneration.', *Journal of cell science*, 118(Pt 19), pp. 4451–4462. doi: 10.1242/jcs.02569.

Thompson, R. F. and Spencer, W. A. (1966) 'Habituation: A model phenomenon for the study of neuronal substrates of behavior.', *Psychological Review*, 73(1), pp. 16–43. doi: 10.1037/h0022681.

Todman, D. (2008) 'Henry Dale and the Discovery of Chemical Synaptic Transmission', *European Neurology*, 60(3), pp. 162–164. doi: 10.1159/000145336.

Tomizawa, K., Inoue, Y. and Nakayasu, H. (2000) 'A monoclonal antibody stains radial glia in the adult zebrafish (Danio rerio) CNS', *Journal of Neurocytology*, 29(2), pp. 119–128. doi: 10.1023/A:1007156529390.

Torborg, C. L. and Feller, M. B. (2005) 'Spontaneous patterned retinal activity and the refinement of retinal projections', *Progress in Neurobiology*, 76(4), pp. 213–235. doi: 10.1016/j.pneurobio.2005.09.002.

Török, K., Staugger, K. and Evans, W. H. (1997) 'Connexin 32 of gap junctions contains two cytoplasmic calmodulin-binding domains', *Biochemical Journal*, 326(2), pp. 479–483. doi: 10.1042/bj3260479.

Traynelis, S. *et al.* (2010) 'Glutamate receptor ion channels: structure, regulation, and function', *Pharmacol Rev*, 62, pp. 405–496.

Urschel, S. *et al.* (2006) 'Protein Kinase A-mediated Phosphorylation of Connexin36 in Mouse Retina Results in Decreased Gap Junctional Communication between AII Amacrine Cells', *Journal of Biological Chemistry*, 281(44), pp. 33163–33171. doi: 10.1074/jbc.M606396200.

Venkatraman, P. *et al.* (2020) 'Rods Contribute to Visual Behavior in Larval Zebrafish', *Investigative Opthalmology & Visual Science*, 61(12), p. 11. doi: 10.1167/iovs.61.12.11.

Verselis, V. K., Ginter, C. S. and Bargiello, T. A. (1994) 'Opposite voltage gating polarities of two closely related connexins.', *Nature*, 368(6469), pp. 348–351. doi: 10.1038/368348a0.

Veruki, M. L. and Hartveit, E. (2002) 'AII (Rod) Amacrine Cells Form a Network of Electrically Coupled Interneurons in the Mammalian Retina', *Neuron*, 33(6), pp. 935–946. doi: 10.1016/S0896-6273(02)00609-8.

Vihtelic, T. S., Doro, C. J. and Hyde, D. R. (1999) 'Cloning and characterization of six zebrafish photoreceptor opsin cDNAs and immunolocalization of their corresponding proteins', *Visual Neuroscience*, 16(3), pp. 571–585. doi: 10.1017/S0952523899163168.

Volff, J.-N. (2005) 'Genome evolution and biodiversity in teleost fish', *Heredity*, 94(3), pp. 280–294. doi: 10.1038/sj.hdy.6800635.

Wade, R. H. (2009) 'On and around microtubules: an overview.', *Molecular biotechnology*, 43(2), pp. 177–91. doi: 10.1007/s12033-009-9193-5.

Wales, P. *et al.* (2016) 'Calcium-mediated actin reset (CaAR) mediates acute cell adaptations.', *eLife*, 5. doi: 10.7554/eLife.19850.

Walton, K. M. (1999) 'GDNF: a novel factor with therapeutic potential for neurodegenerative disorders', *Molecular Neurobiology*, 19(1), pp. 43–59. doi: 10.1007/BF02741377.

Wang, H. Y. *et al.* (2015) 'Two-color fluorescent analysis of connexin 36 turnover: relationship to functional plasticity.', *Journal of cell science*, pp. 3888–3897. doi: 10.1242/jcs.162586.

Wang, H. Y. *et al.* (2015) 'Two-color fluorescent analysis of connexin 36 turnover: relationship to functional plasticity', *Journal of Cell Science*, 128(21), pp. 3888–3897. doi: 10.1242/jcs.162586.

Wang, X. *et al.* (2017) 'A novel mechanism for Ca2+/calmodulin-dependent protein kinase II targeting to L-type Ca2+ channels that initiates long-range signaling to the nucleus', *Journal of Biological Chemistry*, 292(42), pp. 17324–

17336. doi: 10.1074/jbc.M117.788331.

Wang, Y. and Belousov, A. B. (2011) 'Deletion of neuronal gap junction protein connexin 36 impairs hippocampal LTP', *Neurosci Lett*, 502(1), pp. 30–32. doi: 10.1016/j.neulet.2011.07.018.Deletion.

Wang, Z. *et al.* (2008) 'Myosin Vb mobilizes recycling endosomes and AMPA receptors for postsynaptic plasticity.', *Cell*, 135(3), pp. 535–48. doi: 10.1016/j.cell.2008.09.057.

Wansley, R. A. and Holloway, F. A. (1975) 'Multiple retention deficits following one-trial appetitive training', *Behavioral Biology*, 14(2), pp. 135–149. doi: 10.1016/S0091-6773(75)90135-2.

Wansley, R. A. and Holloway, F. A. (1976) 'Oscillations in retention performance after passive avoidance training', *Learning and Motivation*, 7(2), pp. 296–302. doi: 10.1016/0023-9690(76)90037-0.

Warmuth-Metz, M. *et al.* (2001) 'Measurement of the Midbrain Diameter on Routine Magnetic Resonance Imaging', *Archives of Neurology*, 58(7), p. 1076. doi: 10.1001/archneur.58.7.1076.

Wassle, H. and Boycott, B. B. (1991) 'Functional architecture of the mammalian retina', *Physiological Reviews*, 71(2), pp. 447–480. doi: 10.1152/physrev.1991.71.2.447.

Watanabe, H., Washioka, H. and Tonosaki, a (1988) 'Gap junction and its cytoskeletal undercoats as involved in invagination-endocytosis.', *The Tohoku journal of experimental medicine*, 156(2), pp. 175–190. doi: 10.1620/tjem.156.175.

Watanabe, M. (2017) 'Gap Junction in the Teleost Fish Lineage: Duplicated Connexins May Contribute to Skin Pattern Formation and Body Shape Determination', *Frontiers in Cell and Developmental Biology*, 5. doi: 10.3389/fcell.2017.00013.

Watanabe, Y., Stone, E. and McEwen, B. S. (1994) 'Induction and habituation of c-fos and zif/268 by acute and repeated stressors', *NeuroReport*, 5(11), pp. 1321–1324. doi: 10.1097/00001756-199406270-00006.

Wayakanon, P. *et al.* (2012) 'The role of the Cx43 C-terminus in GJ plaque formation and internalization', *Biochemical and Biophysical Research Communications*. Elsevier Inc., 420(2), pp. 456–461. doi: 10.1016/j.bbrc.2012.03.018.

Weber, P. A. *et al.* (2004) 'The permeability of gap junction channels to probes of different size is dependent on connexin composition and permeant-pore affinities.', *Biophysical journal*, 87(2), pp. 958–973. doi: 10.1529/biophysj.103.036350.

Wei, C. J. *et al.* (2005) 'Connexin43 associated with an N-cadherin-containing multiprotein complex is required for gap junction formation in NIH3T3 cells', *Journal of Biological Chemistry*, 280(20), pp. 19925–19936. doi: 10.1074/jbc.M412921200.

Weidmann, S. (1952) 'The electrical constants of Purkinje fibres.', *The Journal of physiology*, 118(3), pp. 348–360.

Weiss, S. A. *et al.* (2006) 'Correlation of C-start behaviors with neural activity recorded from the hindbrain in free-swimming goldfish (Carassius auratus)', *Journal of Experimental Biology*, 209(23), pp. 4788–4801. doi: 10.1242/jeb.02582.

Wen, L. *et al.* (2008) 'Visualization of monoaminergic neurons and neurotoxicity of MPTP in live transgenic zebrafish', *Developmental Biology*, 314(1), pp. 84–92. doi: 10.1016/j.ydbio.2007.11.012.

Westberg, L. *et al.* (2009) 'Colocalization of connexin 36 and corticotropin-releasing hormone in the mouse brain', *BMC Neuroscience*, 10(1), p. 41. doi: 10.1186/1471-2202-10-41.

Wheeler, D. G. *et al.* (2008) 'CaMKII locally encodes L-type channel activity to signal to nuclear CREB in excitation–transcription coupling', *Journal of Cell Biology*, 183(5), pp. 849–863. doi: 10.1083/jcb.200805048.

White, J. G. *et al.* (1986) 'The structure of the nervous system of the nematode Caenorhabditis elegans', *Philosophical Transactions of the Royal Society of London. B, Biological Sciences*, 314(1165), pp. 1–340. doi: 10.1098/rstb.1986.0056.

Wilkerson, C. G., King, S. M. and Witman, G. B. (1994) 'Molecular analysis of the gamma heavy chain of Chlamydomonas flagellar outer-arm dynein.', *Journal of cell science*, 107 (Pt 3, pp. 497–506. Available at: http://www.ncbi.nlm.nih.gov/pubmed/7516341.

Witkovsky, P. (2004) 'Dopamine and retinal function', *Documenta Ophthalmologica*, 108(1), pp. 17–39. doi:

10.1023/B:DOOP.0000019487.88486.0a.

Witman, G. B. (1992) 'Axonemal dyneins', *Curr Opin Cell Biol*, 4(1), pp. 74–79. doi: 10.1016/0960-9822(92)90275-F.

Wolff, J. *et al.* (1996) 'Cation selective promotion of tubulin polymerization by alkali metal chlorides Cation selective promotion of tubulin polymerization by alkali metal chlorides', *Protein Science*, pp. 2020–2028.

Wyart, C. *et al.* (2009) 'Optogenetic dissection of a behavioural module in the vertebrate spinal cord', *Nature*, 461(7262), pp. 407–410. doi: 10.1038/nature08323.

Xie, R. *et al.* (2019) 'Normalization of large-scale behavioural data collected from zebrafish', *PLOS ONE*. Edited by S. C. F. Neuhauss, 14(2), p. e0212234. doi: 10.1371/journal.pone.0212234.

Xiong, Z. *et al.* (2021) 'In vivo proteomic mapping through GFP-directed proximity-dependent biotin labelling in zebrafish', *eLife*, 10. doi: 10.7554/eLife.64631.

Xu, Q. *et al.* (2012) 'Gating of connexin 43 gap junctions by a cytoplasmic loop calmodulin binding domain.', *American journal of physiology. Cell physiology*, 302(10), pp. C1548-56. doi: 10.1152/ajpcell.00319.2011.

Yamamoto, K. *et al.* (2013) 'Evolution of Dopamine Receptor Genes of the D1 Class in Vertebrates', *Molecular Biology and Evolution*, 30(4), pp. 833–843. doi: 10.1093/molbev/mss268.

Yoshida, M. and Macklin, W. B. (2005) 'Oligodendrocyte development and myelination in GFP-transgenic zebrafish', *Journal of Neuroscience Research*, 81(1), pp. 1–8. doi: 10.1002/jnr.20516.

Young, E. . *et al.* (2014) 'Selective, retrieval-independent disruption of methamphetamine- associated memory by actin depolymerization', *Biol. Psychiatry*, 75, pp. 96–104.

Yum, S. W. *et al.* (2007) 'Human connexin26 and connexin30 form functional heteromeric and heterotypic channels', *American Journal of Physiology-Cell Physiology*, 293(3), pp. C1032–C1048. doi: 10.1152/ajpcell.00011.2007.

Zeroka, D., Jensen, J. O. and Samuels, A. C. (1998) 'Rotation / Inversion Study of the Amino Group in Ethylamine', 5639(98), pp. 6571–6579. doi: 10.1021/jp982031a.

Zhang, H. *et al.* (2005) 'Synaptic Fatigue is More Pronounced in the APP/PS1 Transgenic Mouse Model of Alzheimers Disease', *Current Alzheimer Research*, 2(2), pp. 137–140. doi: 10.2174/1567205053585936.

Zhang, K. *et al.* (2004) 'Regulation of Working Memory by Dopamine D4 Receptor in Rats', *Neuropsychopharmacology*, 29(9), pp. 1648–1655. doi: 10.1038/sj.npp.1300491.

Zhdanova, I. V. *et al.* (2001) 'Melatonin promotes sleep-like state in zebrafish', *Brain Research*, 903(1–2), pp. 263–268. doi: 10.1016/S0006-8993(01)02444-1.

Zheng, X. *et al.* (2016) 'Molecular basis for CPAP-tubulin interaction in controlling centriolar and ciliary length', *Nature Communications*, 7, p. 11874. doi: 10.1038/ncomms11874.

Zhou, Y. *et al.* (2007) 'Interactions between the NR2B receptor and CaMKII modulate synaptic plasticity and spatial learning', *Journal of Neuroscience*, 27, pp. 13843–53.

Zhou, Y. *et al.* (2009) 'Calmodulin mediates the Ca2+-dependent regulation of Cx44 gap junctions.', *Biophysical journal*, 96(7), pp. 2832–48. doi: 10.1016/j.bpj.2008.12.3941.

Zhou, Y. *et al.* (2014) 'Quantification of larval zebrafish motor function in multiwell plates using open-source MATLAB applications.', *Nature protocols*, 9(7), pp. 1533–48. doi: 10.1038/nprot.2014.094.

Zikopoulos, B., García-Cabezas, M. Á. and Barbas, H. (2018) 'Parallel trends in cortical gray and white matter architecture and connections in primates allow fine study of pathways in humans and reveal network disruptions in autism', *PLOS Biology*. Edited by C. Darian-Smith, 16(2), p. e2004559. doi: 10.1371/journal.pbio.2004559.

Zlomuzica, a *et al.* (2012) 'Behavioral alterations and changes in Ca/calmodulin kinase II levels in the striatum of connexin36 deficient mice.', *Behavioural brain research*. Elsevier B.V., 226(1), pp. 293–300. doi: 10.1016/j.bbr.2011.08.028.

Zoidl, G. *et al.* (2002) 'Evidence for a role of the N-terminal domain in subcellular localization of the neuronal connexin36 (Cx36)', *Journal of Neuroscience Research*, 69(4), pp. 448–465. doi: 10.1002/jnr.10284.

Zottoli, S. J. (1977) 'Correlation of the startle reflex and Mauthner cell auditory responses in unrestrained goldfish.',

The Journal of experimental biology, 66(1), pp. 243–54. Available at: http://www.ncbi.nlm.nih.gov/pubmed/858992.

Zottoli, S. J., Hordes, A. R. and Faber, D. S. (1987) 'Localization of optic tectal input to the ventral dendrite of the goldfish Mauthner cell.', *Brain research*, 401(1), pp. 113–21. Available at: http://www.ncbi.nlm.nih.gov/pubmed/3815088.

APPENDIX A: CONNEXIN/PANNEXIN PRIMERS

Gene	*Accession Nr*	*Function*	*Primer – 5‘*	*Primer – 3‘*	*amplicon (bp)*
18s rRNA	NM_001098396	ribosomal RNA	TGCATGGCCGTTCTTAGTTG	AGTCTCGTTCGTTATCGGAATGA	86
panx 1a	NM_200916	channel	TGGATACAAACAGCTCTGTGATAG	ATCCTTTAGAGTAGCGCTTGG	96
panx 1b	NM_001100030	channel	AAGTATAAAGGCGTGCGGCTGG	TGATCTGAGTACCCACAGAGAC	129
panx 2	NM_001256641	channel	TCGACTGAGAGGACAAACCC	TCGCCACCAACTTCACAACTC	99
panx 3	XM_001919826	channel	CATACAACCGCTCTGTCCGT	GCTTGCGTTTGGCTCTCTC	105
Cx27.5	NM_131811	gap - junction channel	GGAGGCGATAAAGAACCAGAAG	CAGATACATAAAGGCGGACTCG	106
Cx30.3	NM_212825	gap - junction channel	TCTTTCCAGTCTCGCACATAC	CTCCTTTACCATTACCTCCACG	150
Cx34.7	NM_001128766	gap - junction channel	GCCTTCCCAATCTCCCATATC	GTGTAACGCTGGTCTTTGTG	122
Cx35b	NM_194420	gap - junction channel	ACTGTGTTCCTCGTCTTCATG	AGCCCAGGTGATTGAGTTC	79
Cx39.9	NM_212826	gap - junction channel	GCCCAGGAACATTCTACAGTG	CTGAGCACCAAGATACGGAAG	74
Cx43	NM_131038	gap - junction channel	TACGTGCTCTTCAAACGAATCAAGGACC	CGTATTTGGTCGTAGACAGTTCCTTCGG	109

Cx44.2	NM_131810	gap - junction channel	CAGGATGAACAGAGCAAGTTTG	AGCCGAGATACACAATGGATG	148
Cx47.1	NM_001004574	gap - junction channel	GCTTTCTCACTCGACTCTTGG	TGAACTTTGTCTGCTCATCCG	144
Cx52.6	NM_212819	gap - junction channel	AGAGTGATTCGGTGGAAAGTG	CCCCTTGAGTGATACGGTTG	141
Cx52.7	NM_001113502	gap - junction channel	GACCATCCTGTTCATTTTCCG	TGAGCGATATTGGGAATGCC	146
Cx52.9	NM_207093	gap - junction channel	CACCATCCTCTTCATCTTCCG	AGTGTTGCAGATGAAGTCGG	91
Cx55.5	NM_131812	gap - junction channel	TTTCCCCATTTCCCTAATCCG	GTTCTCGTCTCAGTGCCATC	146
actb1	NM_131031	actin, cytoplasmic	TGAGCAGGAGATGGGAACC	CAACGGAAACGCTCATTGC	102
actb2	NM_181601	actin, cytoplasmic	GCCCCTAGCACAATGAAGATC	GACTCATCGTACTCCTGCTTG	134
tuba1b	NM_194388	tubulin, cytoplasmic	GAGCGTCCTACTTACACCAAC	AGGGAAGTGGATACGAGGATAG	147

APPENDIX B: DOPAMINERGIC GENE PRIMERS

Gene	*Accession Nr*	*Function*	*Primer – 5‘*	*Primer – 3‘*	*amplicon (bp)*
18s rRNA	NM_001098396	rRNA	TGCATGGCCGTTCTTAGTTG	AGTCTCGTTCGTTATCGGAATGA	86
drd1a	XM_017359120	G-protein coupled receptor	CTCATCTCCTTCATCCCAGTG	ATATGTTCGGTTGAGGCTGG	126
drd1b	NM_001135976	G-protein coupled receptor	ACGCTGTCCATCCTTATCTC	TGTCCGATTAAGGCTGGAG	135
drd2a	NM_183068	G-protein coupled receptor	ATCGGGATGGGTGCATTTC	TGGTACTCCGGAAAAGACG	101
drd2b	NM_197936	G-protein coupled receptor	ACCTCCAAGTCCCAATCATG	GTTCGGGTTTTGCCATTAGG	134
drd2c	AY333792	G-protein coupled receptor	ACCTCCAAGTCCCAATCATG	GTTCGGGTTTTGCCATTAGG	147
drd3	NM_183067	G-protein coupled receptor	ATCAGTATCGACAGGTATACAGC	CCAAACAGTAGAGGGCAGG	137
drd4a	NM_001012616	G-protein coupled receptor	CTTACCGCTGTTTGTGTATGC	ATGAACCTGTCTATGCTGATGG	144
drd4b	NM_001012618	G-protein coupled receptor	TTACCCCTGTTTGTCTATGCTG	GGCTATAAACCTGTCCACACTG	147
drd5a	XM_003199767	G-protein coupled receptor	ACCAACTCTTCGCTCAACC	TCGTTGCTGATGTTGACCG	125
th2	NM_001001829	monooxygenase	TTGTGTCCGAGAGCTTTGAG	AAGCATTCTGGATCTTGGAGG	141

slc18a2 (VMAT2)	NM_001256225	transporter	AGCTCCTTTTCTTATCCTGGC	TGCAATGAGGATGTATGGGTC	145
actb1	NM_131031	actin, cytoplasmic	TGAGCAGGAGATGGGAACC	CAACGGAAACGCTCATTGC	102
actb2	NM_181601	actin, cytoplasmic	GCCCCTAGCACAATGAAGATC	GACTCATCGTACTCCTGCTTG	134
tuba1b	NM_194388	tubulin, cytoplasmic	GAGCGTCCTACTTACACCAAC	AGGGAAGTGGATACGAGGATAG	147

APPENDIX C: COGNITIVE INDEXING PRIMERS

Gene	*Accession Nr*	*Function*	*Primer – 5‘*	*Primer – 3‘*	*amplicon (bp)*
18s rRNA *#*	NM_001098396	ribosomal RNA	TGCATGGCCGTTCTTAGTTG	AGTCTCGTTCGTTATCGGAATGA	86
bdnf	NM_001308648	growth factor	CGCCGTTACTCTTTCTCTTGG	GTCACCCACTGGCTAATACTG	136
egr1	NM_131248	transcriptional regulator	TCAACATATCCCAGTGCCAAG	TGTGTCTGGATGGGTTTCTG	128
egr2a	NM_001328404	transcriptional regulator	CTTCTCCTGTGACTTCTGCG	GCTTTCTGTCCTTATGTCTCTGG	92
egr2b	NM_130997	transcriptional regulator	GATGCGGAGAGGTCTATCAAG	AGGAGTAGGATGGCGGAG	84
egr4	NM_001114453	transcriptional regulator	ACAGCACCTCAAAGACTACAG	ACGACAAGGTAAAAGACTGGAG	149
fosab	NM_205569	transcriptional regulator	GTGAACGAAACAAGATGGCTG	TTTCATCCTCAAGCTGGTCAG	96
c-jun	NM_199987	transcriptional regulator	CACAAGGCTCTGAAACACAAC	TGATGCCAGTTTGAGAAGTCC	129
creb1a	NM_200909	transcriptional regulator	CAATAACGGGACGGATGGAG	TGCTGGGAACAAGTATCTGC	131
creb1b	NM_001017818	transcriptional regulator	CCAGATTTCCACAGTAGCAGAG	GACAGGTCGTTCAAGATTTTCC	126

camk2a	NM_001017741	kinase	GAAGACGGATGGTGTGAAGG	CTCTCGAAGTCTCCATTGCTG	138
camk4	NM_001017607	kinase	GAGACCTGAAACCCGAGAAC	GGAGCACAATATCCTGGAGTG	142
fyna	NM_001328163	kinase	AAGTGGAGCGTGGTTACAG	AGTGGCAGTGAAGTAATCCTC	149
dlg4b	NM_214728	synaptic transmission	CCACGCATACACACCTCAG	ATTCAACATCTCCGTCCATACC	119
gria1a	NM_205598	receptor	AGATGACTGTGAGGACGGAG	GGTTCTGGTTTTGCTGGTTCTG	89
gria2b	NM_131895	receptor	AGCTGACATCGCAGTGGC	GGCTTCTTGATCATGATGGAGATGC	108
grin1a	NM_001076714	receptor	AGAGTTTCGCTGGAATCACATC	CAGTTGGTCTTGGTTTTCATAGTTC	139
slc6a4a	NM_001039972	neurotransmitter transporter	GCCACAGGCCCCGCTGTTA	ACCAGGGGCGAAGCCAAGCA	117
tuba1a[#]	AF029250	microtubules	GAGCGTCCTACTTACACCAAC	AGGGAAGTGGATACGAGGATAG	147
actb1[#]	NM_131031	actin, cytoplasmic	TGAGCAGGAGATGGGAACC	CAACGGAAACGCTCATTGC	102

APPENDIX D: LIST OF CONNEXIN HOMOLOGS

Zebrafish Connexin gene	Zebrafish Connexin protein	Human Connexin gene	Human Connexin protein
gja1a	Cx40.8	GJA1	CX43
gja1b	Cx43		
gja2	Cx39.9	—	—
gja3	Cx46	GJA3	CX46
gja4	Cx39.4	GJA4	CX37
gja5a	Cx45.6	GJA5	CX40
gja5b	Cx41.8		
—	—	GJA6P	CX43px
gja8a	Cx79.8	GJA8	CX50
gja8b	Cx44.1		
gja9a	Cx55.5	GJA9	CX58
gja9b	Cx52.9		
gja10a	Cx52.7	GJA10	CX62
gja10b	Cx52.6		
gja11	Cx34.5	—	—
gja12.1	Cx28.9	—	—
gja12.2	Cx28.1	—	—
gja13.1	Cx32.3	—	—
gja13.2	Cx32.2	—	—
gjb1a	Cx27.5	GJB1	GJB1/CX32
gjb1b	Cx31.7		
gjb3	Cx35.4	GJB3	CX31
gjb7	Cx28.8	GJB7	CX25
gjb8	Cx30.3	GJB2	CX26
		GJB6	CX30
gjb9a	Cx28.6	—	—
gjb9b	Cx30.9		
gjb10	Cx34.4	GJB4	CX30.3
		GJB5	CX31.1
gjc1	Cx52.8	GJC1	CX45
gjc2	Cx47.1	GJC2	CX47 or Cx45
—	—	GJC3	CX29
gjc4a.1	Cx44.2	—	—
gjc4a.2	Cx44.5		
gjc4b	Cx43.4		
gjd1a	Cx34.1	GJD2	CX36
gjd1b	Cx34.7		
gjd2a	Cx35.5		
gjd2b	Cx35.1		
—	—	GJD3	CX31.9
gjd4	Cx46.8	GJD4	CX40.1
gjd5	Cx40.5	—	—
gjd6	Cx36.7	—	—
gje1a	*Cx23.9*	GJE1	CX23
gje1b	*Cx20.3*		
gjz1	*Cx26.3*	—	—